ABSTRACT

Title of Dissertation: ASYMPTOTIC AND NUMERICAL ANALYSIS IN KÄHLER GEOMETRY: EDGE METRICS, EINSTEIN METRICS AND SOLITONS

Yuxiang Ji
Doctor of Philosophy, 2024

Dissertation Directed by: Professor Yanir A. Rubinstein
Department of Mathematics

This thesis is divided into two parts. The first part focuses on theoretical problems arising from the study of Kähler edge geometry. The second part introduces a practical method for finding Kähler–Einstein and soliton metrics that exist on toric Fano surfaces. This method is based on a numerical implementation of the Ricci iteration, which essentially solves a sequence of Monge–Ampère equations.

Let M be a compact Kähler manifold and $D = D_1 + \dots D_r$ be a simple normal crossing divisor. Given that $K_M + D$ is ample, there exist Kähler–Einstein crossing edge metrics on M with edge singularities of cone angle β_i along each component D_i for small β_i. The first result in the thesis shows that such negatively curved Kähler–Einstein crossing edge metrics converge to the Kähler–Einstein mixed cusp and edge metrics smoothly away from the divisor, as some of the cone angles approach 0. We further show that, near the divisor, a family of appropriately renormalized Kähler–Einstein crossing edge metrics converges to a mixed cylinder

and edge metric in the pointed Gromov–Hausdorff sense as some of the cone angles approach 0 at (possibly) different speeds.

Generalizing $\mathbb{P}^1$, Calabi–Hirzebruch manifolds are constructed by adding an infinite section to the total space of a tensor product of the hyperplane bundle over the projective space, leading to two disjoint divisors: the zero and infinite sections.

The second main result in the thesis is the discovery of Kähler–Einstein edge metrics with singularities along the two divisors on Calabi–Hirzebruch manifolds, and the study on Gromov–Hausdorff limits of these metrics when either cone angle tends to its extreme value. As a very special case, we show that the Eguchi–Hanson metric arises in this way naturally as a Gromov–Hausdorff limit. We also completely describe all other (possibly rescaled) Gromov–Hausdorff limits which exhibit a wide range of behaviors, resolving in this setting a conjecture of Cheltsov–Rubinstein. This gives a new interpretation of both the Eguchi–Hanson space and Calabi's Ricci flat spaces as limits of compact singular Einstein spaces.

The second part of the thesis focuses on numerical implementation of the Ricci iteration on toric del Pezzo surfaces: $\mathbb{P}^2$, $\mathbb{P}^1 \times \mathbb{P}^1$, and blow-up of $\mathbb{P}^2$ at one, two or three distinct points in general position. The Ricci iteration on these surfaces can be reduced to solving a sequence of real Monge–Ampère equations in $\mathbb{R}^2$ with the second boundary value condition.

As the third contribution of the thesis, we successfully conduct the Ricci iteration on the aforementioned surfaces. We find that the resulting solutions numerically converge to either the unique Kähler–Einstein metric on $\mathbb{P}^2, \mathbb{P}^1 \times \mathbb{P}^1$, and $\mathbb{P}^2 \# 3\overline{\mathbb{P}^2}$, or the unique Kähler–Ricci soliton metric on $\mathbb{P}^2 \# \overline{\mathbb{P}^2}$ and $\mathbb{P}^2 \# 2\overline{\mathbb{P}^2}$. This provides a novel numerical approach to finding Kähler–Einstein and soliton metrics on these manifolds.

Our numerical results also provide evidence that, in the toric case, the Ricci iteration may converge and produce canonical metrics without the necessity of modifying the metrics obtained during the iterations by automorphisms.

ASYMPTOTIC AND NUMERICAL ANALYSIS IN KÄHLER GEOMETRY: EDGE METRICS, EINSTEIN METRICS AND SOLITONS

by

Yuxiang Ji

Dissertation submitted to the Faculty of the Graduate School of the
University of Maryland, College Park in partial fulfillment
of the requirements for the degree of
Doctor of Philosophy
2024

Advisory Committee:
Professor Yanir A. Rubinstein, Chair/Advisor
Professor Tamás Darvas
Professor Antoine Mellet
Professor Ricardo H. Nochetto
Professor Howard Elman, Dean's representative

© Copyright by
Yuxiang Ji
2024

Dedication

To Yanchao and my parents.

Acknowledgments

First and foremost, I would like to thank my advisor, Yanir, for all the math you taught me, and all the time you spent on me. Thank you for introducing me to the world of geometry. Your advice, both in math and in life, has been invaluable to me. Your support and understanding have always been there, and it is my great honor and my great fortune to be your student.

I would also like to express my sincere thanks to Prof. Darvas, Prof. Mellet, Prof. Nochetto and Prof. Elman for serving on my committee. It was my great pleasure to present what I have done over these years to all of you. Your feedback and comments make my thesis better. I also thank Prof. Wentworth for serving on the committee of my preliminary oral exam and offering valuable suggestions.

I want to thank Prof. Zhang and Prof. Bonnet for many helpful discussions and advice. I want to thank Prof. Guenancia and Prof. Sturm for helpful conversations. I am grateful to Prof. Huang and the referees for their careful reading and comments for certain parts of the thesis.

I am grateful for the environment that UMD and our math department have created. I especially want to thank Cristina, Ruth, To Anh, Jemma and Trystan, for the assistance and kindness I received from you.

I want to thank my fellow geometry students, Matt, Mirna, Vlassis, Chenzi, Vasanth, Prakhar, Yu-Chi and Dijia. My academic life would have been alone without discussions, reading groups and presentations with you all. I want to thank Ruijie, Yuancheng, Xiyao and Xiaoyu, and our 5AMUMD group. A special thanks to Furong for all those delicious family dinners and that unforgettable New Year's Eve.

I just feel lucky that I am the son of you two, Fang Liu and Zhi Ji, my mother and my father. Thank you for bringing me to the world, teaching me how to love, and making me the man I am now. I will always be proud of being your son.

My life would have been incomplete without you, Yanchao, my soul mate. It is because you that every place in Maryland and our school, every minute during my PhD career, and every up and down I experienced become so wonderfully irreplaceable. It was the greatest moment of my life when I first met you.

Finally, I am grateful for the support from Michael Brin Graduate Student Endowed Fellowship and Patrick & Marguerite Sung Fellowship. I gratefully acknowledge the support of the National Science Foundation through the grant DMS-1906370.

Table of Contents

List of Tables

List of Figures

Chapter 1: Introduction

1.1 Background

1.1.1 Kähler manifold

A complex manifold is a smooth manifold M on whose charts the transition functions are holomorphic. It admits an almost-complex structure acting on its tangent bundle:

$$J : T_pM \to T_pM, \quad p \in M,$$
$$\text{s.t. } J^2 = -\operatorname{Id}.$$

Example 1.1.1 (The complex spaces $\mathbb{C}^n$ and $\mathbb{P}^n$)**.** The complex space $\mathbb{C}^n$ can be equipped with a natural almost-complex structure: by letting $(z_1, \dots, z_n) = (x_1 + \sqrt{-1}y_1, \dots x_n + \sqrt{-1}y_n)$ be its Euclidean coordinates, and defining

$$J\left(\frac{\partial}{\partial x_i}\right) = \frac{\partial}{\partial y_i},\ i = 1, \dots, n$$
$$J\left(\frac{\partial}{\partial y_i}\right) = -\frac{\partial}{\partial x_i},\ i = 1, \dots, n.$$

The projective space $\mathbb{P}^n$ is defined as the space $\mathbb{C}^{n+1} \setminus \{0\}$ modulo the equivalence relation where two elements z_1 and z_2 in $\mathbb{C}^{n+1} \setminus \{0\}$ are considered equivalent if there exists $0 \neq \lambda \in \mathbb{C}$

such that $z_1 = \lambda z_2$. On $\mathbb{P}^n$ we use the homogeneous coordinate $[Z_0 : \ldots, Z_n]$. An atlas of $\mathbb{P}^n$ includes charts $\{Z_i \neq 0\}, i = 0, \ldots, n$. Each chart is identical to $\mathbb{C}^n$ and this implies that $\mathbb{P}^n$ admits a natural complex structure. Thus, $\mathbb{P}^n$ is a complex manifold. The spaces $\mathbb{C}^n$ and $\mathbb{P}^n$ are respectively examples of non-compact and compact complex manifolds.

Let g be a Riemannian metric on a complex manifold (M, J), that is

$$g : T_pM \times T_pM \to \mathbb{R}, \quad p \in M,$$

such that g is bilinear, positive-definite and varies smootly over M. We call g compatible with J if

$$g(\cdot, \cdot) = g(J\cdot, J\cdot).$$

Given a compatible Riemannian metric g, one can associate a 2-form defined as

$$\omega(\cdot, \cdot) := g(J\cdot, \cdot).$$

The triple (M, J, ω) is called Kähler if

$$d\omega = 0,$$

and then such ω is called a Kähler form, or sometimes by abuse of language, a Kähler metric.

A fundamental result on the Kähler manifold is the $\partial\bar{\partial}$-lemma.

Lemma 1.1.2. [52, Lemma 1.14] *Let M be a compact Kähler manifold. If ω_1 and ω_2 are two real $(1,1)$-forms in the same cohomology class in $H^2(M, \mathbb{R})$, i.e., $\omega_1 - \omega_2 = d\eta$ for some real*

1-form η, then there exists $f : M \to \mathbb{R}$ such that

$$\omega_1 - \omega_2 = \sqrt{-1}\partial\bar{\partial}f.$$

From now on, let (M, ω) be a compact Kähler manifold. Then, for any point $p \in M$ there exists a smooth real function ρ in a neighborhood of p such that

$$\omega = \sqrt{-1}\partial\bar{\partial}\rho = \sqrt{-1}\sum_{i,j=1}^{n} g_{i\bar{j}} dz^i \wedge d\bar{z}^j. \tag{1.1}$$

The function ρ is called a Kähler potential.

The Ricci form of ω, denoted by $\operatorname{Ric}\omega$, has the following formula in local coordinates

$$\operatorname{Ric}\omega = -\sqrt{-1}\partial\bar{\partial}\log\det(g_{i\bar{j}}). \tag{1.2}$$

Example 1.1.3 (Fubini–Study metric)**.** The projective space $\mathbb{P}^n$ admits a naturally defined Kähler metric, namely the Fubini–Study metric. Indeed, on the local chart with homogeneous coordinate $[Z_0 : Z_1 : \cdots Z_n]$ that satisfies $Z_0 \neq 0$, consider the complex coordinate $(z_1, \ldots, z_n) := \left(\frac{Z_1}{Z_0}, \ldots, \frac{Z_n}{Z_0}\right)$ and define

$$\rho := \log\left(1 + \sum_{i=1}^{n} |z_i|^2\right). \tag{1.3}$$

By (1.3), the function ρ defined on different charts only differs by a quantity that vanishes after taking the $\partial\bar{\partial}$-operation. Thus, we can define the Fubini–Study metric $\omega_{\mathrm{FS}} := \sqrt{-1}\partial\bar{\partial}\rho$

Computing using (1.2), the Fubini–Study metric on $\mathbb{P}^n$ that is defined by (1.3) satisfies

$$\operatorname{Ric}\omega_{\mathrm{FS}} = 2(n+1)\omega_{\mathrm{FS}}. \tag{1.4}$$

Definition 1.1.4. A Kähler metric ω is Kähler–Einstein if there exists some constant $\mu \in \mathbb{R}$ such that

$$\operatorname{Ric}\omega = \mu\omega. \tag{1.5}$$

The formula (1.2) shows that $\operatorname{Ric}\omega$ is a real closed $(1,1)$-form and its cohomology class is independent of the choice of ω. Indeed, the first Chern class of M can be defined by

$$c_1(M) := \frac{1}{2\pi}[\operatorname{Ric}\omega].$$

Clearly, if ω is Kähler–Einstein , then the first Chern class of M needs to be definite. Under this assumption, one can rewrite (1.5) in terms of Kähler potentials by considering a reference metric ω in the class $\frac{2\pi}{\mu}c_1(M)$. Given a Kähler metric $\omega \in \frac{2\pi}{\mu}c_1(M)$, by Lemma 1.1.2, there exists a smooth function f_ω on M such that

$$\operatorname{Ric}\omega = \mu\omega + \sqrt{-1}\partial\bar{\partial}f_\omega.$$

Denote by

$$\omega_\varphi := \omega + \sqrt{-1}\partial\bar{\partial}\varphi$$

another Kähler metric in the same class, and assume ω_φ solves (1.5).

Lemma 1.1.5. *For ω_φ there holds*

$$(\omega + \sqrt{-1}\partial\bar{\partial}\varphi)^n = e^{f_\omega - \mu\varphi}\omega^n,$$

after renormalizing f_ω by an appropriate constant.

Proof. Subtracting the following

$$\operatorname{Ric}\omega = \mu\omega + \sqrt{-1}\partial\bar{\partial}f_\omega$$

from

$$\operatorname{Ric}\omega_\varphi = \mu\omega_\varphi,$$

we obtain

$$\operatorname{Ric}\omega_\varphi - \operatorname{Ric}\omega = \sqrt{-1}\partial\bar{\partial}(\mu\varphi - f_\omega).$$

Combining this with (1.2), there holds

$$\sqrt{-1}\partial\bar{\partial}\log\frac{\omega^n}{\omega_\varphi^n} = \sqrt{-1}\partial\bar{\partial}(\mu\varphi - f_\omega).$$

Using the fact that M is compact, there exists some constant c such that

$$\log\frac{\omega^n}{\omega_\varphi^n} - (\mu\varphi - f_\omega) = c.$$

We renormalize f_ω by that c, then it follows that the Kähler–Einstein metric ω_φ satisfies

$$(\omega + \sqrt{-1}\partial\bar{\partial}\varphi)^n = e^{f_\omega - \mu\varphi}\omega^n. \tag{1.6}$$

□

Locally by writing

$$\omega = \sqrt{-1}\sum_{j,k} g_{j\bar{k}} dz^j \wedge d\bar{z}^k$$

we can rewrite (1.6) as

$$\det\left(g_{j\bar{k}} + \frac{\partial^2\varphi}{\partial z_j \partial \bar{z}_k}\right) = e^{f_\omega - \mu\varphi}\det\left(g_{j\bar{k}}\right). \tag{1.7}$$

The equation (1.7) is a complex Monge–Ampère equation in φ. It has been extensively studied by geometers and analysts in both the smooth and singular cases, partly due to its geometric interpretation as we just explained.

In summary, the Kähler–Einstein equation (1.5) can be reformulated in the form of (1.6), and locally, it is a complex Monge–Ampère equation (1.7).

1.1.2 Kähler edge metric

In this thesis we are concerned with the aforementioned Kähler–Einstein metrics, as well as two generalizations. The first generalization is the Kähler–Einstein edge (KEE) metric, which as implied by its name, is both Einstein and possesses Kähler edge singularities. A model edge metric on $\mathbb{C}^n$ with a cone angle β along the divisor $\{z_1 = 0\}$ is given by

$$\omega_{\text{cone},\beta} := \frac{\beta^2\sqrt{-1}dz^1 \wedge d\bar{z}^1}{|z_1|^{2(1-\beta)}} + \sum_{i=2}^{n} \sqrt{-1}dz^i \wedge d\bar{z}^i.$$

Let M be a compact Kähler manifold of dimension n and $D \subset M$ a smooth hypersurface. Then:

Definition 1.1.6. A Kähler edge metric ω on M with angle $2\pi\beta$ ($0 < \beta \leq 1$) along D is a Kähler current on M that is smooth on $M \setminus D$ and, there exists some $C > 0$ such that in any coordinate chart where $D = \{z_1 = 0\}$,

$$\frac{1}{C}\omega_{\text{cone},\beta} \leq \omega \leq C\omega_{\text{cone},\beta}.$$

A Kähler edge metric ω is called *Kähler–Einstein edge* (KEE) if there exists $\mu \in \mathbb{R}$ such that

$$\operatorname{Ric}\omega = \mu\omega + 2\pi(1-\beta)[D], \quad 0 < \beta \leq 1, \tag{1.8}$$

where $[D]$ represents the current associated to the integration along D.

1.1.3 Kähler–Ricci soliton

The second generalization of Kähler–Einstein metrics is the concept of Kähler–Ricci soliton. Assume X is a real smooth vector field on M, and θ is the complete flow of X. For any $p \in M$ and sufficiently small t, the map $\theta_t : M \to M$ is a diffeomorphism from a neighborhood of p to a neighborhood of $\theta_t(p)$. Hence, $d(\theta_t)_p^*$ pulls back tensors at $\theta_t(p)$ to ones at p. Given any smooth tensor field A on M, the Lie derivative of A with respect to X is defined by

$$(\mathcal{L}_X A)_p := \frac{d}{dt}\bigg|_{t=0} (\theta_t^* A)_p = \lim_{t\to 0} \frac{d(\theta_t)_p^*(A_{\theta_t(p)}) - A_p}{t}, \tag{1.9}$$

and $\mathcal{L}_X A$ is a smooth tensor field on M.

Let $\mathrm{Aut}(M, J)$ be the complex Lie group of automorphisms (i.e., biholomorphisms) of (M, J) and denote by $\mathrm{aut}(M, J)$ its Lie algebra of infinitesimal automorphisms composed of real vector fields X satisfying $\mathcal{L}_X J = 0$, where $\mathcal{L}$ is the Lie derivative defined in (1.9).

The following definition generalizes the concept of Kähler–Einstein metrics.

Definition 1.1.7. A Kähler metric ω is called a Kähler–Ricci soliton if there exists a real holomorphic vector field $X \in \mathrm{aut}(M, J)$ such that

$$\mathrm{Ric}\,\omega = \mu\omega + \mathcal{L}_X\omega. \tag{1.10}$$

Given a Fano manifold and a Kähler metric ω, any real holomorphic vector field X induces a smooth function θ_ω^X such that $\mathcal{L}_X\omega = \sqrt{-1}\partial\bar{\partial}\theta_\omega^X$ [47, (42)]. When (ω, X) exists in Definition 1.1.7, we can rewrite (1.10) as follows:

$$\mathrm{Ric}\,\omega = \mu\omega + \sqrt{-1}\partial\bar{\partial}\theta_\omega^X. \tag{1.11}$$

Now, fix a reference metric ω and denote by f_ω its Ricci potential. Assume ω_φ and a real holomorphic vector field X satisfy (1.10). Then there hold

$$\operatorname{Ric}\omega = \mu\omega + \sqrt{-1}\partial\bar{\partial} f_{\omega}, \tag{1.12}$$

$$\operatorname{Ric}\omega_{\varphi} = \mu\omega_{\varphi} + \sqrt{-1}\partial\bar{\partial}\theta^{X}_{\omega_{\varphi}}. \tag{1.13}$$

We normalize θ^X_ω for any ω such that

$$\int_M e^{\theta^X_\omega}\omega^n = \int_M \omega^n,$$

then there holds $\theta^X_{\omega_\varphi} = \theta^X_\omega + X(\varphi)$ [47, p. 1550, line 1]. Thus, (1.13) becomes

$$\operatorname{Ric}\omega_{\varphi} = \mu\omega_{\varphi} + \sqrt{-1}\partial\bar{\partial}(\theta^{X}_{\omega} + X(\varphi)). \tag{1.14}$$

By the same reduction procedure for (1.7), subtracting (1.14) from (1.12) leads to

$$\det\left(g_{j\bar{k}} + \frac{\partial^2\varphi}{\partial z_j \partial \bar{z}_k}\right) = e^{f_\omega - \mu\varphi - \theta^X_\omega - X(\varphi)} \det\left(g_{j\bar{k}}\right). \tag{1.15}$$

1.2 Limit behavior of Kähler–Einstein edge manifolds

Recalling the definition of KEE metrics in (1.8), an analogue of Calabi's conjecture was made by Tian [54] regarding the existence of such metrics. The following theorem resolves Tian's conjecture:

Theorem 1.2.1. [38, Theorem 2] *Let (M, ω_0) be a compact Kähler manifold with $D \subset M$ a smooth divisor. Suppose that $\frac{\mu}{2\pi}[\omega_0] + (1-\beta)[D] = c_1(M)$, where $\beta \in (0,1]$ and $\mu \in \mathbb{R}$. If*

$\mu > 0$, *additionally assume that the twisted K-energy* E^0_β *is proper. Then there exists a KEE metric with Ricci curvature* μ *and with an angle of* $2\pi\beta$ *along* D. *This metric is unique when* $\mu < 0$, *unique in its Kähler class when* $\mu = 0$, *and unique up to automorphisms that preserve* D *when* $\mu > 0$.

One reason that KEE metrics receive attention is Donaldson's idea to employ them in studying the existence problem of smooth Kähler–Einstein metrics of positive curvature by deforming the cone angle to 2π [18]. Since then much research has gone into understanding the large angle limits (when $\beta \to 1$) of Kähler (–Einstein) edge metrics in connectino with the Yau–Tian–Donaldson conjecture.

Cheltsov and Rubinstein initiated the program of studying KEE metrics in another extreme, where the cone angle goes to zero [14]. One topic of their program is to understand the limit, when such exists, of KEE metrics as the cone angle tends to 0. In particular, they made the conjecture:

Conjecture 1.2.2. [14, Conjecture 1.11] *Suppose that* (M, D) *is strongly asymptotically log Fano manifold with* D *smooth and irreducible. Suppose that* $\kappa := \inf\{k \in \mathbb{N} : (K_M + D)^k = 0\} \leq \dim M$, *and that there exist KEE metrics* ω_β, *for* $\beta \in (0, \epsilon)$ *on* (M, D) *and some* $\epsilon > 0$. *Then,* (M, D, ω_β) *converges in an appropriate sense as* β *tends to zero to a generalized Kähler–Einstein metric* ω_∞ *that is Calabi–Yau along its generic* $(\dim M + 1 - \kappa)$*-dimensional fibers.*

In this thesis, we consider two situations regarding the behavior of KEE metrics when the cone angles vary.

1.2.1 Small angle limits of Kähler–Einstein crossing edge metrics

The first part of the thesis treats the Kähler–Einstein crossing edge metrics on compact Kähler manifold M that has edge singularities along a *simple normal crossing* divisor $D = D_1 + \cdots + D_r$ in M with cone angles $2\pi\beta_1, \ldots, 2\pi\beta_r$. The existence of such metrics is confirmed in [27, 44]:

Theorem 1.2.3. *Let M be a compact Kähler manifold, and $D = \sum_i (1-\beta_i) D_i$ an $\mathbb{R}$-divisor with simple normal crossing support such that $\beta_i \in (0,1)$ for all i. If $K_M + D$ is ample, then there exists a unique KEE metric with negative curvature. If $K_M + D$ is numerically trivial, then there exists in each Kähler class a unique KEE metric. If $-(K_M + D)$ is ample and the log-Mabuchi functional is proper, then there exists a unique KEE metric with positive curvature.*

The cone angles of crossing edge metrics can vary along each component in D and we study the limit behavior of such Kähler–Einstein crossing edge metrics when multiple angles converge to zero at (possibly) different rates. In particular, we prove that

Theorem 1.2.4. *Let M be a compact Kähler manifold and $D = \sum_{i=1}^r (1-\beta_i) D_i$ a simple normal crossing divisor such that $K_M + D$ is ample. The Kähler–Einstein crossing edge metrics ω_β converges to the Kähler–Einstein cusp metric on (M, D) globally in a weak sense of currents and locally in the smooth sense when $(\beta_1, \ldots, \beta_r) =: \beta \to 0 \in [0,1)^r$.*

We also prove the following result regarding the local limit behavior of Kähler–Einstein crossing edge metrics near the divisor:

Theorem 1.2.5. *Let $\{\beta_{1,k}\}_{k\in\mathbb{N}}$ be a sequence of positive numbers converging to 0. Assume further that for any $i = 2, \ldots, r$ such that $\{\beta_{i,k}\}_{k\in\mathbb{N}}$ also converges to 0, there holds $\lim_{k\to\infty} \frac{\beta_{1,k}}{\beta_{i,k}} \in [0,1]$.*

Assume $\beta_{i,k} \in (0, \frac{1}{2}]$ for $i = 1, 2, \ldots, r$ and all $k \in \mathbb{N}$. Let ω_{β_k} be the Kähler–Einstein crossing edge metric on $(X, D_k = \sum_{i=1}^{r}(1 - \beta_{i,k})D_i)$. Then there exists a subsequence of the metric spaces consisting of a neighborhood of D_k, denoted as $(U_{\beta_k}, \omega_{\phi_{\beta_k}}/\beta_{1,k}^2)$ converging in pointed Gromov–Hausdorff topology to $((\mathbb{C}^*)^m \times \mathbb{C}^{n-m}, \bar{\omega}_\infty)$, where $\bar{\omega}_\infty$ is a mixed cylinder and edge metric and $0 < m \leq n$.

A detailed overview of this part starts from Section 2.1. The main results are listed in Section 2.1.3.

1.2.2 Large and small angle limits of KEE metrics on Calabi–Hirzebruch manifolds

In the second part of the thesis, we focus on a specific family of Kähler manifolds, Calabi–Hirzebruch manifolds, denoted by $\mathbb{F}_{n,k}$, where $n, k \in \mathbb{N}$, and defined as follows:

$$\mathbb{F}_{n,k} := \mathbb{P}(-kH_{\mathbb{P}^{n-1}} \oplus \mathbb{C}_{\mathbb{P}^{n-1}}), \quad n, k \in \mathbb{N},$$

where $H_{\mathbb{P}^{n-1}}$ is the hyperplane bundle over $\mathbb{P}^{n-1}$ and $\mathbb{C}_{\mathbb{P}^{n-1}}$ is the trivial one.

Calabi–Hirzebruch manifolds are $\mathbb{P}^1$-fibrations over $\mathbb{P}^{n-1}$ base. Hence, it is a generalization of $\mathbb{P}^1$ to higher dimensions. By identifying $\mathbb{P}^1$ as the round sphere S^2, we realize that it has two disjoint divisors (that are points in this case): the north and the south poles. The Calabi–Hirzebruch manifolds also has two disjoint divisors: the zero and infinite section along each $\mathbb{P}^1$-fiber.

We will construct KEE metrics on Calabi–Hirzebruch manifolds using Calabi ansatz, and show that the cone angle at either divisor then determines the angle on the other divisor. As a result, we construct two families of KEE metrics.

We then study the different large and small-angle limits that arise from these KEE metrics when the cone angles approach to extreme values. In particular, we show the following:

Theorem 1.2.6. *The Eguchi–Hanson metric defined on the total space of $-2H_{\mathbb{P}^1}$ and Calabi's Ricci-flat metrics on the total space of $-nH_{\mathbb{P}^{n-1}}$ are respectively pointed Gromov–Hausdorff limits of the KEE metrics we constructed on $\mathbb{F}_{2,2}$ and $\mathbb{F}_{n,n}$ as the cone angle along the zero section approaches* 1.

The motivation for this part starts from Section 3.1. The main results are summarized in Section 3.2.

1.3 Numerical implementation of the Ricci iteration for finding Kähler–Einstein and soliton metrics

The last part of the thesis focuses on numerical implementation of the Ricci iteration, and in turn provides a novel method to find Kähler–Einstein and Kähler–Ricci soliton metrics on toric del Pezzo surfaces.

While there are celebrated theoretical studies on the existence of Kähler–Einstein metrics, cf. Definition 1.1.4, explorations into them from a numerical point of view are also of great importance. The direction was pioneered by Headrick–Wiseman [33] and Donaldson [17], and later captured attention from both mathematicians and physicists [6, 19, 20, 30, 34].

To this end, we introduce a systematic way of finding numerical approximations to Kähler–Einstein metrics and Kähler–Ricci solitons that exist on toric del Pezzo surfaces. Our method relies on the fundamental framework known as the Ricci iteration, which is introduced by Rubinstein [45–47] and later studied in-depth by Hunter in the real case [36, 37]. The Ricci iteration provides a unified way to treat both Kähler–Einstein and Kähler–Ricci soliton metrics.

It has been pointed out in [47, §10.5] that one can iteratively employ Donaldson's algorithm [17] to perform a given step in the Ricci iteration to numerically compute Kähler–Einstein metrics. In this thesis, we instead perform each step by solving a second boundary value problem of a real Monge–Ampère equations. Specifically, our focus is on the Ricci iteration on toric del Pezzo surfaces. In this case, the Calabi–Yau equations arising from each iteration reduce to a second boundary value problem of Monge–Ampère equations. This problem exhibits a PDE nature and also has connection to the optimal transport theory. Numerical methods to address it have been proposed by Lindsey–Rubinstein [43], where an algorithm based on solving a convex optimization problem is introduced, accompanied by a convergence theorem [43, Theorem 6].

In our numerical implementation, we use Guillemin's potential (cf. (4.101)) to help choose a suitable finite domain instead of the whole $\mathbb{R}^2$ to perform the Ricci iteration. We also use the mass balance condition (cf. (4.102)) to normalize the solution obtained through the Ricci iteration. In each iteration step, we employed the numerical method proposed by Bonnet–Mirebeau [5]. We configure their numerical implementation by setting the parameters according to our geometric problems. The choice of a numerical solver in each iteration step is flexible.

The numerical method [5] provides an efficient way to solve the second boundary value problem of the real Monge–Ampère equations when the dimension is 2. For dimension 3, implementing the Ricci iteration can be achieved using either the method in [43] or [5]. However, in higher dimensions, the discretization required in the method [5] becomes challenging, while the optimization approach in [43] remains standard.

Our experimental results show that the solutions obtained through the Ricci iteration do converge to the potential functions of Kähler–Einstein and Kähler–Ricci soliton metrics. Consequently, our numerical implementation of the Ricci iteration provides a way to approximate the aforementioned metrics. Compared to existing works, one advantage of our numerical method is that minimal modification in the implementation is needed when seeking canonical metrics between different manifolds. Furthermore, the convergence is achieved within several minutes.

Our numerical results provide an evidence that the convergence of the Ricci iteration occurs for toric del Pezzo surfaces without the necessity of twisting the metrics by automorphisms. This suggests the possibility of a stronger convergence result in the toric case, compared to the existing best result:

Theorem 1.3.1. [15, Theorem 1.2] *Let (M, J, ω_0) be a compact Kähler manifold admitting a Kähler–Einstein metric. Suppose the Kähler class associated to ω_0 is $2\pi c_1(M, J)$ and let $\{\omega_i\}_{i\in\mathbb{N}}$ by given by $\operatorname{Ric}\omega_{i+1} = \omega_i$. Then there exist holomorphic diffeomorphisms h_i such that $h_i^*\omega_i$ converges smoothly to a Kähler–Einstein metric.*

The convergence of the numerical Ricci iteration observed in the experiments also raises the question of whether a convergence theorem for numerical Ricci iterations can be established, in comparison to the convergence theorem proved for a single second boundary value problem of Monge–Ampère equations, cf. [43, Theorem 6 and 9] and [5, Theorem 5.25].

We provide comprehensive background in geometry in Section 4.2, which includes necessary definitions and results for readers who are not experts in toric Kähler geometry. In Section 4.3, we present the formulation of the Ricci iteration in the toric case, and more precisely three slightly different equations for either Kähler–Einstein or Kähler–Ricci soliton metrics. From Section 4.4 to Section 4.8, we present a self-contained exposition of the numerical method [5]. Then, we use this numerical scheme to solve Monge–Ampère equations sequentially and implement the Ricci iteration. The numerical results of our method are summarized in Chapters 5 and 6.

Chapter 2: Small angle limits of negatively curved Kähler–Einstein metrics with crossing edge singularities

2.1 Introduction

2.1.1 One-dimensional observation

Let $\mathbb{D}^* = \{z \in \mathbb{C} : 0 < |z| < 1\}$ be the punctured unit disc in $\mathbb{C}$. Consider for $\eta \in (0, 1)$, the following Kähler metric

$$\begin{aligned} \omega_{\eta,\mathbb{D}^*} :&= -\sqrt{-1}\partial\bar{\partial}\log(1 - |z|^{2\eta}) \\ &= \frac{\sqrt{-1}\eta^2|z|^{2\eta-2}}{(1 - |z|^{2\eta})^2} dz \wedge d\bar{z}. \end{aligned} \tag{2.1}$$

It has negative constant curvature and cone singularity with cone angle $2\pi\eta$ at $0 \in \mathbb{C}$, as shown by the following calculation

$$\begin{aligned} \mathrm{Ric}\,\omega_{\eta,\mathbb{D}^*} &= \sqrt{-1}\partial\bar{\partial}\log\left(\frac{\eta^2|z|^{2\eta-2}}{(1 - |z|^{2\eta})^2}\right) \\ &= 2\pi(1-\eta)\delta_0 - 2\omega_{\eta,\mathbb{D}^*}, \end{aligned} \tag{2.2}$$

where δ_0 denotes the Dirac measure at 0.

For a fixed $z \in \mathbb{D}^*$,

$$\lim_{\eta \to 0} \frac{\eta^2 |z|^{2\eta - 2}}{(1 - |z|^{2\eta})^2} = \frac{1}{|z|^2 \left(\log |z|^2\right)^2}. \tag{2.3}$$

Thus, for any compact $K \Subset \mathbb{D}^*$, the metric $\omega_{\eta, \mathbb{D}^*}$ converges uniformly to the Poincaré metric defined as follows

$$\omega_{P, \mathbb{D}^*} := \frac{\sqrt{-1} dz \wedge d\bar{z}}{|z|^2 \left(\log |z|^2\right)^2}, \tag{2.4}$$

when η tends to 0.

The same calculation as (2.2) shows that

$$\operatorname{Ric} \omega_{P, \mathbb{D}^*} = 2\pi \delta_0 - 2\omega_{P, \mathbb{D}^*}.$$

Thus, the metric $\omega_{P, \mathbb{D}^*}$ is a Kähler–Einstein cusp metric on $\mathbb{D}^*$ with cusp singularity at 0. And we have shown that it is also a limit of the Kähler–Einstein edge metrics.

2.1.2 Guenancia's convergence result

The one-dimensional observation can be generalized to higher dimensions. Consider the pair (X, D) where X is a compact Kähler manifold of dimension n and D is a smooth divisor.

Definition 2.1.1. A metric ω_0 on $X \setminus D$ is said to have cusp singularities along D if whenever D is locally given by $\{z_1 = 0\}$, there exists a constant $C > 0$ such that

$$C^{-1} \omega_{\text{cusp}} \leq \omega_0 \leq C \omega_{\text{cusp}},$$

where ω_{cusp} is the model cusp metric:

$$\omega_{\mathrm{cusp}} := \frac{\sqrt{-1}dz_1 \wedge d\bar{z}_1}{|z_1|^2 \log^2 |z_1|^2} + \sum_{i=2}^{n} \sqrt{-1}dz_i \wedge d\bar{z}_i.$$

Assuming that $K_X + D$ is ample, Kobayashi [40, Theorem 1] and Tian–Yau [55, Theorem 2.1] showed that there exists a unique complete Kähler–Einstein metric ω_0 on $X \setminus D$ with cusp singularity along D such that $\operatorname{Ric}\omega_0 = -\omega_0$.

Since ampleness is an open condition [42, Theorem 1.2.17], there exists some β_0 such that $K_X + (1-\beta)D$ is also ample for $0 < \beta < \beta_0$. Under this condition, Theorem 1.2.1 guarantees the existence of a unique negatively curved KEE metric ω_β for each such small $\beta \in (0, \beta_0]$. The family of metrics $\{\omega_\beta\}_{0\leq\beta<\beta_0}$ can be seen as currents on X satisfying the twisted Kähler–Einstein equation (note that here we allow $\beta = 0$, cf. (1.8)):

$$\operatorname{Ric}\omega_\beta = -\omega_\beta + (1-\beta)[D], \quad 0 \leq \beta < \beta_0.$$

As a generalization of the one-dimensional observation discussed in §2.1.1, Guenancia related these two metrics as follows:

Theorem 2.1.2. [26, Theorem A and B] *For $\beta \in (0, 1/2]$, there exists a constant $C > 0$ independent of β such that on any coordinate chart U where D is given by $\{z_1 = 0\}$, the KEE metric ω_β satisfies*

$$C^{-1}\omega_{\beta,\mathrm{mod}} \leq \omega_\beta \leq C\omega_{\beta,\mathrm{mod}}, \tag{2.5}$$

where

$$\omega_{\beta,\mathrm{mod}} := \frac{\beta^2\sqrt{-1}dz_1 \wedge d\bar{z}_1}{|z_1|^{2(1-\beta)}(1-|z_1|^{2\beta})^2} + \sum_{i=2}^{n} \sqrt{-1}dz_i \wedge d\bar{z}_i.$$

In particular, the metric $\{\omega_\beta\}_{0<\beta<\beta_0}$ *converges to* ω_0 *in both the weak topology of currents and the* $C^\infty_{\mathrm{loc}}(X \setminus D)$*-topology as* $\beta \to 0$.

The relation between the convergence result in Theorem 2.1.2 and (2.5) is that the weak convergence from $(\omega_\beta)_{0<\beta<\beta_0}$ to ω_0 can be recovered from (2.5) by using Lebesgue's Dominated Convergence Theorem. A very useful observation is that the limit behavior of the model metric $\omega_{\beta,\mathrm{mod}}$ relates the edge metric to the cusp metric, cf. Lemma 2.2.7.

As an application of Theorem 2.1.2, Guenancia studied the asymptotic behavior of ω_β near D as $\beta \to 0$. Fix a point $p \in D$, let U_β denote the punctured metric ball $B_{\omega_\beta}(p,1)$ of radius 1 centered at p with respect to the metric ω_β. Then after renormalization by β^{-2}, there exists a subsequence of the metric spaces $(U_\beta, \frac{1}{\beta^2}\omega_\beta)$ converging to $(\mathbb{C}^* \times \mathbb{C}^{n-1}, \omega_{\mathrm{cyl}})$ in the pointed Gromov–Hausdorff sense, where ω_{cyl} is a so-called cylindrical metric:

Definition 2.1.3. Let $\pi : \mathbb{C}^n \to \mathbb{C}^* \times \mathbb{C}^{n-1}$ be the universal cover of $\mathbb{C}^* \times \mathbb{C}^{n-1}$ given by $\pi(z_1 \ldots, z_n) = (e^{z_1}, z_2, \ldots, z_n)$. A Kähler metric ω_{cyl} on $\mathbb{C}^* \times \mathbb{C}^{n-1}$ is called cylindrical if $\pi^*\omega = F^*\omega_{\mathrm{eucl}}$, where $F \in \mathrm{GL}(n, \mathbb{C})$ and ω_{eucl} is the usual Euclidean metric on $\mathbb{C}^n$.

Theorem 2.1.4. [26, Theorem C] *Let* $(\beta_k)_{k\in\mathbb{N}}$ *be a sequence of positive numbers converging to* 0*. Then, up to extracting a subsequence, there exists a cylindrical metric* ω_{cyl} *on* $\mathbb{C}^* \times \mathbb{C}^{n-1}$ *such that the metric spaces* $(U_{\beta_k}, \beta_k^{-2}\omega_{\beta_k})$ *converge in pointed Gromov-Hausdorff topology to* $(\mathbb{C}^* \times \mathbb{C}^{n-1}, \omega_{\mathrm{cyl}})$ *when* k *tends to* $+\infty$.

2.1.3 Our results

A natural problem is to generalize Theorems 2.1.2 and 2.1.4 to the snc case when all or some of the cone angles tend to 0.

From now on, let X be an n-dimensional compact Kähler manifold. Fix a divisor $D_\beta := \sum_{i=1}^{r}(1-\beta_i)D_i$, where $\beta_i \in (0,1)$ for $i = 1, \ldots, r$. Assume each D_i is smooth and irreducible. We further assume that D_β has simple normal crossing support, i.e., for any $p \in \operatorname{supp}(D_\beta)$ lying in the intersection of exactly m components $D_1, \ldots, D_m$, there exists a coordinate chart $(U, \{z_i\}_{i=1}^n)$ containing p such that $D_j|_U = \{z_j = 0\}$ for $j = 1, \ldots, m$, $m \le n$. Suppose $K_X + \sum_{i=1}^{r} D_i$ is ample. Let s_i denote a defining section of D_i and $h_i = |\cdot|_{h_i}$ be a smooth hermitian metric on L_{D_i}, which is the line bundle induced by D_i. We normalize h_i such that $\log|s_i|^2_{h_i} + 1 < 0$ for each i. Denote

$$\beta := (\beta_1, \ldots, \beta_r) \in (0,1)^r.$$

Let ω be a fixed smooth Kähler metric with $[\omega] = c_1\left(K_X + \sum_{i=1}^r D_i\right)$. We introduce a reference metric,

$$\Omega_\beta := \omega - \sum_{i=1}^{r} \sqrt{-1}\partial\bar{\partial}\log\left[\frac{1-|s_i|^{2\beta_i}_{h_i}}{\beta_i}\right]^2. \tag{2.6}$$

Let $\omega_{\phi_\beta} = \omega + \sqrt{-1}\partial\bar{\partial}\phi_\beta$ be the KEE metric on X whose existence is guaranteed by Theorem 1.2.3. Our first result is as follows.

Theorem 2.1.5. *Let ω_{ϕ_β} be given by Theorem 1.2.3. Let Ω_β be given by (2.6). There exists a* *uniform constant $C > 0$, independent of $\beta \in (0, \frac{1}{2}]^r$, such that*

$$C^{-1}\Omega_\beta \le \omega_{\phi_\beta} \le C\Omega_\beta.$$

The key point of Theorem 2.1.5 is that the constant C is uniform with respect to small $\beta_i, i = 1, \dots, r$. According to Theorem 2.1.5 and Lebesgue's Dominated Convergence Theorem, we obtain the weak convergence from ω_{ϕ_β} to the Kähler–Einstein mixed cusp and edge metric ω_0 constructed in [25] as some of the cone angles tend to 0. In particular, when $\beta \to 0 \in [0, 1)^r$, the limiting metric of such ω_{ϕ_β} is the unique Kähler–Einstein cusp metric on $(X, \sum_{i=1}^{r} D_i)$ constructed in [40, 55]. More precisely, the following result is shown in Section 2.2.3.

Theorem 2.1.6. *The Kähler–Einstein crossing edge metric ω_{ϕ_β} converges to a Kähler–Einstein mixed cusp and edge metric on (X, D_β) globally in a weak sense of currents and locally in a smooth sense when some of the cone angles tend to 0. In particular, ω_{ϕ_β} converges to the Kähler–Einstein cusp metric on $(X, \sum_{i=1}^{r} D_i)$ when $\beta \to 0 \in [0, 1)^r$.*

As an application of Theorem 2.1.5, we study the asymptotic behavior of the Kähler–Einstein crossing edge metric ω_{ϕ_β} near D_β when the smallest cone angle approaches 0, with possibly other cone angles also converging to 0.

To state the result, without loss of generality, we assume for $\beta = (\beta_1, \dots, \beta_r)$ there holds $\beta_1 \le \beta_2 \le \cdots \le \beta_r$. Fix a point $p \in D_\beta$. Choose a coordinate chart $(U, \{z_i\}_{i=1}^n)$ containing p such that $D_j|_U = \{z_j = 0\}$ for $j = 1, \dots, m$, $m \le n$. Consider a small neighborhood U_β about

p defined by

$$U_\beta := \left\{ z \in (\mathbb{C}^*)^m \times \mathbb{C}^{n-m} : |z_1| < e^{-\frac{1}{2\beta_1}}, |z_j| < \left(\frac{\beta_1}{\beta_j}\right)^{\frac{1}{\beta_j}}, j = 2, \ldots, m, |z_\ell| < 1, \ell = m+1, \ldots, n \right\}.$$

We show that after normalization by factor β_1^{-2}, a subsequence of metrics ω_{ϕ_β} converges to a mixed cylinder and edge metric on $(\mathbb{C}^*)^m \times \mathbb{C}^{n-m}$ (see Definition 2.3.1 for more details. Note that Definition 2.3.1 is in a weaker sense of quasi-isometry comparing to Definition 2.1.3.) as β_1 tends to 0. The limiting metric has cylindrical part along the component D_1 where the cone angle β_1 approaches 0 while has edge singularities along other components. More precisely, the third result is as follows:

Theorem 2.1.7. *Let $\{\beta_{1,k}\}_{k\in\mathbb{N}}$ be a sequence of positive numbers converging to 0. Assume further that $\{\beta_{i,k}\}_{k\in\mathbb{N}}$ does not converge to 0 for each $i = 2, \ldots, r$ and all $\beta_{i,k} \in (0, \frac{1}{2}]$. Let $\omega_{\phi_{\beta_k}}$ be the (negatively curved) Kähler–Einstein crossing edge metric on $(X, D_k = \sum_{i=1}^r (1-\beta_{i,k})D_i)$. Then there exists a subsequence of the metric spaces $(U_{\beta_k}, \omega_{\phi_{\beta_k}}/\beta_{1,k}^2)$ converging in pointed Gromov-Hausdorff topology to $((\mathbb{C}^*)^m \times \mathbb{C}^{n-m}, \omega_\infty)$ where ω_∞ is a mixed cylinder and edge metric.*

Regarding complex dimension 1, i.e., in the Riemann surface case, but in the positive curvature regime, Rubinstein–Zhang showed that the (American) football equipped with the Ricci soliton metric converges to the cone-cigar soliton on $\mathbb{R}_+$ as two cone angles converge to 0 at a different speed and to a flat cylindrical metric as two cone angles converge to 0 at a comparable speed [49, Theorem 1.1-1.3]. In higher dimensions, we generalize Theorem 2.1.7 to allow more than one cone angles to tend to 0 and study the limit behavior of metrics under this joint degeneration of cone angles. The result is as follows.

Theorem 2.1.8. *Let $\{\beta_{1,k}\}_{k\in\mathbb{N}}$ be a sequence of positive numbers converging to 0. Assume further that for any $i \in \{2,\ldots,r\}$ such that $\{\beta_{i,k}\}_{k\in\mathbb{N}}$ also converges to 0, there holds $\lim_{k\to\infty}\frac{\beta_{1,k}}{\beta_{i,k}} \in [0,1]$ and all $\beta_{i,k} \in (0,\frac{1}{2}]$. Let $\omega_{\phi_{\beta_k}}$ be the (negatively curved) Kähler–Einstein crossing edge metric on $(X, D_k = \sum_{i=1}^{r}(1-\beta_{i,k})D_i)$. Then there exists a subsequence of the metric spaces $(U_{\beta_k}, \omega_{\phi_{\beta_k}}/\beta_{1,k}^2)$ converging in pointed Gromov-Hausdorff topology to $((\mathbb{C}^*)^m \times \mathbb{C}^{n-m}, \omega_\infty)$, where ω_∞ is a mixed cylinder and edge metric with cylindrical part along components whose cone angles converge to 0 and conical part along other components.*

2.1.4 Ingredients of the proof

We first recall that the key ingredient in the proof of Theorem 2.1.2 is the boundedness of the holomorphic bisectional curvature of the model metric $\omega_{\beta,\mathrm{mod}}$, which makes it possible to use the Chern–Lu inequality to obtain the Laplacian estimates. Therefore, to prove our result in the snc setting, we extend [26, Theorem 3.2] to the snc setting, i.e., prove boundedness of holomorphic bisectional curvature of the model metric Ω_β (see (2.6) for details). This is done in Lemma 2.2.3 by adapting arguments in [38, Lemma 2.3] and making use of the fact that we only need to deal with small β_i's. Then the proof of Theorem 2.1.5 uses a modified maximum principle argument and Chern–Lu's inequality to give respectively the C^0 and Laplacian estiamte. A useful fact in the proof is the observation that Ω_β shares the same crossing edge singularities as ω_{ϕ_β} (see Claim 2.2.5 for the detail).

An important observation is that the reference metric Ω_β has the property of converging to a Kähler metric with mixed cusp and edge singularities when some of the cone angles tend to 0. This observation, combined with the content of Theorem 2.1.5, give us the result of Theorem

2.1.6 as a corollary. As another consequence of Theorem 2.1.5, Theorem 2.1.7 and Theorem 2.1.8 treat the limit behavior of the Kähler–Einstein crossing edge metric ω_{ϕ_β} near the divisor D_β when some of the cone angles approach 0. After fixing a point in the divisor D_β, we first rescale the reference metric to obtain its convergence to a mixed cylinder and edge metric (see Definition 2.3.1) as the smallest cone angle tends to 0 in a small neighborhood of D_β. To obtain the pointed Gromov–Hausdorff convergence of the rescaled Kähler–Einstein crossing edge metric ω_{ϕ_β} near the divisor, we actually show a stronger local smooth convergence result. We use Theorem 2.1.5 and the limit behavior of Ω_β mentioned above to obtain C^0-estimates of rescaled ω_{ϕ_β}. By a standard use of Evans–Krylov theory and Arzelà–Ascoli Theorem, we obtain the C^∞_{loc}-convergence of the rescaled ω_{ϕ_β} as some of the cone angles tend to 0.

2.2 Small angle limits of the Kähler–Einstein crossing edge metrics

2.2.1 A reference metric

The metric Ω_β defined in (2.6) can be seen as a generalization of $\omega_{\eta,\mathbb{D}^*}$ defined in (2.1) to higher dimensional manifolds.

Lemma 2.2.1. [26, Lemma 3.1] *The previously defined Ω_β is a Kähler edge form with cone angle $2\pi\beta_i$ along D_i for $i = 1, \ldots, r$. More precisely,*

$$\Omega_\beta = \omega + 2 \cdot \sum_{i=1}^{r} \left(\sqrt{-1} \frac{\beta_i^2}{|s_i|_{h_i}^{2-2\beta_i}(1 - |s_i|_{h_i}^{2\beta_i})^2} \langle D^{1,0} s_i, D^{1,0} s_i \rangle - \frac{\beta_i |s_i|_{h_i}^{2\beta_i}}{1 - |s_i|_{h_i}^{2\beta_i}} \theta_i \right), \tag{2.7}$$

where $D^{1,0}$ is the $(1,0)$-part of the Chern connection of (L_{D_i}, h_i) for each i. Up to rescaling $\{h_i\}_{i=1,\ldots,r}$, there holds $\Omega_\beta \geq \frac{1}{2}\omega$.

Proof. It suffices to show (2.7) when $r = 1$. Hence, below we suppose $r = 1$ and drop the subscript i for simplicity.

If we set

$$f(x) = -\log\left(\frac{1-x^\beta}{\beta}\right)^2,$$
$$\phi = |s|_h^2 = h \cdot |s|^2,$$

then $\Omega_\beta = \omega + \sqrt{-1}\partial\bar{\partial} f \circ \phi$. Recall there holds $\sqrt{-1}\partial\bar{\partial} f\circ\phi = \sqrt{-1}(f''(\phi)\partial\phi\wedge\bar{\partial}\phi + f'(\phi)\partial\bar{\partial}\phi)$. We calculate

$$f' = \frac{2\beta x^{\beta-1}}{1-x^\beta},$$
$$f'' = \frac{-2\beta x^{\beta-2}}{1-x^\beta} + \frac{2\beta^2 x^{\beta-2}}{(1-x^\beta)^2}.$$

Then

$$\Omega_\beta = \omega + \sqrt{-1}\cdot\frac{2\beta|s|_h^{2\beta-2}}{1-|s|_h^{2\beta}}\partial\bar{\partial}|s|_h^2 + \sqrt{-1}\cdot\left(\frac{2\beta^2|s|_h^{2\beta-4}}{(1-|s|_h^{2\beta})^2} - \frac{2\beta|s|_h^{2\beta-4}}{1-|s|_h^{2\beta}}\right)\partial|s|_h^2\wedge\bar{\partial}|s|_h^2.$$

Note

$$\partial\bar{\partial}|s|_h^2 = \bar{s}\partial s\wedge\bar{\partial}h + |s|^2\partial\bar{\partial}h + h\partial s\wedge\bar{\partial}\bar{s} + s\partial h\wedge\bar{\partial}\bar{s}, \tag{2.8}$$

$$\partial|s|_h^2\wedge\bar{\partial}|s|_h^2 = |s|^4\partial h\wedge\bar{\partial}h + sh|s|^2\partial h\wedge\bar{\partial}\bar{s} + \bar{s}h|s|^2\partial s\wedge\bar{\partial}h + |s|^2h^2\partial s\wedge\bar{\partial}\bar{s}, \tag{2.9}$$

and the fact

$$\theta = -\sqrt{-1}\partial\bar{\partial}\log h = \sqrt{-1}(\frac{\partial h \wedge \bar{\partial} h}{h^2} - \frac{\partial\bar{\partial} h}{h}) \tag{2.10}$$

$$\begin{aligned} \langle D^{1,0}s, D^{1,0}s\rangle &= \langle \partial s \cdot e + \frac{\partial h}{h} s \cdot e, \partial s \cdot e + \frac{\partial h}{h} s \cdot e\rangle & (2.11) \\ &= h\partial s \wedge \bar{\partial}\bar{s} + \bar{s}\partial s \wedge \bar{\partial} h + s\partial h \wedge \bar{\partial}\bar{s} + \frac{|s|^2}{h}\partial h \wedge \bar{\partial} h. & (2.12) \end{aligned}$$

We calculate

$$\begin{aligned} \Omega_\beta &= \omega + \sqrt{-1}\frac{2\beta|s|_h^{2\beta-2}}{1-|s|_h^{2\beta}}\partial\bar{\partial}|s|_h^2 + \sqrt{-1}\left(\frac{2\beta^2|s|_h^{2\beta-4}}{(1-|s|_h^{2\beta})^2} - \frac{2\beta|s|_h^{2\beta-4}}{1-|s|_h^{2\beta}}\right)\partial|s|_h^2 \wedge \bar{\partial}|s|_h^2 \\ &= \omega + \left(\sqrt{-1}\frac{2\beta|s|_h^{2\beta-2}}{1-|s|_h^{2\beta}}|s|^2\partial\bar{\partial} h - \sqrt{-1}\frac{2\beta|s|_h^{2\beta-4}}{1-|s|_h^{2\beta}}|s|^4\partial h \wedge \bar{\partial} h\right) \\ &+ \sqrt{-1}\frac{2\beta|s|_h^{2\beta-2}}{1-|s|_h^{2\beta}}(\bar{s}\partial s \wedge \bar{\partial} h + h\partial s \wedge \bar{\partial}\bar{s} + s\partial h \wedge \bar{\partial}\bar{s}) \\ &+ \sqrt{-1}\left(\frac{2\beta^2|s|_h^{2\beta-4}}{(1-|s|_h^{2\beta})^2} - \frac{2\beta|s|_h^{2\beta-4}}{1-|s|_h^{2\beta}}\right)(sh|s|^2\partial h \wedge \bar{\partial}\bar{s} + \bar{s}h|s|^2\partial s \wedge \bar{\partial} h + |s|^2h^2\partial s \wedge \bar{\partial}\bar{s}) \\ &+ \sqrt{-1}\frac{2\beta^2|s|_h^{2\beta-4}}{(1-|s|_h^{2\beta})^2}|s|^4\partial h \wedge \bar{\partial} h \\ &= \omega - \frac{2\beta|s|_h^{2\beta}}{1-|s|_h^{2\beta}}\sqrt{-1}(\frac{\partial h \wedge \bar{\partial} h}{h^2} - \frac{\partial\bar{\partial} h}{h}) \\ &+ \sqrt{-1}\frac{2\beta^2|s|_h^{2\beta-2}}{(1-|s|_h^{2\beta})^2}(h\partial s \wedge \bar{\partial}\bar{s} + \bar{s}\partial s \wedge \bar{\partial} h + s\partial h \wedge \bar{\partial}\bar{s} + \frac{|s|^2}{h}\partial h \wedge \bar{\partial} h) \\ &= \omega + 2 \cdot \sqrt{-1}\frac{\beta^2|s|_h^{2\beta-2}}{(1-|s|_h^{2\beta})^2}\langle D^{1,0}s, D^{1,0}s\rangle - 2 \cdot \frac{\beta|s|_h^{2\beta}}{1-|s|_h^{2\beta}}\theta, \end{aligned}$$

which is what we need. Since $\sqrt{-1}\frac{\beta_i^2}{|s_i|_{h_i}^{2-2\beta_i}(1-|s_i|_h^{2\beta_i})^2}\langle D^{1,0}s_i, D^{1,0}s_i\rangle$ contributes as a non-negative $(1,1)$-form for each i, we will show that up to rescaling h_i, $\frac{\beta_i|s_i|_{h_i}^{2\beta_i}}{1-|s_i|_{h_i}^{2\beta_i}}$ can be made arbitrarily small to conclude that $\Omega_\beta \geq \frac{1}{2}\omega$. To see this, consider the function $f_{\beta_i}(t) := \frac{\beta_i t^{\beta_i}}{1-t^{\beta_i}}$.

$f_{\beta_i}(t)$ is increasing in $(0,1)$ and satisfies $f_{\beta_i}(0)=0$. Hence for any $\delta>0$, $\exists t_\delta\in(0,1)$, such that for $t\in(0,t_\delta]$, $f_{\beta_i}(t)\leq\delta$ for each $i=1,\ldots,r$. Now take $\delta=\dfrac{1}{4r\cdot\sup_{X,i}||\theta_i||_\omega}$ and rescale each h_i such that $|s_i|^2_{h_i}\leq t_\delta$. Then

$$2\cdot\sum_{i=1}^{r}-\frac{\beta_i|s_i|^{2\beta_i}_{h_i}}{1-|s_i|^{2\beta_i}_{h_i}}\theta_i\geq-\frac{1}{2}\omega$$

and therefore $\Omega_\beta\geq\frac{1}{2}\omega$. □

When $r=1$ and $\beta=\beta_1\in(0,\frac{1}{2}]$, the following result of Guenancia states that the reference metric Ω_β has uniformly bounded holomorphic bisectional curvatures on $X\setminus D_\beta$.

Lemma 2.2.2. [26, Theorem 3.2] *When $r=1$, there exists a constant $C>0$ depending only on X such that for all $\beta\in(0,\frac{1}{2}]$, the holomorphic bisectional curvature of Ω_β is bounded by C.*

We generalize this result to the snc case by adapting arguments from [38, Lemma 2.3].

Lemma 2.2.3. *There exists a constant $C>0$ depending only on X such that for all β where $\beta_i\in(0,1/2]$ for each $i=1,\ldots,r$, the holomorphic bisectional curvature of Ω_β is uniformly bounded by C on $X\setminus D$.*

Proof. Since the idea of the proof is the same for general $r>1$, we assume $r=2$ for simplicity.

Step 1: Estimate the metric tensor.

Fix a point $p\in X\setminus D$. We can find local holomorphic coordinates such that $s_1=z_1$, $s_2=z_2$ and the hermitian metric h_k on L_{D_k} is given by $h_k=e^{-\phi_k}$ with $\phi_k(p)=0$ and $d\phi_k(p)=0$

for $k=1,2$. In these local coordinates, write

$$\omega = \sqrt{-1}\tilde{g}_{i\bar{j}} dz^i \wedge d\bar{z}^j,$$
$$\theta^k = \sqrt{-1}\theta^k_{i\bar{j}} dz^i \wedge d\bar{z}^j,$$

where $\tilde{g}_{i\bar{j}}$ and $\theta^k_{i\bar{j}}$ are smooth functions of the coordinate z and $k=1,2$. Moreover, for $k=1,2$, we have

$$\begin{aligned}
\langle D^{1,0}s_k, D^{1,0}s_k\rangle &= \langle dz_k \cdot e_k - z_k \partial\phi_k \cdot e_k, dz_k \cdot e_k - z_k\partial\phi_k \cdot e_k\rangle \\
&= e^{-\phi_k}\left(1 - \bar{z}_k \frac{\partial \phi_k}{\partial \bar{z}_k} - z_k \frac{\partial \phi_k}{\partial z_k} + |z_k|^2 \frac{\partial \phi_k}{\partial z_k}\frac{\partial \phi_k}{\partial \bar{z}_k}\right) dz^k \wedge d\bar{z}^k \\
&+ \sum_{i\neq k}^n e^{-\phi_k}\left(-\bar{z}_k \frac{\partial \phi_k}{\partial \bar{z}_i} + |z_k|^2 \frac{\partial \phi_k}{\partial z_k}\frac{\partial \phi_k}{\partial \bar{z}_i}\right) dz^k \wedge d\bar{z}^i \\
&+ \sum_{j\neq k}^n e^{-\phi_k}\left(-z_k \frac{\partial \phi_k}{\partial z^j} + |z_k|^2 \frac{\partial \phi_k}{\partial z_j}\frac{\partial \phi_k}{\partial \bar{z}_k}\right) dz^j \wedge d\bar{z}^k \\
&+ \sum_{i,j\neq k}^n e^{-\phi_k} |z_k|^2 \frac{\partial \phi_k}{\partial z_i}\frac{\partial \phi_k}{\partial \bar{z}_j} dz^i \wedge d\bar{z}^j.
\end{aligned}$$

For the sake of brevity, we introduce the following notations for $k=1,2$:

$$\begin{aligned}
a_k &= -\bar{z}_k \frac{\partial \phi_k}{\partial \bar{z}_k} - z_k \frac{\partial \phi_k}{\partial z_k} + |z_k|^2 \frac{\partial \phi_k}{\partial z_k}\frac{\partial \phi_k}{\partial \bar{z}_k}, \\
b^k_j &= \frac{\partial \phi_k}{\partial z^j} + \bar{z}_k \frac{\partial \phi_k}{\partial z_j}\frac{\partial \phi_k}{\partial \bar{z}_k}, \quad j \neq k, \\
c^k_{i\bar{j}} &= \frac{\partial \phi_k}{\partial z_i}\frac{\partial \phi_k}{\partial \bar{z}_j}, \quad i,j\neq k.
\end{aligned}$$

Then a_k, b^k_j and $c^k_{i\bar{j}}$ are smooth and vanish at p. Writing $\Omega_\beta = \sqrt{-1}g_{i\bar{j}} dz^i \wedge d\bar{z}^j$, by (2.7) we have

$$
\begin{aligned}
g &= \tilde{g}_{i\bar{j}} - 2 \cdot \sum_{k=1}^{2} \frac{\beta_k |s_k|_{h_k}^{2\beta_k}}{1-|s_k|_{h_k}^{2\beta_k}} \theta_{i\bar{j}}^k + 2 \cdot \sum_{k=1}^{2} \frac{\beta_k^2 |s_k|_{h_k}^{2\beta_k - 2}}{(1-|s_k|_{h_k}^{2\beta_k})^2} \langle D^{1,0} s_k, D^{1,0} s_k \rangle \\
&= \tilde{g}_{i\bar{j}} - 2 \cdot \sum_{k=1}^{2} \frac{\beta_k e^{-\beta_k \phi_k} |z_k|^{2\beta_k}}{1-|z_k|^{2\beta_k} \cdot e^{-\beta_k \phi_k}} \theta_{i\bar{j}}^k + 2 \cdot \sum_{k=1}^{2} \frac{\beta_k^2 e^{-(\beta_k - 1)\phi_k} |z_k|^{2\beta_k - 2}}{(1-|z_k|^{2\beta_k} e^{-\beta_k \phi_k})^2} \langle D^{1,0} s_k, D^{1,0} s_k \rangle .
\end{aligned}
$$

For each component, we have

$$
\begin{aligned}
g_{1\bar{1}} &= \tilde{g}_{1\bar{1}} - 2 \cdot \sum_{k=1}^{2} \frac{\beta_k e^{-\beta_k \phi_k} |z_k|^{2\beta_k}}{1-|z_k|^{2\beta_k} \cdot e^{-\beta_k \phi_k}} \theta_{1\bar{1}}^k + 2 \cdot \frac{\beta_1^2 e^{-(\beta_1 - 1)\phi_1} |z_1|^{2\beta_1 - 2}}{(1-|z_1|^{2\beta_1} e^{-\beta_1 \phi_1})^2} e^{-\phi_1} (1 + a_1) \\
&\quad + 2 \cdot \frac{\beta_2^2 e^{-(\beta_2 - 1)\phi_2} |z_2|^{2\beta_2 - 2}}{(1-|z_2|^{2\beta_2} e^{-\beta_2 \phi_2})^2} e^{-\phi_2} |z_2|^2 c_{1\bar{1}}^2, \\
g_{1\bar{2}} &= \tilde{g}_{1\bar{2}} - 2 \cdot \sum_{k=1}^{2} \frac{\beta_k e^{-\beta_k \phi_k} |z_k|^{2\beta_k}}{1-|z_k|^{2\beta_k} \cdot e^{-\beta_k \phi_k}} \theta_{1\bar{2}}^k + 2 \cdot \frac{\beta_1^2 e^{-(\beta_1 - 1)\phi_1} |z_1|^{2\beta_1 - 2}}{(1-|z_1|^{2\beta_1} e^{-\beta_1 \phi_1})^2} e^{-\phi_1} \bar{z}_1 \bar{b}_2^1 \\
&\quad + 2 \cdot \frac{\beta_2^2 e^{-(\beta_2 - 1)\phi_2} |z_2|^{2\beta_2 - 2}}{(1-|z_2|^{2\beta_2} e^{-\beta_2 \phi_2})^2} e^{-\phi_2} z_2 b_1^2, \\
g_{i\bar{j}} &= \tilde{g}_{i\bar{j}} - 2 \cdot \sum_{k=1}^{2} \frac{\beta_k e^{-\beta_k \phi_k} |z_k|^{2\beta_k}}{1-|z_k|^{2\beta_k} \cdot e^{-\beta_k \phi_k}} \theta_{i\bar{j}}^k + 2 \cdot \sum_{k=1}^{2} \frac{\beta_k^2 e^{-(\beta_k - 1)\phi_k} |z_k|^{2\beta_k - 2}}{(1-|z_k|^{2\beta_k} e^{-\beta_k \phi_k})^2} e^{-\phi_k} |z_k|^2 c_{i\bar{j}}^k, \quad i, j = 3, \ldots, n.
\end{aligned}
$$

Note that $g_{2\bar{2}}$ (respectively $g_{2\bar{1}}$) can be treated similarly as $g_{1\bar{1}}$ (respectively $g_{1\bar{2}}$). The first observation is that the term $\beta_k/(1 - |z_k|^{2\beta_k} \cdot e^{-\beta_k \phi_k})$ (and also its square) which appears in each $g_{i\bar{j}}$ will not blow up as $\beta_k \to 0$ for $k = 1, 2$. Indeed, the function $x \mapsto \beta/(1 - x^\beta)$ is uniformly bounded for all small β under the assumption $x < e^{-1}$. Since we always assume $|s_k|_{h_k}^2 < e^{-1}$ for $k = 1, 2$, we only need to consider a point p that is near D (i.e., $|z_1|$ and $|z_2|$ are small) and show the holomorphic bisectional curvature at p is uniformly bounded in β. To achieve this, we consider a change of coordinate $\xi_k = z_k^{\beta_k}/\beta_k$ for $k = 1, 2$. Such ξ_k is multi-valued. Thus, we need to choose a single-valued branch of the Riemann surface associated to $z_k \mapsto z_k^{\beta_k}$. More specifically, whenever we work with ξ_k, denoting the polar coordinates of ξ_k by (r_k, θ_k), we always assume $\theta_k \in [0, 2\pi\beta_k)$. Under this assumption, ξ_k always take values in the space $\{(r,\theta) \in \mathbb{C} : \theta \in [0,\pi)\}$ for $k = 1,2$ for varying β_k as we have $\beta_k \in (0, 1/2]$. Moreover, when we consider the inverse map of the change of coordinates $z_k = (\beta_k \xi_k)^{1/\beta_k}$, we assume $\xi_k \in \{(r,\theta) \in \mathbb{C} : \theta \in [0, 2\pi\beta_k)\}$ and hence $z_k \in \{(r,\theta) \in \mathbb{C} : \theta \in [0, 2\pi)\}$ for varying β_k. In the new coordinates, we have

$$
\begin{aligned}
dz_1 \wedge d\bar{z}_1 &= |\beta_1 \xi_1|^{\frac{2}{\beta_1} - 2} d\xi_1 \wedge d\bar{\xi}_1, \\
dz_1 \wedge d\bar{z}_2 &= \beta_1^{\frac{1}{\beta_1} - 1} \beta_2^{\frac{1}{\beta_2} - 1} \xi_1^{\frac{1}{\beta_1} - 1} \bar{\xi}_2^{\frac{1}{\beta_2} - 1} d\xi_1 \wedge d\bar{\xi}_2.
\end{aligned}
$$

From now on, we make the change of coordinates summarized as above:

$$
\begin{aligned}
\xi_k &= \frac{z_k^{\beta_k}}{\beta_k}, \quad k = 1, 2 \\
\xi_\ell &= z_\ell, \quad \ell = 3, \dots, n.
\end{aligned}
$$

We record the components of Ω_β, denoted by $\Omega_\beta = \sqrt{-1}h_{i\bar{j}}d\xi^i \wedge d\xi^j$, in the new coordinates:

$$
\begin{aligned}
h_{1\bar{1}} &= |\beta_1\xi_1|^{\frac{2}{\beta_1}-2}\tilde{g}_{1\bar{1}} - 2\cdot\frac{\beta_1^{\frac{2}{\beta_1}+1}e^{-\beta_1\phi_1}|\xi_1|^{\frac{2}{\beta_1}}}{1-e^{-\beta_1\phi_1}|\beta_1\xi_1|^2}\theta^1_{1\bar{1}} - 2\cdot\frac{\beta_2^3e^{-\beta_2\phi_2}|\xi_2|^2|\beta_1\xi_1|^{\frac{2}{\beta_1}-2}}{1-e^{-\beta_2\phi_2}|\beta_2\xi_2|^2}\theta^2_{1\bar{1}} \\
&\quad + 2\cdot\frac{\beta_1^2e^{-\beta_1\phi_1}}{(1-e^{-\beta_1\phi_1}|\beta_1\xi_1|^2)^2}(1+a_1) + 2\cdot\frac{\beta_2^4|\xi_2|^2|\beta_1\xi_1|^{\frac{2}{\beta_1}-2}}{(1-e^{-\beta_2\phi_2}|\beta_2\xi_2|^2)^2}c^2_{1\bar{1}}, \\
h_{1\bar{2}} &= \left(\beta_1^{\frac{1}{\beta_1}-1}\beta_2^{\frac{1}{\beta_2}-1}\xi_1^{\frac{1}{\beta_1}-1}\bar{\xi}_2^{\frac{1}{\beta_2}-1}\right)\tilde{g}_{1\bar{2}} - 2\cdot\frac{e^{-\beta_1\phi_1}\bar{\xi}_1}{1-e^{-\beta_1\phi_1}|\beta_1\xi_1|^2}\left(\beta_1^{\frac{1}{\beta_1}+2}\beta_2^{\frac{1}{\beta_2}-1}\xi_1^{\frac{1}{\beta_1}}\bar{\xi}_2^{\frac{1}{\beta_2}-1}\right)\theta^1_{1\bar{2}} \\
&\quad - 2\cdot\frac{e^{-\beta_2\phi_2}\xi_2}{1-e^{-\beta_2\phi_2}|\beta_2\xi_2|^2}\left(\beta_1^{\frac{1}{\beta_1}-1}\beta_2^{\frac{1}{\beta_2}+2}\xi_1^{\frac{1}{\beta_1}-1}\bar{\xi}_2^{\frac{1}{\beta_2}}\right)\theta^2_{1\bar{2}} + 2\cdot\frac{\beta_1^3e^{-\beta_1\phi_1}\bar{\xi}_1\beta_2^{\frac{1}{\beta_2}-1}\bar{\xi}_2^{\frac{1}{\beta_2}-1}}{(1-e^{-\beta_1\phi_1}|\beta_1\xi_1|^2)^2}\bar{b}^1_2 \\
&\quad + 2\cdot\frac{\beta_2^3e^{-\beta_2\phi_2}\xi_2\beta_1^{\frac{1}{\beta_1}-1}\xi_1^{\frac{1}{\beta_1}-1}}{(1-e^{-\beta_2\phi_2}|\beta_2\xi_2|^2)^2}b^2_1, \\
h_{1\bar{j}} &= \beta_1^{\frac{1}{\beta_1}-1}\xi_1^{\frac{1}{\beta_1}-1}\tilde{g}_{1\bar{j}} - 2\cdot\frac{\beta_1^{\frac{1}{\beta_1}+2}e^{-\beta_1\phi_1}\bar{\xi}_1\xi_1^{\frac{1}{\beta_1}}}{1-e^{-\beta_1\phi_1}|\beta_1\xi_1|^2}\theta^1_{1\bar{j}} - 2\cdot\frac{\beta_1^{\frac{1}{\beta_1}-1}\beta_2^3e^{-\beta_2\phi_2}|\xi_2|^2\xi_1^{\frac{1}{\beta_1}-1}}{1-e^{-\beta_2\phi_2}|\beta_2\xi_2|^2}\theta^2_{1\bar{j}} \\
&\quad + 2\cdot\frac{\beta_1^3e^{-\beta_1\phi_1}\bar{\xi}_1}{(1-e^{-\beta_1\phi_1}|\beta_1\xi_1|^2)^2}\bar{b}^1_j + 2\cdot\frac{\beta_2^4\beta_1^{\frac{1}{\beta_1}-1}e^{-\beta_2\phi_2}|\xi_2|^2\xi_1^{\frac{1}{\beta_1}-1}}{(1-e^{-\beta_2\phi_2}|\beta_2\xi_2|^2)^2}c^2_{1\bar{j}}, \quad j=3,\ldots,n \\
h_{i\bar{j}} &= \tilde{g}_{i\bar{j}} - 2\sum_{k=1}^{2}\frac{\beta_ke^{-\beta_k\phi_k}|\beta_k\xi_k|^2}{1-e^{-\beta_k\phi_k}|\beta_k\xi_k|^2}\theta^k_{i\bar{j}} + 2\sum_{k=1}^{2}\frac{\beta_k^2e^{-\beta_k\phi_k}|\beta_k\xi_k|^2}{(1-e^{-\beta_k\phi_k}|\beta_k\xi_k|^2)^2}c^k_{i\bar{j}}, \quad i,j=3,\ldots,n.
\end{aligned}
\tag{2.13}
$$

Note that $h_{2\bar{i}}$ can be treated similarly as $h_{1\bar{j}}$. A first observation is that since $\beta_k \in (0,1/2]$, both $\beta_k^{\frac{2}{\beta_k}-2}$ and $|\xi_k|^{\frac{2}{\beta_k}-2}$ are uniformly bounded. Regarding the metric tensor of Ω_β, terms that involve $\tilde{g}_{i\bar{j}}$ or $\theta^k_{i\bar{j}}$ are also uniformly bounded. Moreover, after the change of coordinates, there does not exist singular term in each component $h_{i\bar{j}}$. In conclusion, $h_{i\bar{j}}$ is uniformly bounded for any i,j, i.e., by (2.13), in coordinates $(\xi_1,\xi_2,\xi_3=z_3,\ldots,\xi_n=z_n)$, there holds

$$
h_{i\bar{j}} = O(1), \quad \text{for } i,j=1,\ldots,n.
$$

In other words, we have shown that the metric tensor $h_{i\bar{j}}$ is bounded from above for all i,j. However, the metric tensor may degenerate as β_1 or β_2 tends to 0. According to (2.13), we have for rather small β_1 and β_2 the following asymptotic behaviors of each metric tensor:

$$\begin{aligned} & h_{1\bar{1}} \sim \beta_1^2, \quad h_{2\bar{2}} \sim \beta_2^2, \\ & h_{1\bar{2}}, h_{2\bar{1}} \sim \beta_1^3\beta_2^3|\xi_1||\xi_2|, \\ & h_{1\bar{j}} \sim \beta_1^3|\xi_1|, \quad j = 3, \dots, n \\ & h_{i\bar{j}} = O(1), \quad i, j = 3, \dots, n. \end{aligned} \tag{2.14}$$

Step 2: Estimate the inverse of the metric tensor

Recall the curvature tensor is given by

$$R_{i\bar{j}k\bar{\ell}} = -h_{i\bar{j},k\bar{\ell}} + h^{s\bar{t}}h_{i\bar{t},k}h_{s\bar{j},\ell}. \tag{2.15}$$

To estimate the holomorphic bisectional curvature, we take two unit vectors (w.r.t. the metric $h_{i\bar{j}}$) $u^i\frac{\partial}{\partial\xi_i}$ and $v^j\frac{\partial}{\partial\xi_j}$. Then by (2.14) there holds

$$\begin{aligned} & u^1, v^1 = O(\beta_1^{-1}), \quad u^2, v^2 = O(\beta_2^{-1}), \\ & u^i, v^i = O(1), \quad i = 3, \dots, n. \end{aligned} \tag{2.16}$$

To finish the proof we need to bound $R_{i\bar{j}k\bar{\ell}}u^i\bar{u}^jv^k\bar{v}^\ell$. We first consider $R_{i\bar{j}k\bar{\ell}}$. We need to analyze $h^{i\bar{j}}$, $h_{i\bar{j},k}$ and $h_{i\bar{j},k\bar{\ell}}$.

We first treat $h^{i\bar{j}}$. By (2.13) and (2.14), one finds that $\det\{h_{i\bar{j}}\}$ is uniformly bounded and tends to 0 as β_1 or β_2 tends to 0. More precisely, by (2.14) there holds

$$\det\{h_{i\bar{j}}\} \sim \beta_1^2\beta_2^2. \tag{2.17}$$

Since $h^{i\bar{j}} = C_{j\bar{i}}/\det\{h_{i\bar{j}}\}$, where $C_{j\bar{i}}$ is the ji-th cofactor of the matrix $\{h_{i\bar{j}}\}$, we deduce from (2.14) and (2.17) that

$$\begin{aligned} h^{1\bar{j}}, h^{i\bar{1}} &\sim \beta_1^{-2}, \quad i, j \neq 2 \\ h^{1\bar{2}} &\sim \beta_1^{-2}\beta_2^{-2}, \\ h^{i\bar{j}} &= O(1), \quad i, j \neq 1, 2, \end{aligned} \tag{2.18}$$

while $h^{2\bar{j}}$ and $h^{j\bar{2}}$ can be treated in the same way. Roughly speaking, $h^{i\bar{j}}$ are bounded for fixed β near p but may tend to infinity with respect to β as described above. However, by (2.13) and (2.14), for any j, $h_{1\bar{j}}$ (respectively $h_{2\bar{j}}$) degenerate at the rate of at least β_1^2 (respectively β_2^2), when β_1 (respectively β_2) is small, and taking derivatives may only cause the terms $h_{i\bar{j},k}$ and $h_{i\bar{j},k\bar{\ell}}$ to converge to 0 at a faster speed in β. Thus, the singularity in $h^{i\bar{j}}$ does not cause a problem when we consider the curvature tensor (2.15), where the $h^{i\bar{j}}$ terms are multiplied by corresponding $h_{i\bar{t},k}$ or $h_{s\bar{j},\ell}$. We explain this in detail later in Step 4.

Step 3: Estimate derivatives of the metric tensor

Now we turn to show that $h_{i\bar{j},k}$ and $h_{i\bar{j},k\bar{\ell}}$ are uniformly bounded and find their dependence on β_1 and β_2. For $k, \ell \in \{3, \ldots, n\}$, as taking derivative w.r.t. $\partial/\partial z_3 = \partial/\partial\xi_3, \ldots, \partial/\partial z_n = \partial/\partial\xi_n$ will not contribute extra singular terms, the uniform boundedness of $h_{i\bar{j}}$ implies that this also holds for such $h_{i\bar{j},k}$ and $h_{i\bar{j},k\bar{\ell}}$. It remains to deal with $h_{i\bar{j},k}$ and $h_{i\bar{j},k\bar{\ell}}$ for $k, \ell \in \{1, 2\}$.

By the exact formula of each $h_{i\bar{j}}$ in (2.13), we find that the exponent of the terms $\xi_1, \bar{\xi}_1, \xi_2, \bar{\xi}_2$ is at least 1 when β_1 and β_2 are rather small, and indeed both the term $h_{i\bar{j}}$ and their first or second order derivatives are smooth in $\xi_1, \bar{\xi}_1, \xi_2, \bar{\xi}_2$. In summary, taking derivatives of the metric tensor does not cause singularities in $\xi_1, \bar{\xi}_1, \xi_2, \bar{\xi}_2$. We only need to derive the asymptotic behavior of the derivatives with respect to β. To achieve this, it is enough to deal with the following term T from

(2.13). The reason is that any other terms in (2.13) have higher order dependence in β_1 and β_2, before and after taking the derivatives. So we consider taking derivatives of the following term

$$\frac{\beta_1^2 e^{-\beta_1\phi_1}}{(1-\beta_1^2|\xi_1|^2 e^{-\beta_1\phi_1})^2} =: T \tag{2.19}$$

w.r.t. $\partial/\partial\xi_1$ and $\partial/\partial\xi_2$, since this is the most singular term appearing in the metric tensor. And by symmetry of indices we only need to consider $\partial/\partial\xi_1(T)$, $\partial^2/\partial\xi_1\partial\bar{\xi}_2(T)$ and $\partial^2/\partial\xi_1\partial\bar{\xi}_1(T)$. In the coordinates $(\xi_1, \xi_2, \xi_3 = z_3, \dots, \xi_n = z_n)$,

$$\begin{aligned}
\frac{\partial}{\partial\xi_1} = \frac{\partial z_1}{\partial\xi_1}\frac{\partial}{\partial z_1} = \beta_1^{1/\beta_1-1}\xi_1^{1/\beta_1-1}\frac{\partial}{\partial z_1},\\
\frac{\partial^2}{\partial\xi_1\partial\bar{\xi}_2} = \frac{\partial\bar{z}_2}{\partial\bar{\xi}_2}\frac{\partial z_1}{\partial\xi_1}\frac{\partial^2}{\partial z_1\partial\bar{z}_2},\\
\frac{\partial^2}{\partial\xi_1\partial\bar{\xi}_1} = \frac{\partial\bar{z}_1}{\partial\bar{\xi}_1}\frac{\partial z_1}{\partial\xi_1}\frac{\partial^2}{\partial z_1\partial\bar{z}_1}.
\end{aligned}$$

Thus, we have

$$\begin{aligned}
\frac{\partial}{\partial\xi_1}(T) &= \frac{\partial}{\partial\xi_1}\frac{\beta_1^2 e^{-\beta_1\phi_1}}{(1-\beta_1^2|\xi_1|^2 e^{-\beta_1\phi_1})^2}\\
&= \frac{\beta_1^{1/\beta_1+1}\xi_1^{1/\beta_1-1}\frac{\partial}{\partial z_1}(e^{-\beta_1\phi_1})}{(1-\beta_1^2|\xi_1|^2 e^{-\beta_1\phi_1})^2} + \frac{2\beta_1^{1/\beta_1+3}e^{-\beta_1\phi_1}\bar{\xi}_1\xi_1^{1/\beta_1}\frac{\partial}{\partial z_1}(e^{-\beta_1\phi_1})}{(1-\beta_1^2|\xi_1|^2 e^{-\beta_1\phi_1})^3} + \frac{2\beta_1^4 e^{-2\beta_1\phi_1}\bar{\xi}_1}{(1-\beta_1^2|\xi_1|^2 e^{-\beta_1\phi_1})^3}\\
&= O(\beta_1^4|\xi_1|) = O(1),
\end{aligned}$$

since $\beta_1 \in (0, 1/2]$ and ϕ_1 is smooth w.r.t. $z_1, \dots, z_n$. Similarly, we get

$$\frac{\partial^2}{\partial\xi_1\partial\bar{\xi}_2}(T) = O(\beta_1^4\beta_2^{1/\beta_2-1}|\xi_1||\xi_2|^{1/\beta_2-1}) = O(1),$$

since we only need to address $\partial/\partial\xi_2(e^{-\beta_1\phi_1})$ when taking derivative of $\partial/\partial\xi_1(T)$ w.r.t. $\partial/\partial\bar{\xi_2}$.

Finally, direct calculations yield

$$\begin{aligned}\frac{\partial^2}{\partial\xi_1\partial\bar{\xi_1}}T &= \frac{\beta_1^{2/\beta_1}|\xi_1|^{2/\beta_1-2}\frac{\partial^2}{\partial z_1\partial\bar{z}_1}e^{-\beta_1\phi_1}}{(1-\beta_1^2|\xi_1|^2e^{-\beta_1\phi_1})^2} + \frac{2\beta_1^{1/\beta_1+3}\xi_1^{1/\beta_1-1}\frac{\partial}{\partial z_1}e^{-\beta_1\phi_1}(\xi_1 e^{-\beta_1\phi_1}+|\xi_1|^2\beta_1^{1/\beta_1-1}\bar{\xi}_1^{1/\beta_1-1}\frac{\partial}{\partial z_1}e^{-\beta_1\phi_1})}{(1-\beta_1^2|\xi_1|^2e^{-\beta_1\phi_1})^3}\\
&+\frac{2\beta_1^4\left(\frac{\partial}{\partial\bar{\xi_1}}e^{-\beta_1\phi_1}\frac{\partial}{\partial\xi_1}(|\xi_1|^2e^{-\beta_1\phi_1})+e^{-\beta_1\phi_1}\frac{\partial^2}{\partial\xi_1\partial\bar{\xi_1}}|\xi_1|^2e^{-\beta_1\phi_1}\right)}{(1-\beta_1^2|\xi_1|^2e^{-\beta_1\phi_1})^3}\\
&+\frac{6\beta_1^6e^{-\beta_1\phi_1}\frac{\partial}{\partial\xi_1}(|\xi_1|^2e^{-\beta_1\phi_1})\frac{\partial}{\partial\bar{\xi_1}}(|\xi_1|^2e^{-\beta_1\phi_1})}{(1-\beta_1^2|\xi_1|^2e^{-\beta_1\phi_1})^4}\\
&= O(\beta_1^4).\end{aligned}$$

In conclusion, we have shown

$$h_{i\bar{j},k} = O(1),$$

$$h_{i\bar{j},k\bar{\ell}} = O(1),$$

for fixed β and any $i, j, k, \ell = 1, \ldots, n$. In other words, the derivative of the metric tensor is bounded for fixed β. Moreover, by taking derivatives of (2.13), we find that the derivatives of the metric tensor degenerate (w.r.t. β_1 and β_2) at the rate shown below:

$$
\begin{aligned}
& h_{1\bar{1},1}, \quad h_{1\bar{1},1\bar{\ell}} = O(\beta_1^4), \quad \ell = 1, \dots, n \\
& h_{1\bar{1},2}, \quad h_{1\bar{1},2\bar{i}} = O(\beta_1^3\beta_2^3), \quad i = 1, \dots, n, \\
& h_{1\bar{1},k\bar{\ell}} = O(\beta_1^3), \quad k \neq 1, 2, \ell = 1, \dots, n \\
& h_{1\bar{2},1} = O(\beta_1^4\beta_2^4), \\
& h_{1\bar{2},k} = O(\beta_1^3\beta_2^3), \quad k \neq 1, \\
& h_{1\bar{2},1\bar{\ell}} = O(\beta_1^4\beta_2^4), \quad \ell = 1, \dots, n, \\
& h_{1\bar{2},k\bar{\ell}} = O(\beta_1^3\beta_2^3), \quad k \neq 1, \ell = 1, \dots, n \\
& h_{1\bar{j},k} = O(\beta_1^3), \quad j \neq 1, 2, k \neq 2, \\
& h_{1\bar{j},2} = O(\beta_1^3\beta_2^3), \quad j \neq 1, 2 \\
& h_{1\bar{j},k\bar{\ell}} = O(\beta_1^3), j \neq 1, 2, k \neq 2, \ell \neq 2, \\
& h_{1\bar{j},k\bar{\ell}} = O(\beta_1^3\beta_2^3), \quad j \neq 1, 2, k = 2 \text{ or } \ell = 2, \\
& h_{i\bar{j},1} = O(\beta_1^{1/\beta_1 - 1}), \quad i, j \neq 1, 2 \\
& h_{i\bar{j},2} = O(\beta_2^{1/\beta_2 - 1}), \quad i, j \neq 1, 2 \\
& h_{i\bar{j},1\bar{1}} = O(\beta_1^{2/\beta_1 - 2}), \quad i, j \neq 1, 2 \\
& h_{i\bar{j},2\bar{2}} = O(\beta_2^{2/\beta_2 - 2}), \quad i, j \neq 1, 2 \\
& h_{i\bar{j},1\bar{2}}, h_{i\bar{j},2\bar{1}} = O(\beta_1^{1/\beta_1 - 1}\beta_2^{1/\beta_2 - 1}), \quad i, j \neq 1, 2 \\
& h_{i\bar{j},k}, h_{i\bar{j},k\bar{\ell}} = O(1), \quad i, j, k, \ell \neq 1, 2.
\end{aligned}
\tag{2.20}
$$

Step 4: Estimate the sum $R_{i\bar{j}k\bar{\ell}}u^i\bar{u}^j v^k\bar{v}^\ell$.

We have shown the derivatives of $h_{i\bar{j}}$ are bounded. To show that $R_{i\bar{j}k\bar{\ell}}u^i\bar{u}^j v^k\bar{v}^\ell$ is bounded, we consider

$$R_{i\bar{j}k\bar{\ell}}u^i\bar{u}^j v^k\bar{v}^\ell = (-h_{i\bar{j},k\bar{\ell}} + h^{s\bar{t}}h_{i\bar{t},k}h_{s\bar{j},\ell})u^i\bar{u}^j v^k\bar{v}^\ell.$$

We consider three different cases.

When none of i, j, k, ℓ, s, t **is** 1 **or** 2**:** then the sum is uniformly bounded because none of the term blow up w.r.t. β_1 or β_2.

When $s, t \neq 1, 2$ **and** i, j, k, ℓ **may take values from** 1 **or** 2**:** then we found from (2.20) that the common factors of powers of β_1 or β_2 in $h_{i\bar{j},k}$ and $h_{i\bar{j},k\bar{\ell}}$ compensate for the degeneracy of u^1, u^2 and v^1, v^2.

When s **or** $t = 1, 2$**:** then in the worst case, where $s = 1, t = 2$, we find from (2.20) that all the derivatives that have 1 or 2 in the subscript have at least a degeneracy rate of β_1^3 or β_2^3. However, $h^{s\bar{t}}$ blows up at the rate of $\beta_1^{-2}\beta_2^{-2}$. Combining this fact with (2.16) we find that the common factors of β_1 and β_2 in the derivatives can still compensate for the degeneracy of $h^{s\bar{t}}$ and u, v.

Then we conclude that when β satisfies that $\beta_k \in (0, 1/2]$ for each k, the holomorphic bisectional curvature of Ω_β is uniformly bounded in β. □

2.2.2 A priori estimates

By Theorem 1.2.3, there exists a unique Kähler–Einstein crossing edge metric on X with cone angle $2\pi\beta_i$ along each D_i, denoted by $\omega_{\phi_\beta} = \omega - \sum_{i=1}^r \beta_i\theta_i + \sqrt{-1}\partial\bar{\partial}\phi_\beta$ such that

$$\begin{cases} \omega_{\phi_\beta}^n = \dfrac{e^{f+\phi_\beta}\omega^n}{\Pi_{i=1}^r |s_i|_{h_i}^{2(1-\beta_i)}}, \\ \omega_{\phi_\beta} = \omega - \displaystyle\sum_{i=1}^r \beta_i\theta_i + \sqrt{-1}\partial\bar{\partial}\phi_\beta > 0, \end{cases} \tag{2.21}$$

where $f \in C^\infty(X)$. In this section, we establish a Laplacian estimate for ω_{ϕ_β} with respect to the reference metric Ω_β by proving the following result.

Theorem 2.2.4. *For $\beta = (\beta_1, \dots, \beta_r) \in (0, \frac{1}{2}]^r$, there exists a constant $C > 0$ (independent of $\beta_1, \dots, \beta_r$) such that*

$$C^{-1}\Omega_\beta \leq \omega_{\phi_\beta} \leq C\Omega_\beta, \tag{2.22}$$

on $X \setminus \mathrm{supp}(D)$.

Define

$$\psi_\beta := -\sum_{i=1}^{r} \log \left[\frac{1 - |s_i|_{h_i}^{2\beta_i}}{\beta_i} \right]^2,$$

then

$$\Omega_\beta = \omega + \sqrt{-1}\partial\bar{\partial}\psi_\beta.$$

Proof of Theorem 2.2.4. We divide the proof into two steps. First, we deduce the C^0-estimate for potential functions ϕ_β and ψ_β by using a modified maximum principle. Then we derive the Laplacian estimate by applying Chern–Lu's inequality to the identity map $(X, \omega_{\phi_\beta}) \to (X, \Omega_\beta)$.

Step 1: C^0-estimate: Comparing ϕ_β with ψ_β.

We first compare the potential functions of ω_{ϕ_β} and Ω_β. Let $\tilde{\phi}_\beta := \phi_\beta - \psi_\beta$, then we get

$$\omega_{\phi_\beta}^n = \frac{e^{\phi_\beta + f}\omega^n}{\prod_{i=1}^r |s_i|_{h_i}^{2(1-\beta_i)}}, \tag{2.23}$$

$$\Rightarrow (\Omega_\beta - \sum_{i=1}^r \beta_i\theta_i + \sqrt{-1}\partial\bar{\partial}\tilde{\phi}_\beta)^n = e^{\tilde{\phi}_\beta + F_\beta}\Omega_\beta^n, \tag{2.24}$$

where $F_\beta = \psi_\beta + f + \log\left(\frac{\omega^n}{\prod_{i=1}^r |s_i|_{h_i}^{2(1-\beta_i)} \cdot \Omega_\beta^n}\right)$. Then we claim that

Claim 2.2.5. For some uniform constant $C > 0$,

$$||F_\beta||_{C^0(X\setminus D)} \leq C. \tag{2.25}$$

Proof. First note that f is smooth on X by construction, hence it is bounded as X is compact. Therefore, it suffices to show

$$\begin{aligned} F_\beta - f &= \psi_\beta + \log\left(\frac{\omega^n}{\prod_{i=1}^r |s_i|_{h_i}^{2(1-\beta_i)} \cdot \Omega_\beta^n}\right) \\ &= \log\left(\frac{\prod_{i=1}^r \beta_i^2 \cdot \omega^n}{\prod_{i=1}^r |s_i|_{h_i}^{2(1-\beta_i)}(1-|s_i|_{h_i}^{2\beta_i})^2 \cdot \Omega_\beta^n}\right) \end{aligned}$$

is bounded. To prove the claim, it is equivalent to showing

$$\Omega_\beta^n = \frac{\prod_{i=1}^r \beta_i^2}{\prod_{i=1}^r |s_i|_{h_i}^{2(1-\beta_i)}(1-|s_i|_{h_i}^{2\beta_i})^2} e^{O(1)}\omega^n$$

near the divisor. This amounts to saying that Ω_β^n has a pole of order $\prod_{i=1}^r |s_i|_{h_i}^{2(1-\beta_i)}$. Without loss of generality, we can assume $r = 1$ and thus below we drop the i in the subscript for simplicity. Let $p \in M \setminus D$ near D. Let e be a local holomorphic frame for L_D, and $(z_1, \ldots, z_n)$ be a local holomorphic coordinate chart such that $s = z_1 e$. Let $h = e^{-\phi}$ be a smooth hermitian metric on $\mathcal{O}_X(D)$ and θ the curvature form of (L_D, h). Denote

$$\omega = \sqrt{-1} g_{i\bar{j}} dz_i \wedge d\bar{z}_j,$$

$$\theta = \sqrt{-1} \phi_{i\bar{j}} dz_i \wedge d\bar{z}_j.$$

Recall the expression (2.7) of Ω_β. We calculate

$$\begin{aligned}
\langle D^{1,0} s, D^{1,0} s \rangle &= e^{-\phi}(dz_1 + z_1 \frac{\partial \phi}{\partial z_k} dz_k) \wedge (d\bar{z}_1 + \bar{z}_1 \frac{\partial \phi}{\partial \bar{z}_k} d\bar{z}_k) \\
&= e^{-\phi}[(1 + \bar{z}_1 \frac{\partial \phi}{\partial \bar{z}_k} + z_1 \frac{\partial \phi}{\partial z_1} + |z_1|^2 \frac{\partial \phi}{\partial z_1} \frac{\partial \phi}{\partial \bar{z}_1}) dz_1 \wedge d\bar{z}_1 \\
&+ \sum_{k=2}^n (\bar{z}_1 \frac{\partial \phi}{\partial \bar{z}_k} + |z_1|^2 \frac{\partial \phi}{\partial z_1} \frac{\partial \phi}{\partial \bar{z}_k}) dz_1 \wedge d\bar{z}_k \\
&+ \sum_{k=2}^n (z_1 \frac{\partial \phi}{\partial z_k} + |z_1|^2 \frac{\partial \phi}{\partial z_k} \frac{\partial \phi}{\partial \bar{z}_1}) dz_k \wedge d\bar{z}_1 \\
&+ \sum_{k,l=2}^n |z_1|^2 \frac{\partial \phi}{\partial z_k} \frac{\partial \phi}{\partial \bar{z}_l} dz_k \wedge d\bar{z}_l].
\end{aligned}$$

Hence,

$$
\begin{aligned}
&\frac{\beta^2}{|s|_h^{2(1-\beta)}(1-|s|_h^{2\beta})^2}\langle D^{1,0}s, D^{1,0}s\rangle \\
&= (\frac{\beta^2}{|s|_h^{2(1-\beta)}(1-|s|_h^{2\beta})^2} + O(1))dz_1 \wedge d\bar{z}_1 + \sum_{k=2}^{n}(\frac{\beta^2|s|_h^{2\beta}}{z_1(1-|s|_h^{2\beta})^2} + O(1))dz_1 \wedge d\bar{z}_k \\
&+ \sum_{k=2}^{n}(\frac{\beta^2|s|_h^{2\beta}}{\bar{z}_1(1-|s|_h^{2\beta})^2} + O(1))dz_k \wedge d\bar{z}_1 + \sum_{k,l=2}^{n}\frac{\beta^2|s|_h^{2\beta}}{(1-|s|_h^{2\beta})^2}dz_k \wedge d\bar{z}_l \\
&= (\frac{\beta^2}{|s|_h^{2(1-\beta)}(1-|s|_h^{2\beta})^2} + O(1))dz_1 \wedge d\bar{z}_1 + \sum_{k=2}^{n}(\frac{\beta^2|s|_h^{2\beta}}{z_1(1-|s|_h^{2\beta})^2} + O(1))dz_1 \wedge d\bar{z}_k \\
&+ \sum_{k=2}^{n}(\frac{\beta^2|s|_h^{2\beta}}{\bar{z}_1(1-|s|_h^{2\beta})^2} + O(1))dz_k \wedge d\bar{z}_1 + \sum_{k,l=2}^{n}O(1)dz_k \wedge d\bar{z}_l.
\end{aligned}
$$

Let

$$
(A_{ij})_{i,j=1}^n = (g_{i\bar{j}})_{i,j=1}^n - \frac{\beta|s|_h^{2\beta}}{1-|s|_h^{2\beta}}(\phi_{i\bar{j}})_{i,j=1}^n + \frac{\beta^2}{|s|_h^{2(1-\beta)}(1-|s|_h^{2\beta})^2}\langle D^{1,0}s, D^{1,0}s\rangle.
$$

Write $(A_{ij})_{i,j=1}^n$ as a block matrix

$$
(A_{ij})_{i,j=1}^n = \begin{bmatrix} A_{11} & \vec{A}_r \\ \vec{A}_c & (A_{ij})_{i,j=2}^n \end{bmatrix}, \tag{2.26}
$$

then

$$
\begin{aligned}
A_{11} &= g_{1\bar{1}} - \frac{\beta|s|_h^{2\beta}}{1-|s|_h^{2\beta}}\phi_{1\bar{1}} + \frac{\beta^2}{|s|_h^{2(1-\beta)}(1-|s|_h^{2\beta})^2} + O(|s|_h^{2\beta-1}) + O(|s|_h^{2\beta})O(1),\\
A_{1j} &= g_{1\bar{j}} - \frac{\beta|s|_h^{2\beta}}{1-|s|_h^{2\beta}}\phi_{1\bar{j}} + O(|s|_h^{2\beta-1}) + O(|s|_h^{2\beta}) + O(1), \quad j = 2, \ldots, n,\\
A_{i1} &= g_{i\bar{1}} - \frac{\beta|s|_h^{2\beta}}{1-|s|_h^{2\beta}}\phi_{i\bar{1}} + O(|s|_h^{2\beta-1}) + O(|s|_h^{2\beta}) + O(1), \quad i = 2, \ldots, n,\\
A_{kl} &= O(|s|_h^{2\beta}) + O(1), \quad k, l = 2, \ldots, n.
\end{aligned}
$$

Recall the formula for determinant of block matrices as in (2.26),

$$
\det(A_{ij})_{i,j=1}^n = \det(A_{ij})_{i,j=2}^n \cdot (A_{11} - \vec{A}_r((A_{ij})_{i,j=2}^n)^{-1}\vec{A}_c). \tag{2.27}
$$

Using (2.27),

$$
\begin{aligned}
\frac{\Omega_\beta^n}{\omega^n} &= \frac{\det(g_{i\bar{j}} - \frac{\beta|s|_h^{2\beta}}{1-|s|_h^{2\beta}}\phi_{i\bar{j}} + \frac{\beta^2}{|s|_h^{2(1-\beta)}(1-|s|_h^{2\beta})^2}\langle D^{1,0}s, D^{1,0}s\rangle)}{\det(g_{i\bar{j}})}\\
&= \frac{\det(A_{ij})_{i,j=1}^n}{\det(g_{i\bar{j}})}\\
&= e^{O(1)} \cdot \det(A_{ij})_{i,j=2}^n \cdot (A_{11} - \vec{A}_r((A_{ij})_{i,j=2}^n)^{-1}\vec{A}_c)\\
&= e^{O(1)} \cdot \left(\frac{\beta^2}{|s|_h^{2(1-\beta)}(1-|s|_h^{2\beta})^2} + O(|s|_h^{4\beta-2}) + O(|s|_h^{2\beta-1}) + O(|s|_h^{4\beta-1}) + O(|s|_h^{2\beta}) + O(|s|_h^{4\beta}) + O(1)\right).
\end{aligned}
$$

Thus, one finds that the dominant term is $\frac{\beta^2}{|s|_h^{2(1-\beta)}(1-|s|_h^{2\beta})^2}$. In another word, we have shown $\Omega_\beta^n = e^{O(1)}\frac{\beta^2}{|s|_h^{2(1-\beta)}(1-|s|_h^{2\beta})^2}\omega^n$, which is exactly what we need. □

Lemma 2.2.6. *There exists a uniform constant $C > 0$ in β such that,*

$$\sup_{X\setminus D} |\tilde{\phi}_\beta| \leq C,$$

when β_i are small enough for every i.

Proof. First note that for a fixed β, $\tilde{\phi}_\beta$ is bounded according to [27, 38]. We aim to derive a uniform bound for $\tilde{\phi}_\beta$ in β. Let $\chi_{\beta,\epsilon} = \tilde{\phi}_\beta + \epsilon \sum_{i=1}^r \log |s_i|^2_{h_i}$ for small $\epsilon > 0$. Since $\chi_{\beta,\epsilon}(p)$ approaches $-\infty$ when $p \to D$, $\chi_{\beta,\epsilon}$ obtains its maximum on $X \setminus D$, at say $p_{\max}$. Then

$$0 \geq \sqrt{-1}\partial\bar{\partial}\tilde{\phi}_\beta(p_{\max}) - \epsilon \sum_{i=1}^r \theta_i(p_{\max}),$$

where θ_i is the curvature of the Chern connection on (L_{D_i}, h_i). Then at $p_{\max}$,

$$(\Omega_\beta - \sum_{i=1}^r \beta_i\theta_i + \sqrt{-1}\partial\bar{\partial}\tilde{\phi}_\beta)^n \leq (\Omega_\beta + \sum_{i=1}^r (\epsilon - \beta_i)\theta_i)^n \tag{2.28}$$

$$\leq 2^n \Omega^n_{\beta_i}, \tag{2.29}$$

by the fact that $\Omega_\beta \geq r(\epsilon - \beta_i)\theta_i$ for small enough ϵ and β_i, as shown in Lemma 2.2.1. Combining (2.24) and (2.29), at $p_{\max}$,

$$\begin{aligned} e^{\tilde{\phi}_\beta + F_\beta}(p_{\max}) &\leq 2^n \\ \Rightarrow \tilde{\phi}_\beta(p_{\max}) &\leq n \log 2 - F_\beta(p_{\max}) \\ &\leq n \log 2 - \inf_{X\setminus D} F_\beta. \end{aligned}$$

For any $p \in X \setminus D$,

$$\begin{aligned}
\tilde{\phi}_\beta(p) &= \chi_{\beta,\epsilon}(p) - \epsilon \sum_{i=1}^{r} \log |s_i|^2_{h_i}(p) \\
&\le \chi_{\beta,\epsilon}(p_{\max}) - \epsilon \sum_{i=1}^{r} \log |s_i|^2_{h_i}(p) \\
&\le n \log 2 - \inf_{X \setminus D} F_\beta + \epsilon \sum_{i=1}^{r} \log |s_i|^2_{h_i}(p_{\max}) - \epsilon \sum_{i=1}^{r} \log |s_i|^2_{h_i}(p) \\
&\le C
\end{aligned}$$

for some constant $C > 0$, when letting $\epsilon \to 0$ and using (2.25). Similarly by considering $\tilde{\chi}_{\beta,\epsilon} := \tilde{\phi}_\beta - \epsilon \sum_{i=1}^{r} \log |s_i|^2_{h_i}$ achieving its minimum on $X \setminus D$, we can show a lower bound for $\tilde{\phi}_\beta$ on $X \setminus D$. $\square$

Step 2: The Laplacian estimates for ω_{ϕ_β} and Ω_β.

In this section, we use Chern–Lu's inequality to deduce the Laplacian estimate of ω_{ϕ_β} with respect to Ω_β.

Consider the identity map

$$\mathrm{id} : (X \setminus D, \omega_{\phi_\beta}) \to (X \setminus D, \Omega_\beta).$$

By definitions, $\operatorname{Ric} \omega_{\phi_\beta} = -\omega_{\phi_\beta}$. From Lemma 2.2.3, $|\operatorname{Bisec}_{\Omega_\beta}| \le C_3$ for some constant $C_3 > 0$ when $\beta_i \in (0, \frac{1}{2}]$ for every i. Then by Chern–Lu's inequality [38, Proposition 7.1] (see also [48, Proposition 7.2]),

$$\Delta_{\omega_{\phi_\beta}} (\log \operatorname{tr}_{\omega_{\phi_\beta}} \Omega_\beta) \ge -1 - 2C_3 \operatorname{tr}_{\omega_{\phi_\beta}} \Omega_\beta. \tag{2.30}$$

Set for $0 < \epsilon \ll 1$,

$$H_{\beta,\epsilon} = \log \operatorname{tr}_{\omega_{\phi_\beta}} \Omega_\beta - 4(C_3+1)\tilde{\phi}_\beta + \epsilon \sum_{i=1}^{r} \log |s_i|^2_{h_i},$$

then

$$\Delta_{\omega_{\phi_\beta}} H_{\beta,\epsilon} = \Delta_{\omega_{\phi_\beta}} (\log \operatorname{tr}_{\omega_{\phi_\beta}} \Omega_\beta - 4(C_3+1)\tilde{\phi}_\beta) - \epsilon \sum_{i=1}^{r} \operatorname{tr}_{\omega_{\phi_\beta}} \theta_i \tag{2.31}$$

$$\geq \Delta_{\omega_{\phi_\beta}} (\log \operatorname{tr}_{\omega_{\phi_\beta}} \Omega_\beta) + 4(C_3+1)\left(\frac{1}{2}\operatorname{tr}_{\omega_{\phi_\beta}} \Omega_\beta - n\right) - \operatorname{tr}_{\omega_{\phi_\beta}\Omega_\beta}, \tag{2.32}$$

where the last inequality is true by noting that $\theta_i \leq M\Omega_\beta$ for some uniform constant $M > 0$ and assuming $\epsilon < \frac{1}{2rM}$ and $\sum_{i=1}^{r} \beta_i < \frac{1}{2M}$.

Combine (2.30) and (2.32),

$$\Delta_{\omega_{\phi_\beta}} H_{\beta,\epsilon} \geq \operatorname{tr}_{\omega_{i,\ell}} \Omega_{\beta_i} - C \tag{2.33}$$

for some uniform constant $C > 0$. $H_{\beta,\epsilon}$ achieves its maximum on $X \setminus D$, at, say $q_{\max}$. Then by (2.33),

$$\operatorname{tr}_{\omega_{\phi_\beta}} \Omega_\beta(q_{\max}) \leq C.$$

For any $q \in X \setminus D$,

$$
\begin{aligned}
\log \operatorname{tr}_{\omega_{\phi_\beta}} \Omega_\beta(q) &= H_{\beta,\epsilon}(q) + 4(C_3+1)\tilde{\phi}_\beta(q) - \epsilon \sum_{i=1}^r \log |s_i|^2_{h_i}(q) \\
&\leq H_{\beta,\epsilon}(q_{\max}) + 4(C_3+1)\tilde{\phi}_\beta(q) - \epsilon \sum_{i=1}^r \log |s_i|^2_{h_i}(q) \\
&\leq C - 4(C_3+1)\tilde{\phi}_\beta(q_{\max}) + \epsilon \sum_{i=1}^r \log |s_i|^2_{h_i}(q_{\max}) \\
&+ 4(C_3+1)\tilde{\phi}_{i,\ell}(q) - \epsilon \sum_{i=1}^r \log |s_i|^2_{h_i}(q) \\
&\leq \text{ some uniform constant } C,
\end{aligned}
$$

where the last inequality is true by Lemma 2.2.6 and letting $\epsilon \to 0$ for fixed q. Hence we have shown

$$
\omega_{\phi_\beta} \geq C \cdot \Omega_\beta, \tag{2.34}
$$

on $X \setminus \operatorname{supp}(D)$ as desired. Since ω_{ϕ_β} and Ω_β are equivalent on X, we obtain the estimate (2.22) on $X \setminus D$.

□

2.2.3 Global convergence of ω_{ϕ_β}

A smooth Kähler metric Ω_{PC} on $X \setminus D$ is said to have mixed cusp and edge singularities along a divisor D if whenever D is locally given by $D = \sum_{i=1}^t \{z_i = 0\} + \sum_{j=t+1}^m (1-\beta_j)\{z_j =$

$0\}$ with $t < m \leq n$, Ω_{PC} is quasi-isometric to the following metric:

$$\omega_{PC} := \sum_{i=1}^{t} \frac{\sqrt{-1}dz_i \wedge d\bar{z}_i}{|z_i|^2 \log^2 |z_i|^2} + \sum_{j=t+1}^{m} \frac{\beta_j^2 \sqrt{-1}dz_j \wedge d\bar{z}_j}{|z_j|^{2(1-\beta_j)}} + \sum_{\ell=m+1}^{n} \sqrt{-1}dz_\ell \wedge d\bar{z}_\ell.$$

In particular, when $t = m$, ω_{PC} has merely cusp singularities along D.

In the case $t = m$, it is well known [40, 55] that if $K_X + D$ is ample, there exists a unique Kähler–Einstein metric on $X \setminus D$ with cusp singularities along D. In general, it is shown that if $K_X + D$ is ample, there exists a unique Kähler–Einstein metric on $X \setminus D$ with mixed cusp and cone singularities along D [25, Theorem A]. As a corollary of Theorem 2.2.4, we study the global weak convergence and local smooth convergence of the Kähler–Einstein crossing edge metrics ω_{ϕ_β} to a Kähler–Einstein mixed cusp and edge metric on (X, D_β) as some of the cone angles tend to 0. The first observation is the following lemma.

Lemma 2.2.7. *Assume $\beta_i \to 0$, for $i = 1, \ldots, t < r$, and $\beta_j \to d_j \in (0,1)$ for $j = t+1, \ldots, r$, then Ω_β weakly converges to some Kähler mixed cusp and edge metric Ω_{PC}. Moreover, Ω_β converges to Ω_{PC} in $C^\infty_{\mathrm{loc}}(X \setminus \mathrm{supp}(D_\beta))$.*

Proof. Recall the definition of Ω_β. Note that $\log\left[(1 - |s_i|^{2\beta_i}_{h_i})/\beta_i\right]^2$ converges to $\log\log^2 |s_i|^2_{h_i}$ in $L^1(X, \omega)$ and $C^\infty_{\mathrm{loc}}(X \setminus \mathrm{supp}(D_\beta))$ as $\beta_i \to 0$ for each $i = 1, \ldots, t$. Thus Ω_β converges to

$$\Omega_{PC} := \omega - \sum_{i=1}^{t} \sqrt{-1}\partial\bar{\partial} \log\log^2 |s_i|^2_{h_i} - \sum_{j=t+1}^{r} \sqrt{-1}\partial\bar{\partial} \log \left[\frac{1 - |s_j|^{2d_j}_{h_j}}{d_j}\right]^2$$

in $C^\infty_{\mathrm{loc}}(X \setminus \mathrm{supp}(D_\beta))$ sense and weakly in the sense of currents. It remains to show that Ω_{PC} has mixed cusp and edge singularities along D_β. To see this, recall we denote by θ_i the Chern curvature form of (L_{D_i}, h_i) for each i, then by (2.8) and (2.10), we calculate that

$$\begin{aligned}
&\sum_{i=1}^{t}\sqrt{-1}\partial\bar{\partial}\log\log^2|s_i|^2_{h_i}\\
=&\sum_{i=1}^{t}2\sqrt{-1}\cdot\frac{(\partial\bar{\partial}|s_i|^2_{h_i})(\log|s_i|^2_{h_i})(|s_i|^2_{h_i})-\partial(\log|s_i|^2_{h_i}|s_i|^2_{h_i})\bar{\partial}|s_i|^2_{h_i}}{(\log|s_i|^2_{h_i})^2(|s_i|^2_{h_i})^2}\\
=&\sum_{i=1}^{r}\frac{2\sqrt{-1}\langle D^{1,0}s_i, D^{1,0}s_i\rangle}{\log^2|s_i|^2_{h_i}|s_i|^2_{h_i}}+\frac{2}{\log|s_i|^2_{h_i}}\theta_i.
\end{aligned}$$

Thus, Ω_{PC} has cusp singularities along D_i for $i = 1, \dots, t$. The result follows. $\square$

Theorem 2.2.8. *The Kähler–Einstein crossing edge metric ω_{ϕ_β} converges to the Kähler–Einstein mixed cusp and edge metric on (X, D_β) globally in a weak sense and locally in a strong sense when $\beta_i \to 0$ for $i = 1, \dots, t < r$ and $\beta_j \to d_j \in (0, 1)$ for $j = t + 1, \dots, r$.*

Proof. By Theorem 2.2.4, the family of ω_{ϕ_β} has uniformly bounded mass. Thus, the family of ω_{ϕ_β} is relatively compact in the weak topology. The same arguments in the proof of Lemma 2.2.6 and elliptic estimates give respectively the C^0-estimate and all higher-order estimates for the family of ω_{ϕ_β}. Therefore, any weak limit ω_0 is smooth on $X \setminus \mathrm{supp}(D_\beta)$ and this C^∞_{loc}-convergence indicates that such ω_0 is Kähler–Einstein outside D_β. Lemma 2.2.7 shows any such ω_0 also admits mixed cusp and edge singularities along D_β. Thus, by the uniqueness argument in this setting [25, Proposition 2.5], all such ω_0 coincides with the unique Kähler–Einstein metric on $X \setminus \mathrm{supp}(D_\beta)$ with mixed cusp and cone singularities along D_β. Hence we have shown the locally strong and globally weak convergence of ω_{ϕ_β} to a Kähler–Einstein mixed cusp and edge metric as $\beta_i \to 0$ for $i = 1, \dots, t$ and $\beta_j \to d_j$ for $j = t + 1, \dots, r$. $\square$

2.3 Asymptotic behavior near divisors in the small angle limit

Theorem 2.2.8 only gives us the smooth convergence of ω_{ϕ_β} to a Kähler–Einstein mixed cusp and edge metric away from the divisor when cone angles approach 0. In this section, we study the asymptotic behavior of ω_{ϕ_β} near D when some of the cone angles tend to 0. More precisely, consider a fixed point $p \in D_\beta$ with a holomorphic coordinate chart $(U, \{z_i\}_{i=1}^n)$ centered at p such that $D_\beta \cap U = \{z_1 \cdots z_m = 0\}$, for $m \le n$ and $D_j \cap U = \{z_j = 0\}$ for $j = 1, \ldots, m$. Let β_i denote the cone angle along D_i for each i. From now on, assume $\beta_1 \le \beta_2 \le \cdots \le \beta_m$. We allow other cone angles to tend to 0, but we always assume that β_1 goes to 0 in the fastest speed, i.e., $\beta_1/\beta_i \nrightarrow +\infty$, for $i = 2, \ldots, m$.

2.3.1 A small neighborhood of D_β

By choosing an appropriate coordinate system [10, Lemma 4.1], whenever D_β is locally given by $\{z_1 \cdots z_m = 0\}$, the reference metric Ω_β is equivalent to the following metric:

$$\omega_{\beta,\mathrm{mod}} := \sum_{i=1}^{m} \frac{\beta_i^2 \sqrt{-1} dz_i \wedge d\bar{z}_i}{|z_i|^{2(1-\beta_i)}(1 - |z_i|^{2\beta_i})^2} + \sum_{j=m+1}^{n} \sqrt{-1} dz_j \wedge d\bar{z}_j. \tag{2.35}$$

Thus, Theorem 2.2.4 tells us on $X \setminus \mathrm{supp}(D_\beta)$, there exists a uniform constant $C > 0$ such that

$$C^{-1}\omega_{\beta,\mathrm{mod}} \le \omega_{\phi_\beta} \le C\omega_{\beta,\mathrm{mod}}. \tag{2.36}$$

Thanks to (2.36), it is enough to consider $((\mathbb{C}^*)^m \times \mathbb{C}^{n-m}, \omega_{\beta,\mathrm{mod}})$ when dealing with a small neighborhood of D_β under the metric ω_{ϕ_β}. Let us fix a point $p \in D_\beta$. Let $(U, z_1, \ldots, z_n)$

be a holomorphic coordinate chart centered at p, such that $U \cap D_\beta = \{z_1 \cdots z_m = 0\}$ and $U \cap D_i = \{z_i = 0\}$ for $i = 1, \ldots, m$. Let $\mathbb{D} := \{|z_i| \leq 1, i = 1, \ldots, n\}$ be the unit polydisk. Then we claim that the distance function d_β induced by the completion of $\omega_{\beta,\mathrm{mod}}$ on $\mathbb{D}$ satisfies

$$d_\beta(0, z) \simeq \sum_{i=1}^{m} \frac{1}{2} \log\left(\frac{1 + |z_i|^{\beta_i}}{1 - |z_i|^{\beta_i}}\right) + \sum_{j=m+1}^{n} |z_j|, \quad z \in \mathbb{D}, \tag{2.37}$$

where "$\simeq$" means "is equivalent up to a constant independent of z to". Indeed, $\frac{1}{2}\log\left(\frac{1+x^{\beta_i}}{1-x^{\beta_i}}\right)$ is the primitive of $\frac{\beta_i}{x^{1-\beta_i}(1-x^{2\beta_i})}$, and (2.37) follows from this fact and (2.35). Summarizing the discussions above, it is enough to study the polydisk in $\mathbb{C}^n$

$$\left\{ |z_i|^{\beta_i} < \frac{1 - e^{-2a}}{1 + e^{-2a}}, i = 1, \ldots, m, z_j < a, j = m+1, \ldots, n \right\}, \quad a > 0,$$

when we study a neighborhood of D_β given by the geodesic ball $B_{\omega_{\phi_\beta}}(p, a)$ centered at p of radius a with respect to the metric ω_{ϕ_β}.

2.3.2 Mixed cylinder and edge metric

In this section, we focus on a small neighborhood of D_β and show that in a neighborhood of D_β, a renormalization of $\omega_{\beta,\mathrm{mod}}$ locally converges to a mixed cylinder and edge metric (see Definition 2.3.1 below) in the C^∞-sense.

Definition 2.3.1. A Kähler metric $\tilde{\omega}$ on $(\mathbb{C}^*)^m \times \mathbb{C}^{n-m}$ is called a mixed cylinder and edge metric if $\tilde{\omega}$ is quasi-isometric to the following metric:

$$\omega_{\text{mix}} := \sum_{i=1}^{t} \frac{\sqrt{-1}dz_i \wedge d\bar{z}_i}{|z_i|^2} + \sum_{j=t+1}^{m} \frac{\beta_j^2 \sqrt{-1}dz_j \wedge d\bar{z}_j}{|z_j|^{2(1-\beta_j)}} + \sum_{\ell=m+1}^{n} \sqrt{-1}dz_\ell \wedge d\bar{z}_\ell,$$

where $\beta_j \in (0,1)$ for $j = t+1, \ldots, m$.

Denote by

$$\mathbb{D}(a_1, \ldots, a_m, b) := \{z \in (\mathbb{C}^*)^m \times \mathbb{C}^{n-m} : |z_i| < a_i, i = 1, \ldots, m, |z_j| < b, j = m+1, \ldots, n\}.$$

Let

$$U_\beta := \mathbb{D}\left(e^{-\frac{1}{2\beta_1}}, \left(\frac{\beta_1}{\beta_2}\right)^{\frac{1}{2\beta_2}}, \ldots, \left(\frac{\beta_1}{\beta_m}\right)^{\frac{1}{2\beta_m}}, 1\right).$$

From Section 2.3.1, one realizes U_β as a neighborhood of D_β. We endow U_β with $\dfrac{1}{\beta_1^2}\omega_{\beta,\text{mod}}$. Define a map

$$\Psi_\beta : \mathbb{D}\left(e^{\frac{1}{2\beta_1}}, \left(\frac{\beta_2}{\beta_1}\right)^{\frac{1}{2\beta_2}}, \ldots, \left(\frac{\beta_m}{\beta_1}\right)^{\frac{1}{2\beta_m}}, \frac{1}{\beta_1}\right) \to U_\beta = \mathbb{D}\left(e^{-\frac{1}{2\beta_1}}, \left(\frac{\beta_1}{\beta_2}\right)^{\frac{1}{2\beta_2}}, \ldots, \left(\frac{\beta_1}{\beta_m}\right)^{\frac{1}{2\beta_m}}, 1\right)$$

$$(w_1, \ldots, w_m, w_{m+1}, \ldots, w_n) \mapsto \left(e^{-\frac{1}{\beta_1}} w_1, \left(\frac{\beta_1}{\beta_2}\right)^{\frac{1}{\beta_2}} w_2, \ldots, \left(\frac{\beta_1}{\beta_m}\right)^{\frac{1}{\beta_m}} w_m, \beta_1 w_{m+1}, \ldots, \beta_1 w_n\right).$$

On $\Psi_\beta^{-1}(U_\beta)$, the pull-back metric reads

$$\Psi_\beta^*(\frac{1}{\beta_1^2}\omega_{\beta,\mathrm{mod}}) = \frac{e^{-2}|w_1|^{2\beta_1}}{(1-e^{-2}|w_1|^{2\beta_1})^2}\cdot\frac{\sqrt{-1}dw_1\wedge d\bar{w}_1}{|w_1|^2} + \sum_{i=2}^{m}\frac{\sqrt{-1}dw_i\wedge d\bar{w}_i}{|w_i|^{2(1-\beta_i)}(1-\frac{\beta_1^2}{\beta_i^2}|w_i|^{2\beta_i})^2} \tag{2.38}$$

$$+\sum_{j=m+1}^{n}\sqrt{-1}dw_j\wedge d\bar{w}_j. \tag{2.39}$$

Note that for $(w_1,\dots,w_m,w_{m+1},\dots,w_n)\in(\mathbb{C}^*)^m\times\mathbb{C}^{n-m}$, $|w_1|^{2\beta_1}\to 1$ as $\beta_1\to 0$ and $\frac{\beta_1^2}{\beta_i^2}|w_i|^{2\beta_i}\to 0$ as $\frac{\beta_1}{\beta_i}\to 0$. Moreover, for any compact subset $K\subset(\mathbb{C}^*)^m\times\mathbb{C}^{n-m}$, when β_1 is small enough, $K\subset\Psi_\beta^{-1}(U_\beta)$. Hence we have indeed shown the following result.

Lemma 2.3.2. *The pull-back of $\frac{1}{\beta_1^2}\omega_{\beta,\mathrm{mod}}$ by Ψ_β on any compact subset $K\subset(\mathbb{C}^*)^m\times\mathbb{C}^{n-m}$ converges to a mixed cylindrical and conical metric in $C^\infty(K)$ when $\beta_1\to 0$ and β_i does not converge to 0 for each $i=2,\dots,m$.*

Proof. Summarizing the discussions above, $\Psi_\beta^*(\frac{1}{\beta_1^2}\omega_{\beta,\mathrm{mod}})$ converges to

$$\frac{e^{-2}}{(1-e^{-2})^2}\cdot\frac{\sqrt{-1}dw_1\wedge d\bar{w}_1}{|w_1|^2}+\sum_{i=2}^{m}\frac{\sqrt{-1}dw_i\wedge d\bar{w}_i}{|w_i|^{2(1-\beta_i)}}+\sum_{j=m+1}^{n}\sqrt{-1}dw_j\wedge d\bar{w}_j =: \hat{\omega},$$

which is a mixed cylinder and edge metric by Definition 2.3.1, in $C^\infty(K)$ as $\beta_1\to 0$ and $\frac{\beta_1}{\beta_i}\to 0, \forall i=2,\dots,m$. □

2.3.3 Convergence of renormalized ω_{ϕ_β} near D_β

For a Kähler metric ξ on $\mathbb{C}^n$, let us denote $\bar{\xi} := \Psi_\beta^*\left(\frac{1}{\beta_1^2}\xi\right)$.

Theorem 2.3.3. *Let $\{\beta_{1,k}\}_{k\in\mathbb{N}}$ be a sequence of positive numbers converging to 0. Assume further that $\lim_{k\to\infty}\beta_{i,k}>0$ for each $i=2,\ldots,r$. Assume all $\beta_{i,k}\in(0,\frac{1}{2}]$. Let $\omega_{\phi_{\beta_k}}$ be the (negatively curved) Kähler–Einstein crossing edge metric on $(X, D_k=\sum_{i=1}^{r}(1-\beta_{i,k})D_i)$. Then there exists a subsequence of the metric spaces $\left(U_{\beta_k}, \frac{1}{\beta_{1,k}^2}\omega_{\phi_{\beta_k}}\right)$ which converges in pointed Gromov-Hausdorff topology to $((\mathbb{C}^*)^m\times\mathbb{C}^{n-m},\bar{\omega}_\infty)$, where $\bar{\omega}_\infty$ is a mixed cylindrical and conical metric. Indeed, a subsequence of $\bar{\omega}_{\phi_{\beta_k}}$ converges in $C^\infty_{\mathrm{loc}}((\mathbb{C}^*)^m\times\mathbb{C}^{n-m})$-topology to $\bar{\omega}_\infty$.*

Proof. First note that ω_{ϕ_β} admits a potential function on U_β since $\omega_{\beta,\mathrm{mod}}$ admits one. Thus, $\bar{\omega}_{\phi_\beta}$ admits a potential function on $\Psi_\beta^{-1}(U_\beta)$, denoted by $\bar{\phi}_\beta$. The proof consists of three steps. We first deduce the C^0-estimate of $\bar{\phi}_\beta$ using Theorem 2.2.4. Then we derive the $C^{2,\alpha}$-estimates for $\bar{\phi}_\beta$ by the standard regularization arguments for Monge–Ampère equations. This combining with Arzelà–Ascoli Theorem gives us a cluster value of the metrics. Finally, we use that smooth convergence to conclude the pointed Gromov–Hausdorff convergence as wanted.

Step 1: C^0-estimates.

Discussions in Section 2.3.1 indicate that there exists a uniform constant $C>0$ (independent of $\beta\in(0,\frac{1}{2}]^r$) such that

$$C^{-1}\omega_{\beta,\mathrm{mod}}\le\omega_{\phi_\beta}\le C\omega_{\beta,\mathrm{mod}}$$

on U_β. Thus

$$C^{-1}\Psi_\beta^*\left(\frac{1}{\beta_1^2}\omega_{\beta,\mathrm{mod}}\right)\le\bar{\omega}_{\phi_\beta}\le C\Psi_\beta^*\left(\frac{1}{\beta_1^2}\omega_{\beta,\mathrm{mod}}\right).$$

By Lemma 2.3.2, $\Psi_\beta^*(\frac{1}{\beta_1^2}\omega_{\beta,\mathrm{mod}})$ converges in $C^\infty(K)$ to $\hat{\omega}$ for any compact $K\subset(\mathbb{C}^*)^m\times\mathbb{C}^{n-m}$.

Hence, there exists a constant $C_K > 0$ (independent of β) such that

$$C_K^{-1}\hat{\omega} \le \bar{\omega}_{\phi_\beta} \le C_K\hat{\omega}. \tag{2.40}$$

By (2.40), $\bar{\omega}_{\phi_\beta}$ is uniformly bounded in mass on K. Then by the weak compactness of positive currents and the equivalence between this and the L^1-convergence of potential functions, we can find a normalized potential function $\bar{\phi}_\beta$ such that it has a uniform L^1_{loc} bound, hence uniform L^p_{loc} bounds, for any $p > 1$. By (2.40), $\Delta\bar{\phi}_\beta$ is uniformly bounded. Thus by standard elliptic regularity results, [23, Theorem 8.17], there exists a constant C independ of β such that

$$||\bar{\phi}_\beta||_{C^0(K)} \le C, \quad \text{for } C = C(K). \tag{2.41}$$

Step 2: Higher-order estimates and the smooth local convergence.

Since ω_{ϕ_β} satisfies the Kähler–Einstein equation outside D_β, $\bar{\omega}_{\phi_\beta}$ satisfies

$$\mathrm{Ric}\,\bar{\omega}_{\phi_\beta} = -\beta_1^2\bar{\omega}_{\phi_\beta} \quad \text{on } K. \tag{2.42}$$

Let dV_{eucl} denote the Euclidean volume form on $(\mathbb{C}^*)^m \times \mathbb{C}^{n-m}$. Define

$$H_\beta := \log \frac{\bar{\omega}_{\phi_\beta}^n e^{-\beta_1^2\bar{\phi}_\beta}}{dV_{\mathrm{eucl}}}.$$

H_β is pluriharmonic by (2.42). By the definition of H_β,

$$(\sqrt{-1}\partial\bar{\partial}\bar{\phi}_\beta)^n = e^{\beta_1^2\bar{\phi}_\beta + H_\beta} dV_{\mathrm{eucl}}. \tag{2.43}$$

By (2.40),

$$||\beta_1^2\bar{\phi}_\beta + H_\beta||_{C^0(K)} < +\infty. \tag{2.44}$$

Combining (2.41) and (2.44), we see $||H_\beta||_{C^0(K)} < +\infty$. Then by gradient estimates for pluri-harmonic functions,

$$||H_\beta||_{C^k(K)} < C(k,K), \quad \text{where } C(k,K) \text{ only depends on } k \text{ and } K \text{ not on } \beta. \tag{2.45}$$

Define

$$\Phi : \phi \mapsto \log \frac{(\sqrt{-1}\partial\bar{\partial}\phi)^n e^{-\beta_1^2\phi}}{dV_{\text{eucl}}}.$$

Φ is a uniform elliptic concave operator as a function of $\partial\bar{\partial}\phi$. Hence by Evans–Krylov theory, $||\phi||_{C^{2,\alpha}(K)}$ is controlled by $||\phi||_{C^0(K')}, ||\Delta\phi||_{C^0(K')}$ and $||\Phi(\phi)||_{C^{0,1}(K')}$ for some $K' \Supset K$. Since $\Phi(\bar{\phi}_\beta) = H_\beta$, by (2.45), (2.41) and the fact $||\Delta\bar{\phi}_\beta||_{C^0(K')} < +\infty$, there exist some $\alpha \in (0,1)$ and a uniform constant $C > 0$ such that

$$||\bar{\phi}_\beta||_{C^{2,\alpha}(K)} \leq C.$$

By standard bootstrapping arguments, every derivative of $\bar{\phi}_\beta$ is uniformly bounded on K. Then Arzelà-Ascoli theorem indicates $(\bar{\phi}_{\beta_k})_{k\in\mathbb{N}}$ has a convergent subsequence in $C^\infty(K)$-topology. Recall (2.42), letting $\beta_1 \to 0$ then due to the C^∞-convergence above we get a cluster value $\bar{\omega}_\infty$

such that

$$\operatorname{Ric}\bar{\omega}_\infty = 0.$$

By (2.40), $\bar{\omega}_\infty$ is quasi-isometric to $\hat{\omega}$, and therefore is a mixed cylinder and edge metric.

Step 3: Pointed Gromov–Hausdorff convergence

It remains to show a subsequence of $(U_{\beta_k}, \frac{1}{\beta_{1,k}^2}\omega_{\phi_{\beta_k}})$ converges in pointed Gromov-Hausdorff topology to $((\mathbb{C}^*)^m \times \mathbb{C}^{n-m}, \bar{\omega}_\infty)$. Fix $q \in (\mathbb{C}^*)^m \times \mathbb{C}^{n-m}$ and fix a radius $a > 0$. First note that by construction, $B_{\bar{\omega}_{\phi_{\beta_k}}}(q,a)$ is isometric to $B_{\frac{1}{\beta_{1,k}^2}\omega_{\phi_{\beta_k}}}(\Psi_{\beta_k}(q),a)$. Secondly, by letting the index $k \in \mathbb{N}$ be large enough, we have $B_{\bar{\omega}_\infty}(q,2a) \subset \Psi_{\beta_k}^{-1}(U_{\beta_k})$. Finally, due to the local C^∞-convergence, $B_{\bar{\omega}_{\phi_{\beta_k}}}(q,a) \subset B_{\bar{\omega}_\infty}(q,2a)$ and $B_{\bar{\omega}_{\phi_{\beta_k}}}(q,a)$ converges to $B_{\bar{\omega}_\infty}(q,a)$ in the Gromov-Hausdorff topology. Therefore $(U_{\beta_k}, \frac{1}{\beta_{1,k}^2}\omega_{\phi_{\beta_k}})$ converges (up to a subsequence) in pointed Gromov-Hausdorff topology to $((\mathbb{C}^*)^m \times \mathbb{C}^{n-m}, \bar{\omega}_\infty)$ by [7, Definition 8.1.1]. □

By the same idea in the proof of Theorem 2.3.3, we have the following results by modifying the result of Lemma 2.3.2.

Theorem 2.3.4. *Let $\{\beta_{1,k}\}_{k\in\mathbb{N}}$ be a sequence of positive numbers converging to 0. Assume further that for any $i = 2,\dots,r$ such that $\{\beta_{i,k}\}_{k\in\mathbb{N}}$ also converges to 0, there holds $\lim_{k\to\infty}\frac{\beta_{1,k}}{\beta_{i,k}} \in [0,1]$. Assume $\beta_{i,k} \in (0,\frac{1}{2}]$ for $i = 1,2,\dots,r$ and all $k \in \mathbb{N}$. Let $\omega_{\phi_{\beta_k}}$ be the (negatively curved) Kähler–Einstein crossing edge metric on $(X, D_k = \sum_{i=1}^r(1-\beta_{i,k})D_i)$. Then there exists a subsequence of the metric spaces $(U_{\beta_k}, \frac{1}{\beta_{1,k}^2}\omega_{\phi_{\beta_k}})$ converging in pointed Gromov-Hausdorff topology to $((\mathbb{C}^*)^m \times \mathbb{C}^{n-m}, \bar{\omega}_\infty)$, where $\bar{\omega}_\infty$ is a mixed cylinder and edge metric with cylindrical part along components whose cone angles converge to 0 and conical part along other components.*

Chapter 3: Large and small angle limits of KEE metrics on Calabi–Hirzebruch manifolds

This is based on joint work with Yanir A. Rubinstein and Kewei Zhang.

3.1 Motivation

In the preceding chapter, we considered the small angle limits of KEE metrics that are *negatively curved*. In this chapter, we will focus on certain KEE metrics that are positively curved.

3.1.1 KEE metrics on $\mathbb{P}^1$

Recall (1.4), there exists a positively curved Kähler–Einstein metric on $\mathbb{P}^n$, namely the Fubini–Study metric. In the simplest case, $\mathbb{P}^1$, let us denote the homogeneous coordinate by $[Z_0 : Z_1]$ and consider the chart $\{Z_0 \neq 0\}$ with local holomorphic coordinate $z := Z_1/Z_0$. The Fubini–Study metric is given by

$$\begin{aligned}\omega_{\mathrm{FS}} &= \sqrt{-1}\partial\bar{\partial}\log(1+|z|^2)\\ &= \frac{\sqrt{-1}}{(1+|z|^2)^2}dz\wedge d\bar{z}.\end{aligned}$$

We identify $\mathbb{P}^1$ with the unit sphere $S^2 \subset \mathbb{R}^3$ such that the north pole N corresponds to $[1:0] \in \mathbb{P}^1$ and the south pole S to $[0:1] \in \mathbb{P}^1$. Under this identification, the chart $\{Z_0 \neq 0\}$ is exactly $S^2 \setminus \{S\}$, on which the standard round metric reads

$$\omega_{\text{round}} = 2\omega_{\text{FS}} = \frac{2\sqrt{-1}}{(1+|z|^2)^2} dz \wedge d\bar{z}. \tag{3.1}$$

From now on, we identify $\mathbb{P}^1$ with S^2 and make no difference between them. The KEE metric on $\mathbb{P}^1$ with edge singularities along $\{Z_0 = 0\}$ and $\{Z_1 = 0\}$ is exactly the KEE metric on S^2 with edge singularities at the two poles. The KEE equation in this case is as follows (cf. (1.8)):

$$\operatorname{Ric} \omega = \omega + 2\pi(1-\beta_1)[N] + 2\pi(1-\beta_2)[S], \tag{3.2}$$

where β_1 and β_2 are cone angles.

The solution to (3.2) is explicitly known as follows. The cone angles must satisfy $\beta_1 = \beta_2$ to admit a solution. Denoting by β the cone angle $\beta_1 = \beta_2$, the KEE metric reads

$$\omega_{S^2,KEE} = \sqrt{-1}\frac{2\beta^2|z|^{2\beta-2}}{(1+|z|^{2\beta})^2} dz \wedge d\bar{z}. \tag{3.3}$$

Remark 3.1.1. Indeed, the KEE metric $\omega_{S^2,KEE}$ can be obtained by pulling back the standard round metric from a wedge to $\mathbb{C}$, under the map $z \mapsto z^\beta$:

$$\begin{aligned} &\mathbb{C} \to \{w = re^{i\theta} \in \mathbb{C} : r > 0, 0 \leq \theta < 2\pi\beta\} \\ &z \mapsto z^\beta. \end{aligned}$$

According to (3.3), the KEE metric on $\mathbb{P}^1$ converges smoothly to the standard round metric

(3.1) on $\mathbb{P}^1$ as $\beta \to 1$. On the other side, the renormalized metric $\omega_{S^2,KEE}/\beta^2$ restricted to $\mathbb{P}^1 \setminus \{Z_0 Z_1 = 0\}$ converges to the cylinder metric

$$\frac{\sqrt{-1}}{2|z|^2} dz \wedge d\bar{z}, \quad z \in \mathbb{C}^*$$

smoothly as $\beta \to 0$.

Remark 3.1.2. In [49], the authors further studied on $\mathbb{P}^1$ the Kähler–Ricci soliton equation with edge singularities, cf. (1.11),

$$\operatorname{Ric} \omega = \omega - \sqrt{-1}\partial\bar{\partial} h + 2\pi(1 - \beta_1)[N] + 2\pi(1 - \beta_2)[S],$$

where h is a real-valued smooth function with holomorphic gradient vector field. Under this setting, the cone angles must be different to recover non-trivial soliton metrics other than the trivial one: the KEE metric on $\mathbb{P}^1$. The small angle limits of such edge soliton metrics lead to either the cigar soliton or cylinder metrics under different renormalizations [50, Theorem 1.2 and 1.3].

3.1.2 Calabi–Hirzebruch manifolds as a generalization of $\mathbb{P}^1$

A natural generalization of $\mathbb{P}^1$ to the higher dimension is $\mathbb{P}^n$. However, by identifying $\mathbb{P}^1$ as a $\mathbb{P}^1$-fibration over a point, there is another way to generalize it to higher dimensional spaces: we consider $\mathbb{P}^1$-fibration over $\mathbb{P}^{n-1}$ base, for $n \geq 2$.

To this end, Hirzebruch [35] constructed a family of complex surfaces

$$\mathbb{F}_k := \mathbb{P}(-kH_{\mathbb{P}^1} \oplus \mathbb{C}_{\mathbb{P}^1}), \quad , k \geq 1$$

where $-kH_{\mathbb{P}^1}$ is the total space of the k-times tensor product of the tautological bundle, and $\mathbb{C}_{\mathbb{P}^1}$ is the trivial bundle over $\mathbb{P}^1$. This construction can be understood as $\mathbb{P}^1$ bundles over the base $\mathbb{P}^1$.

Calabi [9] generalized the idea of Hirzrbruch to $\mathbb{P}^1$-fibrations over the base $\mathbb{P}^{n-1}$, and introduced the following definition, which will be the focus of this chapter:

Definition 3.1.3. The Calabi–Hirzebruch manifold, denoted by $\mathbb{F}_{n,k}$, where $n, k \in \mathbb{N}$, is defined as follows:

$$\mathbb{F}_{n,k} := \mathbb{P}(-kH_{\mathbb{P}^{n-1}} \oplus \mathbb{C}_{\mathbb{P}^{n-1}}), \quad n, k \in \mathbb{N},$$

where $H_{\mathbb{P}^{n-1}}$ is the hyperplane bundle over $\mathbb{P}^{n-1}$ and $\mathbb{C}_{\mathbb{P}^{n-1}}$ is the trivial one.

The similarity between $\mathbb{F}_{n,k}$ and $\mathbb{P}^1$ lies in the fact that they both admit disjoint divisors: on $\mathbb{P}^1$, we have the KEE metrics (3.3) that admit edge singularities at the north and south poles. On $\mathbb{F}_{n,k}$, we denote by $[Z_1 : \cdots : Z_n]$ the homogeneous coordinates on the base $\mathbb{P}^{n-1}$. Working on the chart $\{Z_i \neq 0\}$, we shall use the nonhomogeneous coordinates $z_j := Z_j/Z_i$ for all $j \neq i$. Denote by w the coordinate along each fiber on $-kH_{\mathbb{P}^{n-1}}$. Then $w \in \mathbb{C}$ for $-kH_{\mathbb{P}^{n-1}}$ and $w \in \mathbb{C} \cup \{\infty\}$ for $\mathbb{F}_{n,k}$. Analogous to $\mathbb{P}^1$, we also have two disjoint divisors on $\mathbb{F}_{n,k}$: the zero section

$$Z_{n,k} := \{w = 0\} \tag{3.4}$$

and the infinity section

$$Z_{n,-k} := \{w = \infty\}. \tag{3.5}$$

In this chapter, we will construct positively curved KEE metrics that admit edge singularities along these two divisors on $\mathbb{F}_{n,k}$, which generalizes the construction of KEE metrics on $\mathbb{P}^1$.

Furthermore, we study the asymptotic behavior of these KEE metrics and show that the limit metrics recover several classical constructions.

3.1.3 Examples of Ricci-flat metric

In the preceding sections, we focused on KEE metrics that are positively curved. In this section, we briefly divert (though not entirely) our attention to introduce two classical constructions of Ricci-flat metrics.

We start from a specific dimension: the complex dimension 2.

Eguchi–Hanson metrics are constructed about half a century ago [21]. It is one of the earliest discovered Ricci-flat metrics that are not flat. They are initially defined locally on $\mathbb{C}^2 \setminus \{0\}$ and soon be extended (so that no longer being singular) to the complex manifold: the total space of the line bundle $-2H_{\mathbb{P}^1}$.

We start from the construction on $\mathbb{C}^2 \setminus \{0\}$. For $(x_1 + \sqrt{-1}y_1, x_2 + \sqrt{-1}y_2) \in \mathbb{C}^2$, the Hopf coordinates are defined as:

$$\begin{aligned} x_1 + \sqrt{-1}y_1 &= \xi \cos\frac{\theta}{2} e^{\frac{\sqrt{-1}}{2}(\psi+\phi)}, \\ x_2 + \sqrt{-1}y_2 &= \xi \sin\frac{\theta}{2} e^{\frac{\sqrt{-1}}{2}(\psi-\phi)}, \end{aligned}$$

for $\xi \geq 0$, $\theta \in [0,\pi]$, $\psi \in [0,4\pi]$ and $\phi \in [0,2\pi]$. Then, we define one-forms on $\mathbb{C}^2$ by

$$\begin{aligned}
\sigma_1 :&= \frac{1}{\xi^2}(x_1 dy_2 - y_2 dx_1 + y_1 dx_2 - x_2 dy_1) = \frac{1}{2}(\sin\psi d\theta - \sin\theta\cos\psi d\phi), \\
\sigma_2 :&= \frac{1}{\xi^2}(y_1 dy_2 - y_2 dy_1 + x_2 dx_1 - x_1 dx_2) = \frac{1}{2}(-\cos\psi d\theta - \sin\theta\sin\psi d\phi), \\
\sigma_3 :&= \frac{1}{\xi^2}(x_2 dy_2 - y_1 dx_2 + x_1 dy_1 - y_1 dx_1) = \frac{1}{2}(d\psi + \cos\theta d\phi).
\end{aligned} \tag{3.6}$$

Direct calculations yield:

$$\begin{aligned}
d\sigma_1 &= 2\sigma_2 \wedge \sigma_3, \\
d\sigma_2 &= 2\sigma_3 \wedge \sigma_1, \\
d\sigma_3 &= 2\sigma_1 \wedge \sigma_2.
\end{aligned} \tag{3.7}$$

The standard Euclidean metric on $\mathbb{C}^2$ can be written as

$$dx_1^2 + dy_1^2 + dx_2^2 + dy_2^2 = d\xi^2 + \xi^2(\sigma_1^2 + \sigma_2^2 + \sigma_3^2).$$

The Eguchi–Hanson metric with parameter $\epsilon > 0$ is defined by

$$g_{\mathrm{EH},\epsilon} := \left(1 - \frac{\epsilon^4}{\xi^4}\right)^{-1} d\xi^2 + \xi^2\left(\sigma_1^2 + \sigma_2^2 + \left(1 - \frac{\epsilon^4}{\xi^4}\right)\sigma_3^2\right), \quad \xi \geq \epsilon. \tag{3.8}$$

Proposition 3.1.4. *Eguchi–Hanson metrics defined in* (3.8) *are Ricci-flat.*

Proof. We provide a proof by directly calculating connection forms and curvature forms of the metric. See Remark 3.1.5 for another proof using Kähler forms of Eguchi–Hanson metrics. Consider a change of variable $\zeta = \zeta(\xi)$ such that $d\zeta = (1 - (\epsilon/\xi)^4)^{-1/2} d\xi$. Then we can write (3.8) in the form

$$g_{\mathrm{EH},\epsilon} = d\zeta^2 + f^2(\zeta)(\sigma_1^2 + \sigma_2^2 + g^2(\zeta)\sigma_3^2),$$

where $f = \xi$ and $g = (1 - (\epsilon/\xi)^4)^{1/2}$. Consider an orthonormal basis

$$(\omega^0, \omega^1, \omega^2, \omega^3) = (d\zeta, fg\sigma_3, f\sigma_1, f\sigma_2).$$

Then $g_{\mathrm{EH},\epsilon} = \sum_{i=0}^{3}(\omega^i)^2$ and $\{\omega^i\}_{i=0}^{3}$ satisfy the following equations:

$$\begin{aligned} d\omega^i &= \omega^j \wedge \omega_j^i, \quad \text{for } i = 0,1,2,3, \\ \omega_i^j + \omega_j^i &= 0, \quad \text{for } i,j = 0,1,2,3, \end{aligned}$$

where $\{\omega_i^j\}_{i,j=0}^{3}$ are connection forms with respect to $\{\omega^i\}_{i=0}^{3}$. Next let us determine connection forms. For $i = 1$, we have

$$d\omega^1 = \frac{f'g + fg'}{fg}\omega^0 \wedge \omega^1 + \frac{2g}{f}\omega^2 \wedge \omega^3,$$

where f' and g' denote the derivative with respect to ζ. Without loss of generality, we let

$$\begin{aligned} \omega_0^1 &= \frac{f'g + fg'}{fg}\omega^1, \\ \omega_2^1 &= \frac{g}{f}\omega^3, \\ \omega_3^1 &= -\frac{g}{f}\omega^2. \end{aligned} \tag{3.9}$$

It remains to find ω_0^2, ω_0^3 and ω_2^3 due to the skew-symmetry of connection forms. By similar calculations we have

$$
\begin{aligned}
d\omega^2 &= \frac{f'}{f}\omega^0 \wedge \omega^2 + \frac{2}{fg}\omega^3 \wedge \omega^1, \\
d\omega^3 &= \frac{f'}{f}\omega^0 \wedge \omega^3 + \frac{2}{fg}\omega^1 \wedge \omega^2.
\end{aligned}
\tag{3.10}
$$

Thus, combining (3.9) and (3.10) we obtain

$$
\begin{aligned}
\omega_0^2 &= \frac{f'}{f}\omega^2, \\
\omega_0^3 &= \frac{f'}{f}\omega^3, \\
\omega_2^3 &= \frac{g^2-2}{fg}.
\end{aligned}
\tag{3.11}
$$

Notice that

$$
\begin{aligned}
&f' = \frac{d\xi}{d\zeta} = (1-(\epsilon/\xi)^4)^{1/2} = g, \\
&g' = 2\epsilon^4 f^{-5}.
\end{aligned}
\tag{3.12}
$$

Combining (3.9), (3.11) and (3.12) we see

$$
\begin{aligned}
\omega_0^1 &= -\omega_2^3, \\
\omega_2^1 &= \omega_0^3, \\
\omega_3^1 &= -\omega_0^2.
\end{aligned}
\tag{3.13}
$$

By (3.13) and the fact that $R_i^j = d\omega_i^j - \omega_i^k \wedge \omega_k^j$, for $i, j = 0, 1, 2, 3$, we obtain that the curvature forms also satisfy

$$R_0^1 = -R_2^3,$$

$$R_2^1 = R_0^3,$$

$$R_3^1 = -R_0^2.$$

Finally, the Ricci-flatness comes from the formula $\mathrm{Ric}_{ij} = \sum_{k=0}^{3} R_{ikj}^k$ and the first Bianchi identity. $\square$

Introduce

$$r^4 = \xi^4 - \epsilon^4, \quad \xi \geq \epsilon,$$

then (3.8) can be written as

$$g_{\mathrm{EH},\epsilon} = \frac{r^2}{(\epsilon^4 + r^4)^{\frac{1}{2}}}(dr^2 + r^2\sigma_3^2) + (\epsilon^4 + r^4)^{\frac{1}{2}}(\sigma_1^2 + \sigma_2^2), \quad r \geq 0. \tag{3.14}$$

From (3.14) we are able to convert Eguchi–Hanson metrics into complex form by letting $(z_1, z_2) \in \mathbb{C}^2$ satisfy

$$\begin{aligned} z_1 &= r\cos\frac{\theta}{2}e^{\frac{\sqrt{-1}}{2}(\psi+\phi)}, \\ z_2 &= r\sin\frac{\theta}{2}e^{\frac{\sqrt{-1}}{2}(\psi-\phi)}. \end{aligned} \tag{3.15}$$

Denote by $\omega_{\mathrm{EH},\epsilon}$ the Kähler form corresponding to $g_{\mathrm{EH},\epsilon}$. Then by (3.14) we have in complex coordinates,

$$\omega_{\mathrm{EH},\epsilon} = \sqrt{-1}\partial\bar{\partial}[\sqrt{r^4+\epsilon^4} + \log r^2 - \log(\epsilon^2 + \sqrt{r^4+\epsilon^4})] \tag{3.16}$$

$$= \frac{\sqrt{-1}r^2}{\sqrt{r^4+\epsilon^4}}(dz_1 \wedge d\bar{z}_1 + dz_2 \wedge d\bar{z}_2) + \frac{\epsilon^4}{\sqrt{r^4+\epsilon^4}}\sqrt{-1}\partial\bar{\partial}\log(r^2). \tag{3.17}$$

Remark 3.1.5. By calculating the Ricci form of $\omega_{\mathrm{EH},\epsilon}$ as in (3.17), we can also derive the Ricci-flatness of Eguchi–Hanson metrics. Indeed, from (3.17) we calculate

$$\begin{aligned}
\operatorname{Ric}\omega_{\mathrm{EH},\epsilon} &= \operatorname{Ric}\sqrt{-1}\Bigg(\left[\frac{r^2}{\sqrt{r^4+\epsilon^4}} + \frac{\epsilon^4|z_2|^2}{\sqrt{r^4+\epsilon^4}r^4}\right]dz_1 \wedge d\bar{z}_1 \\
&\quad - \frac{\epsilon^4 z_2\bar{z}_1}{\sqrt{r^4+\epsilon^4}r^4}dz_1 \wedge d\bar{z}_2 - \frac{\epsilon^4 z_1\bar{z}_2}{\sqrt{r^4+\epsilon^4}r^4}dz_2 \wedge d\bar{z}_1 \\
&\quad + \left[\frac{r^2}{\sqrt{r^4+\epsilon^4}} + \frac{\epsilon^4|z_1|^2}{\sqrt{r^4+\epsilon^4}r^4}\right]dz_2 \wedge d\bar{z}_2\Bigg) \\
&= -\sqrt{-1}\partial\bar{\partial}\log\Bigg(\left[\frac{r^2}{\sqrt{r^4+\epsilon^4}} + \frac{\epsilon^4|z_2|^2}{\sqrt{r^4+\epsilon^4}r^4}\right]^2 \\
&\quad - \frac{\epsilon^4|z_1|^2|z_2|^2}{(r^4+\epsilon^4)r^8}\Bigg) \\
&= -\sqrt{-1}\partial\bar{\partial}\log 1 \\
&= 0.
\end{aligned}$$

From (3.14) one finds that $g_{\mathrm{EH},\epsilon}$ is defined on $\mathbb{C}^2$ with singularity at $r = 0$. Since $g_{\mathrm{EH},\epsilon}$ is invariant under the antipodal reflection, we have an induced metric on $(\mathbb{C}^2 \setminus \{0\})/\mathbb{Z}_2$ that admits no singularity. The last step is to consider the blow-up of $(\mathbb{C}^2 \setminus \{0\})/\mathbb{Z}_2$ at the origin, which is biholomorphic to the total space of the line bundle $-2H_{\mathbb{P}^1}$, then a calculation in (3.76) below shows that $\sigma_1^2 + \sigma_2^2$ is the pull-back of the Fubini–Study metric from the exceptional divisor.

Hence $g_{\mathrm{EH},\epsilon}$ extends to a metric on the total space $-2H_{\mathbb{P}^1}$ by letting $r = 0$ when restricting $g_{\mathrm{EH},\epsilon}$ to the exceptional divisor, as in (3.17).

More generally, Calabi constructed the following family of Ricci-flat (See Theorem 3.6.1 for a proof of Ricci-flatness) metrics that generalizes the construction of Eguchi and Hanson, on the total space of $-nH_{\mathbb{P}^{n-1}}$. To streamline the presentation, we recall the coordiante system we used when defining (3.4) and (3.5).

Consider the Hermitian norm on $-kH_{\mathbb{P}^{n-1}}$ (and also $\mathbb{F}_{n,k}$) that is defined as

$$||(z_1, \ldots, \hat{z}_i, \ldots, z_n, w)|| := |w|^2 \left(1 + \sum_{j \neq i}^{n} |z_j|^2\right)^k,$$

on the chart $\{Z_i \neq 0\}$. Let s be the logarithm of this fiberwise norm, i.e.,

$$s := \log |w|^2 + k \log \left(1 + \sum_{j \neq i} |z_j|^2\right). \tag{3.18}$$

Let s be defined in (3.18). Fix $k = n$, i.e., assume that the fibers are those of the line bundle $-nH_{\mathbb{P}^{n-1}}$. Considers a change of coordinate $\lambda \in (1, +\infty)$ such that

$$\lambda = (e^s + 1)^{\frac{1}{n}}. \tag{3.19}$$

Note that $\{\lambda = 1\}$ corresponds to the zero section $Z_{n,n} = \{w = 0\}$ on $-nH_{\mathbb{P}^{n-1}}$. Calabi's metrics, denoted by $\omega_{\mathrm{ceh},n}$ is defined by giving its potential function as follows:

$$f(\lambda) := n\lambda + n \int \frac{1}{\lambda^n - 1}\, d\lambda, \tag{3.20}$$

where the last term denotes an indefinite integral, and

$$\omega_{\mathrm{ceh},n} := \sqrt{-1}\partial\bar{\partial}f(\lambda). \tag{3.21}$$

3.1.4 Relating the KEE and Ricci-flat metrics

The contribution of us is to first construct KEE metrics on $\mathbb{F}_{n,k}$ and then study the limit behavior of these metrics. We summarize all the interesting limit behaviors in Table 3.1, and in particular, we show that the Eguchi–Hanson metric and Calabi's Ricci flat metrics defined on non-compact spaces are pointed Gromov–Hausdorff limits of the singular metrics defined on compact spaces.

3.2 Results

In Section 3.3, we will define two (families of) model metrics. The first are Ricci-flat edge metrics on the total space of the (non-compact) line bundle $-kH_{\mathbb{P}^{n-1}}$,

$$\omega_{\mathrm{eh},n,k},$$

and an edge singularity of the angle $2\pi n/k$ along $Z_{n,k}$. The second are compact Kähler–Einstein edge spaces with positive Ricci curvature $(n+1)/k$ and an edge singularity of angle $2\pi/k$,

$$\omega_{\mathrm{orb},n,k},$$

on the weighted projective space $\mathbb{P}^n(1,\ldots,1,k)$, cf. Definition 3.3.3. These two model spaces turn out to be the different Gromov–Hausdorff limits of large-angle limits of the KEE metrics we construct on the Calabi–Hirzebruch manifolds.

3.2.1 Large angle limits

The following result describes precisely the different large-angle limits that arise from the KEE metrics we construct, by either using different pointed limits or else parametrizing the angles in different ways. Denote by η_{β_1} the KEE metrics that exist on $\mathbb{F}_{n,k}$ with cone angle β_1 along $Z_{n,k}$, and by ξ_{β_2} the one with cone angle β_2 along $Z_{n,-k}$. It will be shown that β_1 ranges in $(0, n/k)$ and β_2 ranges in $(0, 1/k)$.

Theorem 3.2.1. *Fix a base point p on the zero section of $\mathbb{F}_{n,k}$ and q on the infinity section. The pointed metric space $(\mathbb{F}_{n,k}, \eta_{\beta_1}, p)$ converges in the pointed Gromov–Hausdorff sense to $(-kH_{\mathbb{P}^{n-1}}, \omega_{\mathrm{eh},n,k}, p)$ as β_1 tends to n/k. On the other hand, $(\mathbb{F}_{n,k}, \xi_{\beta_2}, q)$ converges in the pointed Gromov–Hausdorff sense to $(\mathbb{P}^n(1,\ldots,1,k), \omega_{\mathrm{orb},n,k}, q)$ as $\beta_2 \to 1/k$.*

In particular, when $n = k = 2$, Theorem 3.2.1 amounts to saying that the Eguchi–Hanson metric (3.14) is the Gromov–Hausdorff limit of *compact* Kähler–Einstein edge metrics that we construct on the second Hirzebruch surface (see Remark 3.6.3 for more details). More generally, when $n = k$, Theorem 3.2.1 recovers Calabi's Ricci-flat metrics (3.21), once again as a limit of *compact* Einstein spaces.

The proof of Theorem 3.2.1 is divided into two parts. In Section 3.5, we study asymptotic behaviors of Kähler–Einstein edge metrics η_{β_1} and ξ_{β_2} when β_1, or respectively β_2, is close to n/k or $1/k$. In Section 3.6, we prove the convergence results by studying a family of ODEs that

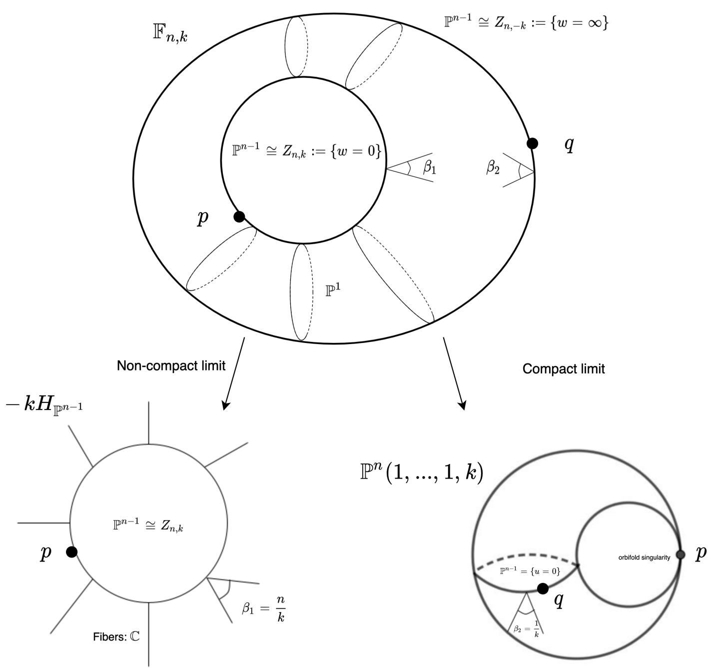

Figure 3.1: The upper part shows the Kähler edge structure on the Calabi–Hirzebruch manifold $\mathbb{F}_{n,k}$. When $n = 2$, $\mathbb{F}_{2,k}$ is the k-th Hirzebruch surface and $Z_{2,\pm k}$ is a $\mp k$-curve. The lower part shows the different limits described in Theorem 3.2.1. Note that on the left, we get a non-compact limit, with q (together with all of $Z_{n,-k}$) pushed-out to infinity. On the right we get a compact limit, with p limiting (together with all of $Z_{n,k}$) to an isolated orbifold point.

arises from the construction of η_{β_1} and ξ_{β_2}.

Remark 3.2.2. The two families of Kähler–Einstein edge metrics η_{β_1} and ξ_{β_2} are related via a simple, but important, rescaling. In Theorem 3.2.1, we see that different limits airse for those two family of metrics. The normalization factor can be obtained by studying the asymptotic behavior of ξ_{β_2}: see Proposition 3.5.5 for details.

Remark 3.2.3. As noted before Theorem 3.2.1, β_1 ranges in $(0, n/k)$ and β_2 ranges in $(0, 1/k)$. In proving Theorem 3.2.1 for the family η_{β_1} one obtains the asymptotic dependence of β_2 on β_1 in terms of a parameter that controls the length of the fibers in the Hirzebruch fibration—see (3.55). This shows that as β_1 tends to its maximal value n/k, β_2 tends to its maximal value as well, $1/k$, and the divisor $Z_{n,k}$ gets pushed-off to infinity. When we consider the family ξ_{β_2} parametrized in terms of β_2, let β_2 tend towards $1/k$, while the parameter β_1 still tends towards its maximal value n/k we get a completely different limiting behavior: instead of a non-compact limit we get a compact limit via a metric degeneration along $Z_{n,k}$. Thus, studying the two families is an essential feature of the setting and leads to two completely different Gromov–Hausdorff limits as in Theorem 3.2.1.

Remark 3.2.4. Abreu [1, §5] and subsequently Atiyah–LeBrun [3, (5.5)–(5.6)] also studied a family of Einstein metrics with orbifold/edge singularities converging (roughly) to the Eguchi–Hanson metric. However, there are important differences between their construction and ours: (i) their metrics are *not* Kähler, (ii) they work on the space $\mathbb{P}^2$ while we work on the second Hirzebruch surface $\mathbb{F}_2$ (which generalizes to $\mathbb{F}_{n,k}$ in higher-dimensions), (iii) the metrics they construct in the sequence are singular along a single $\mathbb{P}^1$ divisor instead of two $\mathbb{P}^1$ divisors, as in our construction, (iv) their limit metric is not precisely the Eguchi–Hanson metric, but rather its double cover (they obtain an angle of 4π along a $\mathbb{P}^1$ divisor).

3.2.2 Small angle limits

Next, we consider small angle limits in the setting of $\mathbb{F}_{n,k}$. Denote by $\widetilde{\eta_{\beta_1}}$ and $\widetilde{\xi_{\beta_2}}$ fiber-wise rescalings of $\eta_{\beta_1}, \xi_{\beta_2}$, respectively (see (3.71) and §3.7).

Theorem 3.2.5. *Both $(\mathbb{F}_{n,k}, \eta_{\beta_1})$ and $(\mathbb{F}_{n,k}, \xi_{\beta_2})$ converge in the Gromov–Hausdorff sense to $(\mathbb{P}^{n-1}, k\omega_{\mathrm{FS}})$ as β_1 or β_2 tends to 0. Moreover, as $\beta_1 \searrow 0$, $(\mathbb{F}_{n,k}, \widetilde{\eta_{\beta_1}}, p)$ converges in the pointed Gromov–Hausdorff sense to $(\mathbb{P}^{n-1} \times \mathbb{C}^*, \frac{k}{n}(n\pi_1^*\omega_{\mathrm{FS}} + \pi_2^*\omega_{\mathrm{Cyl}}), p)$ and similarly for $(\mathbb{F}_{n,k}, \widetilde{\xi_{\beta_2}}, q)$, where $p, q \in \mathbb{F}_{n,k}$ are as in Theorem 3.2.1.*

A compendium of the limit theorems in [49, 50] and the present work is shown in Table 1.

n	k	β_1	β_2	Sequence	Limit	Reference
1	k	$\beta_1 \searrow 0$	$\beta_2(\beta_1) \equiv \beta_1$	football metrics	$(\mathbb{C}^*, \omega_{\mathrm{Cyl}})$	folklore, [49, Thm 1.3]
1	k	$\beta_1 \nearrow 1$	$\beta_2(\beta_1) \equiv \beta_1$	football metrics	$(\mathbb{P}^1, \omega_{\mathrm{FS}})$	folklore, [49, Thm 1.2]
2	k	$\beta_1 \searrow 0$	$\beta_2(\beta_1) = \beta_1 + O(\beta_1^2)$	KEE metrics	$(\mathbb{P}^1, k\omega_{\mathrm{FS}})$	[50, Thm 1.2]
2	k	$\beta_1 \searrow 0$	$\beta_2(\beta_1) = \beta_1 + O(\beta_1^2)$	rescaled KEE metrics	$(\mathbb{P}^1 \times \mathbb{C}^*, k\pi_1^*\omega_{\mathrm{FS}} + k\pi_2^*\omega_{\mathrm{Cyl}})$	[50, Thm 1.2]
2	1	$\beta_1 \to 1$	$\beta_2(\beta_1) \to \sqrt{3} - 1$	KEE metrics	KEE metric on $(\mathbb{F}_1, Z_{-1})$	[50, Cor 1.5]
2	1	$\beta_1 \nearrow 2$	$\beta_2(\beta_1) \nearrow 1$	KEE metrics	Ricci-flat metric on $(-H_{\mathbb{P}^1}, Z_1)$	Thm 3.9.3
2	1	the metric degenerates on Z_1	$\beta_2 \nearrow 1$	KEE metrics	$(\mathbb{P}^2, \omega_{\mathrm{FS}})$	Thm 3.9.5.
2	1	$\beta_1(\beta_2) \nearrow 2$	$\beta_2 \nearrow 1$	rescaled KEE metrics	Ricci-flat metric on $(-H_{\mathbb{P}^1}, Z_1)$	Thm 3.9.7
2	2	$\beta_1 \nearrow 1$	$\beta_2(\beta_1) \nearrow 2$	KEE metrics	Eguchi–Hanson metric ($\epsilon = 1$)	Thm 3.6.1
2	k	the metric degenerates on $Z_{2,k}$	$\beta_2(\beta_1) \nearrow 1/k$	KEE metrics	$(\mathbb{P}^2(1,1,k), \omega_{\mathrm{orb},2,k})$	Thm 3.6.4
n	1	the metric degenerates on $Z_{n,1}$	$\beta_2(\beta_1) \nearrow 1$	KEE metrics	$(\mathbb{P}^n, \omega_{\mathrm{FS}})$	Thm 3.6.4
n	k	$\beta_1 \nearrow n/k$	$\beta_2(\beta_1) \nearrow 1/k$	KEE metrics	$(-kH_{\mathbb{P}^{n-1}}, \omega_{\mathrm{eh},n,k})$	Thm 3.6.1
n	k	$\beta_1 \searrow 0$	$\beta_2(\beta_1) = \beta_1 + O(\beta_1^2)$	rescaled KEE metrics	$(\mathbb{P}^{n-1} \times \mathbb{C}^*, \frac{k}{n}(n\pi_1^*\omega_{\mathrm{FS}} + \pi_2^*\omega_{\mathrm{Cyl}}))$	Thm 3.7.6
n	k	the metric degenerates on $Z_{n,k}$	$\beta_2 \nearrow 1/k$	KEE metrics	$(\mathbb{P}^n(1,\ldots,1,k), \omega_{\mathrm{orb},n,k})$	Thm 3.6.4
n	k	$\beta_1(\beta_2) \nearrow n/k$	$\beta_2 \nearrow 1/k$	rescaled KEE metrics	$(-kH_{\mathbb{P}^{n-1}}, \omega_{\mathrm{eh},n,k})$	Cor 3.6.5
n	k	$\beta_1(\beta_2) = \beta_2 + O(\beta_2^2)$	$\beta_2 \searrow 0$	rescaled KEE metrics	$(\mathbb{P}^{n-1} \times \mathbb{C}^*, \frac{k}{n}(n\pi_1^*\omega_{\mathrm{FS}} + \pi_2^*\omega_{\mathrm{Cyl}}))$	Thm 3.7.11

Table 3.1: Limits of Kähler–Einstein edge metrics on $\mathbb{F}_{n,k}$, the k-th Calabi–Hirzebruch manifold of dimension n.

3.2.3 Organization

In Section 3.3, we define two families of model metrics respectively on the total space of line bundles $-kH_{\mathbb{P}^{n-1}}$ and the weighted projective space. In Section 3.4, we construct Kähler–Einstein edge metrics on the Calabi–Hirzebruch manifolds following Calabi ansatz. In Section 3.5, we study the asymptotic behaviors of Kähler–Einstein edge metrics by reducing it to the study of some ODEs. In Section 3.6, we consider the Gromov–Hausdorff limits of the Kähler–Einstein edge metrics on the Calabi–Hirzebruch manifolds and find out the model metrics in the limit. Theorem 3.2.1 is then proved in two parts: Theorem 3.6.1 and Theorem 3.6.4. The first statement of Theorem 3.2.5 about the non-rescaled limits is proved in Theorems 3.7.1 and 3.7.10. The second statement of Theorem 3.2.5 concerning rescaled limits and pointed limits is contained in Theorems 3.7.6 and 3.7.11. We also discuss the relation between Theorem 3.6.1 and Theorem 3.6.4 as mentioned in Remark 3.2.2 in Corollary 3.6.5. $\mathbb{P}^1$-fibrations over the base $\mathbb{P}^{n-1}$ Appendices 3.8 explain how to understand Eguchi–Hanson metrics as Gromov–Hausdorff limits of Kähler–Einstein edge metrics. In Appendix 3.9, we provide more examples of Kähler–Einstein edge metrics and their Gromov–Hausdorff limit metrics.

3.3 Model metrics

In this section, we introduce two model metrics $\omega_{\mathrm{eh},n,k}$ and $\omega_{\mathrm{orb},n,k}$, that are defined respectively on the total space of line bundles $-kH_{\mathbb{P}^{n-1}}$ and the weighted projective space $\mathbb{P}^n(1,\dots,1,k)$, cf. Definition 3.3.3. They will serve as the candidates of limit metrics in the latter sections.

Recalling the logarithmic of the fiberwise norm (3.18), we will define model metrics that depend only on s on $-kH_{\mathbb{P}^{n-1}}$ and $\mathbb{P}^n(1,\dots,1,k)$.

3.3.1 Non-compact case: model metrics on $-kH_{\mathbb{P}^{n-1}}$

The first model metric, $\omega_{\mathrm{eh},n,k}$, is a Ricci-flat edge metric with edge singularity of angle $2n\pi/k$ along the zero section $Z_{n,k}$ of $-kH_{\mathbb{P}^{n-1}}$. In particular, when $n = k$, this metric is smooth. Indeed, when $n = k$, $\omega_{\mathrm{eh},n,k}$ coincides with the Ricci-flat metric on the canonical bundle of $\mathbb{P}^{n-1}$ that was constructed by Calabi [8].

Definition 3.3.1. Let s be defined in (3.18). To define $\omega_{\mathrm{eh},n,k}$, introduce another coordinate $\lambda \in (1, +\infty)$ such that

$$\lambda = (e^{\frac{n}{k}s} + 1)^{\frac{1}{n}}. \tag{3.22}$$

Thus $\{\lambda = 1\}$ corresponds to the zero section $Z_{n,k} = \{w = 0\}$ on $-kH_{\mathbb{P}^{n-1}}$. We define $\omega_{\mathrm{eh},n,k}$ by giving its potential function as follows:

$$f(\lambda) := k\lambda + k \int \frac{1}{\lambda^n - 1}\, d\lambda, \tag{3.23}$$

where the last term denotes an indefinite integral, and

$$\omega_{\mathrm{eh},n,k} := \sqrt{-1}\partial\bar{\partial} f(s).$$

The metric $\omega_{\mathrm{eh},n,k}$ is a Ricci-flat metric on $-kH_{\mathbb{P}^{n-1}}$ with edge singularity of angle $2n\pi/k$ along the zero section (See Theorem 3.6.1 for details). It can be seen as a generalization of Eguchi–Hanson metrics to higher dimensional manifolds (See Remark 3.3.2 for details). More precisely, in local coordinates,

$$\omega_{\mathrm{eh},n,k} = k(e^{\frac{n}{k}s}+1)^{\frac{1}{n}}\pi_1^*\omega_{\mathrm{FS}} + \frac{e^{\frac{n}{k}s}}{k(e^{\frac{n}{k}s}+1)^{\frac{n-1}{n}}}\left(\frac{\sqrt{-1}dw\wedge d\bar{w}}{|w|^2} + \sqrt{-1}\alpha\wedge\bar{\alpha} + \right.$$
$$\left. \sqrt{-1}\alpha\wedge\frac{d\bar{w}}{\bar{w}} + \sqrt{-1}\frac{dw}{w}\wedge\bar{\alpha}\right),$$

where

$$\alpha = k\frac{\sum_{i\neq j}\bar{z}_i dz_i}{1+\sum_{i\neq j}|z_i|^2}, \quad \text{on the chart } \{z_j\neq 0\},$$

and

$$\pi_1([Z_1:\cdots:Z_n],w) = [Z_1:\cdots:Z_n]$$

is the projection map from the total space $-kH_{\mathbb{P}^{n-1}}$ to the base space $\mathbb{P}^{n-1}$.

Remark 3.3.2. Fixing $n=k=2$ in (3.22) and (3.23), we obtain that on $-2H_{\mathbb{P}^1}$ the model metric $\omega_{\mathrm{eh},n,k}$ has the expression

$$\sqrt{-1}\partial\bar{\partial}(2\lambda + \log(\lambda-1) - \log(\lambda+1)), \quad \lambda > 1. \tag{3.24}$$

Set

$$r := e^{\frac{1}{4}s}, \quad r>0. \tag{3.25}$$

Plugging (3.22) and (3.25) in (3.24), one finds $\omega_{\mathrm{eh},n,k}$ has the following expression on $-2H_{\mathbb{P}^1}$:

$$\sqrt{-1}\partial\bar{\partial}[\sqrt{r^4+1} + \log r^2 - \log(\sqrt{r^4+1}+1)]. \tag{3.26}$$

Equation (3.26) coincides with (3.16) when we put $\epsilon=1$. In other words, when $n=k=2$, the metric $\omega_{\mathrm{eh},n,k}$ recovers the famous Eguchi–Hanson metric [21] that is constructed on the total space of $-2H_{\mathbb{P}^1}$.

It is recalled in Proposition 3.1.4 that the Eguchi–Hanson metric is Ricci-flat. The metric $\omega_{\mathrm{eh},n,k}$, which is also Ricci-flat but with edge singularities along $Z_{n,k}$ when $n \neq k$, can be seen as a generalization of Eguchi–Hanson metrics to the total space of $-kH_{\mathbb{P}^{n-1}}$ for arbitrary $n, k \in \mathbb{N}_{>0}$.

3.3.2 Compact case: model metrics on $\mathbb{P}^n(1, \ldots, 1, k)$

In this section, we introduce another model metric $\omega_{\mathrm{orb},n,k}$ that is defined on the weighted projective space $\mathbb{P}^n(1, \ldots, 1, k)$. We first recall the construction of the weighted projective space and its orbifold structure.

Definition 3.3.3. For $k \in \mathbb{N}$, consider the group action of $\mathbb{C}^*$ on $\mathbb{C}^{n+1} \setminus \{0\}$ given by

$$\lambda \cdot (z_0, \ldots, z_{n-1}, z_n) = (\lambda z_0, \ldots, \lambda z_{n-1}, \lambda^k z_n), \quad \lambda \in \mathbb{C}^*,\ (z_0, \ldots, z_{n-1}, z_n) \in \mathbb{C}^{n+1} \setminus \{0\}.$$

Then the weighted projective space $\mathbb{P}^n(1, \ldots, 1, k)$ is defined as the quotient of this group action:

$$\mathbb{P}^n(1, \ldots, 1, k) := (\mathbb{C}^{n+1} \setminus \{0\})/\mathbb{C}^*.$$

We use homogeneous coordinates on $\mathbb{P}^n(1, \ldots, 1, k)$. A point $[x_0 : \cdots : x_{n-1} : x_n] \in \mathbb{P}^n(1, \ldots, 1, k)$ corresponds to an equivalence class in $\mathbb{C}^{n+1} \setminus \{0\}$. More precisely,

$$[x_0 : \cdots : x_{n-1} : x_n] := \{\lambda x_0, \ldots, \lambda x_{n-1}, \lambda^k x_n : \lambda \in \mathbb{C}^*\}. \tag{3.27}$$

Consider the $\mathbb{Z}_k$ action on $\mathbb{C}^n$ such that the $\mathbb{Z}_k$ orbit of a point $(z_1, \ldots, z_n) \in \mathbb{C}^n$ is

$$\{e^{\frac{2\pi\sqrt{-1}\ell}{k}} z_1, \ldots, e^{\frac{2\pi\sqrt{-1}\ell}{k}} z_n : \ell = 0, \ldots, k-1\}.$$

Then near the point $[0 : 0 \cdots : 0 : 1] \in \mathbb{P}^n(1, \ldots, 1, k)$ the local structure is $\mathbb{C}^n/\mathbb{Z}_k$. The next lemma shows the relation between $\mathbb{P}^n(1, \ldots, 1, k)$ and $\mathbb{F}_{n,k}$.

Lemma 3.3.4. *The total space of the line bundle $kH_{\mathbb{P}^{n-1}}$ can be embedded in the weighted projective space $\mathbb{P}^n(1, \ldots, 1, k)$ and the complement is a single point $p = [0 : \cdots : 0 : 1] \in \mathbb{P}^n(1, \ldots, 1, k)$. Moreover, $\mathbb{F}_{n,k}$ is the blow up of $\mathbb{P}^n(1, \ldots, 1, k)$ at p.*

Proof. Since for any vector bundle A and line bundle L we have $\mathbb{P}(A \otimes L) = \mathbb{P}(A)$, it follows that $\mathbb{F}_{n,-k}$ is biholomorphic to $\mathbb{F}_{n,k}$ by taking $L = 2kH_{\mathbb{P}^{n-1}}$ in Definition 3.1.3 with the biholomorphism exchanging the zero and the infinity sections $Z_{n,k}$ and $Z_{n,-k}$. Thus, we identify $\mathbb{F}_{n,k}$ as

$$\mathbb{F}_{n,k} = \mathbb{P}(kH_{\mathbb{P}^{n-1}} \oplus \mathbb{C}_{\mathbb{P}^{n-1}}). \tag{3.28}$$

We first show the total space of $kH_{\mathbb{P}^{n-1}}$ can be naturally embedded in $\mathbb{P}^n(1, \ldots, 1, k)$.

Consider $\mathbb{P}^n(1, \ldots, 1, k)$ with homogeneous coordinate $[x_0 : \cdots, x_n]$ and embed $\mathbb{P}^{n-1}$ in $\mathbb{P}^n$ as $\{x_n = 0\}$. Recall the transition function at a point $[x_0 : \cdots : x_{n-1}] \in \mathbb{P}^{n-1}$ of the line bundle $kH_{\mathbb{P}^{n-1}}$ is given by

$$g_{ij}([x_0 : \cdots : x_{n-1}]) = \left(\frac{x_j}{x_i}\right)^k. \tag{3.29}$$

Then the fiber of $kH_{\mathbb{P}^{n-1}}$ at an arbitrary point $[x_0 : \cdots, x_{n-1} : 0] \in \mathbb{P}^n(1, \ldots, 1, k)$ can be identified as the set of all $[x_0 : \cdots : x_{n-1} : \lambda]$ for $\lambda \in \mathbb{C}$, where $[x_0 : \cdots : x_{n-1} : \lambda]$ is defined in (3.27). By definition of the weighted projective space and (3.29), this is well-defined.

Thus, $kH_{\mathbb{P}^{n-1}}$ can be naturally embedded in $\mathbb{P}^n(1,\ldots,1,k)$ and the complement is the point $[0:\cdots:0:1]$. We have mentioned that the local structure of $\mathbb{P}^n(1,\ldots,1,k)$ near this point is $\mathbb{C}^n/\mathbb{Z}_k$.

Next, we blow up $\mathbb{P}^n(1,\ldots,1,k)$ at $[0:\cdots:0:1]$. The exceptional divisor can be identified as adding an infinity section that is biholomorphic to $\mathbb{P}^{n-1}$ to the total space $kH_{\mathbb{P}^{n-1}}$. Combining this observation with (3.28), one realizes the manifold upstairs is the Calabi–Hirzebruch manifold $\mathbb{F}_{n,k}$. We henceforth denote by π the blow down map. □

Now we are ready to define $\omega_{\mathrm{orb},n,k}$. To do so, we first define another family of model metrics $\tilde{\omega}_{\mathrm{orb},n,k}$ on $\mathbb{F}_{n,k}$. $\tilde{\omega}_{\mathrm{orb},n,k}$ is a Kähler–Einstein edge metric with Ricci curvature $(n+1)/k$ and an edge singularity of angle $2\pi/k$ along $Z_{n,-k}$ that degenerates on $Z_{n,k}$. In particular, this metric is smooth along $Z_{n,-k}$ when $k=1$ and collapses along $Z_{n,k}$. Indeed, when $k=1$ this metric coincides with the Fubini–Study metric on $\mathbb{P}^n$. We will then define $\omega_{\mathrm{orb},n,k}$ as the pull-back of the metric $\tilde{\omega}_{\mathrm{orb},n,k}$ under the blow up map.

Definition 3.3.5. Let s be defined in (3.18). To define $\tilde{\omega}_{\mathrm{orb},n,k}$, introduce another coordinate $\nu\in(0,1)$ such that

$$\nu = 1-(e^{\frac{s}{k}}+1)^{-1}.$$

Note that $\{\nu=0\}$ and $\{\nu=1\}$ correspond to the zero section $Z_{n,k}$ and the infinity section $Z_{n,-k}$ respectively. We define $\tilde{\omega}_{\mathrm{orb},n,k}$ by giving its potential function as follows:

$$g(\nu) := -k\log(1-\nu), \quad \nu\in(0,1),$$

and

$$\tilde{\omega}_{\mathrm{orb},n,k} := \sqrt{-1}\partial\bar{\partial}g(s).$$

Note that $\tilde{\omega}_{\mathrm{orb},n,k}$ is a degenerate Kähler–Einstein edge metric on $\mathbb{F}_{n,k}$ with Ricci curvature $(n+1)/k$ and an edge singularity of the angle $2\pi/k$ along $Z_{n,-k}$, while $\tilde{\omega}_{\mathrm{orb},n,k}$ collapses along $Z_{n,k}$ (See Theorem 3.6.4 for details). More precisely, in local coordinates,

$$\tilde{\omega}_{\mathrm{orb},n,k} = \frac{ke^{\frac{s}{k}}}{e^{\frac{s}{k}}+1}\pi_1^*\omega_{\mathrm{FS}} + \frac{e^{\frac{s}{k}}}{k(e^{\frac{s}{k}}+1)}\left(\frac{\sqrt{-1}dw\wedge d\bar{w}}{|w|^2} + \sqrt{-1}\alpha\wedge\bar{\alpha} + \sqrt{-1}\alpha\wedge\frac{d\bar{w}}{\bar{w}} + \sqrt{-1}\frac{dw}{w}\wedge\bar{\alpha}\right),$$

where

$$\alpha = k\frac{\sum_{i\neq j}\bar{z}_i dz_i}{1+\sum_{i\neq j}|z_i|^2}, \quad \text{on the chart } \{z_j \neq 0\},$$

and

$$\pi_1([Z_1:\cdots:Z_n],w) = [Z_1:\cdots:Z_n]$$

is the projection map from $\mathbb{F}_{n,k}$ to the zero section $Z_{n,k}$ identified as $\mathbb{P}^{n-1}$.

Definition 3.3.6. For $k>1$, the model metric $\omega_{\mathrm{orb},n,k}$ on $\mathbb{P}^n(1,\ldots,1,k)$ is defined away from $[0:\cdots:0:1]$ as the pull-back of the metric $\tilde{\omega}_{\mathrm{orb},n,k}$ on $\mathbb{F}_{n,k}\setminus\{Z_{n,k}\}$ under the inverse of the blow up map. For $k=1$, we define $\omega_{\mathrm{orb},n,1}$ as the Fubini–Study metric on $\mathbb{P}^n(1,\ldots,1,1)=\mathbb{P}^n$.

3.4 Construction of KEE metrics

In this section, we aim to construct Kähler–Einstein edge metrics defined on the Calabi–Hirzebruch manifold $\mathbb{F}_{n,k}$ with edge singularities along the zero section $Z_{n,k}$ and the infinity section $Z_{n,-k}$ using Calabi ansatz. By Kähler–Einstein edge metrics we mean Kähler edge currents that satisfy the Kähler–Einstein equation on smooth locus. The reader may refer to [48] for detailed exposition of Kähler edge metrics.

3.4.1 Construction of η_{β_1} on $\mathbb{F}_{n,k}$

Recall, the coordinate s is defined in (3.18), where w and z_j, $j \neq i$ are coordinates we use when working on the chart $\{Z_i \neq 0\} \subset \mathbb{F}_{n,k}$. We seek a Kähler–Einstein edge metric

$$\eta := \sqrt{-1}\partial\bar{\partial} f(s)$$

for some smooth function f on $\mathbb{F}_{n,k}$. Define

$$\begin{aligned} \tau(s) &:= f'(s), \quad s \in (-\infty, +\infty) \\ \varphi(s) &:= f''(s) = \tau'(s), \quad s \in (-\infty, +\infty). \end{aligned} \tag{3.30}$$

Let π_1 and π_2 be projections from $\mathbb{F}_{n,k}$ to the zero section $Z_{n,k}$ and each fiber respectively, i.e.,

$$\begin{aligned} &\pi_1([Z_1 : \cdots : Z_n], w) = [Z_1 : \cdots : Z_n], \\ &\pi_2([Z_1 : \cdots : Z_n], w) = w. \end{aligned}$$

Denote by ω_{FS} the Fubini–Study metric on $\mathbb{P}^{n-1}$ and define

$$\begin{aligned}\omega_{\mathrm{Cyl}} &:= \frac{\sqrt{-1}dw\wedge d\bar{w}}{|w|^2},\\ \alpha &:= \frac{k\sum_{j\neq i}\bar{z}_j dz_j}{1+\sum_{j\neq i}|z_j|^2}, \quad \text{on the chart } \{Z_i\neq 0\}.\end{aligned}$$

Then direct calculation (cf. [50, Section 3.3] for detailed computations in dimension n=2) yields

$$\begin{aligned}\eta = k\tau\pi_1^*\omega_{\mathrm{FS}} + \varphi\Big(\pi_2^*\omega_{\mathrm{Cyl}} + \sqrt{-1}\alpha\wedge\bar{\alpha} + \\ \sqrt{-1}\alpha\wedge\frac{d\bar{w}}{\bar{w}} + \sqrt{-1}\frac{dw}{w}\wedge\bar{\alpha}\Big).\end{aligned} \tag{3.31}$$

Positive definiteness of η then implies $f'\geq 0$ and $f''\geq 0$ for $s\in(-\infty,+\infty)$.

Proposition 3.4.1. *Assume that $Z_{n,k}$ is non-collapsed, then $\inf_{s\in\mathbb{R}}\tau(s)>0$. Moreover, there holds $\sup_{s\in\mathbb{R}}\tau(s)<+\infty$.*

Proof. Assume by contradiction that $\inf_{s\in\mathbb{R}}\tau(s)=0$. Then by (3.31), η is identically zero when restricted to $Z_{n,k}$. However, we assume $Z_{n,k}$ is non-collapsed. Thus we must have $\inf_{s\in\mathbb{R}}\tau(s)>0$. To see $\sup_{s\in\mathbb{R}}\tau(s)<+\infty$, we follow the arguments in [50, Lemma 3.2]. Indeed, restricting η to the fiber $\{Z_j=0,\forall j\neq i\}$, in (3.31) we get

$$\begin{aligned}\eta &= \varphi\pi_2^*\omega_{\mathrm{Cyl}}\\ &= \varphi\frac{\sqrt{-1}dw\wedge d\bar{w}}{|w|^2},\end{aligned} \tag{3.32}$$

and also in this case $s=\log|w|^2$. Then we use the coordinate $w=e^{s/2+\sqrt{-1}\theta}$ on this fiber, and by (3.32) η restricted on the fiber gives a metric

$$g_\eta = \frac{1}{2\varphi(\tau)}d\tau^2 + 2\varphi(\tau)d\theta^2. \tag{3.33}$$

Thus, the volume form on the fiber is $d\tau \wedge d\theta$, and the volume of the fiber is $2\pi(\sup_{s\in\mathbb{R}} \tau(s) - \inf_{s\in\mathbb{R}} \tau(s))$. Since for any Kähler edge metric the volume of a complex submanifold is finite, we conclude $\sup_{s\in\mathbb{R}} \tau(s) < \infty$. □

By Proposition 3.4.1, we may rescale f by a positive constant such that $\inf \tau = 1$ and $\sup \tau = T < \infty$. Thus, we henceforth assume that τ ranges from $[1, T]$.

Proposition 3.4.2. *If η is a Kähler edge metric with conic singularities along $Z_{n,k}$ and $Z_{n,-k}$, then*

$$\begin{aligned} \varphi(1) &= 0, \quad \frac{d\varphi}{d\tau}(1) = \beta_1, \\ \varphi(T) &= 0, \quad \frac{d\varphi}{d\tau}(T) = -\beta_2, \end{aligned} \tag{3.34}$$

if we denote by $2\pi\beta_1$ and $2\pi\beta_2$ respectively the angles of η along $Z_{n,k}$ and $Z_{n,-k}$.

Proof. Recall we assume τ ranges from $[1, T]$. In particular, this implies that

$$\lim_{s\to\pm\infty} \frac{d\tau}{ds} = 0,$$

which combines with (3.30) show that

$$\varphi(1) = \varphi(T) = 0.$$

Next, we follow the arguments in the proof of [50, Proposition 3.3]. Indeed, it follows from [38, Theorem 1, proposition 4.4] that the potential function f of η has complete asymptotic expansions near both $w = 0$ and $w = \infty$. Near $w = 0$, the leading term in the expansion is $|w|^{2\beta_1}$. More precisely, by (3.18),

$$\begin{aligned}\varphi &\sim C_1 + C_2|w|^{2\beta_1} + (C_3 \sin\theta + C_4 \cos\theta)|w|^2 + O(|w|^{2+\epsilon}) \\ &= C_1 + C_2 e^{\beta_1 s} + (C_3 \sin\theta + C_4 \cos\theta)e^s + O(e^{(1+\epsilon)s}).\end{aligned}$$

We first find $C_1 = 0$ by the fact that $\varphi(1) = \varphi(T) = 0$ in (3.34). Moreover, the expansion can be differentiated term-by-term as $|w| \to 0$ or $s \to -\infty$. As $\varphi'(\tau) = \frac{\partial\varphi}{\partial s}\frac{ds}{d\tau} = \frac{\partial\varphi}{\partial s}/\varphi$, we obtain

$$\varphi'(1) = \beta_1.$$

The same arguments imply that

$$\varphi'(T) = -\beta_2,$$

where the minus sign comes from the fact that the leading term in this expansion is $|w|^{-2\beta_2} = e^{-\beta_2 s}$. □

Definition 3.4.3. A Kähler–Einstein edge metric ω is a Kähler edge metric that has constant Ricci curvature away from the singular locus.

By Definition 3.4.3, η is a Kähler–Einstein edge metric if and only if it satisfies the following Kähler–Einstein edge equation:

$$\operatorname{Ric}\eta = \lambda\eta + (1-\beta_1)[Z_{n,k}] + (1-\beta_2)[Z_{n,-k}], \tag{3.35}$$

where by λ we denote the Ricci curvature.

The next proposition shows that (3.35) is equivalent to an ODE satisfied by τ and φ with boundary conditions given in (3.34).

Proposition 3.4.4. *The Kähler edge metric η given in* (3.31) *satisfies the Kähler–Einstein edge equation* (3.35) *if and only if*

$$\lambda = \frac{n}{k} - \beta_1, \quad \beta_1 \in \left(0, \frac{n}{k}\right), \tag{3.36}$$

$$\varphi(\tau) = \frac{1}{k}\frac{\tau^n - 1}{\tau^{n-1}} + \frac{1}{n+1}(\beta_1 - \frac{n}{k})\frac{\tau^{n+1} - 1}{\tau^{n-1}}, \quad \tau \geq 1. \tag{3.37}$$

Moreover, β_2 and T are determined by β_1 such that $T > 1$ and $\beta_2 > 0$.

Proof. By (3.31), we calculate $\operatorname{Ric}\eta$:

$$\begin{aligned}
\operatorname{Ric}\eta &= -\sqrt{-1}\partial\bar{\partial}\log\eta^n \\
&= -\sqrt{-1}\partial\bar{\partial}\log\left(k^{n-1}\tau^{n-1}\varphi(\pi_1^*\omega_{\mathrm{FS}})^{n-1} \wedge \pi_2^*\omega_{\mathrm{Cyl}}\right) \\
&= (1-\beta_1)[Z_{n,k}] + (1-\beta_2)[Z_{n,-k}] + \left(n - k(n-1)\frac{\varphi}{\tau} - k\frac{d\varphi}{d\tau}\right)\pi_1^*\omega_{\mathrm{FS}} \\
&- \varphi\frac{d}{d\tau}\left((n-1)\frac{\varphi}{\tau} + \frac{d\varphi}{d\tau}\right)\left(\pi_2^*\omega_{\mathrm{Cyl}} + \sqrt{-1}\alpha\wedge\bar{\alpha} + \right. \\
&\left. \sqrt{-1}\alpha\wedge\frac{d\bar{w}}{\bar{w}} + \sqrt{-1}\frac{dw}{w}\wedge\bar{\alpha}\right).
\end{aligned} \tag{3.38}$$

Plugging (3.31) and (3.38) in (3.35), (3.35) is equivalent to

$$n - k(n-1)\frac{\varphi}{\tau} - k\frac{d\varphi}{d\tau} = \lambda k\tau, \tag{3.39}$$

$$-\varphi\frac{d}{d\tau}((n-1)\frac{\varphi}{\tau} + \frac{d\varphi}{d\tau}) = \lambda\varphi. \tag{3.40}$$

Now we first observe that (3.39) and (3.40) are equivalent since taking derivative of (3.39) with respect to τ gives (3.40). Thus we conclude (3.35) is equivalent to the ODE (3.39) together with boundary conditions (3.34). Solving this ODE with boundary conditions gives (3.36) and (3.37). We need the assumption $\beta_1 \in (0, n/k)$ to ensure the existence of T and β_2 that satisfy (3.34). Indeed, β_2 and T are determined by β_1 due to (3.34) and (3.37). More precisely, T should be a root of the polynomial that appears in the right hand side of (3.37) and $-\beta_2$ should be determined by the derivative $d\varphi/d\tau$ at T. Writing (3.37) as $\varphi(\tau) = P(\tau)/\tau^{n-1}$, we factor $P(\tau)$ as

$$\begin{aligned} P(\tau) &= (\tau - 1)\left[\frac{1}{k}(\tau^{n-1} + \cdots + 1) + \frac{1}{n+1}\left(\beta_1 - \frac{n}{k}\right)(\tau^n + \cdots + 1)\right] \\ &= \frac{(\tau-1)}{n+1}\left[\left(\beta_1 - \frac{n}{k}\right)\tau^n + \left(\frac{1}{k} + \beta_1\right)(\tau^{n-1} + \cdots + 1)\right]. \end{aligned} \tag{3.41}$$

Under the assumption $\beta_1 \in (0, n/k)$, one finds $P(\tau) > 0$ for $1 < \tau \ll 2$ and $P(\tau) < 0$ for $\tau \to \infty$. Thus, $P(\tau)$ has at least one real root that is greater than 1. Denote by T the first root of P after 1. In particular, $d\varphi/d\tau(T) < 0$. By (3.34), this implies that $\beta_2 > 0$ as claimed. □

By (3.30), there holds

$$\frac{ds}{d\tau} = \frac{1}{\varphi(\tau)}. \tag{3.42}$$

Combining (3.31), (3.42) and Proposition 3.4.4 altogether, we realize that given $\beta_1 \in (0, n/k)$ we can construct a Kähler–Einstein edge metric η on $\mathbb{F}_{n,k}$ using coordinates τ and φ. This Kähler–Einstein edge metric has Ricci curvature $\lambda = n/k - \beta_1$, and has edge singularities of angle $2\pi\beta_1$ along $Z_{n,k}$ and angle $2\pi\beta_2$ along $Z_{n,-k}$. Note that β_2 is determined by β_1. In other words, we can construct a family of Kähler–Einstein edge metrics on $\mathbb{F}_{n,k}$ parametrized by $\beta_1 \in (0, n/k)$. In Section 3.5, we study the asymptotic behavior of this family of metrics when β_1 approaches the two extremes: n/k or 0.

Recall, in the construction of η we rescale the metric such that τ ranges from $[1, T]$. Note that T is determined by β_1. By Proposition 3.4.1, we may also rescale the metric such that τ ranges from $[t, 1]$ for some $0 < t < 1$. In such a way, we construct another family of Kähler–Einstein edge metrics on $\mathbb{F}_{n,k}$ parametrized by β_2 in the remainder of this section. Such metrics can be seen as obtained after renormalizing metrics in the family that is parametrized by β_1. However, when studying their asymptotic behaviors they give rise to different limit metric.

3.4.2 Construction of ξ_{β_2} on $\mathbb{F}_{n,k}$

Now consider a change of coordinate $u := 1/w$. Then (3.18) can be written as

$$s = -\log |u|^2 + k \log \left(1 + \sum_{j \neq i}^{n} |z_j|^2\right).$$

We still denote by $f(s)$ a smooth function on $\mathbb{F}_{n,k}$ and seek Kähler–Einstein edge metrics that have the form $\sqrt{-1}\partial\bar{\partial} f(s)$. Recall $\tau(s)$ and $\varphi(s)$ are defined in (3.30). Let

$$\begin{aligned} \xi : &= \sqrt{-1}\partial\bar{\partial} f(s) \\ &= k\tau\pi_1^*\omega_{\mathrm{FS}} + \varphi\left(\pi_2^*\omega_{\mathrm{Cyl}} + \sqrt{-1}\alpha \wedge \bar{\alpha} - \right. \\ &\left. \sqrt{-1}\alpha \wedge \frac{d\bar{u}}{\bar{u}} - \sqrt{-1}\frac{du}{u} \wedge \bar{\alpha}\right), \end{aligned} \tag{3.43}$$

where π_1, π_2 and α are the same as those in (3.31). Recall by Proposition 3.4.1,

$$0 < \inf_{s \in \mathbb{R}} \tau(s) < \sup_{s \in \mathbb{R}} \tau(s) < +\infty.$$

We rescale the potential function f such that for some $t > 0$,

$$\sup_{s\in\mathbb{R}} \tau(s) = 1, \quad \inf_{s\in\mathbb{R}} \tau(s) = t. \tag{3.44}$$

Assume ξ is a Kähler edge metric on $\mathbb{F}_{n,k}$. Then, under the renormalization given by (3.44), Proposition 3.4.2 and Proposition 3.4.4, which respectively describe the boundary conditions for φ and the ODE satisfied by φ, translate to the following two Propositions.

Proposition 3.4.5. *Assume ξ has edge singularities of angle $2\pi\beta_1$ and $2\pi\beta_2$ respectively along $Z_{n,k}$ and $Z_{n,-k}$. Recall φ in (3.43). Then,*

$$\begin{aligned} \varphi(t) &= 0, \quad \frac{d\varphi}{d\tau}(t) = \beta_1, \\ \varphi(1) &= 0, \quad \frac{d\varphi}{d\tau}(1) = -\beta_2. \end{aligned} \tag{3.45}$$

Proposition 3.4.6. *Under the same assumptions in Proposition 3.4.5, the Kähler edge metric ξ satisfies the Kähler–Einstein edge equation if and only if*

$$\begin{aligned} &\mu = \frac{n}{k} + \beta_2, \quad \beta_2 \in \left(0, \frac{1}{k}\right), \\ &\varphi(\tau) = \frac{1}{k}\frac{\tau^n - 1}{\tau^{n-1}} - \frac{1}{n+1}\left(\frac{n}{k} + \beta_2\right)\frac{\tau^{n+1} - 1}{\tau^{n-1}}, \quad \tau \in (t, 1), \end{aligned} \tag{3.46}$$

where by μ we denote the Ricci curvature of ξ. Moreover, β_1 and t are determined by β_2.

By Propositions 3.4.5 and 3.4.6, we realize that given β_2 we can construct a family of Kähler–Einstein edge metrics on $\mathbb{F}_{n,k}$ parametrized by β_2 such that β_1 and t are determined by β_2. This family of metrics can be obtained by renormalizing the family of metrics parametrized by β_1.

3.5 Angle asymptotics

In this section, we study the asymptotic behaviors of Kähler–Einstein edge metrics η in (3.31) (respectively, ξ in (3.43)) as β_1 (respectively, β_2) approaches either of its extremes.

We first study the limit behavior of η when $\beta_1 \nearrow n/k$. It is enough to study the limiting behavior of φ and τ thanks to Proposition 3.4.4.

Proposition 3.5.1. *When β_1 is close to n/k, we have $T > 1$ and $T \to \infty$ as $\beta_1 \nearrow n/k$.*

Proof. Recall by (3.34), 1 and T are both roots of $\varphi(\tau)$. By Proposition 3.4.4, $T > 1$. To prove $T \to \infty$ as $\beta_1 \nearrow n/k$, we write (3.37) as

$$\varphi(\tau) = \frac{1}{\tau^{n-1}} \cdot \frac{1}{n+1}(\beta_1 - \frac{n}{k})(\tau - 1)(\tau - \alpha_1)\cdots(\tau - \alpha_{n-1})(\tau - T), \tag{3.47}$$

where $\alpha_1, \ldots, \alpha_{n-1} \in \mathbb{C}$. Comparing (3.37) to (3.47), we have

$$(\tau - \alpha_1)\cdots(\tau - \alpha_{n-1})(\tau - T) = \tau^n + \frac{1 + k\beta_1}{k\beta_1 - n}(\tau^{n-1} + \cdots + 1).$$

By Vieta's formulas,

$$(-1)^n \alpha_1 \cdots \alpha_{n-1} \cdot T = \frac{1 + k\beta_1}{k\beta_1 - n}, \tag{3.48}$$

$$\alpha_1 + \cdots + \alpha_{n-1} + T = \frac{1 + k\beta_1}{n - k\beta_1}. \tag{3.49}$$

By (3.37), $\varphi(\tau)$ has $n+1$ (possibly complex) roots. Since

$$\varphi(\tau) \to \frac{1}{k}\frac{\tau^n - 1}{\tau^{n-1}}, \qquad \text{as } \beta_1 \nearrow n/k,$$

we conclude that the n roots of φ except T converge to the nth root of unity as $\beta_1 \nearrow n/k$. In particular, $|\alpha_1|, \ldots, |\alpha_{n-1}|$ converge to 1 as $\beta_1 \nearrow n/k$. However, by (3.48) we see

$$|\alpha_1| \cdots |\alpha_{n-1}||T| \to +\infty, \quad \text{as } \beta_1 \nearrow n/k.$$

Thus we must have $T \to +\infty$ as $\beta_1 \nearrow n/k$. □

Proposition 3.5.2. *As $\beta_1 \nearrow n/k$, the length of the path on each fiber between the intersection point of the fiber with $Z_{n,k}$ and that of the fiber with $Z_{n,-k}$ tends to infinity. In other words, $Z_{n,-k}$ gets pushed–off to infinity as $\beta_1 \nearrow n/k$ if we fix a base point on $Z_{n,k}$.*

Proof. Restricted to each fiber, by (3.33), $\eta = \varphi\sqrt{-1}dw \wedge d\bar{w}/|w|^2$ gives a metric

$$g = \frac{1}{2\varphi(\tau)}d\tau^2 + 2\varphi(\tau)d\theta^2.$$

Up to some constant, the distance between $\{\tau = 1\}$ and $\{\tau = T\}$ is given by

$$\begin{aligned} &\int_1^T \frac{1}{\sqrt{\varphi(\tau)}}\, d\tau = \\ &\int_1^T \frac{\tau^{\frac{n-1}{2}}}{\sqrt{\frac{n/k-\beta_1}{n+1}} \cdot \sqrt{(\tau-1)(\tau-\alpha_1)\cdots(\tau-\alpha_{n-1})(T-\tau)}}\, d\tau. \end{aligned} \tag{3.50}$$

Recall in the proof of Proposition 3.5.1, we have shown

$$T \sim \frac{1+k\beta_1}{n-k\beta_1} \sim \frac{1+n}{k} \cdot \frac{1}{n/k-\beta_1}, \quad \text{as } \beta_1 \nearrow n/k. \tag{3.51}$$

For any fixed $\epsilon > 0$, consider

$$\int_{T-\epsilon}^{T} \frac{\tau^{\frac{n-1}{2}}}{\sqrt{\frac{n/k-\beta_1}{n+1}} \cdot \sqrt{(\tau-1)(\tau-\alpha_1)\cdots(\tau-\alpha_{n-1})(T-\tau)}}\, d\tau.$$

We can find β_1 close to n/k such that

$$T - \epsilon > \frac{1}{2}T.$$

Then in $[T-\epsilon, T]$, we have

$$\begin{aligned} &\tau^{\frac{n-1}{2}} > (T-\epsilon)^{\frac{n-1}{2}} > \left(\frac{1}{2}T\right)^{\frac{n-1}{2}}, \\ &\sqrt{(\tau-1)(\tau-\alpha_1)\cdots(\tau-\alpha_{n-1})} < \sqrt{2(\tau^n-1)} < \sqrt{2T^n}. \end{aligned} \tag{3.52}$$

By (3.51) and (3.52), there exists a constant $C > 0$ that is independent of ϵ such that

$$\begin{aligned} &\int_{T-\epsilon}^{T} \frac{\tau^{\frac{n-1}{2}}}{\sqrt{\frac{n/k-\beta_1}{n+1}} \cdot \sqrt{(\tau-1)(\tau-\alpha_1)\cdots(\tau-\alpha_{n-1})(T-\tau)}}\, d\tau \\ &> C \cdot \frac{T^{\frac{n-1}{2}}}{\sqrt{n/k-\beta_1} \cdot T^{\frac{n}{2}}} \int_{T-\epsilon}^{T} \frac{1}{\sqrt{T-\tau}}\, d\tau \\ &> C\epsilon. \end{aligned}$$

Since ϵ is arbitrarily chosen, the integral in (3.50) diverges as $\beta_1 \nearrow n/k$. Thus, we have shown

$Z_{n,-k}$ gets pushed-off to infinity as $\beta_1 \nearrow n/k$ if we choose a base point on $Z_{n,k}$. $\square$

Proposition 3.5.3. $\lim\limits_{\beta_1 \nearrow \frac{n}{k}} \beta_2(\beta_1) = \dfrac{1}{k}$.

Proof. We calculate

$$\frac{d\varphi}{d\tau} = \frac{1}{k}\frac{\tau^{n-2}}{(\tau^{n-1})^2}(n+\tau^n-1) + \frac{1}{n+1}(\beta_1 - \frac{n}{k})\frac{\tau^{n-2}}{(\tau^{n-1})^2}(2\tau^{n+1}+n-1).$$

By $\varphi_\tau(T) = -\beta_2$ we have

$$\frac{1}{kT^n}(n+T^n-1) + \frac{1}{n+1}(\beta_1 - \frac{n}{k})\frac{1}{T^n}(2T^{n+1}+n-1) = -\beta_2. \tag{3.53}$$

Recall $\varphi(T) = 0$, then we have

$$\frac{T^n-1}{k} + \frac{1}{n+1}(\beta_1 - \frac{n}{k})(T^{n+1}-1) = 0. \tag{3.54}$$

Combining (3.53) and (3.54),

$$\Big(\frac{1}{k} - \beta_2\Big)T^n = \beta_1 + \frac{1}{k}. \tag{3.55}$$

Since $T \to \infty$ as $\beta_1 \nearrow n/k$, there holds $\beta_2 \to 1/k$ as $\beta_1 \nearrow n/k$. $\square$

In Section 3.6, we use asymptotic behaviors discussed above to study the limit metric of η as β_1 approaches n/k or 0. In the remainder of this section, we focus on the family of metrics ξ that is parametrized by β_2. Inspired by Proposition 3.5.3, we study the asymptotic behaviors of ξ as $\beta_2 \nearrow 1/k$.

Proposition 3.5.4. *When $\beta_2 \nearrow \frac{1}{k}$, as an analogue of* (3.55)*, there holds*

$$\left(\frac{1}{k} + \beta_1\right) t^n = \frac{1}{k} - \beta_2.$$

Proof. Let $\varphi(\tau)$ and t be as in (3.45) and (3.46). We calculate

$$\frac{d\varphi}{d\tau} = \frac{1}{k}\frac{\tau^{n-2}}{(\tau^{n-1})^2}(\tau^n + n - 1) - \frac{1}{n+1}\left(\frac{n}{k} + \beta_2\right)\frac{\tau^{n-2}}{(\tau^{n-1})^2}(2\tau^{n+1} + n - 1).$$

By the fact that $d\varphi/d\tau(t) = \beta_1$,

$$\beta_1 = \frac{1}{kt^n}(n + t^n - 1) - \frac{1}{n+1}\left(\frac{n}{k} + \beta_2\right)\frac{1}{t^n}(2t^{n+1} + n - 1).$$

Combining this with the fact that $\varphi(t) = 0$, there holds

$$\begin{aligned} \beta_1 t^n &= \frac{1}{k}(n + t^n - 1) - \frac{2(t^n - 1)}{k} - \frac{n}{k} - \beta_2 \\ &= -\frac{1}{k}t^n + \frac{1}{k} - \beta_2, \end{aligned}$$

which implies

$$\left(\beta_1 + \frac{1}{k}\right) t^n = \frac{1}{k} - \beta_2$$

as claimed.

□

Proposition 3.5.5. *As $\beta_2 \nearrow \dfrac{1}{k}$, $t = O\left(\left(\dfrac{k}{n+1}\right)^{\frac{1}{n}}\left(\dfrac{1}{k} - \beta_2\right)^{\frac{1}{n}}\right)$. In particular, t tends to 0 when $\beta_2 \nearrow 1/k$. Moreover, the length of the path on each fiber between the intersection point of the fiber with $Z_{n,k}$ and that of the fiber with $Z_{n,-k}$ converges to a finite number as $\beta_2 \nearrow 1/k$.*

Proof. Recall t is a root of

$$\varphi(\tau) = \frac{1}{k}\frac{\tau^n - 1}{\tau^{n-1}} - \frac{1}{n+1}\left(\frac{n}{k} + \beta_2\right)\frac{\tau^{n+1} - 1}{\tau^{n-1}} = 0.$$

Direct calculations yield

$$\frac{\varphi(\tau)}{\tau - 1} = \frac{1}{\tau^{n-1}}\left(-\frac{1}{n+1}\left(\frac{n}{k} + \beta_2\right)\tau^n + \frac{1/k - \beta_2}{n+1}(\tau^{n-1} + \cdots + \tau + 1)\right).$$

Then it is easy to see that every root of $\varphi(\tau)$ except for $\tau = 1$, denoted by α, satisfies that $|\alpha| = O((k/(n+1))^{1/n}(1/k - \beta_2)^{1/n})$ when $\beta_2 \nearrow 1/k$. In particular, as $\beta_2 \nearrow 1/k$, all roots of $\varphi(\tau) = 0$ except for $\tau = 1$ converge to 0. We conclude that $t \to 0$. To see that the length between $Z_{n,k}$ and $Z_{n,-k}$ converges to a finite number in the limit, one follows the arguments in the proof of Proposition 3.5.2 and Proposition 3.9.4. $\square$

3.6 Large angle limits

In this section, we first study the Gromov–Hausdorff limit of the family of metrics η when the parameter β_1 approaches n/k.

Theorem 3.6.1. *Fix an arbitrary base point p on $Z_{n,k}$. As $\beta_1 \nearrow n/k$, the Kähler–Einstein edge metric $(\mathbb{F}_{n,k}, \eta_{\beta_1}, p)$ converges in the pointed Gromov–Hausdorff sense to a Ricci-flat Kähler edge metric $(-kH_{\mathbb{P}^{n-1}}, \eta_\infty, p)$ described in (3.60). Moreover, away from $Z_{n,k}$, one has $\eta_{\beta_1} \xrightarrow{C^k_{\mathrm{loc}}} \eta_\infty$ for any $k \geq 0$ on the total space of $-kH$ (seen as an open subset in $\mathbb{F}_{n,k}$), and the limit metric η_∞ coincides with the model metric $\omega_{\mathrm{eh},n,k}$ defined in Section 3.3.*

Proof. We use notation η_{β_1}, $\tau(\beta_1)$ and $\varphi(\beta_1)$ to emphasize the dependence of metrics and coordinates on β_1. Combining (3.30) and (3.37), we have

$$\frac{ds}{d\tau(\beta_1)} = \frac{1}{\varphi(\beta_1)} = \frac{\tau(\beta_1)^{n-1}}{\frac{1}{k}(\tau(\beta_1)^n - 1) + \frac{\beta_1 - n/k}{n+1}(\tau(\beta_1)^{n+1} - 1)}. \tag{3.56}$$

Claim 3.6.2. The pointwise limits of functions

$$\tau_\infty(s) := \lim_{\beta_1 \nearrow n/k} \tau(\beta_1, s), \quad s \in (-\infty, +\infty),$$

$$\varphi_\infty(s) := \lim_{\beta_1 \nearrow n/k} \varphi(\beta_1, s), \quad s \in (-\infty, +\infty)$$

exist. Moreover, $\tau_\infty(s)$ and $\varphi_\infty(s)$ are smooth in s.

Proof of the Claim. By the continuous dependence of ODEs in (3.56) on the parameter β_1, the pointwise limit function τ_∞ exists. Since $\tau(\beta_1, s)$ is smooth in s for each β_1, $\tau_\infty(s)$ is smooth in s. By (3.37) and the existence of $\tau_\infty(s)$, $\varphi_\infty(s)$ also exists. Moreover, $\varphi_\infty(s)$ is smooth in s due to the smoothness of $\tau_\infty(s)$. □

Thanks to Claim 3.6.2, τ_∞ and φ_∞ satisfy

$$\begin{aligned} \frac{ds}{d\tau_\infty} &= \frac{\tau_\infty^{n-1}}{\frac{1}{k}(\tau_\infty^n - 1)}, \\ \varphi_\infty(\tau_\infty) &= \frac{1}{k}\frac{\tau_\infty^n - 1}{\tau_\infty^{n-1}}. \end{aligned} \tag{3.57}$$

Solving the first equation in (3.57), we get

$$\tau_\infty(s) = (1 + e^{(s-C)\frac{n}{k}})^{1/n}, \quad \text{for some constant } C. \tag{3.58}$$

By considering a change of coordinate $w' = C'w$ for some appropriate C' in (3.18), we may choose C in (3.58) to be 0. Plugging (3.58) into the second equation in (3.57), one finds

$$\varphi_\infty(s) = \frac{1}{k} \cdot \frac{e^{s\cdot \frac{n}{k}}}{(e^{s\cdot \frac{n}{k}}+1)^{\frac{n-1}{n}}}. \tag{3.59}$$

Plugging (3.58) and (3.59) into (3.31), we obtain the convergence of Kähler–Einstein edge metric η_{β_1} on any compact subsets of $\mathbb{F}_{n,k}$ in every C^k-norm to the following metric:

$$\begin{aligned} \eta_\infty &:= \lim_{\beta_1 \nearrow n/k} \eta_{\beta_1} \\ &= k(1+e^{s\cdot\frac{n}{k}})^{1/n}\pi_1^*\omega_{\mathrm{FS}} + \frac{1}{k}\cdot\frac{e^{s\cdot \frac{n}{k}}}{(e^{s\cdot \frac{n}{k}}+1)^{\frac{n-1}{n}}}\Big(\pi_2^*\omega_{\mathrm{Cyl}} + \sqrt{-1}\alpha\wedge\bar{\alpha} \\ &+ \sqrt{-1}\alpha\wedge\frac{d\bar{w}}{\bar{w}} + \sqrt{-1}\frac{dw}{w}\wedge\bar{\alpha}\Big). \end{aligned} \tag{3.60}$$

Recall by (3.36), the Ricci curvature of η_{β_1} is given by $\lambda_{\beta_1} = n/k - \beta_1$, which converges to 0 as $\beta_1 \nearrow n/k$. Thus, η_∞ is a Ricci-flat Kähler edge metric on $-kH_{\mathbb{P}^{n-1}}$. η_∞ has edge singularity of angle $2n\pi/k$ along $Z_{n,k} \subset -kH_{\mathbb{P}^{n-1}}$. Indeed, η_∞ coincides with the model metric $\omega_{\mathrm{eh},n,k}$ defined in Section 3.3. To obtain the convergence in the pointed Gromov–Hausdorff sense, we first recall by Proposition 3.5.2 the distance between $Z_{n,-k}$ and $Z_{n,k}$ tends to infinity as $\beta_1 \nearrow n/k$. Once we choose a base point on $Z_{n,k}$. Since η_{β_1} converges to η_∞ on any compact geodesic balls centered at the base point, we conclude that η_{β_1} converges in the pointed Gromov–Hausdorff sense to η_∞ on $-kH_{\mathbb{P}^{n-1}}$. □

Remark 3.6.3. If we let $n = k = 2$ in Theorem 3.6.1, then by Remark 3.3.2 we obtain in the limit the Eguchi–Hanson metric with parameter ϵ set as 1 (see (3.16)). In other words, the Eguchi–Hanson metric arises as the pointed Gromov–Hausdorff limit of Kähler–Einstein edge metrics

η_{β_1} when $\beta_1 \nearrow 1$. This interesting observation has been conjectured in [50, Remark 5.1].

Next, we fix a base point on the infinity section $Z_{n,-k}$ to study the Gromov–Hausdorff limit of the family of Kähler–Einstein edge metrics ξ on $\mathbb{F}_{n,k}$. In the limit, we obtain an orbifold Kähler–Einstein edge metric instead of the Ricci-flat edge metric obtained in Theorem 3.6.1.

From now on, we use $\xi_{\beta_2}, \tau(\beta_2)$ and $\varphi(\beta_2)$ to emphasize the dependence of metrics and coordinates on β_2. We consider the case $\beta_2 \nearrow 1/k$.

Theorem 3.6.4. *Fix an arbitrary base point p on the infinity section $Z_{n,-k}$. As $\beta_2 \nearrow 1/k$, the Kähler–Einstein edge metric $(\mathbb{F}_{n,k}, \xi_{\beta_2}, p)$ on $\mathbb{F}_{n,k}$ converges in the pointed Gromov–Hausdorff sense to an orbifold Kähler–Einstein edge metric $(\mathbb{P}^n(1,\ldots,1,k), \xi_\infty, p)$ on the weighted projective space $\mathbb{P}^n(1,\ldots,1,k)$ with an edge singularity of angle $2\pi/k$ along $Z_{n,-k}$. This limit metric coincides with the model metric $\omega_{\mathrm{orb},n,k}$ defined in Definition 3.3.6.*

Proof. By similar notation and calculations as in the proof of Theorem 3.6.1, we have

$$\frac{ds}{d\tau(\beta_2)} = \frac{1}{\varphi(\beta_2)} = \frac{\tau(\beta_2)^{n-1}}{\frac{1}{k}(\tau(\beta_2)^n - 1) - \frac{n/k+\beta_2}{n+1}(\tau(\beta_2)^{n+1} - 1)}.$$

As $\beta_2 \nearrow 1/k$, we have

$$\begin{aligned} \frac{ds}{d\tau_\infty} &= \frac{k}{\tau_\infty - \tau_\infty^2}, \\ \varphi_\infty(\tau_\infty) &= \frac{1}{k}(\tau_\infty - \tau_\infty^2). \end{aligned} \tag{3.61}$$

Solving (3.61) and considering a change of coordinate $u' = C'u$ for some appropriate C, we have

$$\begin{aligned} \tau_\infty(s) &= 1 - \frac{1}{e^{\frac{s}{k}} + 1}, \quad s \in (-\infty, +\infty), \\ \varphi_\infty(s) &= \frac{1}{k}\frac{e^{s/k}}{(e^{s/k}+1)^2}, \quad s \in (-\infty, +\infty). \end{aligned}$$

Thus, the limit metric on $\mathbb{F}_{n,k}$ is as follows:

$$\begin{aligned}\tilde{\xi}_\infty = k\frac{e^{s/k}}{e^{s/k}+1}\pi_1^*\omega_{\mathrm{FS}} + \frac{1}{k}\frac{e^{s/k}}{(e^{s/k}+1)^2}\Big(\pi_2^*\omega_{\mathrm{Cyl}} + \sqrt{-1}\alpha\wedge\bar{\alpha} \\ +\sqrt{-1}\alpha\wedge\frac{d\bar{w}}{\bar{w}} + \sqrt{-1}\frac{dw}{w}\wedge\bar{\alpha}\Big).\end{aligned}$$

Recall the Ricci curvature μ_{β_2} is given in (3.46) by $n/k+\beta_2$ and converges to $(n+1)/k$ in the limit. Thus $\tilde{\xi}_\infty$ has Ricci curvature $(n+1)/k$. Moreover, $\tilde{\xi}_\infty$ has an edge singularity of angle $2\pi/k$ along $Z_{n,-k}$. It degenerates on $Z_{n,k}$ since $\tau\equiv 0$ on $Z_{n,k}$. Indeed, $\tilde{\xi}_\infty$ coincides with the model metrics defined in Definition 3.3.5. Then by Definition 3.3.6, we denote by ξ_∞ the model metric on $\mathbb{P}^n(1,\ldots,1,k)$ that is the pull-back of $\tilde{\xi}_\infty$ under the blow up map.

We have shown that $\tilde{\xi}_\infty$ is the limit of ξ_{β_2} as tensors in the pointwise smooth sense. Next, fix an arbitrary base point on $Z_{n,-k}$. By Proposition 3.5.5 and the local smooth convergence result, we conclude that $(\mathbb{P}^n(1,\ldots,1,k),\xi_\infty)$ is the limit of $(\mathbb{F}_{n,k},\xi_{\beta_2})$ in the pointed Gromov–Hausdorff sense when $\beta_2\nearrow 1/k$. Moreover, the limit metric coincides with the model metric $\omega_{\mathrm{orb},n,k}$ defined in Section 3.3. □

As we pointed out in Section 3.5, the family of metrics ξ_{β_2} can be obtained by renormalizing the family of metrics η_{β_1}. Comparing Theorem 3.6.1 to Theorem 3.6.4, we obtain different limit metrics for those two family of metrics. However, we show that after a proper normalization of ξ_{β_2}, we obtain the same limit metric for both ξ_{β_2} and η_{β_1}. The normalization factor is actually given by Proposition 3.5.5.

Corollary 3.6.5. *Rescale the Kähler–Einstein edge metric ξ_{β_2} by $((n+1)/k)^{1/n}/(1/k-\beta_2)^{1/n}$, then the normalized metric converges in the pointed Gromov–Hausdorff sense to a Ricci-flat* *metric on $-kH_{\mathbb{P}^{n-1}}$ when $\beta_2 \nearrow 1/k$, where the base point is chosen from $Z_{n,k}$. See the proof for a more precise explanation. Moreover, this Ricci-flat metric coincides with the one obtained in Theorem 3.6.1, i.e., the model metric $\omega_{\mathrm{eh},n,k}$.*

Proof. Consider a change of coordinate

$$y(\beta_2) := \left(\frac{n+1}{k}\right)^{\frac{1}{n}} \cdot \frac{\tau(\beta_2)}{(\frac{1}{k}-\beta_2)^{\frac{1}{n}}}.$$

By Proposition 3.5.5, the interval of definition of $y(\beta_2)$ converges to $[1,+\infty]$ as $\beta_2 \nearrow 1/k$. The rescaled metric reads

$$\begin{aligned}&\left(\frac{n+1}{k}\right)^{\frac{1}{n}} \cdot \frac{\xi_{\beta_2}}{(\frac{1}{k}-\beta_2)^{\frac{1}{n}}}\\ &= ky\pi_1^*\omega_{\mathrm{FS}} + \left(\frac{n+1}{k}\right)^{\frac{1}{n}} \cdot \frac{\varphi(\beta_2)}{(\frac{1}{k}-\beta_2)^{\frac{1}{n}}} \left(\pi_2^*\omega_{\mathrm{Cyl}} + \sqrt{-1}\alpha\wedge\bar{\alpha} - \right.\\ &\left.\sqrt{-1}\alpha\wedge\frac{d\bar{u}}{\bar{u}} - \sqrt{-1}\frac{du}{u}\wedge\bar{\alpha}\right).\end{aligned}$$

Recall

$$\begin{aligned}&\left(\frac{n+1}{k}\right)^{\frac{1}{n}} \cdot \frac{\varphi(\beta_2)}{(\frac{1}{k}-\beta_2)^{\frac{1}{n}}} =\\ &\left(\frac{n+1}{k}\right)^{\frac{1}{n}} \cdot \frac{\frac{1}{k}(\tau(\beta_2)^n-1) - \frac{1}{n+1}(\frac{n}{k}+\beta_2)(\tau(\beta_2)^{n+1}-1)}{(\tau(\beta_2)^{n-1})(\frac{1}{k}-\beta_2)^{\frac{1}{n}}}.\end{aligned} \tag{3.62}$$

Denote by y the coordinate in the limit. Letting $\beta_2 \nearrow 1/k$, the right hand side of (3.62) converges to

$$\frac{y^n-1}{ky^{n-1}}, \quad y\in[1,+\infty].$$

Solving

$$\frac{ds}{d\tau_{\beta_2}} = \frac{1}{\varphi_{\beta_2}(\tau_{\beta_2})} \Rightarrow \frac{ds}{dy_{\beta_2}} \frac{1}{(\frac{1}{k} - \beta_2)^{\frac{1}{n}}} \cdot \left(\frac{n+1}{k}\right)^{\frac{1}{n}} = \frac{1}{\varphi_{\beta_2}(y_{\beta_2})},$$

we obtain in the limit

$$s = \frac{k}{n} \log\left(y^n - 1\right), \quad y \in (1, +\infty). \tag{3.63}$$

Thus the limit metric is given by

$$\begin{aligned} \tilde{\xi}_\infty = ky\pi_1^*\omega_{\mathrm{FS}} + \frac{y^n - 1}{ky^{n-1}} \Big(\pi_2^*\omega_{\mathrm{Cyl}} + \sqrt{-1}\alpha \wedge \bar{\alpha} - \\ \sqrt{-1}\alpha \wedge \frac{d\bar{u}}{\bar{u}} - \sqrt{-1}\frac{du}{u} \wedge \bar{\alpha}\Big), \end{aligned} \tag{3.64}$$

where y and s satisfy (3.63). This limit metric is Ricci-flat. And it coincides with the limit metric in Theorem 3.6.1, i.e., the model metric $\omega_{\mathrm{eh},n,k}$ defined in Section 3.3. Fix an arbitrary base point on $Z_{n,k}$. By Proposition 3.5.5, the distance between $Z_{n,k}$ and $Z_{n,-k}$ tends to $+\infty$ in the limit under the renormalized metric. Thus, $Z_{n,-k}$ gets pushed-off to infinity in the limit. We obtain the pointed Gromov–Hausdorff convergence of $(\mathbb{F}_{n,k}, ((n+1)/k)^{1/n}\xi_{\beta_2}/(\frac{1}{k} - \beta_2)^{1/n})$ to $-kH_{\mathbb{P}^{n-1}}$ with the metric obtained in (3.64). $\square$

3.7 Small angle limits and fiberwise rescaling

In this section we first consider the $\beta_1 \searrow 0$ case for η_{β_1}.

Theorem 3.7.1. *As β_1 tends to 0, $(\mathbb{F}_{n,k}, \eta_{\beta_1})$ converges in the Gromov–Hausdorff sense to $(\mathbb{P}^{n-1}, k\omega_{\mathrm{FS}})$.*

Proof. As $\beta_1 \searrow 0$, by (3.37) we have

$$\begin{aligned}\varphi_0 := \lim_{\beta_1 \searrow 0} \varphi_{\beta_1} &= \frac{1}{\tau^{n-1}}\left(\frac{1}{k}(\tau^n - 1) - \frac{n}{k(n+1)}(\tau^{n+1} - 1)\right) \\ &= \frac{1}{k(n+1)} \cdot \frac{1}{\tau^{n-1}}(-n\tau^{n+1} + (n+1)\tau^n - 1).\end{aligned}$$

Then we observe φ_0 does not have any root greater than 1. Indeed, notice that

$$\begin{aligned}-n\tau^{n+1} + (n+1)\tau^n - 1 &= (\tau - 1)(1 + \cdots + \tau^{n-1} - n\tau^n) \\ &= (\tau - 1)(1 - \tau^n + \tau - \tau^n + \cdots + \tau^{n-1} - \tau^n).\end{aligned}$$

Thus φ_0 is always positive when $\tau > 1$. However, combining this fact with (3.47), we conclude that

$$\lim_{\beta_1 \searrow 0} T = 1. \tag{3.65}$$

Since $\varphi(1) = \varphi(T) = 0$, we have $\varphi(\beta_1) \to 0$ as $\beta_1 \searrow 0$. Since τ ranges from 1 to T, by (3.31) we conclude that as $\beta_1 \searrow 0$, η_{β_1} converges to $k\pi_1^*\omega_{\mathrm{FS}}$. Thus we have shown $(\mathbb{F}_{n,k}, \eta_{\beta_1})$ converges in the Gromov–Hausdorff sense to $(\mathbb{P}^{n-1}, k\omega_{\mathrm{FS}})$ when $\beta_1 \searrow 0$. $\square$

Roughly speaking, Theorem 3.7.1 says that as $\beta_1 \searrow 0$, the fibers collapse to the zero section. This motivates us to rescale the metric η_{β_1} along the fiber so that we can obtain a non-collapsed metric in the limit. We first need the following lemma.

Lemma 3.7.2. *For $\beta_1 > 0$ and close to zero, $T = T(\beta_1) = 1 + O(\beta_1)$.*

Proof. By Proposition 3.4.4, $T(\beta_1)$ is determined by β_1, and $T(\beta_1)$ is the first root of the polynomial in (3.41). We rewrite the polynomial in (3.41) as

$$P(\tau) = \frac{k\beta_1 - n}{k(n+1)}(\tau - 1)\left(\tau^n + \frac{k\beta_1 + 1}{k\beta_1 - n}(\tau^{n-1} + \cdots + 1)\right).$$

Letting $y = \tau - 1$,

$$\begin{aligned} P(y) &= \frac{k\beta_1 - n}{k(n+1)} y \left((y+1)^n + \frac{k\beta_1 + 1}{k\beta_1 - n}\big((y+1)^{n-1} + \cdots + (y+1) + 1\big)\right) \\ &= \frac{k\beta_1 - n}{k(n+1)} y \left(y^n + \ldots + y\left(n + \frac{k\beta_1 + 1}{k\beta_1 - n}(1 + \ldots + n - 1)\right) + \frac{k(n+1)\beta_1}{k\beta_1 - n}\right) \\ &= \frac{k\beta_1 - n}{k(n+1)} y \left(yQ(y) + \frac{k(n+1)\beta_1}{k\beta_1 - n}\right), \end{aligned} \tag{3.66}$$

where $Q(y)$ is a polynomial of degree $n-1$ whose coefficients depend on β_1 and whose constant term is

$$Q(0) = n + \frac{k\beta_1 + 1}{k\beta_1 - n}(1 + \ldots + n - 1) = n\frac{(n-1)(k\beta_1 + 1)}{2(k\beta_1 - n)} = \frac{n+1}{2}\frac{nk\beta_1 - n}{k\beta_1 - n}. \tag{3.67}$$

By Proposition 3.4.4, $T - 1$ is a root of the term in the parenthesis of the second equation in (3.66), i.e.,

$$0 = (T-1)Q(T-1) + \frac{k(n+1)\beta_1}{k\beta_1 - n}.$$

In particular, it follows that $Q(T-1) \neq 0$ for small enough β_1. Thus, dividing we obtain

$$T - 1 = \frac{k(n+1)\beta_1}{(-k\beta_1 + n)Q(T-1)}.$$

By (3.65) $\lim_{\beta_1 \searrow 0} T = 1$, and so $\lim_{\beta_1 \searrow 0} Q(T-1) = (n+1)/2$ by (3.67). Altogether,

$$T - 1 = \frac{2k}{n}\beta_1 + o(\beta_1), \tag{3.68}$$

as claimed. □

Remark 3.7.3. The last display generalizes [50, (5.1)] from the surface case $n = 2$ to any dimension. Note that in op. cit. n corresponds to our k.

It follows that in the small angle limit, both angles approach zero at the same rate:

Lemma 3.7.4. *For $\beta_1 > 0$ and close to zero, $\beta_2 = \beta_2(\beta_1) = \beta_1 + O(\beta_1^2)$.*

Proof. Combining (3.65) and (3.55) it follows that $\lim_{\beta_1 \searrow 0} \beta_2 = 0$. Using this, and plugging (3.68), in (3.55) we find that

$$\beta_1 + \frac{1}{k} = \frac{1}{k} + 2\beta_1 - \beta_2 + o(\beta_1),$$

so $\beta_2 = \beta_1 + o(\beta_1)$, and so bootstrapping we obtain $\beta_2 = \beta_1 + O(\beta_1^2)$, as claimed. □

Lemma 3.7.4 motivates treating the angles $2\pi\beta_1$ and $2\pi\beta_2$ on the same footing in the small angle regime, so that it reasonable to hope that under some appropriate rescaling the fibers converge to cylinders, as in [49, 50]. This is precisely what we prove next.

We change variable from $\tau \in (1, T)$ in (3.31) and (3.37) to

$$x := \frac{\tau - 1 - \frac{k\beta_1}{n}}{\frac{k\beta_1^2}{n}}, \tag{3.69}$$

with $x \in \left(-\frac{1}{\beta_1}, \frac{1}{\beta_1} + O(1)\right)$ by (3.68). Note that $x = 0$ roughly corresponds to the middle section between $Z_{n,k}$ and $Z_{n,-k}$. By (3.37) and (3.69),

$$\varphi(x) = \frac{k}{2n}\beta_1^2 + \frac{k}{n}\beta_1^3 x + o(\beta_1^2), \quad x \in \left(-\frac{1}{\beta_1}, \frac{1}{\beta_1} + O(1)\right). \tag{3.70}$$

Let $p \in \mathbb{F}_{n,k}$ be a fixed base point chosen from the section $\{x = 0\}$, which will serve as the base point we use later for pointed Gromov–Hausdorff convergence.

To find a fiberwise-rescaled limit, we next rescale the metric η_{β_1} in (3.31) along each fiber, i.e., we define

$$\widetilde{\eta_{\beta_1}} := k\tau\pi_1^*\omega_{\mathrm{FS}} + \frac{1}{\beta_1^2}\varphi\pi_2^*\omega_{\mathrm{Cyl}} + \varphi(\sqrt{-1}\alpha \wedge \bar{\alpha} + \sqrt{-1}\alpha \wedge \overline{dw/w} + \sqrt{-1}dw/w \wedge \bar{\alpha}). \tag{3.71}$$

Remark 3.7.5. This fiberwise rescaled metric is no longer Kähler. Indeed, since the metric η_{β_1} in (3.31) is Kähler, i.e., $d\eta_{\beta_1} = 0$, there holds

$$\begin{aligned} d\widetilde{\eta_{\beta_1}} &= d\left(\eta_{\beta_1} - \left(1 - \frac{1}{\beta_1^2}\right)\varphi\pi_2^*\omega_{\mathrm{Cyl}}\right) \\ &= -\left(1 - \frac{1}{\beta_1^2}\right) d\varphi \wedge \pi_2^*\omega_{\mathrm{Cyl}} \\ &\neq 0. \end{aligned}$$

Theorem 3.7.6. *As $\beta_1 \searrow 0$, $(\mathbb{F}_{n,k}, \widetilde{\eta_{\beta_1}}, p)$ converges in the pointed Gromov–Hausdorff sense to $(\mathbb{P}^{n-1} \times \mathbb{C}^*, \frac{k}{n}(n\pi_1^*\omega_{\mathrm{FS}} + \pi_2^*\omega_{\mathrm{Cyl}}), p)$.*

Proof. We first show on compact subsets, the following pointwise convergence holds:

Claim 3.7.7. The restriction of $\widetilde{\eta_{\beta_1}}$ to a fiber converges to a cylindrical metric pointwise on compact subsets. More precisely,

$$\lim_{\beta_1 \searrow 0} \frac{1}{\beta_1^2} \varphi \pi_2^* \omega_{\mathrm{Cyl}} = \frac{k}{n} \pi_2^* \omega_{\mathrm{Cyl}}.$$

Proof of the Claim. As shown in (3.33), the restriction of η_{β_1} is given by

$$\frac{1}{2\varphi(\tau)} d\tau^2 + 2\varphi(\tau) d\theta^2,$$

thus the restriction of $\widetilde{\eta_{\beta_1}}$ to a fiber, using the new coordinates (3.69) is given by

$$\frac{k^2 \beta_1^2}{2n^2 \varphi(x)} dx^2 + \frac{2\varphi(x)}{\beta_1^2} d\theta^2. \tag{3.72}$$

As $\beta_1 \searrow 0$, by (3.70), (3.72) converges pointwise on compact subsets to

$$\frac{k}{n} dx^2 + \frac{k}{n} d\theta^2 = \frac{k}{n} \omega_{\mathrm{Cyl}},$$

as claimed. □

By the collapsing arguments in the proof of Theorem 3.7.1 and the claim above, we have shown $\widetilde{\eta_{\beta_1}}$ converges pointwise to $\frac{k}{n}(n\pi_1^* \omega_{\mathrm{FS}} + \pi_2^* \omega_{\mathrm{Cyl}})$ on compact subsets as $\beta_1 \searrow 0$. It remains to prove the pointed Gromov–Hausdorff convergence. Indeed, by arguments in the proof of Proposition 3.5.2, the distance between $Z_{n,k}$ and $\{x = 0\}$ and the distance between $Z_{n,-k}$ and $\{x = 0\}$ tend to infinity under the metric $\widetilde{\eta_{\beta_1}}$. Thus in the limit $\beta_1 \searrow 0$, we get the product differential structure on $\mathbb{P}^{n-1} \times \mathbb{C}^*$ as claimed. Choosing the point p as the base point, the pointwise convergence result implies that

$$\lim_{\beta_1 \searrow 0} \widetilde{\eta_{\beta_1}} = \frac{k}{n}(n\pi_1^*\omega_{\mathrm{FS}} + \pi_2^*\omega_{\mathrm{Cyl}})$$

in the pointed Gromov–Hausdorff sense. □

The $\beta_2 \searrow 0$ case for ξ_{β_2} is similar to Theorem 3.7.1 and Theorem 3.7.6.

The asymptotic behaviors of $t(\beta_2)$ and $\beta_1(\beta_2)$ when $\beta_2 \searrow 0$ are similar to those described in Lemma 3.7.2 and Lemma 3.7.4. We collected them as follows.

Lemma 3.7.8. *For $\beta_2 > 0$ and close to zero,*

$$t = t(\beta_1) = 1 - \frac{2k}{n}\beta_2 + o(\beta_2).$$

Lemma 3.7.9. *For $\beta_2 > 0$ and close to zero,*

$$\beta_1 = \beta_1(\beta_2) = \beta_2 + O(\beta_2^2).$$

Now we state the non-rescaling limit of ξ_{β_2} as $\beta_2 \searrow 0$.

Theorem 3.7.10. *As β_2 tends to 0, $(\mathbb{F}_{n,k}, \xi_{\beta_2})$ converges in the Gromov–Hausdorff sense to $(\mathbb{P}^{n-1}, k\omega_{\mathrm{FS}})$.*

Proof. By Proposition 3.4.5 and Proposition 3.4.6, t tends to 1 as $\beta_2 \searrow 0$. The remaining proof is similar to that of Theorem 3.7.1. □

To obtain a non-collapsed metric in the limit, we consider rescaling ξ_{β_2} in the way of (3.71) and denote the rescaled metric by $\widetilde{\xi_{\beta_2}}$:

$$\widetilde{\xi_{\beta_2}} := k\tau\pi_1^*\omega_{\mathrm{FS}} + \frac{1}{\beta_2^2}\varphi\pi_2^*\omega_{\mathrm{Cyl}} + \varphi(\sqrt{-1}\alpha\wedge\bar{\alpha} - \sqrt{-1}\alpha\wedge\overline{du/u} - \sqrt{-1}du/u\wedge\bar{\alpha}).$$

Moreover, we consider a change of variable as (3.69):

$$u := \frac{\tau - 1 + \frac{k}{n}\beta_2}{\frac{k}{n}\beta_2^2}.$$

As before, we choose a fixed base point from the section $\{u = 0\}$.

Theorem 3.7.11. *As* $\beta_2 \searrow 0$, $(\mathbb{F}_{n,k}, \widetilde{\xi_{\beta_2}}, q)$ *converges in the pointed Gromov–Hausdorff sense to* $(\mathbb{P}^{n-1}\times\mathbb{C}^*, \frac{k}{n}(n\pi_1^*\omega_{\mathrm{FS}} - \pi_2^*\omega_{\mathrm{Cyl}}), q)$.

Proof. By Lemma 3.7.8 and Lemma 3.7.9, we have similar asymptotic behaviors as Lemma 3.7.2 and Lemma 3.7.4 in the β_2 case. Then we can apply similar arguments as in the proof of Theorem 3.7.6. □

3.8 Appendix on Eguchi–Hanson metric as Gromov–Hausdorff limits of KEE metrics

In this section we give a direct proof of a special case of Theorem 3.6.1 when $n = k = 2$. We already know we will obtain Eguchi–Hanson metrics in the limit.

Recall in (3.31) we denote by η a Kähler–Einstein edge metric on Calabi–Hirzebruch manifolds $\mathbb{F}_{n,k}$ that has the following form:

$$\eta = k\tau\pi_1^*\omega_{\mathrm{FS}} + \varphi\left(\pi_2^*\omega_{\mathrm{Cyl}} + \sqrt{-1}\alpha\wedge\bar{\alpha} + \sqrt{-1}\alpha\wedge\frac{d\bar{w}}{\bar{w}} + \sqrt{-1}\frac{dw}{w}\wedge\bar{\alpha}\right), \tag{3.73}$$

where π_1, π_2 and α are defined below (3.31).

From now on, we assume $k = 2$ and $n = 2$, i.e., consider the second Hirzebruch surface $\mathbb{F}_2$. To build a connection between $g_{\mathrm{EH},\epsilon}$ and the Kähler edge metric η on $\mathbb{F}_2$, we first write η in terms of one forms introduced in (3.6).

Consider a change of coordinate $w = v^2$. The reason to do this is that w is the coordinate along each fiber of the line bundle $-2H_{\mathbb{P}^1}$. Recall (3.15), then we have the following correspondence:

$$\begin{aligned} z_1 = vz = r\cos\frac{\theta}{2}e^{\frac{\sqrt{-1}}{2}(\psi+\phi)}, \\ z_2 = v = r\sin\frac{\theta}{2}e^{\frac{\sqrt{-1}}{2}(\psi-\phi)}. \end{aligned} \tag{3.74}$$

In particular,

$$\begin{aligned} r^2 &= |v|^2(1+|z|^2) \\ &= |w|(1+|z|^2). \end{aligned} \tag{3.75}$$

By the definition of α in (3.31), $(1,1)$-forms that appear in η are

$$\frac{dz\wedge d\bar{z}}{(1+|z|^2)^2},\ \alpha\wedge\bar{\alpha},\ \frac{4dv\wedge d\bar{v}}{|v|^2},\ \alpha\wedge\frac{2d\bar{v}}{\bar{v}},\ \frac{2dv}{v}\wedge\bar{\alpha}.$$

Let us first calculate $\sigma_1^2 + \sigma_2^2$ in terms of the coordinate z and v. By (3.6) and (3.74) we have

$$\begin{aligned}
\sigma_1^2+\sigma_2^2 &= \frac{1}{4}d\theta^2+\frac{1}{4}\sin^2\theta d\phi^2 \\
&= \frac{1}{4}\left(-\frac{|z|dz}{(1+|z|^2)z}-\frac{|z|d\bar{z}}{(1+|z|^2)\bar{z}}\right)^2+ \\
&\frac{1}{4}\left(\frac{2|z|}{1+|z|^2}\right)^2\cdot\left(\frac{1}{2\sqrt{-1}}\left(\frac{dz}{z}-\frac{d\bar{z}}{\bar{z}}\right)\right)^2 \\
&= \operatorname{Re}\frac{dz\otimes d\bar{z}}{(1+|z|^2)^2}.
\end{aligned} \tag{3.76}$$

For dr^2 and σ_3, By (3.6) and (3.74) we have

$$\begin{aligned}
4r^2dr^2 &= \frac{r^4}{4}\left(\alpha+\bar{\alpha}+\frac{2dv}{v}+\frac{2d\bar{v}}{\bar{v}}\right)^2, \\
\sigma_3^2 &= -\frac{1}{16}\left(\alpha-\bar{\alpha}+\frac{2dv}{v}-\frac{2d\bar{v}}{\bar{v}}\right)^2. \\
dr^2+r^2\sigma_3^2 &= \frac{r^2}{4}\operatorname{Re}\left(\frac{4dv\otimes d\bar{v}}{|v|^2}+\alpha\otimes\bar{\alpha}+\alpha\otimes\frac{2d\bar{v}}{\bar{v}}+\frac{2dv}{v}\otimes\bar{\alpha}\right).
\end{aligned} \tag{3.77}$$

Denote by g_η the corresponding Riemannian metric on $-2H_{\mathbb{P}^1}$ with respect to η. Then combining (3.73), (3.76) and (3.77) we obtain

$$g_\eta = 2\tau(\sigma_1^2+\sigma_2^2)+\varphi\cdot\frac{4}{r^2}(dr^2+r^2\sigma_3^2). \tag{3.78}$$

For τ and φ in (3.78), results in Section 3.4 apply after we fix $n=k=2$ there. A key feature when $n=2$ is the right hand side in (3.37) is a cubic polynomial, which is easy to handle. In other words, we will be able to derive more precise dependence of T and β_2 on β_1 comparing to results in Proposition 3.5.1 and Proposition 3.5.3. Indeed, this was done in the work of [50]. In this and the next section, we fix $n=2$ and make use of several results obtained in [50].

Since $n = k = 2$, we find $\beta_1 \in (0, 1)$. We will study the asymptotic behaviors of Kähler–Einstein edge metrics η when $\beta_1 \to 1$. Recall [50, (4.20)]

$$\beta_2 = \frac{1}{4}(2\beta_1 + \sqrt{3(3 - 2\beta_1)(1 + 2\beta_1)} - 3).$$

So we have $\beta_2 \to \frac{1}{2}$ as $\beta_1 \to 1$. Recall, τ ranges from $[1, T]$ and T is given by [50, (5.1)]

$$T = 1 + 3\frac{\sqrt{1 + \frac{4}{3}\beta_1 - \frac{4}{3}\beta_1^2} + 2\beta_1 - 1}{4 - 4\beta_1}.$$

Thus, $T \to +\infty$ as $\beta_1 \to 1$. Moreover, recall in (3.37) $\varphi(\tau)$ is given by

$$\begin{aligned}\varphi(\tau) &= \frac{1}{2}\frac{\tau^2 - 1}{\tau} + \frac{1}{3}(\beta_1 - 1)\frac{\tau^3 - 1}{\tau} \\ &= \frac{1}{3}(\beta_1 - 1)(\tau - 1)(\tau - \alpha_1)(\tau - T)/\tau, \quad \text{for } \tau \in [1, T],\end{aligned} \tag{3.79}$$

where α_1 is given in [50, (5.2)] by $\alpha_1 = 1 + 3\dfrac{-\sqrt{1 + \frac{4}{3}\beta_1 - \frac{4}{3}\beta_1^2} + 2\beta_1 - 1}{4 - 4\beta_1}$ and α_1 tends to -1 as $\beta_1 \to 1$. Below we first recall as $\beta_1 \to 1$, the divisor Z_{-2} gets pushed-off to infinity. This result is a special case of Proposition 3.5.2.

Proposition 3.8.1. *The length of the path on each fiber between the intersection point of the fiber with Z_2 and that of the fiber with Z_{-2} tends to infinity as $\beta_1 \to 1$.*

From now on, we use β_1 as a subscript to emphasize the dependence on angles. By (3.73) and (3.79), on any compact subsets of $\mathbb{F}_2$ we have the following convergence in the C^k-norm for every k:

$$
\begin{aligned}
\eta_\infty :&= \lim_{\beta_1 \to 1} \eta_{\beta_1} \\
&= 2\tau_{\beta_1} \frac{\sqrt{-1} dz \wedge d\bar{z}}{(1+|z|^2)^2} + \frac{1}{2}\left(\tau_{\beta_1} - \frac{1}{\tau_{\beta_1}}\right)\left(\frac{\sqrt{-1} dw \wedge d\bar{w}}{|w|^2} + \sqrt{-1}\alpha \wedge \bar{\alpha}\right. \\
&\left. + \sqrt{-1}\alpha \wedge \frac{d\bar{w}}{\bar{w}} + \sqrt{-1}\frac{dw}{w} \wedge \bar{\alpha}\right).
\end{aligned} \tag{3.80}
$$

Recall the Ricci curvature tensor of η_{β_1} is given by

$$
\begin{aligned}
\mathrm{Ric}\, \eta_{\beta_1} &= (1-\beta_1)[C_1] + (1-\beta_2)[C_2] + 2\frac{\sqrt{-1} dz \wedge d\bar{z}}{(1+|z|^2)^2} - \sqrt{-1}\partial\bar{\partial} \log \tau_{\beta_1} \\
&- \sqrt{-1}\partial\bar{\partial} \log \varphi_{\beta_1}.
\end{aligned} \tag{3.81}
$$

The Ricci curvature λ_{β_1} of η_{β_1} is given by $\lambda_{\beta_1} = 1 - \beta_1$. Notice that $\lambda_{\beta_1} \to 0$ as $\beta_1 \to 1$. Hence, by (3.81) and facts that $\varphi \to (\tau^2 - 1)/2\tau$ in the limit and τ is a function of $r^4 = |w|^2(1+|z|^2)^2$ (recall (3.75)) we have

$$
\begin{aligned}
&2\frac{\sqrt{-1} dz \wedge d\bar{z}}{(1+|z|^2)^2} - \sqrt{-1}\partial\bar{\partial} \log \tau_\infty - \sqrt{-1}\partial\bar{\partial} \log \varphi_\infty = 0, \\
&\Rightarrow \tau_\infty \varphi_\infty = C|w|^2(1+|z|^2)^2, \\
&\Rightarrow \tau_\infty = C^{-\frac{1}{2}}(C + r^4)^{\frac{1}{2}}, \quad \text{for some constant } C > 0.
\end{aligned} \tag{3.82}
$$

Replacing τ and φ in (3.78) using (3.82), we have

$$
\eta_\infty = 2C^{-\frac{1}{2}}\left((C+r^4)^{\frac{1}{2}}(\sigma_1^2 + \sigma_2^2) + \frac{r^2}{(C+r^4)^{\frac{1}{2}}}(dr^2 + r^2\sigma_3^2)\right). \tag{3.83}
$$

Comparing (3.83) to (3.14) we see η converges on compact subsets to an Eguchi–Hanson metric as $\beta_1 \to 1$. Summarizing discussions above, we have shown the following result. It is a special case of Theorem 3.6.1 and provides a new way of understanding Eguchi–Hanson metrics.

Theorem 3.8.2. *Fix an arbitrary base point* p *on the zero section. The Kähler–Einstein edge metric* $(\mathbb{F}_2, \eta_{\beta_1}, p)$ *on* $\mathbb{F}_2$ *converges in the pointed Gromov–Hausdorff sense to the following Eguchi–Hanson metric* $(-2H_{\mathbb{P}^1}, \eta_\infty), p$ *on* $-2H_{\mathbb{P}^1}$ *as* $\beta_1 \to 1$*:*

$$\eta_\infty = 2C^{-\frac{1}{2}} \left((C + r^4)^{\frac{1}{2}} (\sigma_1^2 + \sigma_2^2) + \frac{r^2}{(C + r^4)^{\frac{1}{2}}} (dr^2 + r^2 \sigma_3^2) \right),$$

where $C > 0$ *is a constant.*

Proof. The convergence on any compact subset of $-2H_{\mathbb{P}^1}$ of such η to an Eguchi–Hanson metric in C^k-norm for every k can be seen from (3.83). Combining this fact, the fact that Z_{-2} gets pushed-off to infinity as $\beta_1 \to 1$ and choosing an arbitrary base point from the exceptional divisor Z_2, we obtain the convergence in the pointed Gromov–Hausdorff sense by considering convergence of η to an Eguchi–Hanson metric on compact geodesic balls centered at the base point. □

3.9 Appendix on examples of limit of KEE metrics

In this section, we fix $k = 1$ and $n = 2$. Then we follow Section 3.5 and Section 3.6 to give more concrete examples as limit of Kähler–Einstein edge metrics. In the previous work, we treated the case $\beta_1 \searrow 0$ and $\beta_1 \to 1$ [50]. In this section, we consider the several cases: $\beta_1 \nearrow 2$, $\beta_2 \nearrow 1$ with no rescaling and $\beta_2 \nearrow 1$ with rescaling. The asymptotic behaviors in such cases are summarized in Table 3.1.

Under the assumption $k = 1$ and $n = 2$, β_1 ranges from $(0, 2)$. τ ranges from $[1, T]$. We will study the limiting behaviors of Kähler–Einstein edge metrics when $\beta_1 \to 2$.

By (3.37) $\varphi(\tau)$ satisfies

$$\begin{aligned}\varphi(\tau) &= \frac{\tau^2 - 1}{\tau} + \frac{1}{3}(\beta_1 - 2)(\tau^3 - 1) \\ &= \frac{1}{3}(\beta_1 - 2)(\tau - 1)(\tau - \alpha_1)(\tau - T)/\tau,\end{aligned}$$

where T and α_1 satisfy [50, (5.1), (5.2)]

$$\begin{aligned}T &= 1 + 3\frac{\sqrt{1 + \frac{2}{3}\beta_1 - \frac{1}{3}\beta_1^2} + \beta_1 - 1}{4 - 2\beta_1}, \\ \alpha_1 &= 1 + 3\frac{-\sqrt{1 + \frac{2}{3}\beta_1 - \frac{1}{3}\beta_1^2} + \beta_1 - 1}{4 - 2\beta_1}.\end{aligned} \tag{3.84}$$

Obviously $T \to +\infty$ and $\alpha_1 \to -1$ as $\beta_1 \to 2$. β_2 is given by [50, (4.20)]

$$\beta_2 = \frac{\beta_1 - 3 + 3\sqrt{1 + \frac{2}{3}\beta_1 - \frac{1}{3}\beta_1^2}}{2}.$$

Thus $\beta_2 \to 1$ as $\beta_1 \to 2$. More precisely, we have the following asymptotic behavior of $\beta_2(\beta_1)$:

Lemma 3.9.1. *For $\beta_1 < 2$ and close to 2, $\beta_2(\beta_1) = \frac{1}{2}\beta_1 + o(1)$.*

The length of the path on each fiber between the intersection point of the fiber with Z_1 and that of the fiber with Z_{-1} is given by the integration of $\varphi(\tau)$ from 1 to T. A similar calculation as in the proof of Proposition 3.8.1 shows the following result.

Proposition 3.9.2. *The length of the path on each fiber between the intersection point of the fiber* *with Z_1 and that of the fiber with Z_{-1} tends to infinity as $\beta_1 \to 2$.*

Recall we assume Kähler–Einstein edge metrics on $\mathbb{F}_1$ have the form as in (3.73). The Ricci curvature form of such Kähler–Einstein edge metrics, denoted by η, is given by (3.81). From now on, we denote by η_{β_1}, τ_{β_1} and φ_{β_1} to emphasize the dependence of metrics and coordinates on β_1. Let us consider on any compact subsets of $\mathbb{F}_1$,

$$
\begin{aligned}
\lim_{\beta_1\to 2}\eta_{\beta_1} = & \lim_{\beta_1\to 2}\tau\frac{\sqrt{-1}dz\wedge d\bar{z}}{(1+|z|^2)^2} + \left(\frac{\tau^2-1}{\tau} + \frac{1}{3}(\beta_1-2)(\tau^3-1)\right)\left(\frac{\sqrt{-1}dw\wedge d\bar{w}}{|w|^2}\right.\\
& \left. +\sqrt{-1}\alpha\wedge\bar{\alpha} + \sqrt{-1}\alpha\wedge\frac{d\bar{w}}{\bar{w}} + \sqrt{-1}\frac{dw}{w}\wedge\bar{\alpha}\right)\\
& = \tau\frac{\sqrt{-1}dz\wedge d\bar{z}}{(1+|z|^2)^2} + \frac{\tau^2-1}{\tau}\left(\frac{\sqrt{-1}dw\wedge d\bar{w}}{|w|^2} + \sqrt{-1}\alpha\wedge\bar{\alpha} + \sqrt{-1}\alpha\wedge\frac{d\bar{w}}{\bar{w}}\right.\\
& \left. +\sqrt{-1}\frac{dw}{w}\wedge\bar{\alpha}\right).\\
& =: \eta_\infty
\end{aligned}
$$

The Ricci curvature λ_{β_1} of η_{β_1} is given by $\lambda_{\beta_1} = 2-\beta_1$. As $\beta_1 \to 2$, the Ricci curvature λ_{β_1} tends to 0. Thus, the limit metric η_∞ has Ricci curvature 0. Hence by (3.81), τ_∞ and φ_∞ satisfy

$$
\begin{aligned}
& 2\frac{\sqrt{-1}dz\wedge d\bar{z}}{(1+|z|^2)^2} - \sqrt{-1}\partial\bar{\partial}\log\tau_\infty - \sqrt{-1}\partial\bar{\partial}\log\varphi_\infty = 0,\\
\Rightarrow & \tau_\infty\varphi_\infty = C|w|^4(1+|z|^2)^2,\\
\Rightarrow & \tau_\infty = (1+C|w|^4(1+|z|^2)^2)^{\frac{1}{2}}, \quad \text{for some constant } C>0.
\end{aligned}
\tag{3.85}
$$

Thus we obtain the following theorem, which is a special case of Theorem 3.6.1.

Theorem 3.9.3. *Fix an arbitrary base point p on $Z_1 \subset \mathbb{F}_1$. As $\beta_1 \to 2$, the Kähler–Einstein edge metric $(\mathbb{F}_1, \eta_{\beta_1}, p)$ on $\mathbb{F}_1$ converges in the pointed Gromov–Hausdorff sense to a Ricci-flat metric*

$(-H_{\mathbb{P}^1}, \eta_\infty, p)$ *on* $-H_{\mathbb{P}^1}$ *with conic singularity of angle* 4π *along* Z_1.

Proof. By (3.85), the limit metric η_∞ has the form

$$
\begin{aligned}
\eta_\infty =& (1 + C|w|^4(1+|z|^2)^2)^{\frac{1}{2}} \frac{\sqrt{-1}dz \wedge d\bar{z}}{(1+|z|^2)^2} \\
&+ \frac{C|w|^4(1+|z|^2)^2}{(1+C|w|^4(1+|z|^2)^2)^{\frac{1}{2}}} \left(\frac{\sqrt{-1}dw \wedge d\bar{w}}{|w|^2} + \sqrt{-1}\alpha \wedge \bar{\alpha} + \sqrt{-1}\alpha \wedge \frac{d\bar{w}}{\bar{w}} \right. \\
&\left. + \sqrt{-1}\frac{dw}{w} \wedge \bar{\alpha} \right),
\end{aligned}
$$

for some constant $C > 0$. Thus η_∞ has edge singularity of angle 4π along Z_1. For a fixed base point on Z_1, Proposition 3.9.2 shows that Z_{-1} gets pushed-off to infinity in the limit. The remaining proof is the same as that of Theorem 3.8.2. ∎

3.9.1 Calculation in β_2

In this section, we choose a base point from the infinity section and then study the limiti behavior of the Kähler–Einstein edge metrics. In the language of Section 3.5, we will consider the Kähler–Einstein edge metrics that are parametrized by β_2.

As in Section 3.5, we consider $u := 1/w$ as the fiber coordinate. Then $\{u = 0\}$ is the infinity section and $\{u = \infty\}$ is the zero section. We still define s as follows:

$$s = \log(1 + |z|^2) - \log |u|^2.$$

Then as before $\{s = -\infty\}$ still corresponds to the zero section while $\{s = +\infty\}$ corresponds to the infinity section.

Denote now by ξ the Kähler–Einstein edge metric that we seek on $\mathbb{F}_1$. Assume $\xi = \sqrt{-1}\partial\bar{\partial}f(s)$ for some smooth function $f(s)$. As (3.43) we calculate

$$\eta = \sqrt{-1}\partial\bar{\partial}f(s) = \tau\pi_1^*\omega_{\mathrm{FS}} + \varphi\left(\frac{\sqrt{-1}du \wedge d\bar{u}}{|u|^2} + \alpha \wedge \bar{\alpha} - \alpha \wedge \frac{d\bar{u}}{\bar{u}} - \frac{du}{u} \wedge \bar{\alpha}\right),$$

where $\alpha := \bar{z}dz/1 + |z|^2$, $\tau = f'(s)$ and $\varphi = f''(s)$ as before. As in Section 3.5, after a renormalization of the metric we may assume

$$\sup f'(s) = 1.$$

We also assume $\inf f'(s) = t$, for some $t > 0$. In other words, τ ranges from $[t, 1]$.

Now we calculate the Ricci curvature form η using coordinates u and z:

$$\begin{aligned}
\operatorname{Ric}\eta &= -\sqrt{-1}\partial\bar{\partial}\log\eta^2 \\
&= -\sqrt{-1}\partial\bar{\partial}\log\frac{\tau\varphi}{|u|^2(1+|z|^2)^2} \\
&= (1-\beta_1)[Z_1] + (1-\beta_2)[Z_{-1}] + 2\pi_1^*\omega_{\mathrm{FS}} - \sqrt{-1}\partial\bar{\partial}\log\tau \\
&- \sqrt{-1}\partial\bar{\partial}\log\varphi.
\end{aligned}$$

Denote the Ricci curvature by μ. The Kähler–Einstein edge equation

$$\operatorname{Ric}\eta = \mu\eta + (1-\beta_1)[Z_1] + (1-\beta_2)[Z_{-1}]$$

is equivalent to

$$2 - \varphi_\tau - \varphi/\tau = \mu\tau, \quad \tau \in [t, 1]. \tag{3.86}$$

Note that (3.86) gives us the same ODE derived in [50, (4.12)]. Now let us determine boundary conditions satisfied by $\varphi(\tau)$. The same arguments in [50, Proposition 3.3] give us that

$$\varphi(t) = \varphi(1) = 0, \quad \varphi'(t) = \beta_1, \quad \varphi'(1) = -\beta_2. \tag{3.87}$$

Plugging boundary conditions in (3.86) implies that

$$\mu = 2 + \beta_2.$$

The solution to (3.86) is

$$\varphi(\tau) = \frac{\tau^2 - 1}{\tau} + \frac{2 + \beta_2}{3}\frac{1 - \tau^3}{\tau}. \tag{3.88}$$

Combining (3.87) and (3.88), we obtain the dependence of t and β_1 on β_2:

$$\begin{aligned} t &= \frac{1 - \beta_2 + \sqrt{(\beta_2 - 1)(-3\beta_2 - 9)}}{2(2 + \beta_2)}, \\ \beta_1 &= \frac{3}{2} + \frac{1}{2}\beta_2 - \frac{1}{2}\sqrt{(1 - \beta_2)(3\beta_2 + 9)}. \end{aligned} \tag{3.89}$$

Next, inspired by the result in Theorem 3.9.3, we study the limiting behavior of Kähler–Einstein edge metrics when β_2 tends to 1. The proof is similar to that of Proposition 3.8.1 and is omitted.

Proposition 3.9.4. *The length of the path on each fiber between the intersection point of the fiber with Z_1 and that of the fiber with Z_{-1} converges to a finite number as $\beta_2 \to 1$.*

From now on, we denote by ξ_{β_2}, τ_{β_2} and φ_{β_2} to indicate the dependence of metrics and coordinates on β_2.

Theorem 3.9.5. *Fix an arbitrary base point p on $Z_{-1} \subset \mathbb{F}_1$. As $\beta_2 \to 1$, the Kähler–Einstein edge metric $(\mathbb{F}_1, \xi_{\beta_2}, p)$ on $\mathbb{F}_1$ converge in the pointed Gromov–Hausdorff sense to the Fubini–Study metric $(\mathbb{P}^2, \omega_{\mathrm{FS}}, p)$. We will show that ξ_{β_2} converges pointwise smoothly to a degenerate metric tensor that is the pull-back of the Fubini–Study metric under the blow-up map on $\mathbb{F}_1$.*

Proof. Denote by ξ_∞, τ_∞ and φ_∞ the metric and coordinates in the limit when $\beta_2 \to 1$. To find a relation between τ_∞, φ_∞ and s, consider the ODE satisfied by s and τ_{β_2}:

$$\frac{ds}{d\tau_{\beta_2}} = \frac{1}{\varphi_{\beta_2}} = \frac{\tau_{\beta_2}}{(\frac{2+\beta_2}{3})(1-\tau_{\beta_2}^3) + \tau_{\beta_2}^2 - 1}. \tag{3.90}$$

Letting $\beta_2 \to 1$ in (3.90), we obtain (up to a constant that can be chosen to be 0)

$$s = \log \frac{\tau_\infty}{1-\tau_\infty}, \quad \tau_\infty \in (0,1), \tag{3.91}$$

where τ_∞ ranges from $(0,1)$ since $t \to 0$ as $\beta_2 \to 1$. Obviously there holds

$$\varphi_\infty = \tau_\infty(1-\tau_\infty). \tag{3.92}$$

Recall $s = \log(1+|z|^2) - \log|u|^2$. Combining (3.91) and (3.92), the limit metric ξ_∞ has the form:

$$
\begin{aligned}
\xi_\infty &= \tau_\infty \pi_1^* \omega_{\mathrm{FS}} + \varphi_\infty \left(\pi_2^* \omega_{\mathrm{Cyl}} + \sqrt{-1}\alpha \wedge \bar{\alpha} - \sqrt{-1}\alpha \wedge \frac{d\bar{u}}{\bar{u}} - \sqrt{-1}\frac{du}{u} \wedge \bar{\alpha} \right) \\
&= \frac{1+|z|^2}{|u|^2+1+|z|^2} \pi_1^* \omega_{\mathrm{FS}} + \frac{1+|z|^2}{(|u|^2+1+|z|^2)^2} \sqrt{-1} du \wedge d\bar{u} \\
&+ \frac{|u|^2(1+|z|^2)}{(|u|^2+1+|z|^2)^2} \left(\sqrt{-1}\alpha \wedge \bar{\alpha} - \sqrt{-1}\alpha \wedge \frac{d\bar{u}}{\bar{u}} - \sqrt{-1}\frac{du}{u} \wedge \bar{\alpha} \right).
\end{aligned}
\tag{3.93}
$$

Next, we derive the explicit formula for ξ_∞. Recall,

$$
\alpha = \frac{\bar{z} dz}{1+|z|^2}. \tag{3.94}
$$

Plugging (3.94) in (3.93) and by calculations:

$$
\begin{aligned}
\xi_\infty &= \frac{1+|z|^2}{|u|^2+1+|z|^2} \cdot \frac{\sqrt{-1} dz \wedge d\bar{z}}{(1+|z|^2)^2} + \frac{1+|z|^2}{(|u|^2+1+|z|^2)^2} \sqrt{-1} du \wedge d\bar{u} \\
&+ \frac{|u|^2(1+|z|^2)}{(|u|^2+1+|z|^2)^2} \left(\sqrt{-1} \cdot \frac{|z|^2 dz \wedge d\bar{z}}{(1+|z|^2)^2} - \sqrt{-1} \frac{\bar{z} dz}{1+|z|^2} \wedge \frac{d\bar{u}}{\bar{u}} - \sqrt{-1} \frac{du}{u} \wedge \frac{z d\bar{z}}{1+|z|^2} \right) \\
&= \sqrt{-1} \left(\frac{1+|u|^2}{(1+|u|^2+|z|^2)^2} dz \wedge d\bar{z} - \frac{\bar{z} u}{(1+|u|^2+|z|^2)^2} dz \wedge d\bar{u} - \frac{\bar{u} z}{(1+|u|^2+|z|^2)^2} du \wedge d\bar{z} \right. \\
&+ \left. \frac{1+|z|^2}{(1+|u|^2+|z|^2)^2} du \wedge d\bar{u} \right) \\
&= \sqrt{-1} \partial \bar{\partial} \log(1+|u|^2+|z|^2).
\end{aligned}
\tag{3.95}
$$

This limit metric does not have singularity along Z_-1 since $\beta_2 \to 1$ in the limit. Moreover, ξ_∞ has Ricci curvature 3 since μ_{β_2} tends to 3 when $\beta_2 \to 1$. Moreover, the metric ξ_∞ degenerates along $Z_1 = \{u = \infty\}$ as $\xi_\infty \to 0$ as $|u| \to +\infty$.

We next show that ξ_∞ is the pull-back of the Fubini–Study metric ω_{FS} on $\mathbb{P}^2$ under the blow-down map $\pi : \mathbb{F}_1 \to \mathbb{P}^2$. Figure 3.2 shows the blow up of $\mathbb{P}^2(1,1,k)$ at p giving rise to $\mathbb{F}_1$. To see this, we regard $\mathbb{F}_1$, which is the blow-up of $\mathbb{P}^2$ at one point p (WLOG assuming $p = [1 : 0 : 0]$), as the variety embedded in $\mathbb{P}^2 \times \mathbb{P}^1$:

$$\mathbb{F}_1 = \{([x_0 : x_1 : x_2], [y_0 : y_1]) \in \mathbb{P}^2 \times \mathbb{P}^1 : x_1 y_1 = x_2 y_0\}.$$

Then the blow-down map π is given by:

$$\pi : \mathbb{F}_1 \to \mathbb{P}^2$$

$$([x_0 : x_1 : x_2], [y_0 : y_1]) \mapsto [x_0 : x_1 : x_2].$$

Restricted on the chart $\{x_1 \neq 0\}$, there hold:

$$u = \frac{x_0}{x_1}, \quad z = \frac{x_2}{x_1}$$

and

$$\pi(u, z) = (u, z) \in \mathbb{P}^2. \tag{3.96}$$

Recall the Fubini–Study metric on $\mathbb{P}^2$ (restriced to the chart $\{x_1 \neq 0\}$) has the formula

$$\omega_{\text{FS}} = \sqrt{-1} \log(1 + |u|^2 + |z|^2).$$

Thus by (3.95) and (3.96) we have shown,

$$\xi_\infty = \pi^* \omega_{\text{FS}},$$

confirming that ξ_∞ degenerates along the exceptional curve Z_1.

We have shown ξ_{β_2} converges on any compact subset of $\mathbb{F}_1$ to ξ_∞. Now fix an arbitrary base point on $Z_{-1} \subset \mathbb{F}_1$. By Proposition 3.9.4, the length between Z_1 and Z_{-1} remains to be finite when $\beta_2 \to 1$. Thus $(\mathbb{F}_1, \xi_{\beta_2}, p)$ converges in the pointed Gromov–Hausdorff sense to $(\mathbb{P}^2, \omega_{\mathrm{FS}}, p)$ when $\beta_2 \to 1$. □

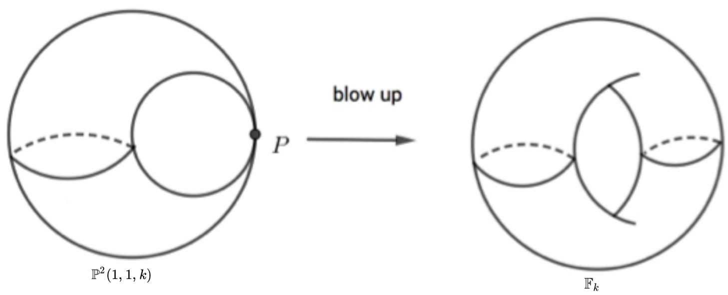

Figure 3.2: Blow up of $\mathbb{P}^2(1,1,k)$ at p (with $k > 1$).

Next, we consider the limiting behavior of properly renormalized Kähler–Einstein edge metrics on $\mathbb{F}_1$ when $\beta_2 \to 1$.

Lemma 3.9.6. *Rescaling the metric ξ by a factor $2(2+\beta_2)/(1-\beta_2+\sqrt{(1-\beta_2)(3\beta_2+9)})$, the interval of definition of τ will change from $[t,1]$ to $[1,T]$ as in (3.84).*

Proof. When we calculate in terms of β_1, we have

$$\beta_2 = \frac{\beta_1 - 3 + 3\sqrt{1+\frac{2}{3}\beta_1 - \frac{1}{3}\beta_1^2}}{2}, \tag{3.97}$$

$$T = 1 + 3\frac{\sqrt{1+\frac{2}{3}\beta_1 - \frac{1}{3}\beta_1^2} + \beta_1 - 1}{4 - 2\beta_1}. \tag{3.98}$$

When we calculate in terms of β_2, we have

$$\beta_1 = \frac{3}{2} + \frac{1}{2}\beta_2 - \frac{1}{2}\sqrt{(\beta_2 - 1)(-3\beta_2 - 9)}, \tag{3.99}$$

$$t = \frac{1 - \beta_2 + \sqrt{(\beta_2 - 1)(-3\beta_2 - 9)}}{2(2 + \beta_2)}. \tag{3.100}$$

Direct calculation shows (3.97) and (3.99) are equivalent. Combining (3.97) and (3.98), we have

$$T = \frac{2(2 + \beta_2)}{4 - 2\beta_1}.$$

Combining (3.99) and (3.100), we have

$$t = \frac{4 - 2\beta_1}{2(2 + \beta_2)}.$$

Thus, $T = 1/t$ and we can rescale the metric η by the factor $1/t$ to change the domain of τ from $[t, 1]$ to $[1, T]$. □

Inspired by Lemma 3.9.6, we normalize ξ_{β_2} by the factor $\sqrt{3}/\sqrt{1 - \beta_2}$ and study its limiting behavior when β_2 tends to 1.

Theorem 3.9.7. *Rescaling the metric ξ_{β_2} by $\sqrt{3}/\sqrt{1 - \beta_2}$, then as $\beta_2 \to 1$, the renormalized metric converges in the pointed Gromov–Hausdorff sense to a Ricci-flat metric on $-H_{\mathbb{P}^1}$, where the base point is chosen from Z_1. See the proof for an explicit explanation. This metric coincides with the one obtained in Theorem 3.9.3.*

Proof. Consider the change of coordinate $y_{\beta_2} := \sqrt{3}\tau_{\beta_2}/\sqrt{1-\beta_2}$ in the following ODE:

$$\frac{ds}{d\tau_{\beta_2}} = \frac{1}{\varphi_{\beta_2}(\tau_{\beta_2})},$$

In the following equations, we omit the subscript β_2:

$$\begin{aligned}
&\frac{ds}{dy}\frac{dy}{d\tau} = \frac{1}{\varphi(y)} \\
&\Rightarrow \frac{ds}{dy} = \frac{\sqrt{3}}{3} \cdot \frac{(1-\beta_2)y}{(\sqrt{1-\beta_2}y)^2 - 1 + \frac{2+\beta_2}{3}(1-(\sqrt{1-\beta_2}y)^3)}.
\end{aligned}$$

By an abuse of notation, still denote by y the coordinate in the limit. As $\beta_2 \to 1$, there holds

$$\frac{ds}{dy} = \frac{y}{y^2-1}, \quad y \in (1, +\infty), \tag{3.101}$$

where the range of y comes from (3.100). Recall the renormalized metric $\sqrt{3}\xi_{\beta_2}/\sqrt{1-\beta_2}$ reads

$$\begin{aligned}
\frac{\sqrt{3}\xi_{\beta_2}}{\sqrt{1-\beta_2}} = \frac{\sqrt{3}\tau_{\beta_2}}{\sqrt{1-\beta_2}}\pi_1^*\omega_{\mathrm{FS}} + \frac{\sqrt{3}\varphi_{\beta_2}}{\sqrt{1-\beta_2}}\Big(&\pi_2^*\omega_{\mathrm{Cyl}} + \sqrt{-1}\alpha\wedge\bar{\alpha} - \sqrt{-1}\alpha\wedge\frac{d\bar{u}}{\bar{u}} \\
&-\sqrt{-1}\frac{du}{u}\wedge\alpha\Big).
\end{aligned} \tag{3.102}$$

Combining (3.101) and (3.102) we obtain the limit metric

$$\begin{aligned}
\tilde{\xi}_\infty = \sqrt{e^{2s}+1}\pi_1^*\omega_{\mathrm{FS}} + \frac{e^{2s}}{\sqrt{e^{2s}+1}}\Big(&\pi_2^*\omega_{\mathrm{Cyl}} + \sqrt{-1}\alpha\wedge\bar{\alpha} - \sqrt{-1}\alpha\wedge\frac{d\bar{u}}{\bar{u}} \\
&-\sqrt{-1}\frac{du}{u}\wedge\alpha\Big).
\end{aligned}$$

Note that this limit metric is Ricci-flat. It coincides with the metric obatined in Theorem 3.9.3 if we choose $C = 1$ there. We have shown the renormalized Kähler–Einstein edge metrics converge to $\tilde{\xi}_\infty$ in smooth local sense. Next, fix a base point from the zero section Z_1. Then by Proposition 3.9.4, we conclude that the infinity section Z_{-1} gets pushed-off to infinity in the limit. Combining this fact with the local smooth convergence, we conclude the pointed Gromov–Hausdorff limit of $(\mathbb{F}_1, \sqrt{3}\eta_{\xi_2}/\sqrt{1-\beta_2})$ is $(-H_{\mathbb{P}^1}, \tilde{\xi}_\infty)$. $\square$

Chapter 4: Numerical Ricci iteration on toric surfaces

4.1 Introduction

Analytical expressions for Kähler–Einstein metrics are unknown except in very few cases. For example, using Calabi ansatz of previous chapter one can write down explicit solutions to the Kähler–Einstein equation (1.5) on certain manifolds (cf. [52, §4.4-4.5]).

Kähler–Einstein metrics are important not only in the study of complex geometry but also other subjects. For example, when setting $\mu = 0$ in (1.5), the resulting equation is known as the Calabi–Yau equation. Solutions to this equation, namely Calabi–Yau metrics, are fundamental building blocks in superstring theory [11, 24]. Typically, explicit formula for such metrics are unavailable. Despite lacking an explicit form, numerical solutions for them, and more generally for Kähler–Einstein metrics have been developed across various settings for the underlying manifolds, and an incomplete list includes [6, 17, 19, 20, 30, 34].

A systematic way to study (1.5) is pioneered by Rubinstein [45–47], where he introduced the Ricci iteration:

Definition 4.1.1. Let M be a Kähler manifold and Ω be a Kähler class satisfying $\mu\Omega = c_1(M)$ for some $\mu \in \mathbb{R}$. Given a Kähler form ω in the class Ω and a number $\tau > 0$, define the time τ

Ricci iteration to be the sequence of forms $\{\omega_{k\tau}\}_{k\geq 0}$, satisfying the equations

$$\begin{aligned} &\omega_{k\tau} = \omega_{(k-1)\tau} + \tau\mu\omega_{k\tau} - \tau \operatorname{Ric}\omega_{k\tau}, \quad k \in \mathbb{N}, \\ &\omega_0 = \omega, \end{aligned}$$

for each $k \in \mathbb{N}$ for which a solution exists.

Our focus is on the case where M is *Fano*, i.e., $c_1(M) > 0$, and $\tau = 1$. In this setting, given $[\omega_0] = 2\pi c_1(M)$, the Ricci iteration reduces to the following dynamical system

$$\operatorname{Ric}\omega_{i+1} = \omega_i, \quad i = 0, 1, \ldots \tag{4.1}$$

The motivations behind the introduction of the Ricci iteration are to discretize the Ricci flow [31, §3] and treat easier equations than original in each iteration step.

The Kähler–Einstein metric is a fixed point of (4.1). Thus, we may expect that convergence of the Ricci iteration will yield Kähler–Einstein metrics. The idea to use the Ricci iteration as a numerical method, as discussed in [45–47], is that, assuming the sequence of metrics produced by Ricci iteration converging to the Kähler–Einstein metric, then numerically computing positively curved Kähler–Einstein metric amounts to solving a sequence of Calabi–Yau equations (4.1). The exploration of numerically solving Calabi–Yau equations commenced with Donaldson's algorithm, proposed in [17], which relies on the theory on balanced metrics.

However, it is not guaranteed that the Ricci iteration will converge to a Kähler–Einstein metric. In (4.1), theoretical results for convergence require a sequence of automorphisms applied to each solution obtained from iterations:

Theorem 4.1.2. [15, Theorem 1.2] *Let (M, J, ω_0) be a compact Kähler manifold admitting a Kähler–Einstein metric. Suppose the Kähler class associated to ω_0 is $2\pi c_1(M, J)$ and let $\{\omega_i\}_{i\in\mathbb{N}}$ by given by* (4.1)*. Then there exist holomorphic diffeomorphisms h_i such that $h_i^*\omega_i$ converges smoothly to a Kähler–Einstein metric.*

We only consider the case where M is a toric manifold (cf. Definition 4.2.3). Then each step in the Ricci iteration reduces to a *real* Monge–Ampère equation. More precisely, we need to solve

$$\begin{aligned} \det \nabla^2 \psi_{i+1}(x) &= e^{-\psi_i(x)}, \quad x \in \mathbb{R}^n, \\ \nabla \psi_{i+1}(\mathbb{R}^n) &= \operatorname{int} P, \end{aligned} \tag{4.2}$$

where $\psi_0(x) : \mathbb{R}^n \to \mathbb{R}$ serves as an initial choice and P is the Delzant polytope (cf. Theorem 4.2.8) of M. Iteration schemes regarding (4.2) are studied by Hunter [36, 37]. In particular, his result [37, Theorem 2.1] recovered the convergence of the Ricci iteration in the toric setting.

Our goal is to numerically implement the Ricci iteration for toric manifolds. In each step, it suffices to solve (4.2), which is known as the second boundary value problem for real Monge–Ampère equations. Such equations are linked to the optimal transport theory, as their solutions give rise to optimal transport maps. Back in 2016, Lindsey and Rubinstein proposed a numerical scheme for solving (4.2) and proved a corresponding convergence theorem [43, Theorem 1.6]. They also pointed out the potential to apply their numerical method to the Ricci iteration [43, §8]. Recently, Bonnet–Mirebeau proposed another numerical method for solving (4.2) with a convergence theorem proved [5, Theorem 5.25].

We successfully implement the Ricci iteration for toric del Pezzo surfaces. In our implementation, we choose the numerical solver in [5] in each step. Their approach is efficient for the specific dimension we are concerned: the real dimension 2. However, in higher dimensions, Lindsey and Rubinstein's method will have the advantage of being straightforward to apply, while in [5] a non-trivial discretization procedure is required, cf. [5, §7].

Our numerical results suggest that the Ricci iteration in the toric surface case converges without the need of applying automorphisms to the metrics obtained from each iteration. This finding leads to the question of whether the theoretical results of Theorem 4.1.2 and also [37, Theorem 2.1] can be further strengthened. Moreover, thanks to the convergence achieved through the Ricci iteration, our numerical implementation provides a new approach for finding canonical metrics on toric del Pezzo surfaces. This will be discussed in Chapters 5 and 6.

The contribution of this work also lies in demonstrating the applicability of the Ricci iteration in the numerical domain. We compare the Ricci iteration as an approach to finding numerical canonical metrics to previous works with the same goal in Sections 5.3 and 6.3. Furthermore, the present work provides a unified way to treat both Kähler–Einstein metrics and Kähler–Ricci soliton metrics on the toric del Pezzo surfaces, as both are governed by real Monge–Ampère equations.

4.1.1 Organization

In Section 4.2, we introduce the definition of toric Kähler surfaces and review existence results of canonical metrics on them. In Section 4.3, we present the formulation of the Ricci iteration on toric surfaces and also present existing theoretical results regarding its convergence.

From Section 4.4 to Section 4.8, we explain in detail the numerical method in [5]. The method is used in this work to solve the Monge–Ampère equations. We present both the convergence and existence results for solutions to their numerical scheme. These theoretical results guarantee the robustness of our numerical implementation.

In Section 4.9, we specify the surfaces on which we implement the Ricci iteration and clarify corresponding boundary conditions. We present detailed settings of our numerical work, including how to choose a suitable domain of solutions and properly normalize solutions.

4.2 Canonical metrics on toric del Pezzo surfaces

4.2.1 Toric Kähler manifold

We introduce the following notation for the n-dimensional real torus:

$$\mathbb{T}^n := \mathbb{R}^n/2\pi\mathbb{Z}^n \cong (S^1)^n$$

and in comparison, the n-dimensional complex torus:

$$\mathbb{T}^n_{\mathbb{C}} := \mathbb{C}^n/2\pi\sqrt{-1}\mathbb{Z}^n \cong \mathbb{R}^n \times \sqrt{-1}\mathbb{T}^n.$$

From now on, we will consider Kähler manifolds that admit toric symmetry, as described in the following definitions.

Just as Kähler geometry can be seen as an intersection of complex and symplectic geometries, a Kähler toric manifold will be both a toric variety, from the complex geometry side and a symplectic toric manifold from the symplectic side. For readers' convenience, we include these definitions here and the main reference is [2].

From the complex geometry side, we have

Definition 4.2.1. A toric variety is a normal variety M that contains the complex torus $\mathbb{T}^n_{\mathbb{C}}$ as a dense open subset, and is equipped with an holomorphic action of $\mathbb{T}^n_{\mathbb{C}}$ on M that extends the natural action of $\mathbb{T}^n_{\mathbb{C}}$ on itself.

From the symplectic geometry side, we have

Definition 4.2.2. A symplectic toric manifold is a symplectic manifold (M, ω) equipped with an effective Hamiltonian action of the real torus $\mathbb{T}^n$ on (M, ω).

The toric Kähler manifold is defined to have both structures.

Definition 4.2.3. An n-dimensional Kähler manifold (M, ω, J) is said to be toric if it is a toric variety that contains $\mathbb{T}^n_{\mathbb{C}}$ as a dense open set, and the induced action $\mathbb{T}^n \subset \mathbb{T}^n_{\mathbb{C}}$ on (M, ω, J) makes it also a symplectic manifold.

From now on, we only consider toric Kähler manifolds, and Kähler metric on which that is invariant under the $\mathbb{T}^n$ action.

By the theory of toric Kähler geometry, cf. [2, Section 2.2], the set

$$M_{\text{open}} := \{p \in M : \mathbb{T}^n \text{ action is free at } p\} \cong \mathbb{T}^n_{\mathbb{C}}$$

is an open dense subset of M, moreover, we have the holomorphic coordinates as follows:

$$M_{\text{open}} \cong \mathbb{C}^n / 2\pi\sqrt{-1}\mathbb{Z}^n = \mathbb{R}^n \times \sqrt{-1}\mathbb{T}^n = \left\{ z = \frac{1}{2}x + \sqrt{-1}\theta : x \in \mathbb{R}^n, \theta \in \mathbb{T}^n \right\},$$

such that the $\mathbb{T}^n$ action is given by

$$t \cdot z = t \cdot \left(\frac{1}{2}x + \sqrt{-1}\theta \right) = \frac{1}{2}x + \sqrt{-1}(t + \theta),\ z \in M_{\mathrm{open}}, t \in \mathbb{T}^n. \tag{4.3}$$

We summarize this fact into the next definition.

Definition 4.2.4. The complex coordinates (x, θ) on M_{open} is defined using the following identification:

$$M_{\mathrm{open}} \cong \mathbb{C}^n / 2\pi\sqrt{-1}\mathbb{Z}^n = \mathbb{R}^n \times \sqrt{-1}\mathbb{T}^n = \left\{ z = \frac{1}{2}x + \sqrt{-1}\theta : x \in \mathbb{R}^n, \theta \in \mathbb{T}^n \right\}. \tag{4.4}$$

On M_{open}, a toric invariant Kähler metric has a local potential function as (1.1):

$$\omega|_{M_{\mathrm{open}}} = \sqrt{-1}\partial_z \partial_{\bar{z}} \psi.$$

Lemma 4.2.5. *In the complex coordinates (x, θ),*

$$\omega|_{M_{\mathrm{open}}} = \sum_{i,j=1}^{n} \frac{\partial^2 \psi}{\partial x_i \partial x_j} dx_i \wedge d\theta_j.$$

Proof. By (4.4), there holds

$$
\begin{aligned}
\omega|_{M_{\text{open}}} &= \sqrt{-1}\partial\bar{\partial}\psi \\
&= \sqrt{-1}\sum_{i,j=1}^{n}\left(\frac{\partial}{\partial z_i}\frac{\partial\psi}{\partial\bar{z}_j}\right)dz_i\wedge d\bar{z}_j \\
&= \sqrt{-1}\sum_{i,j=1}^{n}\left(\frac{\partial}{\partial x_i}-\sqrt{-1}\frac{\partial}{\partial\theta_i}\right)\left(\frac{\partial\psi}{\partial x_j}+\sqrt{-1}\frac{\partial\psi}{\partial\theta_j}\right)\left(\frac{1}{2}dx_i+\sqrt{-1}d\theta_i\right)\left(\frac{1}{2}dx_j-\sqrt{-1}d\theta_j\right) \\
&= \sum_{i,j}^{n}\frac{\partial^2\psi}{\partial x_i\partial x_j}dx_i\wedge d\theta_j,
\end{aligned}
\tag{4.5}
$$

where we assume that ω is toric invariant, so that $\partial\psi/\partial\theta_i \equiv 0$ due to (4.3). □

The positivity of ω implies that the potential function $\psi(x)$ is strongly convex, which allows us to consider the Legendre transform of $\psi(x)$ and also its gradient image.

Lemma 4.2.6. *The gradient map*

$$\nabla\psi(x) : \mathbb{R}^n \to \operatorname{int} P \tag{4.6}$$

is a diffeomorphism of $\mathbb{R}^n$ *onto the interior* int P *of a convex polytope* $P \subset \mathbb{R}^n$.

Such polytopes satisfy several combinatorial properties and form a set called Delzant polytopes, as we define below.

Definition 4.2.7. A convex polytope P in $\mathbb{R}^n$ is Delzant if:

1. there are n edges meeting at each vertex p;

2. the edges meeting at a vertex p satisfy that each edge is of the form $p+tv_i$, for $0 \le t < \infty$, $i = 1, \ldots, n$ and $v_i \in \mathbb{Z}^n$;

3. the $v_1, \ldots, v_n$ in (2) can be chosen to be a basis of $\mathbb{Z}^n$.

Theorem 4.2.8. [12, Theorem 28.2] *There is an one-to-one correspondence between Delzant polytopes and symplectic toric manifolds.*

Let $x \in \mathbb{R}^n$ as in (4.4) be the real part of the complex coordinates on M_{open}. Define

$$y := \nabla \psi(x). \tag{4.7}$$

By Lemma 4.2.6, we can define a second coordinate system on M_{open}.

Definition 4.2.9. The symplectic coordinates on M_{open} is defined as

$$M_{\text{open}} \cong \operatorname{int} P \times \mathbb{T}^n = \{(y, \theta) : y \in \operatorname{int} P \text{ as in (4.7)}, \theta \text{ is the same as before}\}. \tag{4.8}$$

Using the symplectic coordinates, the Kähler form ω has the simplest form $\omega = \sum dy \wedge d\theta$ and the complex structure J is determined by a potential function $\psi^*(y)$, which is the Legendre transform of $\psi(x)$ [2].

The complex coordinate x and the symplectic coordinate y will both be used. Next, we write down the concerned real equations arising from geometric equations using the real coordinates $x \in \mathbb{R}^n$. Consider two toric invariant Kähler metrics which are given by $\omega_1 = \sqrt{-1}\partial\bar{\partial}\psi_1(x)$ and $\omega_2 = \sqrt{-1}\partial\bar{\partial}\psi_2(x)$ on M_{open}.

Proposition 4.2.10. [36, Lemma 3.3.2] *If there exists $f \in C^\infty(M)$ such that*

$$\operatorname{Ric} \omega_1 = \omega_2 + \sqrt{-1}\partial\bar{\partial} f,$$

then

$$\det \nabla^2 \psi_1(x) = e^{-\psi_2(x) - f(x) + c},$$

for some constant c*.*

4.2.2 Kähler–Einstein metrics on toric del Pezzo surfaces

We only consider toric del Pezzo surfaces, i.e., complex dimension 2 toric manifold with positive first Chern class. They are

$$\mathbb{P}^2,\ \mathbb{P}^1 \times \mathbb{P}^1,\ \mathbb{P}^2 \# \overline{\mathbb{P}^2},\ \mathbb{P}^2 \# 2\overline{\mathbb{P}^2},\ \mathbb{P}^2 \# 3\overline{\mathbb{P}^2}, \tag{4.9}$$

where $\mathbb{P}^2 \# n\overline{\mathbb{P}^2}$ is the blowup of $\mathbb{P}^2$ at n distinct points in general position.

By Theorem 4.2.8, each toric Kähler surface is associated with a convex polytope $P \subset \mathbb{R}^2$, namely the Delzant polytope. There is a canonical choice of the formula for such polytopes, cf. [39, (27)]:

$$P = \bigcap_\alpha \{ y \in \mathbb{R}^n : \langle n_\alpha, y \rangle + 1 \geq 0 \}, \tag{4.10}$$

where $\{n_\alpha\}$ denotes a set of inward pointing normal vectors in $\mathbb{Z}^n$ and the components of each n_α are required to be relatively prime over $\mathbb{Z}$. From now on, when we refer to a Delzant polytope this canonical formula is used.

More precisely, the Delzant polytope of $\mathbb{P}^2$ is a triangle, denoted by P_1, with vertices

$$(-1,-1), (2,-1), (-1,2).$$

The Delzant polytope of $\mathbb{P}^1 \times \mathbb{P}^1$ is a square P_2 with vertices

$$(-1,-1), (1,-1), (1,1), (-1,1).$$

The Delzant polytope of $\mathbb{P}^2 \# 3\overline{\mathbb{P}^2}$ is a hexagon P_3 with vertices

$$(-1,0), (0,-1), (1,-1), (1,0), (0,1), (-1,1).$$

The Delzant polytope of $\mathbb{P}^2 \# 2\overline{\mathbb{P}^2}$ is a pentagon P_4 with vertices

$$(1,-1), (1,0), (0,1), (-1,1), (-1,-1).$$

The Delzant polytope of $\mathbb{P}^2 \# \overline{\mathbb{P}^2}$ is a trapezoid P_5 with vertices

$$(2,-1), (0,-1), (-1,0), (-1,2).$$

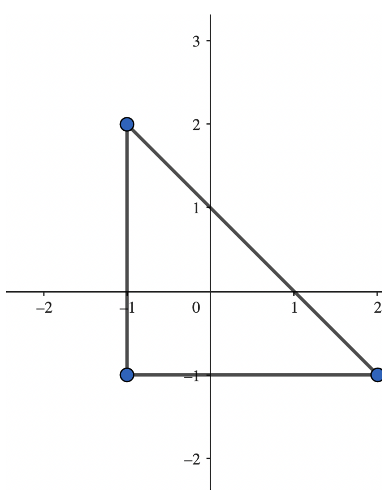

Figure 4.1: Delzant polytope of $\mathbb{P}^2$

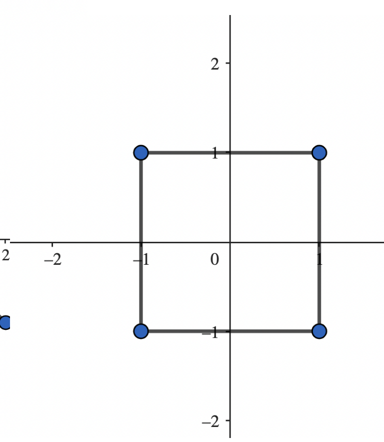

Figure 4.2: Delzant polytope of $\mathbb{P}^1 \times \mathbb{P}^1$

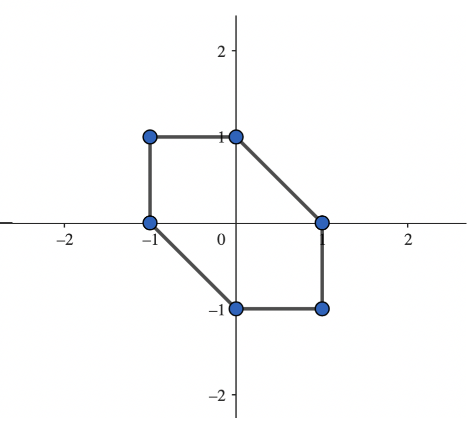

Figure 4.3: Delzant polytope of $\mathbb{P}^2 \# 3\overline{\mathbb{P}^2}$

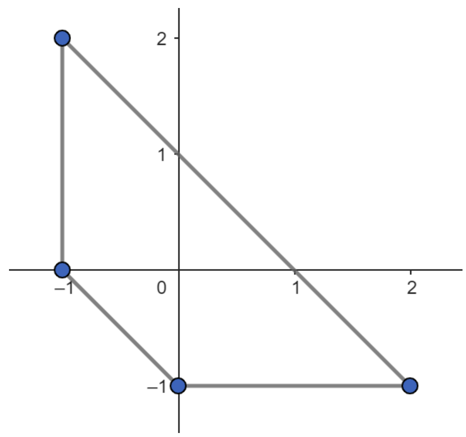

Figure 4.4: Delzant polytope of $\mathbb{P}^2\#\overline{\mathbb{P}^2}$

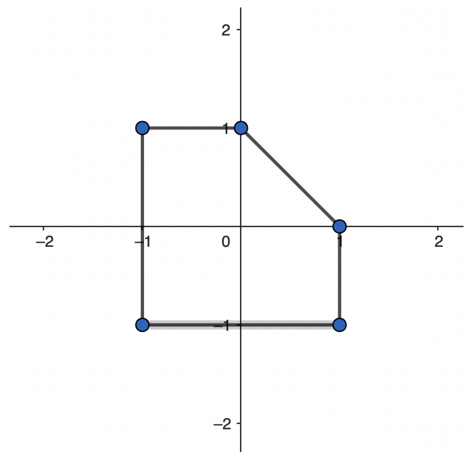

Figure 4.5: Delzant polytope of $\mathbb{P}^2\#2\overline{\mathbb{P}^2}$

The problem of existence of Kähler–Einstein metrics on del Pezzo surfaces is solved by Tian [53, Main theorem]. By Tian's theorem, among all toric del Pezzo surfaces, only $\mathbb{P}^2$, $\mathbb{P}^1\times\mathbb{P}^1$ and $\mathbb{P}^2\#3\overline{\mathbb{P}^2}$ admit Kähler–Einstein metrics.

By Theorem 4.2.8 and Proposition 4.2.10, existence of Kähler–Einstein metrics requires certain real Monge–Ampère equation to be solvable:

Theorem 4.2.11. *When P equals P_1, P_2 or P_3, the following equation is solvable:*

$$\begin{aligned} \det \nabla^2\psi(x) &= e^{-\psi(x)}, \quad x\in\mathbb{R}^2, \\ \nabla\psi(\mathbb{R}^2) &= \operatorname{int} P. \end{aligned} \tag{4.11}$$

From the geometry point of view, a solution ψ corresponds to a Kähler–Einstein metric ω on a surface S such that on the open orbit $\omega|_{S_{\text{open}}} = \sqrt{-1}\partial\bar\partial\psi$.

4.2.3 Kähler–Ricci solitons on toric del Pezzo surfaces

The existence result of Kähler–Ricci solitons on toric Fano manifolds is proved by Wang and Zhu [56, Theorem 1.1]:

Theorem 4.2.12. *Any toric Fano manifold admits a Kähler–Ricci soliton, unique up to holomorphic automorphisms.*

Denote by $p \in \mathbb{R}^2$ the barycenter of Delzant polytope P. By [16, p. 53, line -12], the *Futaki invariant* of a toric manifold vanishes if and only if p is the origin. By [56, Corollary 1.2], the Ricci soliton on a toric del Pezzo surface is Kähler–Einstein if and only if the Futaki invariant vanishes. Thus, among all toric del Pezzo surfaces only $\mathbb{P}^2\#\overline{\mathbb{P}^2}$ and $\mathbb{P}^2\#2\overline{\mathbb{P}^2}$ admit Ricci solitons that are not Kähler–Einstein, as only the barycenter of P_4 or P_5 is not the origin.

We only consider the surface S to be $\mathbb{P}^2\#\overline{\mathbb{P}^2}$ or $\mathbb{P}^2\#2\overline{\mathbb{P}^2}$. Let ω be a Kähler–Ricci soliton on S that solves (1.10) for $\mu = 1$. Let X be the soliton vector field. Let θ_ω^X be the soliton potential such that $\mathcal{L}_X\omega = \sqrt{-1}\partial\bar\partial\theta_\omega^X$, cf. Section 1.1.3. Given $\omega|_{S_{\text{open}}} = \sqrt{-1}\partial\bar\partial\psi$, by Proposition 4.2.10, up to a constant the metric potential ψ satisfies

$$\begin{aligned} \det\nabla^2\psi(x) &= e^{-\psi(x)-\theta_\omega^X(x)}, \quad x\in\mathbb{R}^2 \\ \nabla\psi(\mathbb{R}^2) &= \operatorname{int} P. \end{aligned} \tag{4.12}$$

The following result gives an explicit formula for the soliton potential in case of $\mathbb{P}^2\#\overline{\mathbb{P}^2}$ and $\mathbb{P}^2\#2\overline{\mathbb{P}^2}$.

Proposition 4.2.13. [56, Lemma 2.2] *Let S be $\mathbb{P}^2\#\overline{\mathbb{P}^2}$ or $\mathbb{P}^2\#2\overline{\mathbb{P}^2}$. Let P be the Delzant polytope. Let $y = (y_1, y_2)$ be the symplectic coordinate in (4.2.9). Then up to a constant, the soliton* *potential is given by*

$$\theta_\omega^X(x) = c_1 \frac{\partial \psi}{\partial x_1}(x) + c_2 \frac{\partial \psi}{\partial x_2}(x)$$

where c_1, c_2 are constant such that

$$\int_P y_i e^{-c_1 y_1 - c_2 y_2} dy_1 dy_2 = 0,$$

for $i = 1, 2$.

Next we use Proposition 4.2.13 to compute an exact formula for the soliton potential on $\mathbb{P}^2 \# 2\overline{\mathbb{P}^2}$ and $\mathbb{P}^2 \# \overline{\mathbb{P}^2}$. Let $y = (y_1, y_2)$ be the symplectic coordinate.

Proposition 4.2.14. *On $\mathbb{P}^2 \# 2\overline{\mathbb{P}^2}$, $c_1 = c_2 \approx 0.434748$.*

Proof. By Proposition 4.2.13, the constant c_1 and c_2 satisfy

$$\int_{P_4} y_i e^{-c_1 y_1 - c_2 y_2} dy_1 dy_2 = 0, \tag{4.13}$$

for $i = 1, 2$. By [29, Corollary 12], there holds $c_1 = c_2 = c$ for some c. Hence, (4.13) reduces to

$$\int_{P_4} y_1 e^{-c(y_1+y_2)} dy_1 dy_2 = 0, \quad \int_{P_4} y_2 e^{-c(y_1+y_2)} dy_1 dy_2 = 0, \tag{4.14}$$

for some c. Adding the two equations in (4.14), we have

$$\int_{P_4} (y_1 + y_2) e^{-c(y_1+y_2)} dy_1 dy_2 = 0. \tag{4.15}$$

It remains to find c that satisfies (4.15). Consider the function of c

$$\mathcal{K}(c) := \int_{P_4} e^{-c(y_1+y_2)} dy_1 dy_2, \tag{4.16}$$

then

$$\mathcal{K}'(c) = \int_{P_4} -(y_1+y_2) e^{-c(y_1+y_2)} dy_1 dy_2.$$

Hence, the constant c satisfies (4.15) if $\mathcal{K}'(c) = 0$.

We calculate using (4.16) that

$$\mathcal{K}(c) = \frac{e^{2c} - 2 + (1-c) \cdot e^{-c}}{c^2}.$$

Now by numerical root finding method, we solve

$$\mathcal{K}'(c) = 0$$

and obtain that $c \approx 0.434748$. □

Proposition 4.2.15. *On* $\mathbb{P}^2 \# \overline{\mathbb{P}^2}$, $c_1 = c_2 = c \approx -0.52762$.

Proof. The proof follows the same steps as Proposition 4.2.14. □

4.3 The Ricci iteration on toric del Pezzo surfaces

Our goal is to find a numerical solution to (4.11) and (4.12) that are associated to toric del Pezzo surfaces. One difficulty in solving these equations, both theoretically and numerically, comes from the fact that the right hand side involves nonlinear terms of $\psi(x)$. A strategy to overcome this is to use the Ricci iteration (4.1). Indeed, it has been pointed out that one can use the Ricci iteration to find numerical approximations to both Kähler–Einstein and Kähler–Ricci soliton metrics in [45–47], e.g., cf. [47, §10.5]. To streamline the presentation, we introduce the following iteration system that is directly related to (4.11) and (4.12):

Definition 4.3.1. [37, (11)] Let $0 \leq i \in \mathbb{N}$. The Monge–Ampère iteration of (4.11) is defined as a sequence of equations

$$\begin{aligned} \det \nabla^2 \psi_{i+1}(x) &= e^{-\psi_i(x)}, \quad x \in \mathbb{R}^2, \\ \nabla \psi_{i+1}(\mathbb{R}^2) &= \operatorname{int} P, \\ \int_{\mathbb{R}^2} e^{-\psi_{i+1}(x)}\, dx &= |P|, \end{aligned} \tag{4.17}$$

with an initial choice $\psi_0(x) : \mathbb{R}^2 \to \mathbb{R}$, where $|P|$ denotes the area of P.

The Monge–Ampère iteration (4.17) is proposed by Hunter [36, 37]. It is a real analogue of the Ricci iteration on general Kähler manifolds.

4.3.1 Kähler–Einstein metrics

We implement the Ricci iteration on $\mathbb{P}^2$, $\mathbb{P}^1 \times \mathbb{P}^1$ and $\mathbb{P}^2 \# 3\overline{\mathbb{P}^2}$ by solving (4.17) sequentially. The convergence result regarding (4.17) is established as follows:

Theorem 4.3.2. [37, Theorem 1.2] *Let $\{\psi_i(x)\}_{i\in\mathbb{N}}$ be solutions to (4.17), then there exists a sequence of $a_i \in \mathbb{R}^2$ such that the $\{\psi_i(x + a_i)\}_{i\in\mathbb{N}}$ converges to a solution to (4.11).*

When P in (4.17) is a Delzant polytope, Theorem 4.3.2 recovers the result in Theorem 4.1.2. In [36, 37], Theorem 4.3.2 is proved for more general convex bodies.

Our numerical results, presented in Section 5.2, indicate that this convergence occurs without needing the translation of variables. Theoretical results to this end remain unknown.

The Monge–Ampère equations (4.17) have the second boundary condition, and we will employ the numerical scheme proposed in [5] to solve such problems.

4.3.2 Solitons

Regarding the soliton case (4.12), the corresponding iterative scheme reads

$$\begin{aligned} \det \nabla^2 \psi_{i+1}(x) &= e^{-\psi_i(x)-\theta_i(x)}, \quad x \in \mathbb{R}^2, \\ \nabla \psi_{i+1}(\mathbb{R}^2) &= \operatorname{int} P, \\ \int_{\mathbb{R}^2} e^{-\psi_{i+1}(x)}\, dx &= |P|, \end{aligned} \tag{4.18}$$

where

$$\theta_i(x) := 0.434748 \left(\frac{\partial \psi_i(x)}{\partial x_1} + \frac{\partial \psi_i(x)}{\partial x_2} \right),$$

for $\mathbb{P}^2 \# 2\overline{\mathbb{P}^2}$ and

$$\theta_i(x) := -0.52762 \left(\frac{\partial \psi_i(x)}{\partial x_1} + \frac{\partial \psi_i(x)}{\partial x_2} \right)$$

for $\mathbb{P}^2 \# \overline{\mathbb{P}^2}$, indicated by Propositions 4.2.14 and 4.2.15.

The convergence of (4.18), or more generally of the Ricci iteration in the soliton case is conjectured by Rubinstein [47, p. 1546, line 1-2]. Our numerical results, presented in 6.2, suggest that the convergence does happen in the toric surface case.

Compared to (4.17), a difficulty in solving (4.18) arises as the right hand side consists not only of the solution obtained from the last iteration but also its first order derivative. A more complicated right hand side usually means more time needed to achieve a numerical solution.

We propose an alternative implementation as a possible way to get around this issue. Recall, the equation (4.18) is obtained by spelling out the soliton equation (1.15) directly. Also, recall the soliton potential function in (1.15) is explicitly known for $\mathbb{P}^2\#\overline{\mathbb{P}^2}$ and $\mathbb{P}^2\#2\overline{\mathbb{P}^2}$, cf. Propositions 4.2.14 and 4.2.15. More precisely, given $x = (x_1, x_2)$ and $y = (y_1, y_2)$ respectively the complex and symplectic coordinates of either $\mathbb{P}^2\#\overline{\mathbb{P}^2}$ or $\mathbb{P}^2\#2\overline{\mathbb{P}^2}$, the push-forward of the soliton potential under the gradient map of the metric potential is linear in y. By (4.7), coordinates y are the gradient image under the metric potential ψ of x. Consequently, under the gradient image of the Legendre transform ψ^*, coordinates y are mapped to x. We consider the following lemma:

Lemma 4.3.3. *Let $\psi(x) : \mathbb{R}^n \to \mathbb{R}$ be a convex function. Let $\psi^*(y)$ be its Legendre transform. For any $v \in \mathbb{R}^n$, the Legendre transform of the function $\psi(x) + \langle v, x\rangle$ is given by*

$$\tilde{\psi}^*(y) = \psi^*(y - v).$$

Proof. By definition of the Legendre transform, for any y in the domain of ψ^*,

$$\psi^*(y) = \sup_{x\in\mathbb{R}^n} \langle y, x\rangle - \psi(x). \tag{4.19}$$

Hence, for any y such that $y - v$ is in the domain of ψ^*,

$$\begin{aligned}\tilde{\psi}^*(y) &= \sup_{x\in\mathbb{R}^n} \langle y, x\rangle - \psi(x) - \langle v, x\rangle \\ &= \sup_{x\in\mathbb{R}^n} \langle y - v, x\rangle - \psi(x) \\ &= \psi^*(y - v).\end{aligned}$$

□

Inspired by Lemma 4.3.3, we realize that the existence of a linear soliton potential in y roughly corresponds to a translation of variable in x for the metric potential ψ. Instead of solving (4.18), we may still solve (4.17) sequentially, but translate the variable in solutions obtained from each iteration by a constant before feeding it into the next step.

Consider

$$\begin{aligned}\det \nabla^2 \psi_{i+1}(x) &= e^{-\psi_i(x_1+c, x_2+c)}, \quad x \in \mathbb{R}^2,\\ \nabla \psi_{i+1}(\mathbb{R}^2) &= \operatorname{int} P,\\ \int_{\mathbb{R}^2} e^{-\psi_{i+1}(x)}\, dx &= |P|,\end{aligned} \tag{4.20}$$

where $c = 0.434748$ for $\mathbb{P}^2 \# 2\overline{\mathbb{P}^2}$ and $c = -0.52762$ for $\mathbb{P}^2 \# \overline{\mathbb{P}^2}$ by Propositions 4.2.14 and 4.2.15. We solve both (4.18) and (4.20) to approximate Ricci solitons.

4.4 Gaveau's reformulation of Monge–Ampère equations

Starting this section, we present an exposition of the numerical method in [5]. In this section, our goal is to revisit Gaveau's reformulation of the Monge–Ampère equations. This result is essentially a characterization of the determinant operator. The key result is an observation in linear algebra, see Lemma 4.4.3.

From now on, let K be an open bounded convex subset of $\mathbb{R}^n$ that contains the origin. In our applications it will always be a cube. Let $f \in L^\infty(K)$. Gaveau gave an ingenious reformulation of the Monge–Ampère equation

$$\det \nabla^2 u(x) = f(x), \quad x \in K, \tag{4.21}$$

that is crucial for the numerical scheme used later.

Denote by $\mathrm{Sym}^2(\mathbb{R}^n)$ the set of $n \times n$ symmetric matrices, and let $\mathcal{P} \subset \mathrm{Sym}^2(\mathbb{R}^n)$ be the set of positive semidefinite matrices. Let $\operatorname{int} \mathcal{P}$ be the set of positive definite matrices. We consider the following operator.

Definition 4.4.1. Define the Monge–Ampère operator $F_{\mathrm{MA}} : K \times \mathcal{P} \to \mathbb{R}$ as

$$F_{\mathrm{MA}}(x, M) := \max_{B \in \mathcal{P}, \operatorname{Tr} B = 1} \left[n(f(x) \cdot \det B)^{1/n} - \operatorname{Tr}(BM) \right] \tag{4.22}$$

The aim of this section is to prove the following result.

Theorem 4.4.2. *The Monge–Ampère equation* (4.21) *is equivalent to*

$$F_{\mathrm{MA}}(x, \nabla^2 u(x)) = 0, \quad \textit{in } K. \tag{4.23}$$

Proof. The key ingredient is the following observation by Gaveau:

Lemma 4.4.3. [22, Lemma 1] *For $M \in \mathcal{P}$,*

$$n(\det M)^{\frac{1}{n}} = \inf_{B \in \operatorname{int} \mathcal{P}, \det B = 1} \operatorname{Tr}(BM). \tag{4.24}$$

Proof of the lemma. Let $\lambda_1, \ldots, \lambda_n$ be eigenvalues of a matrix Q, then $\det Q = \lambda_1 \cdots \lambda_n$ and $\operatorname{Tr}(Q) = \lambda_1 + \cdots + \lambda_n$. Assume that $Q \in \mathcal{P}$, then for each i there holds $\lambda_i \geq 0$. Applying the inequality of arithmetic and geometric means, we obtain

$$n(\det Q)^{1/n} \leq \operatorname{Tr}(Q),$$

and the equality holds when Q has equal eigenvalues. We apply this fact to the matrix BM, where $M \in \mathcal{P}, B \in \operatorname{int} \mathcal{P}$, and $\det B = 1$,

$$n(\det M)^{1/n} = n(\det(BM))^{1/n} \leq \text{Tr}(BM).$$

Finally, to show $n(\det M)^{\frac{1}{n}}$ is the limit of a sequence of $\operatorname{Tr}(BM)$, where $B \in \operatorname{int} \mathcal{P}$ and $\det B = 1$, we choose a sequence of B_t so that all the eigenvalues of $B_t M$ approach to the same value. More precisely, one choice can be $B_t = (M + tI)^{-1} \cdot \det(M + tI)^{1/n}$ and in the limit we let $t \to 0$. □

By Lemma 4.4.3, equation (4.21) can be reformulated as follows.

$$\begin{aligned}
&\det \nabla^2 u(x) = f(x), \quad \text{in } K, \\
\Longleftrightarrow \; &\sup_{B \in \operatorname{int} \mathcal{P}, \det B = 1} \left[n f(x)^{1/n} - \operatorname{Tr}(B \nabla^2 u(x)) \right] = 0, \quad \text{in } K. \qquad (4.25) \\
\Longleftrightarrow \; &\sup_{B \in \mathcal{P}, \operatorname{Tr} B = 1} \left[n(f(x) \cdot \det B)^{1/n} - \operatorname{Tr}(B \nabla^2 u(x)) \right] = 0, \quad \text{in } K.
\end{aligned}$$

Lemma 4.4.4. *The supremum in (4.25) is attained, i.e.,*

$$\begin{aligned}
&\sup_{B \in \mathcal{P}, \operatorname{Tr} B = 1} \left[n(f(x) \cdot \det B)^{1/n} - \operatorname{Tr}(B \nabla^2 u(x)) \right] = 0, \quad \textit{in } K, \\
\Longleftrightarrow \; &\max_{B \in \mathcal{P}, \operatorname{Tr} B = 1} \left[n(f(x) \cdot \det B)^{1/n} - \operatorname{Tr}(B \nabla^2 u(x)) \right] = 0, \quad \textit{in } K.
\end{aligned}$$

Proof of the lemma. The set $\{B \in \mathcal{P} : \operatorname{Tr} B = 1\}$ is a compact subset of $\operatorname{Sym}^2(\mathbb{R}^n)$, where we identify $\operatorname{Sym}^2(\mathbb{R}^n)$ as a subset of $\mathbb{R}^{n \times n}$ and use its Euclidean topology. Consider the map

$$B \in \operatorname{Sym}^2(\mathbb{R}^n) \mapsto C \cdot (\det B)^{1/n} - \operatorname{Tr}(BM),$$

where C is a real number and $M \in \mathrm{Sym}^2(\mathbb{R}^n)$. The map is a continuous map, when considering $\mathrm{Sym}^2(\mathbb{R}^n)$ as a subset of $\mathbb{R}^{n\times n}$ and use its topology. Hence, the concerned supremum is taken over a compact set for a continuous function, which implies the maximum can be attained. □

By Lemma 4.4.3 and 4.4.4, the following two equations are equivalent:

$$\begin{aligned} &\det \nabla^2 u(x) = f(x), \quad \text{in } K, \\ \Longleftrightarrow &\max_{B\in\mathcal{P}, \mathrm{Tr}\, B=1} \left[n(f(x)\cdot \det B)^{1/n} - \mathrm{Tr}(B\nabla^2 u(x)) \right] = 0, \quad \text{in } K. \end{aligned} \tag{4.26}$$

Hence, by the definition of F_{MA}, we have shown the equivalence between (4.21) and (4.23).

□

In summary, given the simplest form of Monge–Ampère type equations, denoted as (4.21), we revisited Gaveau's reformulation. The reformulation essentially involves substituting the determinant operator in (4.21) with a maximum operator applied to a certain subset of semi-positive matrices, defined as follows:

$$\mathcal{P}_0 := \{B \in \mathcal{P} : \mathrm{Tr}\, B = 1\}. \tag{4.27}$$

One crucial input in [5] entails an additional reformulation of the Monge–Ampère equation, achieved by studying this set $\mathcal{P}_0$.

4.5 An approximation result for semi-positive matrices with trace one

In this section, we provide a detailed explanation of the discretization process applied to the set $\mathcal{P}_0$ in (4.27). The primary result is Theorem 4.5.9. It is important that this theorem is specifically valid for dimension $n = 2$. Built upon Theorem 4.4.2, this result on $\mathcal{P}_0$ leads to a further reformulation for Monge–Ampère equations.

4.5.1 Motivation, summation of rank one matrices, and Selling's formula

The motivation behind investigating $\mathcal{P}_0$ stems from the necessity to discretize the equation (4.26). In our applications, it is unfeasible to numerically find a maximum over $\mathcal{P}_0$ as required in (4.22) or (4.26). Therefore, we aim to approximate this set using finitely many matrices.

Let

$$N := n(n+1)/2.$$

Let

$$\mathbf{v} = \{v_1, \ldots, v_N\}$$

represent a collection of N vectors in $\mathbb{Z}^n$ (to be specified later), and let

$$\gamma = (\gamma_1, \ldots, \gamma_N) \in \mathbb{R}^N_+.$$

Define

$$P(\mathbf{v}, \gamma) := \sum_{i=1}^{N} \gamma_i v_i v_i^T, \tag{4.28}$$

which is a symmetric matrix expressed as a *positive linear* (as opposed to merely a linear (i.e., $\gamma \in \mathbb{R}^N$) combination of rank one matrices. Our goal is to show that any matrix in $\mathcal{P}_0$ can be approximated in a sense by such $P(\mathbf{v}, \gamma)$.

Remark 4.5.1. The requirement that $\gamma \in \mathbb{R}^N_+$ as opposed to $\gamma \in \mathbb{R}^N$ arises since we intend to develop a *monotonic* numerical scheme (See Definition 4.8.1). For instance, when $n = 2$, if we were to allow γ to take values in the whole $\mathbb{R}^3$ rather than only non-negative values, then the standard choice $\mathbf{v}_{\mathrm{std}} = (v_1, v_2, v_3) = ((1,0)^T, (0,1)^T, (-1,-1)^T)$ already gives that for any $M \in \mathcal{P}_0$,

$$M = \begin{pmatrix} a & b \\ b & d \end{pmatrix} = (a-b)v_1v_1^T + (d-b)v_2v_2^T + bv_3v_3^T.$$

Consequently, by setting $\gamma = (a-b, d-b, b)$, we then have $M = P(\mathbf{v}_{\mathrm{std}}, \gamma)$. However, such γ not necessarily in $\mathbb{R}^3_+$. The fact that, in dimension 2, given M and $\mathbf{v}_{\mathrm{std}}$ a corresponding γ can be produced such that $M = P(\mathbf{v}_{\mathrm{std}}, \gamma)$, will be generalized in Proposition 4.5.4. below.

The 3-tuple of vectors $\mathbf{v}_{\mathrm{std}}$ in Remark 4.5.1 is an example of the following:

Definition 4.5.2. A set of vectors $\mathbf{v} = \{v_1, v_2, v_3\} \subset \mathbb{Z}^2$ is called a superbase of $\mathbb{Z}^2$ if

$$v_1 + v_2 + v_3 = 0 \in \mathbb{Z}^2,$$

and

$$\det[v_1, v_2] = 1 \text{ or } -1.$$

A superbase can be considered either as a 3-tuple of vectors, or equivalently as a 2-by-3 integer matrix,

$$\mathbf{v} \in \mathbb{Z}^{2\times 3},$$

whose columns are v_1, v_2, v_3.

In summary, one easily has $P(\mathbf{v}_{\mathrm{std}}, \mathbb{R}^3) = \mathcal{P}_0$, however, this will not be enough for a monotone numerical scheme used later on. As a compromise, we instead will use *many* superbases and only consider their images under $P(\,\cdot\,, \mathbb{R}^3_+)$. The main result, Theorem 4.5.9, is that a certain well-chosen collection of superbases will approximate $\mathcal{P}_0$.

By treating the set $\mathcal{P}_0$ as a subset of $\mathbb{R}^{n\times n}$ and considering the Euclidean distance on the latter space, we see the former set is a metric space. Consequently, the Hausdorff distance, which we define below, serves as a natural measure of whether another set of matrices approximates the set.

Definition 4.5.3. Let X and Y be two non-empty subsets of a metric space with distance function d. The Hausdorff distance is given by

$$d_H(X,Y) := \max\Big\{\sup_{x\in X} d(x,Y), \sup_{y\in Y} d(y,X)\Big\}.$$

From now on, and as in [5], fix

$$n = 2,$$

i.e., we will only consider 2×2 matrices in $\mathcal{P}_0$. So,

$$N = n(n+1)/2 = 3, \quad \mathbf{v} = \{v_1, v_2, v_3\} \subset \mathbb{Z}^2, \quad \gamma \in \mathbb{R}^3_+.$$

To conclude this section, we prove the following Selling's formula, which provides a way to write any symmetric matrix in the form of (4.28) for a fixed $\mathbf{v}$, with the caveat that the resulted γ may take its value in $\mathbb{R}^3$.

For any vector $w = (w_1, w_2) \in \mathbb{R}^2$, denote by

$$\begin{aligned} w^\perp &:= (-w_2, w_1), \\ \tilde{w} &:= (w_1, -w_2). \end{aligned} \tag{4.29}$$

For any superbase $\mathbf{v} = (v_1, v_2, v_3)$ and any $M \in \mathrm{Sym}^2(\mathbb{R}^2)$, define

$$\gamma(\mathbf{v}, M) := \left(-\langle v_2^\perp, M v_3^\perp\rangle, -\langle v_3^\perp, M v_1^\perp\rangle, -\langle v_1^\perp, M v_2^\perp\rangle\right). \tag{4.30}$$

The following is the 2-dimensional version of the Selling's formula [51].

Proposition 4.5.4. *Let $P(\cdot,\cdot)$ be defined as in (4.28) with $N = 3$ and $\gamma(\cdot,\cdot)$ as in (4.30). If $\mathbf{v} = (v_1, v_2, v_3)$ is a superbase as in Definition 4.5.2, then for any $M \in \mathrm{Sym}^2(\mathbb{R}^2)$,*

$$M = P(\mathbf{v}, \gamma(\mathbf{v}, M)).$$

Proof. Let $\mathbf{v} = (v_1, v_2, v_3)$ be a superbase. By Definition 4.5.2, v_1 and v_2 form a basis of $\mathbb{R}^2$. And so do $v_1^\perp$ and $v_2^\perp$ as defined by (4.29). Thus, to prove the proposition it suffices to show that for any $1 \le i \le j \le 2$,

$$\langle v_i^\perp, M v_j^\perp\rangle = \langle v_i^\perp, P(\mathbf{v}, \gamma(\mathbf{v}, M) v_j^\perp\rangle. \tag{4.31}$$

We write out the right hand side in (4.31):

$$\begin{align} \langle v_i^\perp, P(\mathbf{v}, \gamma(\mathbf{v}, M) v_j^\perp\rangle &= (v_i^\perp)^T \left[\sum_{k=1}^{3} -(v_{k+1}^\perp)^T M v_{k+2}^\perp \cdot v_k v_k^T\right] v_j^\perp \tag{4.32}\\ &= \sum_{k=1}^{3} -(v_{k+1}^\perp)^T M v_{k+2}^\perp \cdot \det[v_i, v_k] \cdot \det[v_j, v_k], \tag{4.33} \end{align}$$

where we use

$$\langle v_i^\perp, v_j\rangle = \det[v_i, v_j], \quad \text{for any } i, j = 1, 2, 3$$

which follows from the definition in (4.29). Now we divide into two cases. First, if $i \ne j$ in

(4.33), then since $1 \leq i \leq j \leq 2$, we have $i = 1, j = 2$, and

$$\begin{aligned}
\langle v_i^\perp, P(\mathbf{v}, \gamma(\mathbf{v}, M)v_j^\perp\rangle &= \sum_{k=1}^{3} -(v_{k+1}^\perp)^T M v_{k+2}^\perp \cdot \det[v_i, v_k] \cdot \det[v_j, v_k] \\
&= -(v_{k+1}^\perp)^T M v_{k+2}^\perp \cdot \det[v_i, v_k] \cdot \det[v_j, v_k], \quad \text{where } i = 1, j = 2, k = 3, \\
&= \langle v_1^\perp, M v_2^\perp\rangle
\end{aligned}$$

as expected. Second, if $i = j$ in (4.33), then if $i = j = 1$, there hold

$$\begin{aligned}
\langle v_i^\perp, P(\mathbf{v}, \gamma(\mathbf{v}, M)v_j^\perp\rangle &= \sum_{k=1}^{3} -(v_{k+1}^\perp)^T M v_{k+2}^\perp \cdot \det[v_i, v_k] \cdot \det[v_j, v_k] \\
&= -(v_3^\perp)^T M v_1^\perp - (v_1^\perp)^T M v_2^\perp \\
&= -(v_1^\perp)^T M v_3^\perp - (v_1^\perp)^T M v_2^\perp \\
&= -(v_1^\perp)^T M (v_3^\perp + v_2^\perp) \\
&= \langle v_1^\perp, M v_1^\perp\rangle
\end{aligned}$$

since $v_1 + v_2 + v_3 = 0$. If $i = j = 2$, then

$$\begin{aligned}
\langle v_i^\perp, P(\mathbf{v}, \gamma(\mathbf{v}, M)v_j^\perp\rangle &= \sum_{k=1}^{3} -(v_{k+1}^\perp)^T M v_{k+2}^\perp \cdot \det[v_i, v_k] \cdot \det[v_j, v_k] \\
&= -(v_2^\perp)^T M v_3^\perp - (v_1^\perp)^T M v_2^\perp \\
&= -(v_2^\perp)^T M v_3^\perp - (v_2^\perp)^T M v_1^\perp \\
&= -(v_2^\perp)^T M (v_1^\perp + v_3^\perp) \\
&= \langle v_2^\perp, M v_2^\perp\rangle.
\end{aligned}$$

$\square$

4.5.2 Strategy to prove the approximation result, Stern–Brocot Tree and its illustration

With Selling's formula in mind, cf. Proposition 4.5.4, the goal to write a matrix $M \in \mathcal{P}_0$ as $M = P(\mathbf{v}, \gamma)$ reduces to finding a superbase $\mathbf{v} = (v_1, v_2, v_3)$, such that $\gamma(\mathbf{v}, M)$ in (4.30) has non-negative components, i.e.,

$$v_i^{\perp} M v_j^{\perp} \leq 0, \tag{4.34}$$

for any $1 \leq i \neq j \leq 3$. The following definition characterizes (4.34).

Definition 4.5.5. Let $M \in \mathcal{P} \subset \mathrm{Sym}^2(\mathbb{R}^2)$. A superbase $\mathbf{v} = (v_1, v_2, v_3)$ of $\mathbb{Z}^2$ is M-obtuse if for any $1 \leq i \leq j \leq 3$,

$$v_i^T M v_j \leq 0.$$

Our strategy to prove the approximation result in Theorem 4.5.9 is by showing how to find such $\mathbf{v}$ for almost all $M \in \mathcal{P}_0$. The proof is constructive and relies on an intriguing structure known as the Stern–Brocot Tree. By Definition 4.5.2 of the superbase, in a superbase $\mathbf{v} = (v_1, v_2, v_3)$, the value of v_3 is completely determined by the other two vectors. Therefore, we consider the following definition of direct basis and then introduce the construction of the Stern–Brocot Tree, which essentially consists of a subset of direct basis.

Definition 4.5.6. An ordered pair of two vectors (v_1, v_2), where $v_1, v_2 \in \mathbb{Z}^2$, is called a direct basis if

$$\det[v_1, v_2] = 1.$$

By Definition 4.5.6 and Definition 4.5.2, given a direct basis (v_1, v_2), a superbase $\mathbf{v} = (v_1, v_2, v_3)$ can be produced by letting $v_3 = -v_1 - v_2$.

Definition 4.5.7. The Stern–Brocot Tree $\mathcal{T}$ is the set of direct basis that satisfies

1. The direct basis consisting of $(1,0)^T, (0,1)^T$ belongs to $\mathcal{T}$.

2. If (v_1, v_2) is a direct basis and $(v_1, v_2) \in \mathcal{T}$, then $(v_1, v_2 + v_1)$ and $(v_1 + v_2, v_2)$ also belong to $\mathcal{T}$.

The set $\mathcal{T}$ has a tree structure because each direct basis $(v_1, v_2) \in \mathcal{T}$, viewed as a node, has exactly two child nodes $(v_1, v_2 + v_1)$ and $(v_1 + v_2, v_2)$. Therefore, $\mathcal{T}$ is indeed a complete binary tree. The tree has the following direct basis as its root:

$$\left((1,0)^T, (0,1)^T\right).$$

The further a direct basis $(v_1, v_2) \in \mathcal{T}$, as a node, is away from the root, the larger both $|v_1|$ and $|v_2|$ are, and the angle between v_1 and v_2 is closer to 0.

Remark 4.5.8. A visualization of the Stern–Brocot Tree $\mathcal{T}$ is given in Figure 4.6. We denote by $v^{l,k}$ the kth node in the lth level of the Stern–Brocot Tree.

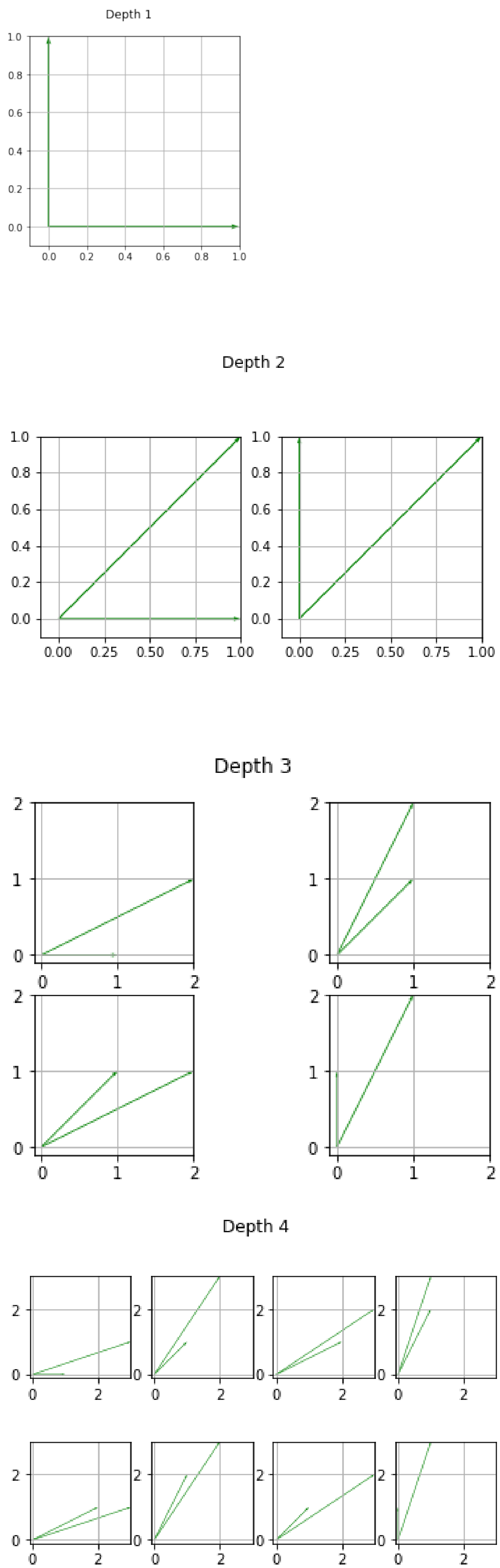

Figure 4.6

The root node of the Stern–Brocot Tree is the direct basis

$$v^{0,1} = (v_1^{0,1}, v_2^{0,1}) = ((1,0)^T, (0,1)^T).$$

The second level of the Stern–Brocot Tree has two child nodes of the root node v^0:

$$v^{1,1} = ((1,0)^T, (1,1)^T)$$

and

$$v^{1,2} = ((1,1)^T, (0,1)^T).$$

They are constructed following Definition 4.5.7:

$$\begin{aligned} v^{1,1} &= (v_1^{0,1}, v_1^{0,1} + v_2^{0,1}), \\ v^{1,2} &= (v_1^{0,1} + v_2^{0}, v_2^{0,1}). \end{aligned}$$

The third level of the Stern–Brocot Tree has four child nodes of the parent nodes $v^{1,1}$ and $v^{1,2}$:

$$\begin{aligned} v^{2,1} &= (v_1^{1,1}, v_1^{1,1} + v_2^{1,1}) = ((1,0)^T, (2,1)^T), \\ v^{2,2} &= (v_1^{1,1} + v_2^{1,1}, v_2^{1,1}) = ((2,1)^T, (1,1)^T), \\ v^{2,3} &= (v_1^{1,2}, v_1^{1,2} + v_2^{1,2}) = ((1,1)^T, (1,2)^T), \\ v^{2,4} &= (v_1^{1,2} + v_2^{1,2}, v_2^{1,2}) = ((1,2)^T, (0,1)^T). \end{aligned}$$

The fourth level:

$$\begin{aligned} v^{3,1} &= (v_1^{2,1}, v_1^{2,1} + v_2^{2,1}) = ((1,0)^T, (3,1)^T), \\ v^{3,2} &= (v_1^{2,1} + v_2^{2,1}, v_2^{2,1}) = ((3,1)^T, (2,1)^T), \\ v^{3,3} &= (v_1^{2,2}, v_1^{2,2} + v_2^{2,2}) = ((2,1)^T, (3,2)^T), \\ v^{3,4} &= (v_1^{2,2} + v_2^{2,2}, v_2^{2,2}) = ((3,2)^T, (1,1)^T), \\ v^{3,5} &= (v_1^{2,3}, v_1^{2,3} + v_2^{2,3}) = ((1,1)^T, (2,3)^T), \\ v^{3,6} &= (v_1^{2,3} + v_2^{2,3}, v_2^{2,3}) = ((2,3)^T, (1,2)^T), \\ v^{3,7} &= (v_1^{2,4}, v_1^{2,4} + v_2^{2,4}) = ((1,2)^T, (1,3)^T), \\ v^{3,8} &= (v_1^{2,4} + v_2^{2,4}, v_2^{2,4}) = ((1,3)^T, (0,1)^T). \end{aligned}$$

4.5.3 A geometric interpretation of the approximation result

In the remainder of the chapter, we prove Theorem 4.5.9, the approximation result for $\mathcal{P}_0$. The set can be reformulated as follows:

$$\mathcal{P}_0 = \{M \in \mathcal{P} : \operatorname{Tr} M = 1\} = \left\{ \rho \in \mathbb{D}^2 : \frac{1}{2} \begin{pmatrix} 1+\rho_1 & \rho_2 \\ \rho_2 & 1-\rho_1 \end{pmatrix} \right\}, \tag{4.35}$$

where $\mathbb{D}^2$ is the unit disk in $\mathbb{R}^2$. Geometrically, the set $\mathcal{P}_0$ can be identified as the unit disk. In Remark 4.5.11 below, we will see that for a fixed superbase $\mathbf{v}$, the matrices in the set $\{P(\mathbf{v},\gamma) : \gamma \in \mathbb{R}^3_+, \operatorname{Tr}(P(\mathbf{v},\gamma)) = 1\}$ correspond to a triangle in the unit disk. Hence, the approximation of $\mathcal{P}_0$ using $\{P(\mathbf{v},\gamma) : \gamma \in \mathbb{R}^3_+, \operatorname{Tr}(P(\mathbf{v},\gamma)) = 1\}$ for different $\mathbf{v}$ is geometrically a triangulation of $\mathbb{D}^2$.

Theorem 4.5.9. *There exists a countable sequence of sets $\{V_\epsilon\}$, indexed by $\epsilon > 0$, such that each V_ϵ consists of a finite number of superbases, i.e., V_ϵ is a finite collection of matrices in $\mathbb{Z}^{2\times 3}$ and*

$$\lim_{\epsilon \to 0^+} d_H\left(\mathcal{P}_0, \{P(\mathbf{v},\gamma) : \mathbf{v} \in V_\epsilon, \gamma \in \mathbb{R}^3_+, \operatorname{Tr} P(\mathbf{v},\gamma) = 1\}\right) = 0.$$

Remark 4.5.10. The Stern–Brocot Tree is used in the proof of Theorem 4.5.9 to construct such V_ϵ. Since the Stern–Brocot Tree consists of 2-dimensional vectors, Theorem 4.5.9 only applies to 2×2 matrices.

Remark 4.5.11. Before proving Theorem 4.5.9, we provide a geometric illustration of it.

Thanks to (4.35), the set $\mathcal{P}_0$ of matrices corresponds to the unit disk in $\mathbb{R}^2$, and it is plotted in Figure 4.7.

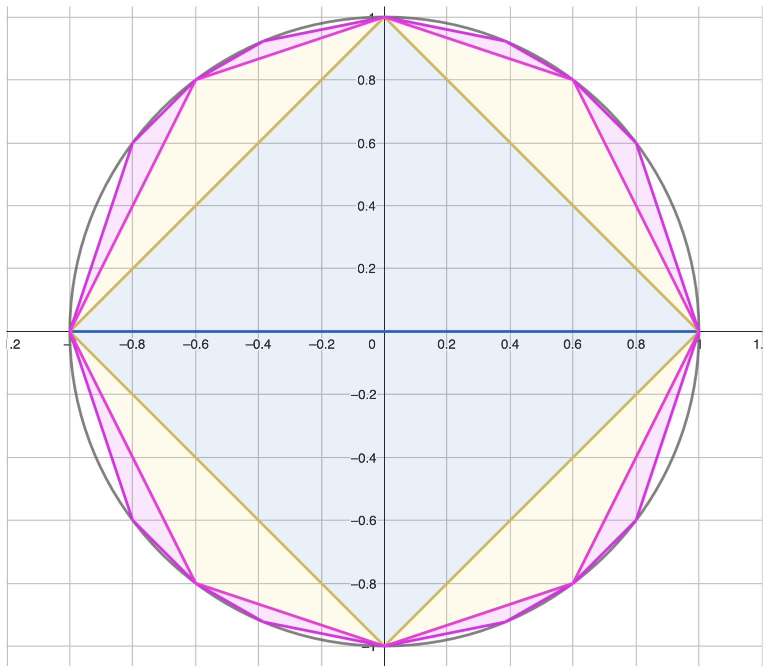

Figure 4.7: $\mathcal{P}_0$ viewed as the unit disk and its triangulation

Henceforth, we use the notation

$$M_\rho := \frac{1}{2}\begin{pmatrix} 1+\rho_1 & \rho_2 \\ \rho_2 & 1-\rho_1. \end{pmatrix}$$

Now fix a superbase $\mathbf{v} = (v_1, v_2, v_3)$, then the set of matrices

$$\{P(\mathbf{v}, \gamma) : \gamma \in \mathbb{R}^3_+, \mathrm{Tr}(P(\mathbf{v}, \gamma)) = 1\}$$

corresponds to a triangle within the unit disk. Indeed, by Proposition 4.5.4, there is a 1-to-1 correspondence between

$$\{P(\mathbf{v}, \gamma) : \gamma \in \mathbb{R}^3_+, \mathrm{Tr}(P(\mathbf{v}, \gamma)) = 1\}$$

and

$$\{\rho \in \mathbb{D}^2 : \gamma(\mathbf{v}, M_\rho) \in \mathbb{R}^3_+\}.$$

The condition $\gamma(\mathbf{v}, M_\rho) \in \mathbb{R}^3_+$, by (4.30) is equivalent to

$$\begin{aligned} -\langle v_1^\perp, M_\rho v_2^\perp \rangle &> 0, \\ -\langle v_2^\perp, M_\rho v_3^\perp \rangle &> 0, \\ -\langle v_3^\perp, M_\rho v_1^\perp \rangle &> 0. \end{aligned} \tag{4.36}$$

For any two vectors $u = (u_1, u_2)$ and $v = (v_1, v_2)$, the inequality

$$-\langle u^\perp, M_\rho v^\perp \rangle > 0$$

is equivalent to

$$\rho_2 > \frac{u_1v_1 - u_2v_2}{-u_1v_2 - u_2v_1}\rho_1 + \frac{u_1v_1 + u_2v_2}{u_1v_2 + u_2v_1}.$$

Therefore, those three inequalities in (4.36) altogether define a triangle within the unit disk.

As a result of how V_ϵ will be constructed in the proof of Theorem 4.5.9, any V_{ϵ_1}, as a collection of superbases, is a subset of V_{ϵ_2} for any $0 < \epsilon_2 < \epsilon_1$. The collection of triangles that arise from superbase $\mathbf{v} \in V_\epsilon$ has the following patterns.

1. The first two superbases included in V_ϵ are

$$((1,0)^T, (0,1)^T(-1,-1)^T)$$

and

$$((1,0)^T,(0,-1)^T,(-1,1)^T).$$

They, identified as two triangles, are the two largest triangles

$$\{|\rho| \in \mathbb{D}^2 : \rho_2 \geq 0, \rho_2 \leq \rho_1 + 1, \rho_2 \geq -\rho_1 + 1\},$$

$$\{|\rho| \in \mathbb{D}^2 : \rho_2 \leq 0, \rho_2 \geq \rho_1 - 1, \rho_2 \geq -\rho_1 - 1\}$$

in Figure 4.7, illustrated in blue. They correspond to the matrices belonging to the following sets:

$$\{P(\mathbf{v}_1,\gamma) : \gamma \in \mathbb{R}^3_+, \mathrm{Tr}(P(\mathbf{v}_1,\gamma)) = 1\}, \text{ where } \mathbf{v}_1 = ((1,0)^T,(0,1)^T,(-1,-1)^T),$$

$$\{P(\mathbf{v}_2,\gamma) : \gamma \in \mathbb{R}^3_+, \mathrm{Tr}(P(\mathbf{v}_2,\gamma)) = 1\}, \text{ where } \mathbf{v}_2 = ((1,0)^T,(0,-1)^T,(-1,1)^T).$$

These triangles share a common edge along the x-axis.

2. As $\epsilon > 0$ becomes smaller, V_ϵ contains more superbases. The subsequent four triangles with the second largest area all share a common edge with the two largest triangles, and are shown in yellow in Figure 4.7. Furthermore, the distinct vertex on each of these four triangles has coordinates $(-0.6, 0.8)$, $(-0.6, -0.8)$, $(0.6, 0.8)$ and $(0.6, -0.8)$ respectively. The eight smaller triangles in magenta share common edges with these four triangles as well.

3. The ratio of the area of the two largest triangles to the unit disk is about 64%. The ratio of the area of the six largest triangles to the unit disk is about 89%. The ratio of the area of the fourteen triangles to the unit disk is about 99%. This result is helpful for determining

the desired accuracy in our experiments. The ratio of the triangle's area to that of the unit disk represents the percentage of matrices in $\mathcal{P}_0$ that can be approximated using V_ϵ.

In Section 4.5.6, we will provide validation for these items.

In conclusion, as ϵ becomes smaller and closer to 0, the set V_ϵ contains more superbases, also generating more triangles in the unit disk. And a finer triangulation of the unit circle is then achieved, which means a larger set of matrices in $\mathcal{P}_0$ has been approximated.

4.5.4 Proof of the approximation result

We prove Theorem 4.5.9 in this section. In the proof, the construction of the collection of superbases V_ϵ relies on the Stern–Brocot Tree defined in Definition 4.5.7. Roughly speaking, each direct basis in Stern–Brocot Tree leads to two superbases, and V_ϵ contains more and more superbases as $\epsilon \to 0^+$.

Proof of Theorem 4.5.9. Let $\mathcal{T}$ be the Stern–Brocot Tree in Definition 4.5.7. Recall that the further a direct basis, as a node, is away from the root node $((1,0)^T, (0,1)^T)$, the vectors in the pair have larger norms and smaller angle between each other. Define

$$\mathcal{T}_s := \{(v_1, v_2) \in \mathcal{T} : v_1^T v_2 \leq s\}. \tag{4.37}$$

Then $\mathcal{T}_s$ is a subtree with a finite number of nodes and contains the root for any given $s > 0$. For any $M \in \operatorname{int} \mathcal{P} \subset \operatorname{Sym}^2(\mathbb{R}^2)$, let $\lambda_2 \geq \lambda_1 > 0$ be eigenvalues of M. Define

$$\mu(M) := \sqrt{\frac{\lambda_2}{\lambda_1}}, \tag{4.38}$$

$$s(M) := \frac{\mu(M) - \mu(M)^{-1}}{2}. \tag{4.39}$$

The following lemma shows that there is an upper bound on the norm of vectors that belong to a direct basis within a given subtree $\mathcal{T}_s$, for $s > 0$.

Lemma 4.5.12. *Let $\mu > 1$. For any direct basis $(v_1, v_2) \in \mathcal{T}_{(\mu-\mu^{-1})/2}$,*

$$\max\{|v_1|, |v_2|\} < \frac{\mu + \mu^{-1}}{2} < \mu.$$

Proof of the lemma. Any pair (v_1, v_2) in $\mathcal{T}$ satisfies $|v_1| \geq 1$ and $|v_2| \geq 1$. We have

$$|v_1|^2 \leq |v_1|^2 |v_2|^2 = \det[v_1, v_2]^2 + (v_1^T v_2)^2. \tag{4.40}$$

Assuming $(v_1, v_2) \in \mathcal{T}_{(\mu-\mu^{-1})/2}$, we also have

$$\det[v_1, v_2]^2 + (v_1^T v_2)^2 < 1 + \left(\frac{\mu - \mu^{-1}}{2}\right)^2 = \left(\frac{\mu + \mu^{-1}}{2}\right)^2. \tag{4.41}$$

Then the desired inequality for v_1 follows from (4.40) and (4.41). The proof for v_2 is the same. □

The next lemma relates M-obtuseness between a pair of vectors in a direct basis, cf. Definition 4.5.5, to their inner product compared to $s(M)$ defined in (4.39).

Lemma 4.5.13. *Let* $(v_1, v_2) \in \mathcal{T}$ *and* $M \in \operatorname{int}\mathcal{P}$. *Let* $s(M)$ *be defined in* (4.39). *Assume* $v_1^T v_2 \geq s(M)$, *then* $v_1^T M v_2 \geq 0$.

Proof of the lemma. Denote by θ the angle between v_1 and v_2. Then

$$\sin\theta = \frac{\det[v_1, v_2]}{\sqrt{(v_1^T v_2)^2 + \det[v_1, v_2]^2}} = \left(1 + (v_1^T v_2)^2\right)^{-1/2}. \tag{4.42}$$

Denote by $\cos(\cdot,\cdot)$ the cosine of the angle between any two vectors. Then for any $w = (w_1, w_2) \in \mathbb{R}^2$ and $M \in \operatorname{int}\mathcal{P}$ with eigenvalues $\lambda_2 \geq \lambda_1 > 0$,

$$\cos(w, Mw) = \frac{w^T M w}{|w||Mw|},$$

and by a change of basis,

$$\cos(w, Mw) = \frac{\lambda_1 w_1^2 + \lambda_2 w_2^2}{\sqrt{w_1^2 + w_2^2}\sqrt{\lambda_1^2 w_1^2 + \lambda_2^2 w_2^2}}. \tag{4.43}$$

Write $k_1 = \lambda_1 w_1^2$ and $k_2 = \lambda_2 w_2^2$, then (4.43) reads

$$\begin{aligned}\cos(w, Mw) &= \frac{k_1 + k_2}{\sqrt{\frac{k_1}{\lambda_1} + \frac{k_2}{\lambda_2}}\sqrt{\lambda_1 k_1 + \lambda_2 k_2}} \\ &\geq \frac{k_1 + k_2}{\frac{1}{2}(k_1 + k_2)(\sqrt{\frac{\lambda_1}{\lambda_2}} + \sqrt{\frac{\lambda_2}{\lambda_1}})} \\ &= \frac{2}{\mu(M) + \mu(M)^{-1}},\end{aligned} \tag{4.44}$$

where the second inequality follows from the following inequality [32, p. 62]

$$\sqrt{\frac{k_1}{\lambda_1}+\frac{k_2}{\lambda_2}}\sqrt{\lambda_1 k_1+\lambda_2 k_2} \le \frac{1}{2}(k_1+k_2)\left(\sqrt{\frac{\lambda_1}{\lambda_2}}+\sqrt{\frac{\lambda_2}{\lambda_1}}\right), \quad \forall k_1, k_2 \ge 0, \lambda_1, \lambda_2 > 0.$$

By (4.44),

$$\cos(v_2, Mv_2)\cdot(\mu(M)+\mu(M)^{-1}) \ge 2. \tag{4.45}$$

Plugging in the following assumption

$$v_1^T v_2 \ge s(M) = \frac{\mu(M)-\mu(M)^{-1}}{2}$$

into (4.42) and comparing (4.42) to (4.45), we have

$$\sin\theta = \sin(v_1, v_2) \le \cos(v_2, Mv_2).$$

Hence, the sum of θ and the angle between v_2, Mv_2 cannot exceed $\pi/2$. Consequently, the angle between v_1 and Mv_2 also cannot exceed $\pi/2$. This is equivalent to the desired result. □

Now, we explain how to choose direct basis from $\mathcal{T}$ that gives rise to a corresponding superbase.

Lemma 4.5.14. *For any $M \in \operatorname{int}\mathcal{P}$, there exists $(v_1, v_2) \in \mathcal{T}$ satisfying that, first, $v_1^T v_2 \le s(M)$, and second, either $(v_1, v_2, -v_1-v_2)$ or $(\tilde{v}_1, \tilde{v}_2, -\tilde{v}_1-\tilde{v}_2)$ is an M-obtuse superbase.*

Proof of the lemma. First, assume the off diagonal entries of M are negative. Consider the set

$$\{(v_1, v_2) \in \mathcal{T} : v_1^T M v_2 < 0\}.$$

The set is non-empty, as the pair consisting of the standard basis satisfies

$$e_1^T M e_2 < 0.$$

By Lemma 4.5.13, any basis (v_1, v_2) belonging to this set satisfies $v_1^T v_2 < s(M)$. Hence, it is guaranteed there exists a pair (v_1, v_2) in the set which achieves the maximum inner product. By this construction, there must hold

$$v_1^T M(v_1 + v_2) \geq 0,$$
$$(v_1 + v_2)^T M v_2 \geq 0,$$

by Lemma 4.5.13 and using $v_1^T(v_1 + v_2) \geq s(M), v_2^T(v_1 + v_2) \geq s(M)$. As a result, the triple $(v_1, v_2, -v_1 - v_2)$ is M-obtuse, and it is also a superbase because (v_1, v_2) is a direct basis.

On the other hand, if the off diagonal entries of M are not negative, we can reverse the orientation of the 2-dimensional coordinate system to make it a matrix having negative off diagonal entries. In other words, the triple $(\tilde{v}_1, \tilde{v}_2, -\tilde{v}_1 - \tilde{v}_2)$ will form a M-obtuse superbase in this case by the same arguments. □

Let us now prove the theorem. For $\epsilon > 0$, we choose a family of real numbers μ_ϵ indexed by ϵ, such that

$$\mu_\epsilon > 1, \quad \forall \epsilon > 0, \tag{4.46}$$

and

$$\lim_{\epsilon \to 0} \mu_\epsilon = +\infty, \tag{4.47}$$

and

$$\lim_{\epsilon \to 0} \epsilon \mu_\epsilon = 0. \tag{4.48}$$

Inspired by Lemma 4.5.12 and Lemma 4.5.14, define

$$V_\epsilon := \bigcup_{(v_1,v_2) \in \mathcal{T}_{(\mu_\epsilon - \mu_\epsilon^{-1})/2}} \{(-v_1^\perp, -v_2^\perp, v_1^\perp + v_2^\perp), (-\tilde{v}_1^\perp, -\tilde{v}_2^\perp, \tilde{v}_1^\perp + \tilde{v}_2^\perp)\}. \tag{4.49}$$

A (rough) visualization of the superbase in set V_ϵ is given in Figure 4.8.

It remains to show that V_ϵ fulfills the desired property in Theorem 4.5.9.

For any $M \in \operatorname{int} \mathcal{P}$, there exists $\epsilon > 0$ such that $\mu(M) < \mu_\epsilon$. Then by (4.39),

$$s(M) < \frac{\mu_\epsilon - \mu_\epsilon^{-1}}{2}.$$

Now, by Lemma 4.5.14, there exists a superbase $\mathbf{v} = (v_1, v_2, v_3) \in V_\epsilon$ such that $(v_1^\perp, v_2^\perp, v_3^\perp)$ is M-obtuse.

Now, fix $\epsilon > 0$. And consider $M \in \operatorname{int} \mathcal{P}$ such that $\mu(M) < \mu_\epsilon$. As previously discussed, let $\mathbf{v} = (v_1, v_2, v_3) \in V_\epsilon$ such that $(v_1^\perp, v_2^\perp, v_3^\perp)$ is M-obtuse. Defining $\gamma := \gamma(M, \mathbf{v})$ as (4.30), we have $\gamma \in \mathbb{R}^3_+$. By Selling's formula,

$$M = P(\mathbf{v}, \gamma).$$

Thus, we have shown

$$\{M \in \operatorname{int} \mathcal{P} : \operatorname{Tr} M = 1, \mu(M) < \mu_\epsilon\} \subset \{P(\mathbf{v}, \gamma) : \mathbf{v} \in V_\epsilon, \gamma \in \mathbb{R}^3_+, \operatorname{Tr}(P(\mathbf{v}, \gamma)) = 1\}.$$

Let ϵ be rather small in (4.49) so that there are many superbases in V_ϵ. Then, the first two superbases in V_ϵ, denoted by $\mathbf{v}^{0,1}$ and $\mathbf{v}^{0,2}$ are constructed using the root node $v^{0,1} = ((1,0)^T, (0,1)^T)$ in Figure 4.49 and the formula (4.49). In this case, v_1 and v_2 in (4.49) are $(1,0)^T$ and $(0,1)^T$. Then, we have

$$\begin{aligned}\mathbf{v}^{0,1} &= (-v_1^\perp, -v_2^\perp, v_1^\perp + v_2^\perp)\\ &= ((0,-1)^T, (1,0)^T, (-1,1)^T)\end{aligned}$$

and

$$\begin{aligned}\mathbf{v}^{0,2} &= (-\tilde{v}_1^\perp, -\tilde{v}_2^\perp, \tilde{v}_1^\perp + \tilde{v}_2^\perp)\\ &= ((0,-1)^T, (-1,0)^T, (1,1)^T).\end{aligned}$$

The second level of superbases in V_ϵ, denoted as $\mathbf{v}^{1,k}$ for $k = 1,2,3,4$, are derived from (4.49) using the two direct basis

$$v^{1,1} = ((1,0)^T, (1,1)^T)$$

and

$$v^{1,2} = ((1,1)^T, (0,1)^T),$$

cf. Remark 4.5.8. More precisely, we have

$$\begin{aligned}\mathbf{v}^{1,1} &= ((0,-1)^T, (1,-1)^T, (-1,2)^T),\\ \mathbf{v}^{1,2} &= ((0,-1)^T, (-1,-1)^T, (1,2)^T),\\ \mathbf{v}^{1,3} &= ((1,-1)^T, (1,0)^T, (-2,1)^T),\\ \mathbf{v}^{1,4} &= ((1,-1)^T, (-1,0)^T, (2,1)^T).\end{aligned}$$

Subsequently, there are eight superbases in the third level in V_ϵ, as originally there are four direct basis $v^{2,1}, v^{2,2}, v^{2,3}, v^{2,4}$ in the third level in the Stern–Brocot Tree, cf. Figure 4.6. Each direct basis leads to two superbases.

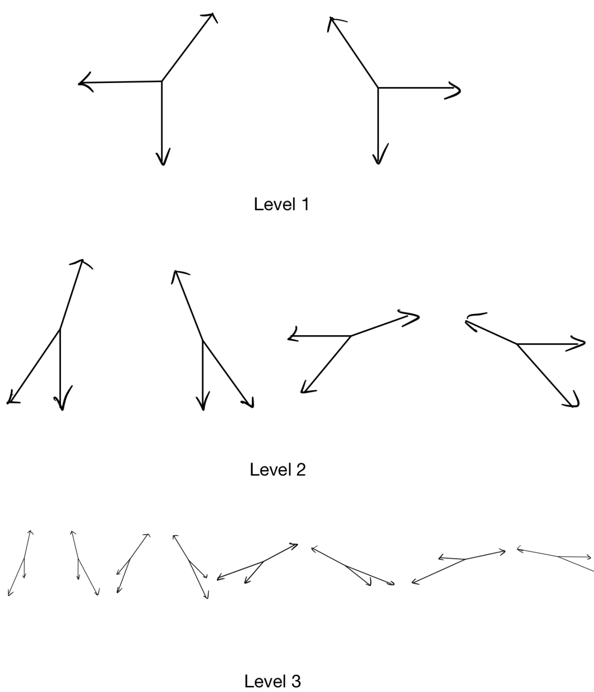

Figure 4.8

Finally, note that any direct basis $(v_1, v_2) \in \mathcal{T}_{(\mu_\epsilon - \mu_\epsilon^{-1})/2}$ satisfies that

$$|v_1|, |v_2| \leq \mu_\epsilon$$

by Lemma 4.5.12. Hence, we conclude

$$\begin{aligned}
&\lim_{\epsilon \to 0} d_H \left(\{M \in \mathcal{P} : \operatorname{Tr} M = 1\}, \{P(\mathbf{v}, \gamma) : \mathbf{v} \in V_\epsilon, \gamma \in \mathbb{R}^3_+, \operatorname{Tr} P(\mathbf{v}, \gamma) = 1\} \right) \\
&\quad \leq \lim_{\epsilon \to 0} d_H \left(\{M \in \mathcal{P} : \operatorname{Tr} M = 1\}, \{M \in \operatorname{int} \mathcal{P} : \operatorname{Tr} M = 1, \mu(M) < \mu_\epsilon\} \right) \\
&\quad = 0.
\end{aligned}$$

In particular, we find that for a fixed V_ϵ, by (4.49) it contains only a finite number of superbases.

□

4.5.5 An example

Example 4.5.15. Adopting notations from the proof of Theorem 4.5.9, we consider two sequences

$$\epsilon_n = \frac{1}{n+1}, \quad n = 1, 2, \ldots$$

and

$$\mu_{\epsilon_n} := \sqrt{n+1}, \quad n = 1, 2, \ldots \tag{4.50}$$

These two sequences satisfy (4.46), (4.47) and (4.48). Therefore, the set V_{ϵ_n} constructed in (4.49) has an explicit form:

$$\begin{aligned} V_{\epsilon_n} &= \bigcup_{(v_1,v_2)\in\mathcal{T}_{(\mu_{\epsilon_n}-\mu_{\epsilon_n}^{-1})/2}} \{(-v_1^\perp, -v_2^\perp, v_1^\perp + v_2^\perp), (-\tilde{v}_1^\perp, -\tilde{v}_2^\perp, \tilde{v}_1^\perp + \tilde{v}_2^\perp)\} \\ &= \bigcup_{(v_1,v_2)\in\mathcal{T}_{\frac{n}{2\sqrt{n+1}}}} \{(-v_1^\perp, -v_2^\perp, v_1^\perp + v_2^\perp), (-\tilde{v}_1^\perp, -\tilde{v}_2^\perp, \tilde{v}_1^\perp + \tilde{v}_2^\perp)\}. \end{aligned} \tag{4.51}$$

If we take $n = 1$ in (4.51), then

$$V_{\epsilon_1} = \bigcup_{(v_1,v_2)\in\mathcal{T}_{\frac{1}{2\sqrt{2}}}} \{(-v_1^\perp, -v_2^\perp, v_1^\perp + v_2^\perp), (-\tilde{v}_1^\perp, -\tilde{v}_2^\perp, \tilde{v}_1^\perp + \tilde{v}_2^\perp)\}.$$

By (4.37), the only direct basis $v = (v_1, v_2)$ in Figure 4.6 that satisfies

$$(v_1, v_2) \in \mathcal{T}_{\frac{1}{2\sqrt{2}}}$$

is $v^{0,1}$. Consequently,

$$\begin{aligned} V_{\epsilon_1} &= \bigcup_{(v_1,v_2)\in\mathcal{T}_{\frac{1}{2\sqrt{2}}}} \{(-v_1^\perp, -v_2^\perp, v_1^\perp + v_2^\perp), (-\tilde{v}_1^\perp, -\tilde{v}_2^\perp, \tilde{v}_1^\perp + \tilde{v}_2^\perp)\} \\ &= \bigcup_{(v_1,v_2)\in\{((1,0)^T,(0,1)^T)\}} \{(-v_1^\perp, -v_2^\perp, v_1^\perp + v_2^\perp), (-\tilde{v}_1^\perp, -\tilde{v}_2^\perp, \tilde{v}_1^\perp + \tilde{v}_2^\perp)\} \\ &= \{((1,1)^T, (0,-1)^T, (-1,0)^T), ((-1,-1)^T, (0,-1)^T, (1,0)^T)\}. \end{aligned}$$

Let $n = 37$ in (4.51), then

$$V_{\epsilon_{37}} = \bigcup_{(v_1,v_2)\in\mathcal{T}_{\frac{37}{2\sqrt{38}}}} \{(-v_1^{\perp}, -v_2^{\perp}, v_1^{\perp} + v_2^{\perp}), (-\tilde{v}_1^{\perp}, -\tilde{v}_2^{\perp}, \tilde{v}_1^{\perp} + \tilde{v}_2^{\perp})\}$$

$$= \bigcup_{(v_1,v_2)\in\mathcal{T}_{3.001}} \{(-v_1^{\perp}, -v_2^{\perp}, v_1^{\perp} + v_2^{\perp}), (-\tilde{v}_1^{\perp}, -\tilde{v}_2^{\perp}, \tilde{v}_1^{\perp} + \tilde{v}_2^{\perp})\}.$$

By (4.37), the direct bases that satisfy

$$(v_1, v_2) \in \mathcal{T}_{3.001}$$

are the following 9 direct bases, cf. Figure 4.6

$$v^{0,1} = ((1,0)^T, (0,1)^T)$$

$$v^{1,1} = ((1,0)^T, (1,1)^T)$$

$$v^{1,2} = ((1,1)^T, (0,1)^T)$$

$$v^{2,1} = ((1,0)^T, (2,1)^T)$$

$$v^{2,2} = ((2,1)^T, (1,1)^T)$$

$$v^{2,3} = ((1,1)^T, (1,2)^T)$$

$$v^{2,4} = ((1,2)^T, (0,1)^T)$$

$$v^{3,1} = ((1,0)^T, (3,1)^T)$$

$$v^{3,8} = ((1,3)^T, (0,1)^T)$$

and in turn $V_{\epsilon_{37}}$ contains 18 superbases

$$((0,-1)^T,(1,0)^T,(-1,1)^T)$$

$$((0,-1)^T,(-1,0)^T,(1,1)^T)$$

$$((0,-1)^T,(1,-1)^T,(-1,2)^T)$$

$$((0,-1)^T,(-1,-1)^T,(1,2)^T)$$

$$((1,-1)^T,(1,0)^T,(-2,1)^T)$$

$$((1,-1)^T,(-1,0)^T,(2,1)^T)$$

$$((0,1)^T,(-1,2)^T,(1,-3)^T)$$

$$((0,1)^T,(1,2)^T,(-1,-3)^T)$$

$$((-1,2)^T,(-1,1)^T,(2,-3)^T)$$

$$((1,2)^T,(1,1)^T,(2,-3)^T)$$

$$((-1,1)^T,(-2,1)^T,(3,-2)^T)$$

$$((1,1)^T,(2,1)^T,(-3,-2)^T)$$

$$((-2,1)^T,(-1,0)^T,(3,-1)^T)$$

$$((2,1)^T,(1,0)^T,(-3,-1)^T)$$

$$((0,1)^T,(-1,3)^T,(1,-4)^T)$$

$$((0,1)^T,(1,3)^T,(-1,-4)^T)$$

$$((-3,1)^T,(-1,0)^T,(4,-1)^T)$$

$$((3,1)^T,(1,0)^T,(-4,-1)^T).$$

By the 3rd item in Remark 4.5.11, the set $\{P(\mathbf{v},\gamma) : \mathbf{v} \in V_{\epsilon_{37}}, \gamma \in \mathbb{R}^3_+, \operatorname{Tr} P(\mathbf{v},\gamma) = 1\}$

already contains more than 99% of matrices in $\mathcal{P}_0$ as defined in (4.27).

The method in [5] uses Theorem 4.5.9 to find a finite set of superbases to approximate all matrices in $\mathcal{P}_0$. In principle, we want to approximate as many matrices in $\mathcal{P}_0$ as possible. However, this also means more and more superbases needed. In practice, the numerical solver in [5] has a parameter, called `condition number`, which is defined as $\mu^2(M)$ for M and μ in (4.38). Users use this parameter to specify how fine the approximation should be, i.e., how to make a choice of the set of superbases.

After one specifies the `condition number` parameter, accordingly a finite set of superbases can be generated. Indeed, by the proof of Theorem 4.5.9 and definitions (4.38) and (4.39), given a positive real number $\mu_0 > 0$, all the matrices in the following set:

$$\{M \in \mathcal{P}_0 : \mu(M) < \mu_0\}$$

can be written as $P(\mathbf{v}, \gamma)$ for some γ determined by Propositon 4.5.4 and some $\mathbf{v}$ that belongs to V_ϵ such that

$$\mu_\epsilon = \mu_0.$$

More precisely, say one inputs `condition number = 15`, then a set of superbases will be produced and it includes all superbases that are constructed using direct basis $v = (v_1, v_2)$ with

$$|v_1| \leq \frac{\sqrt{15} - \sqrt{15}^{-1}}{2},$$
$$|v_2| \leq \frac{\sqrt{15} - \sqrt{15}^{-1}}{2}.$$

These direct bases are exactly the first three direct bases in Figure 4.6. They in turn give the first six superbases in Figure 4.8.

We will discuss in Section 5.2.1, Remark 5.2.1 how we choose this parameter in our applications.

4.5.6 Properties of the set of superbases

We address the items mentioned in Remark 4.5.11. Recalling the construction of V_ϵ from the proof of Theorem 4.5.9, each direct basis $\tilde{v} = (v_1, v_2)$ in the Stern–Brocot Tree leads to two superbases

$$(-v_1^\perp, -v_2^\perp, v_1^\perp + v_2^\perp),$$

$$(-\tilde{v}_1^\perp, -\tilde{v}_2^\perp, \tilde{v}_1^\perp + \tilde{v}_2^\perp).$$

These superbases are corresponding to two triangles in the unit disk. In particular, the standard basis $((1,0)^T, (0,1)^T)$ gives rise to two superbases and, consequently, the two largest triangles in Figure 4.7.

The children nodes of any direct basis $\tilde{v}$, denoted as $\tilde{v}^{(1)} = (v_1+v_2, v_2)$ and $\tilde{v}^{(2)} = (v_1, v_1+v_2)$ will give rise to four triangles. These four triangles share common edges with the triangles associated with the parent node. To see this, note that the superbase $(-v_1^\perp, -v_2^\perp, v_1^\perp+v_2^\perp)$, derived from $\tilde{v}$, and the superbase $(-v_1^\perp - v_2^\perp, -v_2^\perp, v_1^\perp + 2v_2^\perp)$, derived from $\tilde{v}^{(1)}$, respectively have components of $-v_2^\perp, v_1^\perp + v_2^\perp$ and $-v_2^\perp, -v_1^\perp - v_2^\perp$. By (4.36), they define the same edge within the unit disk. In particular, the four superbases that arise from child nodes of $((1,0)^T, (0,1)^T)$ give rise to the four yellow triangles in Figure 4.7.

In this section, we conclude by introducing two additional properties of the set V_ϵ, which has been constructed in the proof of Theorem 4.5.9. Furthermore, we briefly describe how V_ϵ will be applied within the numerical scheme.

Henceforth, we adopt the notation $h > 0$ to index this set and refer to the sequence using

$$\{V_h\}_{h>0}.$$

Indeed, the notation $h > 0$ will be used for the grid size that we later need in the discretization of the domain where the equation is solved. In principle, as h approaches 0, the grid points approximate the domain more precisely. Correspondingly, the set V_h is expected to, and indeed can provide a better approximation to $\mathcal{P}_0$ for smaller $h > 0$, as suggested by Theorem 4.5.9.

Based on the construction of V_h, we have the following result.

Proposition 4.5.16. *Let V_h be defined as in the proof of Theorem 4.5.9. Then*

$$\lim_{h\to 0} \max_{v\in V_h} \max_{e\in v} |e| = 0. \tag{4.52}$$

Furthermore, for any $h > 0$,

$$(1,0)^T = e_1 \in \bigcup_{v\in V_h} \bigcup_{e\in v} \{\pm e\}. \tag{4.53}$$

Proof. To prove (4.52), we fix $h > 0$ and consider any $\mathbf{v} = (v_1, v_2, v_3) \in V_h$. By Lemma 4.5.12 and the construction (4.49), we have

$$\max_{1\le i\le 3} |v_i| \le 2\mu_h.$$

Consequently, (4.52) can be derived from (4.48).

Next, to prove (4.53), we have from the Definition 4.5.7 that any subtree $\mathcal{T}_{(\mu_h-\mu_h^{-1})/2}$ contains the basis $(e_1, e_2) = ((1,0)^T, (0,1)^T)$. Now by (4.49), it is evident that $(-e_2, e_1, e_2 - e_1)$ always belongs to V_h. $\square$

4.6 Reformulation of the second boundary value problem for Monge–Ampère equations

In this section, our objective is to expound Bonnet–Mirebeau's approach to reformulating the second boundary value problem for the Monge–Ampère equations.

- In Section 4.6.1, we explain how they reformulate the equation under consideration, cf. Theorems 4.6.2 and 4.6.5. This reformulation relies on Gaveau's result, along with the discretization of the set $\mathcal{P}_0$, which we have seen from the preceding section, and elementary convex geometry.
- In Section 4.6.2, we show that this reformulation, when viewed as an optimization problem, has a partially closed-form solution, as illustrated in Theorem 4.6.8. This feature enhances its computational efficiency when applied in the numerical work.

4.6.1 Bonnet–Mirebeau's reformulation

In their work [5], the authors developed a numerical scheme for a type of Monge–Ampère equations in a more generalized form, as we will define in the forthcoming Definition 4.6.1. The reformulation utilizes Gaveau's results (4.22) and (4.23), and subsequently employs Theorem 4.5.9 to discretize the set $\mathcal{P}_0$.

Let K be the same open bounded convex subset as in (4.21) and P a convex polytope defined in (4.6). Let $A(x,p) : \overline{K} \times \mathbb{R}^n \to \mathrm{Sym}^2(\mathbb{R}^n)$ and $B(x,p) : \overline{K} \times \mathbb{R}^n \to \mathbb{R}_{\geq 0}$ be two bounded maps. The following definition is the second boundary value problem that we will solve.

Definition 4.6.1. The second boundary value problem of Monge–Ampère equation is the following equation

$$\det(\nabla^2 u(x) - A(x, \nabla u(x))) = B(x, \nabla u(x)) \quad \text{in } K, \tag{4.54}$$

combined with a constraint on the solution's gradient image:

$$\nabla u(K) \in \overline{P}. \tag{4.55}$$

We reformulate the equation (4.54) and (4.55) respectively. For (4.54):

Proposition 4.6.2. *Let $\{V_h\}_{h>0}$ be a sequence of collection of superbases that is constructed in Theorem 4.5.9. The equation (4.54) is equivalent to*

$$\lim_{h\to 0^+} \max_{\mathbf{v}\in V_h} \max_{\substack{\gamma\in\mathbb{R}^N_+ \\ \operatorname{Tr} P(\mathbf{v},\gamma)=1}} \Big[n \left(B(x,\nabla u(x)) \det P(\mathbf{v},\gamma) \right)^{1/n} - \operatorname{Tr}(P(\mathbf{v},\gamma)(\nabla^2 u(x) - A(x,\nabla u(x)))) \Big] = 0, \text{ in } K. \tag{4.56}$$

Proof. By Lemma 4.4.3 and 4.4.4, the equation (4.54) is equivalent to

$$\max_{M\in\mathcal{P}_0} \left[n(B(x,\nabla u(x)) \det M)^{1/n} - \operatorname{Tr}(M(\nabla^2 u(x) - A(x, \nabla u(x)))) \right] = 0. \tag{4.57}$$

This can be also proved by using Theorem 4.4.2 and replacing $f(x)$ in (4.23) with $B(x, \nabla u(x))$ and M with $\nabla^2 u(x) - A(x, \nabla u(x))$.

Since we only consider 2×2 matrices in (4.57), Theorem 4.5.9 is valid and can be used to discretize the set $\mathcal{P}_0$. We have that for any $M \in \operatorname{int} \mathcal{P}$ that belongs to a compact subset of $\mathcal{P}_0$, there exists $h > 0$ such that $M = P(\mathbf{v}, \gamma)$ for some $\mathbf{v} \in V_h$ and $\gamma \in \mathbb{R}^3_+$. Hence, (4.57) can be seen to be equivalent to (4.56) by approximating $\mathcal{P}_0$ using $\{V_h\}_{h>0}$ and the matrices $P(\mathbf{v}, \gamma)$ derived from it. □

Henceforth, denote by

$$F_{\mathrm{MA}}(u(x)) :=$$

$$\lim_{h \to 0^+} \max_{\mathbf{v} \in V_h} \max_{\gamma \in \mathbb{R}^n_+, \operatorname{Tr} P(\mathbf{v},\gamma)=1} \left[n \left(B(x, \nabla u(x)) \det P(\mathbf{v}, \gamma) \right)^{1/n} - \operatorname{Tr}(P(\mathbf{v}, \gamma)(\nabla^2 u(x) - A(x, \nabla u(x)))) \right], \tag{4.58}$$

for $x \in K$.

In addressing the boundary condition (4.55), note that this condition essentially requires that a vector $\nabla u(x) \in \mathbb{R}^n$ resides either inside a convex set $P \subset \mathbb{R}^n$ or on its boundary, for a given function u and any $x \in K$. Hence, we can employ tools from convex geometry to reformulate this condition.

Let P be a convex polytope as in Definition 4.6.1. The following definition is classic in convex geometry.

Definition 4.6.3. The support function $h_P : \mathbb{R}^n \to \mathbb{R}$ of P is given by

$$h_P(v) := \sup_{p \in P} \{v \cdot p\}.$$

Definition 4.6.4. The boundary operator is defined for $p \in \mathbb{R}^n$ as

$$F_{\text{BV}}(p) := \max_{v \in \mathbb{R}^n, |v|=1} (v \cdot p - h_P(v)) \tag{4.59}$$

Proposition 4.6.5. *The boundary condition* (4.55) *is equivalent to*

$$F_{BV}(\nabla u(x)) \leq 0, \quad x \in K.$$

Proof. It suffices to prove that a vector $w \in \mathbb{R}^n$ belongs to $\overline{P}$ if and only if $F_{\text{BV}}(w) \leq 0$. Assume $w \in \overline{P}$, then by Definition 4.6.3, for any v such that $|v| = 1$,

$$v \cdot w \leq h_P(v) = \sup_{p \in P} v \cdot p.$$

Hence, we have $F_{\text{BV}}(w) \leq 0$ in this case.

It remains to prove the other direction. For any vector $b \in \partial P$, denote by $n(b)$ the outward normal vector to ∂P at b. The function

$$H(p) := \max_{b \in \partial P} \{n(b) \cdot (p - b)\}$$

satisfies that $H(p) \leq 0$ if and only if $p \in \overline{P}$. Instead of considering such $b \in \partial P$, for any v such that $|v| = 1$ we denote by $b(v)$ a point on ∂P whose normal vector has the same direction as v. Then the function

$$\widetilde{H}(p) := \max_{v \in \mathbb{R}^n, |v|=1} \{v \cdot (p - b(v))\}$$

also satisfies that $H(p) \leq 0$ if and only if $p \in \overline{P}$. For any vector v such that $|v| = 1$, there holds $h_P(v) = v \cdot b(v)$. Thus,

$$F_{\text{BV}}(p) = \widetilde{H}(p)$$

and it follows that $w \in \overline{P}$ if $F_{\text{BV}}(w) \leq 0$. $\square$

Finally, we combine the reformulation for (4.54) and (4.55) to rewrite the second boundary value problem.

Theorem 4.6.6. *Assume that we consider a second boundary value problem in Definition 4.6.1 whose solutions are smooth. An equivalent formulation of* (4.54) *along with* (4.55)*, is as follows:*

$$\max\{F_{\text{MA}}(u(x)), F_{\text{BV}}(\nabla u(x))\} = 0, \quad x \in K. \tag{4.60}$$

Proof. For $x \in K$ such that $\nabla u(x) \in \operatorname{Int} P$, there holds $F_{\text{BV}}(\nabla u(x)) < 0$ by Proposition 4.6.5. In that case, the equation (4.60) reduces to $F_{\text{MA}}(u(x)) = 0$. For other $x \in K$, there still holds $F_{\text{MA}}(u(x)) = 0$ due to the continuity of u. The result then follows from Proposition 4.6.2. $\square$

4.6.2 Properties of the reformulation

In this section, we digress briefly to explore the key advantages of the reformulation (4.60) when applied later in the numerical method.

Firstly, Theorem 4.5.9 ensures that the collection of matrices $\{P(\mathbf{v}, \gamma) : \mathbf{v} \in V_h, \gamma \in \mathbb{R}^3_+\}$ approximates the set $\mathcal{P}_0$ as $h \to 0^+$, and each V_h only contains a finite number of superbases v. In practical terms, this implies that we can choose a small $h > 0$ such that all the matrices in the set $\{P(\mathbf{v}, \gamma) : \mathbf{v} \in V_h, \gamma \in \mathbb{R}^3_+, \operatorname{Tr}(P(\mathbf{v}, \gamma)) = 1\}$ already cover a large portion of matrices in

$\mathcal{P}_0$. Simultaneously, there is only a finite number of $\mathbf{v}$ in such V_h. By Remark 4.5.11, as long as V_h contains the first six superbases, 89% of matrices in $\mathcal{P}_0$ will have been included. In the numerical experiments, when taking maximum in (4.58), we fix h such that V_h contains the first six superbases.

Secondly, for any given superbase v, the maximum in (4.56) over $\gamma \in \mathbb{R}^3_+$, after a modification, can be determined through a closed form solution, which we will now describe. This and the aforementioned properties provide us a way to achieve numerical efficiency: we only need to consider finitely many superbases, and for each superbase the maximum can be computed using a closed form formula.

Definition 4.6.7 below is a modified version of the quantity presented within the brackets in (4.56). The modification is valid, since

$$\begin{aligned}\operatorname{Tr}\left(P(\mathbf{v},\gamma)(\nabla^2 u(x) - A(x,\nabla u(x)))\right) &= \operatorname{Tr}\left(\sum_{i=1}^{3} \gamma_i v_i v_i^T (\nabla^2 u(x) - A(x,\nabla u(x)))\right) \\ &= \sum_{i=1}^{3} \gamma_i \left(\operatorname{Tr}(v_i v_i^T (\nabla^2 u(x) - A(x,\nabla u(x))))\right).\end{aligned} \tag{4.61}$$

In other words, the trace operator can be reformulated as an inner product involving γ.

Definition 4.6.7. Let $N = 2, 3$. Let $v = (v_1, \ldots, v_N)$ and $\gamma \in \mathbb{R}^N$. Let $b \in \mathbb{R}$ and $m \in \mathbb{R}^N$. Define

$$L_{v,\gamma}(b,m) := n \cdot b^{1/n} \cdot (\det P(v,\gamma))^{1/n} - \langle \gamma, m \rangle, \tag{4.62}$$

Using Definition 4.6.7, the equation (4.56) can be expressed as

$$\lim_{h\to 0^+} \max_{\mathbf{v}\in V_h} \max_{\gamma\in\mathbb{R}^N_+, \operatorname{Tr} P(\mathbf{v},\gamma)=1} L_{\mathbf{v},\gamma}(B(x,\nabla u(x)), m)$$

where $m = (m_1, m_2, m_3)$ such that

$$m_i = \mathrm{Tr}(v_i v_i^T (\nabla^2 u(x) - A(x, \nabla u(x)))), \quad i = 1, 2, 3.$$

Theorem 4.6.8. [5, Theorem 1.2] *Let the operator $L_{v,\gamma}$ be defined in (4.62). If $v = (v_1, v_2)$ is a direct basis of $\mathbb{Z}^2$, then for any $b \geq 0$ and $m \in \mathbb{R}^2$,*

$$\max_{\gamma \in \mathbb{R}^2_+, \mathrm{Tr}(P(v,\gamma))=1} L_{v,\gamma}(b, m) = \tilde{H}_v(b, m), \tag{4.63}$$

where

$$\tilde{H}_v(b, m) := \left(\frac{b}{|v_1|^2 |v_2|^2} + \left(\frac{m_1}{2|v_1|^2} - \frac{m_2}{2|v_2|^2} \right)^2 \right)^{1/2} - \frac{m_1}{2|v_1|^2} - \frac{m_2}{2|v_2|^2}.$$

Furthermore, if $\mathbf{v} = (v_1, v_2, v_3)$ is a superbase of $\mathbb{Z}^2$, then for any $b \geq 0$ and $m \in \mathbb{R}^3$,

$$\max_{\gamma \in \mathbb{R}^3_+, \mathrm{Tr}(P(\mathbf{v},\gamma))=1} L_{\mathbf{v},\gamma}(b, m) = \max \left\{ H_v(b, m), \max_{1 \leq i < j \leq 3} \tilde{H}_{(v_i, v_j)}(b, m) \right\},$$

where

$$H_v(b, m) := \begin{cases} (b + \langle m, Q_v m \rangle)^{\frac{1}{2}} + \langle w_v, m \rangle, & \textit{if } Q_v m + (b + \langle m, Q_v m \rangle)^{\frac{1}{2}} w_v <_{vec} 0, \\ -\infty, & \textit{else}, \end{cases}$$

and

$$Q_v := \frac{1}{4} \begin{pmatrix} |v_2|^2 |v_3|^2 & \langle v_1, v_2 \rangle |v_3|^2 & \langle v_1, v_3 \rangle |v_2|^2 \\ \langle v_1, v_2 \rangle |v_3|^2 & |v_1|^2 |v_3|^2 & \langle v_2, v_3 \rangle |v_1|^2 \\ \langle v_1, v_3 \rangle |v_2|^2 & \langle v_2, v_3 \rangle |v_1|^2 & |v_1|^2 |v_2|^2 \end{pmatrix},$$

and

$$w_v := \frac{1}{2}\begin{pmatrix} \langle v_2, v_3\rangle \\ \\ \langle v_1, v_3\rangle \\ \\ \langle v_1, v_2\rangle \end{pmatrix},$$

and for $a \in \mathbb{R}^d$, we write $a <_{vec} 0$ if all components of a are negative.

We conclude this section after proving the preceding theorem.

Proof of the Theorem. We first prove the result when $v = (v_1, v_2)$ is a direct basis. The set under consideration can be parameterized by a single variable:

$$\{\gamma \in \mathbb{R}_2^+ : \operatorname{Tr}(P(v,\gamma)) = 1\} = \left\{ \left(\frac{1+t}{2|v_1|^2}, \frac{1-t}{2|v_2|^2}\right) : t \in [-1,1] \right\}. \tag{4.64}$$

This set is a collection of points on the segment with endpoints

$$\left(\frac{1}{|v_1|^2, 0}\right), \quad \text{and} \quad \left(0, \frac{1}{|v_2|^2}\right).$$

By (4.64), the left hand side of (4.63) can be written as

$$\max_{\gamma\in\mathbb{R}_+^2, \operatorname{Tr}(P(v,\gamma))=1} L_{v,\gamma}(b,m) = \max_{t\in[-1,1]} \left(2b^{\frac{1}{2}} \cdot \left(\left(\det P\left(v, \left(\frac{1+t}{2|v_1|^2}, \frac{1-t}{2|v_2|^2}\right)\right)\right)^{\frac{1}{2}} - \frac{1+t}{2|v_1|^2}m_1 - \frac{1-t}{2|v_2|^2}m_2\right)\right). \tag{4.65}$$

A direct calculation yields

$$\begin{aligned}\det P\left(v,\left(\frac{1+t}{2|v_1|^2},\frac{1-t}{2|v_2|^2}\right)\right) &= \det\left(\frac{1+t}{2|v_1|^2}v_1\cdot v_1^T+\frac{1-t}{2|v_2|^2}v_2\cdot v_2^T\right)\\ &= \frac{1}{4}(1-t^2)\frac{\det[v_1,v_2]^2}{|v_1|^2|v_2|^2}\\ &= \frac{1-t^2}{4|v_1|^2|v_2|^2}.\end{aligned} \tag{4.66}$$

To simplify notations, we introduce

$$\begin{aligned}\omega_v^0 &:= \frac{1}{|v_1|^2|v_2|^2}\\ \omega_v^1 &:= \frac{1}{2}\left(\frac{1}{|v_1|^2},\frac{-1}{|v_2|^2}\right),\\ \omega_v^2 &:= \frac{1}{2}\left(\frac{1}{|v_1|^2},\frac{1}{|v_2|^2}\right).\end{aligned} \tag{4.67}$$

Substituting (4.66) in (4.65) and using (4.67), we have

$$\max_{\gamma\in\mathbb{R}_+^2,\operatorname{Tr}P(v,\gamma)=1} L_{v,\gamma}(b,m)=\max_{t\in[-1,1]}\left((\omega_v^0)^{\frac{1}{2}}b^{\frac{1}{2}}(1-t^2)^{\frac{1}{2}}-\langle\omega_v^1,m\rangle-\langle\omega_v^2,m\rangle\right). \tag{4.68}$$

Taking the derivative with respect to t in, we find the optimal t satisfies

$$t^2=\frac{\langle\omega_v^1,m\rangle^2}{b\cdot\omega_v^0+\langle\omega_v^1,m\rangle^2}.$$

Plugging this into (4.68), we obtain

$$\max_{\gamma\in\mathbb{R}_+^2,\operatorname{Tr}P(v,\gamma)=1} L_{v,\gamma}(b,m)=\left(b\cdot\omega_v^0+\langle\omega_v^1,m\rangle^2\right)^2-\langle\omega_v^2,m\rangle$$

which precisely aligns with the definition of $\tilde{H}_v(b, m)$.

Now, let us prove the result when $\mathbf{v} = (v_1, v_2, v_3)$ is a superbase. Define a map

$$\mathcal{D} : \mathbb{R}^2 \to \mathrm{Sym}^2(\mathbb{R}^n),$$
$$\rho = (\rho_1, \rho_2) \mapsto \frac{1}{2}\begin{pmatrix} 1+\rho_1 & \rho_2 \\ \rho_2 & 1-\rho_1 \end{pmatrix}.$$

Then, the set $\mathcal{P}_0$ satisfies

$$\mathcal{P}_0 = \{M \in \mathcal{P} : \operatorname{Tr} M = 1\} = \{\mathcal{D}(\rho) : |\rho| \leq 1\}. \tag{4.69}$$

For any $\rho \in \mathbb{R}^2$,

$$\det \mathcal{D}(\rho) = \frac{1}{4}(1 - |\rho|^2)$$
$$\kappa(\mathcal{D}(\rho)) = \frac{1+|\rho|}{1-|\rho|}.$$

Recall that the following map

$$f : M \mapsto \det(M)^{\frac{1}{2}}$$

is concave in $\mathcal{P}$. Hence, for

$$\gamma \in \{\gamma \in \mathbb{R}^3 : P(\mathbf{v}, \gamma) \in \mathcal{P}, \operatorname{Tr}(P(\mathbf{v}, \gamma)) = 1\},$$

the map

$$\gamma \mapsto L_{\mathbf{v},\gamma}(b, m)$$

is also concave by Definition 4.62. The following is well-defined:

$$\gamma(\mathbf{v}, b, m) := \underset{\gamma \in \mathbb{R}^3, P(\mathbf{v},\gamma) \in \mathcal{P}, \mathrm{Tr}(P(\mathbf{v},\gamma))=1}{\operatorname{argmax}} L_{\mathbf{v},\gamma}(b, m).$$

There are two possibilities. Firstly, if there exist any components in $\gamma(\mathbf{v}, b, m)$ that are non-positive, then

$$\max_{\gamma \in \mathbb{R}^3_+, \mathrm{Tr}\, P(\mathbf{v},\gamma)=1} L(\mathbf{v}, \gamma)(b, m) = \max_{1 \leq i < j \leq 3} \tilde{H}(v_i, v_j)(b, m).$$

On the other hand, if $\gamma(\mathbf{v}, b, m) \in \mathbb{R}^3_+$, then Proposition 4.5.4 and (4.69) imply that

$$\max_{\gamma \in \mathbb{R}^3, P(\mathbf{v},\gamma) \in \mathcal{P}, \mathrm{Tr}(P(\mathbf{v},\gamma))=1} L_{\mathbf{v},\gamma}(b, m) = \max_{|\rho| \leq 1} L_{\mathbf{v},\gamma(\mathbf{v},\mathcal{D}(\rho))}(b, m).$$

Define

$$\rho(\mathbf{v}, b, m) := \operatorname{argmax}_{|\rho| \leq 1} L_{\mathbf{v},\gamma(\mathbf{v},\mathcal{D}(\rho))}(b, m),$$

then

$$\gamma(\mathbf{v}, b, m) = \gamma(\mathbf{v}, \mathcal{D}(\rho(\mathbf{v}, b, m))). \tag{4.70}$$

Observe that Q_v can be factorized as

$$Q_v = W_v \cdot W_v^T$$

where

$$W_v := \frac{1}{2}\begin{pmatrix} v_{2,1}v_{3,1} - v_{2,2}v_{3,2}, & v_{2,1}v_{3,2} + v_{2,2}v_{3,1} \\ v_{1,1}v_{3,1} - v_{1,2}v_{3,2}, & v_{1,1}v_{3,2} - v_{1,2}v_{3,1} \\ v_{1,1}v_{2,1} - v_{1,2}v_{2,2}, & v_{1,1}v_{2,2} - v_{1,2}v_{2,1}. \end{pmatrix}.$$

By (4.30), we have

$$\gamma(\mathbf{v}, \mathcal{D}(\rho)) = W_v\rho - w_v. \tag{4.71}$$

Plugging (4.71) into the Definition 4.6.7, we obtain

$$L_{\mathbf{v},\gamma(\mathbf{v},\mathcal{D}(\rho))}(b, m) = b^{1/2}(1 - |\rho|^2)^{\frac{1}{2}} - \langle W_v\rho - w_v, m\rangle. \tag{4.72}$$

Setting the derivative with respect to ρ in (4.72) to be zero, we have

$$\begin{aligned}\rho(\mathbf{v}, b, m) &= -\frac{W_v^T m}{(b + |W_v^T m|^2)^{\frac{1}{2}}} \\ &= -\frac{W_v^T m}{(b + \langle m, Q_v m\rangle)^{\frac{1}{2}}}.\end{aligned}$$

Plugging this into (4.70), we have

$$\begin{aligned}\gamma(\mathbf{v}, b, m) &= \gamma(\mathbf{v}, \mathcal{D}(\rho(\mathbf{v}, b, m))) \\ &= -\frac{Q_v m}{(b + \langle m, Q_v m\rangle)^{\frac{1}{2}}} - w_v.\end{aligned}$$

Finally, substituting $\gamma(\mathbf{v}, b, m)$ in Definition 4.6.7 yields

$$L_{\mathbf{v},\gamma(\mathbf{v},b,m)} = (b + \langle m, Q_v m\rangle)^{\frac{1}{2}} + \langle w_v, m\rangle.$$

This equality has matched with $H_v(b, m)$. The proof is finished. $\square$

4.7 Discretization

In this section, we use the finite difference method to discretize the reformulated problem (4.60) and then construct a corresponding numerical scheme. The numerical scheme is presented in equation (4.79).

4.7.1 An overview on numerical schemes

Ultimately, our aim is to solve the problem (4.60) numerically. The approach we use will be the finite difference method. It consists of the following steps. We discretize the domain on which the equation is defined, which is K. And then we define finite difference operators which are approximations to derivative terms that appear in the equation. Finally, on each grid point, by replacing the exact solution with these approximations, we obtain a resulting linear system of equations. Solving this linear system gives us a numerical solution.

From now on, let $h > 0$. This h should be understood as the grid size. Denote by

$$\mathcal{G}_h := K \cap h\mathbb{Z}^n \tag{4.73}$$

the set of integer points in K with grid size h.

Definition 4.7.1. A numerical scheme is a function $S : \mathbb{R}^{\mathcal{G}_h} \to \mathbb{R}^{\mathcal{G}_h}$.

Usually a numerical scheme is denoted as S^h to indicate its dependence on the grid size h. For a function $u : K \to \mathbb{R}$, which we may think of as a solution to certain PDEs, the set

$\{u(x) : x \in \mathcal{G}_h\}$ is indexed by x and thus will be identified as a vector in $\mathbb{R}^{\mathcal{G}_h}$. For any numerical scheme S^h, we introduce the notation

$$S^h u[x] := S^h\Big(\{u(x) : x \in \mathcal{G}_h\}\Big)(x), \quad \forall x \in \mathcal{G}_h.$$

In the following sections, we construct a numerical scheme S that is closely related to the second boundary value problem (4.60).

Roughly speaking, we discretize all components in their reformulation (4.60) by the finite difference method, and then aim to solve a resulting system of equations for its associated numerical scheme S^h:

$$S^h u[x] = 0, \quad \forall x \in \mathcal{G}_h.$$

The solution $\{u(x) : x \in \mathcal{G}_h\}$ is expected to be an approximation of the true solution values evaluated on $\mathcal{G}_h$.

The numerical scheme will be shown to be consistent with the original PDE, by Definition 4.8.5 below. More importantly, we will prove the existence of solutions to such numerical scheme in Theorem 4.8.10 below, and present the fact that the numerical solution to the scheme is an approximation to solutions to the original problem in next chapter's Theorem 4.8.18.

4.7.2 Bonnet–Mirebeau's numerical scheme

In this section, we revisit the construction of the numerical scheme for (4.60).

Step 1: reformulation of the problem. By Theorem 4.6.6, the original second value problem (4.54) and (4.55) is equivalent to (4.60). The two components in (4.60) have the following forms:

$$F_{\text{MA}}(u(x)) = 0, \quad x \in K,$$
$$F_{\text{BV}}(\nabla u(x)) \leq 0, \quad x \in K, \tag{4.74}$$

where F_{MA} is defined in (4.58) and F_{BV} in (4.59).

From now on, we aim to discretize each component in (4.74) by finite difference method. We assume that in (4.74) $A(\cdot,\cdot)$ is bounded from below and Lipschitz continuous, and $B(\cdot,\cdot)^{1/n}$ is Lipschitz continuous. More precisely, assume that there exist constants $a_1 \geq 0, a_2 \leq 0, b_1 \geq 0$ such that for any $x \in K$ and $v_1, v_2 \in \mathbb{R}^n$,

$$\begin{aligned} |A(x,v_1) - A(x,v_2)|_2 &\leq a_1|v_1 - v_2|_1, \\ |B(x,v_1)^{1/n} - B(x,v_2)^{1/n}| &\leq b_1|v_1 - v_2|_1, \\ A(x,v_1) &\geq a_2 I_n. \end{aligned} \tag{4.75}$$

These assumptions are made so that the proposed numerical scheme is monotonic, as defined in Definition 4.8.1 below.

Step 2: Discretizations of the equation and the boundary condition. The discretization of (4.74) is based on the *finite difference method*. Let h be the grid size and $\mathcal{G}_h$ the grid integer points as in Definition 4.7.1. Always denote by $e \in \mathbb{Z}^n$ an arbitrary vector. Let $(e_1, \ldots, e_n)$ always be the standard basis $(1,0,\ldots,0)^T, \ldots, (0,0,\ldots,1)^T$ of $\mathbb{Z}^n$.

Since (4.60) is a second order PDE, below we will define the first order and second order finite difference operators, in particular the gradient operator and the Laplace operator, and based on which the discrete expression of functions A, B and F_{BV}.

Definition 4.7.2. Let $u : \mathcal{G}_h \to \mathbb{R}$, and $x \in \mathcal{G}_h$. The first order finite difference operator $\delta_h^e u[x]$ is defined as

$$\delta_h^e u[x] := \begin{cases} \frac{u[x+he]-u[x]}{h}, & \text{if } x+he \in \mathcal{G}_h. \\ \\ +\infty, & \text{else.} \end{cases}$$

Definition 4.7.3. Let u and x be the same as in Definition 4.7.2. The second order finite difference operator $\Delta_h^e u[x]$ is defined as follows.

$$\Delta_h^e u[x] := \begin{cases} \frac{u[x+he]+u[x-he]-2u[x]}{h^2}, & \text{if } x \pm he \in \mathcal{G}_h. \\ \\ +\infty, & \text{else.} \end{cases}$$

The discretizations $\delta_h^e u[x]$ and $\Delta_h^e u[x]$ are used as approximations to the directional derivatives along direction e.

Definition 4.7.4. Let u and x be as in Definition 4.7.2. The finite difference operator for the gradient is defined as

$$\nabla_h u[x] := \left(\frac{\delta_h^{e_i} u[x] - \delta_h^{-e_i} u[x]}{2} \right)_{1 \le i \le n}$$

such that $\nabla_h u[x] \in (\mathbb{R} \cup +\infty)^n$.

Definition 4.7.5. Let u and x be as in Definition 4.7.2. The finite difference operator of Laplacian is given by

$$\Delta_h u[x] := \sum_{i=1}^{n} \Delta_h^{e_i} u[x]$$

recalling that $\{e_i\}_{1 \le i \le n}$ is the set of standard basis of $\mathbb{R}^n$. We have that $\Delta_h u[x] \in \mathbb{R} \cup +\infty$.

The discretizations of $A(x, \nabla u(x))$ and $B(x, \nabla u(x))$ on $\mathcal{G}_h$, denoted by $A_h^e u[x]$ and $B_h u[x]$, are then as follows.

Definition 4.7.6. Define

$$A_h^e u[x] := \begin{cases} \max\left\{\left(\langle e, A(x, \nabla_h u[x])e\rangle - \frac{h}{2}a_1|e|^2\Delta_h u[x]\right), a_2|e|^2\right\}, & \text{if } \Delta_h u[x] < +\infty, \\ a_2|e|^2, & \text{else.} \end{cases}$$

$$B_h u[x] := \begin{cases} \max\left\{\left(B(x, \nabla_h u[x])^{1/n} - \frac{h}{2}b_1\Delta_h u[x]\right)^n, 0\right\}, & \text{if } \Delta_h u[x] < +\infty \\ 0, & \text{else.} \end{cases}$$

where a_1, a_2, b_1 are the same constants in (4.75).

Remark 4.7.7. A more natural way to discretize $A(x, \nabla u(x))$ or $B(x, \nabla u(x))$ is as follows:

$$\tilde{A}_h^e u[x] := \langle e, A(x, \nabla_h u[x])e\rangle,$$

$$\tilde{B}_h u[x] := B(x, \nabla_h u[x]).$$

However, the reason to use Definition 4.7.6 in the construction of the numerical scheme lies in the fact that this definition allows us to prove several properties enjoyed by the scheme. For example, we prove the monotonicity in Proposition 4.8.2 below by using Definition 4.7.6.

The discretization in Definition 4.7.6 is called Lax–Friedrichs approximations. A straightforward yet helpful observation is that, as $h \to 0$, when $\Delta_h u[x] < +\infty$, we have

$$A_h^e u[x] \to \max\left\{\langle e, A(x, \nabla_h u[x])e\rangle, a_2|e|^2\right\}$$

$$B_h u[x] \to \max\{B(x, \nabla_h u[x]), 0\}$$

which is in accordance with intuition.

In summary, in the discretization of $B(x, \nabla u(x))$ we replaces $\nabla u(x)$ with $\nabla_h u(x)$. And for

$A(x, \nabla u(x))$, which is a symmetric matrix, we consider the value $e^T A(x, \nabla u(x))e$ for arbitrary e. For each e, we replace $\nabla u(x)$ in $e^T A(x, \nabla u(x))e$ with $\nabla_h u(x)$.

Definition 4.7.8. Let $\Delta_h^e u[x]$ be defined in Definition 4.7.3. Let $A_h^e u[x]$ be defined in 4.7.6. Let $\mathbf{v}$ be a superbase. Define

$$\Delta_h^{\mathbf{v}} u[x] := (\Delta_h^{v_i} u[x])_{v_i \in \mathbf{v}},$$

$$A_h^{\mathbf{v}} u[x] := (A_h^{v_i} u[x])_{v_i \in \mathbf{v}}.$$

Hence, for any superbase $\mathbf{v}$, the vector $\Delta_h^{\mathbf{v}} u[x]$ or $A_h^{\mathbf{v}} u[x]$ is of size that is equal to the cardinality of $\mathbf{v}$.

Remark 4.7.9. By the observation made in (4.61), it is enough to take care of

$$v_i^T \cdot (\nabla^2 u(x) - A(x, \nabla u(x)))v_i \tag{4.76}$$

for each $v_i \in \mathbf{v}$ in (4.74) when considering the trace operator. This is why we consider $\Delta_h^{\mathbf{v}}$ and $A_h^{\mathbf{v}}$ in Definition 4.7.8.

To discretize the boundary condition, we define a different finite difference operator for the gradient, compared to Definition 4.7.4, also in order to maintain the properties enjoyed by the numerical scheme.

Definition 4.7.10. Let u and x be as in Definition 4.7.4. We define the upwind gradient operator to be

$$\nabla_h^e u[x] := \sum_{i=1}^{n} \left(\min\{0, e^T e_i\} \delta_h^{e_i} u[x] - \max\{0, e^T e_i\} \delta_h^{-e_i} u[x] \right)$$

so that $\nabla_h^e u[x] \in \mathbb{R} \cup +\infty$.

With all the preparations, we discretize (4.74) as follows.

Definition 4.7.11. Let V_h be the same as V_ϵ in (4.74), with only the notation ϵ written as h. Let h, $\mathcal{G}_h$ be as in Definition 4.7.1. Let $L_{v,\gamma}$ be defined in (4.62). Define

$$S^h_{\mathrm{MA}} u[x] := \max_{\mathbf{v} \in V_h} \max_{\substack{\gamma \in \mathbb{R}^3_+ \\ \mathrm{Tr}(P(\mathbf{v},\gamma)=1)}} L_{\mathbf{v},\gamma}(B_h u[x], \Delta^{\mathbf{v}}_h u[x] - A^{\mathbf{v}}_h u[x]), \tag{4.77}$$

for $x \in \mathcal{G}_h$.

Remark 4.7.12. The function S^h_{MA} is the discretization that we will use for the first equation in (4.74). The term

$$\Delta^{\mathbf{v}}_h u[x] - A^{\mathbf{v}}_h u[x]$$

appears since the following term

$$\mathrm{Tr}\left(P(\mathbf{v},\gamma)\left(\nabla^2 u(x) - A(x, \nabla u(x))\right)\right)$$

in (4.74) can be approximated by

$$\begin{aligned}
\mathrm{Tr}\left(P(\mathbf{v},\gamma)\left(\nabla^2 u(x) - A(x, \nabla u(x))\right)\right) &= \mathrm{Tr}\left(\sum_{i=1}^{3} \gamma_i v_i v_i^T \left(\nabla^2 u(x) - A(x, \nabla u(x))\right)\right) \\
&= \sum_{i=1}^{3} \gamma_i \,\mathrm{Tr}\left(v_i v_i^T \left(\nabla^2 u(x) - A(x, \nabla u(x))\right)\right) \\
&= \sum_{i=1}^{3} \gamma_i \,\mathrm{Tr}\left(v_i^T \left(\nabla^2 u(x) - A(x, \nabla u(x))\right) v_i\right) \\
&= \langle \gamma, (\Delta^{\mathbf{v}}_h u[x] - A^{\mathbf{v}}_h u[x]) \rangle + O(h^2).
\end{aligned}$$

Definition 4.7.13. Let h and $\mathcal{G}_h$ be as in Definition 4.7.1. Let h_P be defined in Definition 4.6.3.

Define

$$S^h_{\text{BV}}u[x] := \max_{v\in\mathbb{R}^n,|v|=1} \left(\nabla^v_h u[x] - h_P(v)\right). \tag{4.78}$$

Remark 4.7.14. The function S^h_{BV} is the discretization of F_{BV} in Definition 4.6.4. The component $v \cdot \nabla u(x)$ in $F_{\text{BV}}(\nabla u(x))$ is discretized by $\nabla^v_h u[x]$. In practice, if P is a polytope then S^h_{BV} reduces to several linear constraints. Indeed, as argued in the proof of Proposition 4.6.5, assume the polytope P is defined as

$$P := \{x \in \mathbb{R}^2 : x \cdot n_i + b_i \leq 0, i = 1, \ldots, m\},$$

where n_i is the outward normal vector of each edge of P with $|n_i| = 1$. Then $S^h_{\text{BV}}u[x] = \max_{i=1,\ldots,m}\{\nabla^{n_i}_h u[x] + b_i\}$.

Step 3: Combine the discretizations for the equation and the boundary condition.

Definition 4.7.15. Let h and $\mathcal{G}_h$ be as in Definition 4.7.1. Let S^h_{MA} be as in Definition 4.7.11 and S^h_{BV} in Definition 4.7.13. Denote by α a real number. Define

$$S^{h,\alpha}_{\text{MABV}}u[x] := \max\{S^h_{\text{MA}}u[x] + \alpha, S^h_{\text{BV}}u[x]\}. \tag{4.79}$$

This definition is the discrete version of (4.60) but with the modification of an extra α. The constant α is introduced, by authors of [5], to guarantee that the numerical scheme has solutions, as will be discussed in Theorem 4.8.10 and Remark 4.8.11.

In our application, to numerically solve (4.74), we first fix a grid size $h > 0$. Then we solve the following equation on $\mathcal{G}_h$:

$$S^{h,\alpha}_{\mathrm{MABV}} u[x] = 0, \quad \forall x \in \mathcal{G}_h. \tag{4.80}$$

The solution to the numerical scheme (4.80) includes a constant α and the value of the function u, denoted by $u[x]$ on the grid points $x \in \mathcal{G}_h$.

4.8 Existence and convergence results of Bonnet–Mirebeau's numerical scheme

In this section, we address two important questions concerning the numerical scheme (4.80): first, is it always solvable? Second, if it is solvable, does the solution converge to the original Monge–Ampère equation as we reduce the grid size h to 0?

- In Section 4.8.1, we demonstrate that the proposed numerical scheme admits several properties, as shown in Propositions 4.8.2, 4.8.3, 4.8.6 and 4.8.8.
- The answers to the previous two questions are in Theorems 4.8.10 and 4.8.18.

The proofs of these theorems primarily rely on various properties that the numerical scheme (4.80) has, as we will describe now.

4.8.1 Properties of the numerical scheme

The first property is the monotonicity.

Definition 4.8.1. A monotonic numerical scheme $S^h : \mathbb{R}^{\mathcal{G}_h} \to \mathbb{R}^{\mathcal{G}_h}$ satisfies that for any $h > 0$, any $x \in \mathcal{G}_h$, and any $u_1, u_2 : \mathcal{G}_h \to \mathbb{R}$ such that $u_1[x] = u_2[x]$ and $u_1 \geq u_2$ on $\mathcal{G}_h$, there holds

$$S^h u_1[x] \leq S^h u_2[x].$$

Proposition 4.8.2. *For any fixed α, the numerical scheme $S^{h,\alpha}_{MABV}$ is a monotone scheme.*

Proof. Let $h > 0$, $\alpha \in \mathbb{R}$, $x \in \mathcal{G}_h$ and consider u_1, u_2 such that $u_1(x) = u_2(x)$ and $u_1 \geq u_2$ in $\mathcal{G}_h$.

We aim to show

$$S^{h,\alpha}_{\text{MABV}} u_1[x] \leq S^{h,\alpha}_{\text{MABV}} u_2[x],$$

which is equivalent to

$$\max\{S^h_{\text{MA}} u_1[x] + \alpha, S^h_{\text{BV}} u_1[x]\} \leq \max\{S^h_{\text{MA}} u_2[x] + \alpha, S^h_{\text{BV}} u_2[x]\}.$$

We will show the following stronger result:

$$S^h_{\text{MA}} u_1[x] \leq S^h_{\text{MA}} u_2[x],$$
$$S^h_{\text{BV}} u_1[x] \leq S^h_{\text{BV}} u_2[x].$$

First, by Definition 4.7.10, it is obvious that for any e, $\nabla^e_h u_1[x] \leq \nabla^e_h u_2[x]$. Then, by the definition of S^h_{BV} in (4.78), there holds

$$S^h_{\text{BV}} u_1[x] \leq S^h_{\text{BV}} u_2[x].$$

Hence, it remains to show for any $\mathbf{v} = (v_1, v_2, v_3)$ and $\gamma \in \mathbb{R}^3_+$,

$$L_{\mathbf{v},\gamma}(B_h u_1[x], \Delta_h^{\mathbf{v}} u_1[x] - A_h^{\mathbf{v}} u_1[x]) \leq L_{\mathbf{v},\gamma}(B_h u_2[x], \Delta_h^{\mathbf{v}} u_2[x] - A_h^{\mathbf{v}} u_2[x]).$$

To achieve so, we use Definition (4.6.7), and will show

$$B_h u_1[x]^{1/n} \leq B_h u_2[x]^{1/n},$$

$$A_h^{\mathbf{v}} u_1[x] \leq A_h^{\mathbf{v}} u_2[x],$$

$$\Delta_h^{\mathbf{v}} u_2[x] \leq \Delta_h^{\mathbf{v}} u_1[x].$$

The last inequality is obvious. For the first inequality, we consider two cases. First, if $B_h u_1[x] = 0$, then we must have

$$0 = B_h u_1[x]^{1/n} \leq B_h u_2[x]^{1/n}$$

as $B_h \geq 0$ for any function. On the other hand, if $B_h u_1[x] > 0$, then first it indicates that

$$x \pm e_i \in \mathcal{G}_h$$

for any $i = 1, \ldots, n$. Then, we use the Lipschitz continuity of B:

$$\begin{aligned}
B_h u_1[x]^{1/n} - B_h u_2[x]^{1/n} &\leq B(x, D_h u_1[x])^{1/n} - B(x, D_h u_2[x])^{1/n} - \frac{h}{2} b_1 \Delta_h (u_1 - u_2)[x] \\
&\leq b_1 (|D_h u_1[x] - D_h u_2[x]|_1 - \frac{h}{2} \Delta_h (u_1 - u_2)[x]) \\
&= \frac{b_1}{2h} \sum_{i=1}^{n} [|(u_1 - u_2)[x + he_i] - (u_1 - u_2)[x - he_i]| - \\
&(u_1 - u_2)[x + he_i] - (u_1 - u_2)[x - he_i]] \\
&\leq 0.
\end{aligned}$$

Hence, we have shown in both cases

$$B_h u_1[x]^{1/n} \leq B_h u_2[x]^{1/n}.$$

Finally, for the A function we also consider two cases. For any $e \in \mathbf{v}$, if $A_h^e u_1[x] = a_2 |e|^2$, then $A_h^e u_1[x] \leq A_h^e u_2[x]$ by Definition 4.7.6. On the other side, if $A_h^e u_1[x] \neq a_2 |e|^2$, then we also use the Lipschitz continuity of A:

$$\begin{aligned}
A_h^e u_1[x] - A_h^e u_2[x] &\leq \langle e, (A(x, D_h u_1[x]) - A(x, D_h u_2[x]))e \rangle - \frac{h}{2} a_1 |e|^2 \Delta_h (u_1 - u_2)[x] \\
&\leq a_1 |e|^2 (|D_h u_1[x] - D_h u_2[x]|_1 - \frac{h}{2} \Delta_h (u_1 - u_2)[x]) \\
&\leq 0.
\end{aligned}$$

Thus, we have proved $A_h^e u_1[x] \leq A_h^e u_2[x]$. Hence by the definition of S_{MA}^h there holds

$$S_{\text{MA}}^h u_1[x] \leq S_{\text{MA}}^h u_2[x].$$

$\square$

The next property is the continuity of the proposed numerical scheme.

Proposition 4.8.3. *Assume for any small $h > 0$ and for any $x \in \mathcal{G}_h$, there exists $e \in \mathbb{R}^n$ such that $|e| = 1$ and $x - he \in \mathcal{G}_h$. Then for such small $h > 0$, the map*

$$\begin{aligned} &\mathbb{R} \times \mathbb{R}^{\mathcal{G}_h} \to \overline{\mathbb{R}}^{\mathcal{G}_h} \\ &(\alpha, u) \mapsto S^{h,\alpha}_{MABV} u \end{aligned} \tag{4.81}$$

takes finite values and is continuous.

Proof. First, the scheme S^h_{MA}, as defined in (4.77), is continuous, because it is a maximum over two compact sets, V_h and $\{\gamma \in \mathbb{R}^3_+ : \text{ for a fixed } \mathbf{v} \in V_h, \mathrm{Tr}(P(\mathbf{v}, \gamma) = 1)\}$, of a continuous function $L_{\mathbf{v},\gamma}$. The continuity of $L_{\mathbf{v},\gamma}$ can be seen by the same argument in the proof of Lemma 4.4.4. Moreover, the scheme S^h_{BV}, defined as in (4.78), is continuous because it is also a maximum over a compact set: $\{v \in \mathbb{R}^n : |v| = 1\}$, of a continuous function. Consequently, the map (4.81) is continuous since it is composed of two previously established continuous components.

It remains to show that the numerical scheme only takes finite values. Based on the constructions in (4.77) and (4.78), if $S^{h,\alpha}_{\mathrm{MABV}}$ takes non-finite values, it must be $-\infty$. To show that this is not possible for sufficiently small $h > 0$, we use the assumption that for small h, for a given $x \in \mathcal{G}_h$, there exists some e such that $x - he \in \mathcal{G}_h$. Then we have

$$S^{h,\alpha}_{\mathrm{MABV}} u[x] \geq S^h_{\mathrm{BV}} u[x] \geq \nabla^e_h u[x] - h_P(e) > -\infty.$$

$\square$

The next property we consider is a crucial one to relate a numerical scheme to a PDE. To state this property, we will consider PDEs that admit the following form:

$$F(x, \nabla u(x), \nabla^2 u(x)) = 0, \quad \forall x \in \overline{K}. \tag{4.82}$$

Usually, the operator F is discontinuous and it may admit different formulae respectively in K and on the boundary. Hence, naturally we will also consider $\limsup F(x)$ and $\liminf F(x)$.

Following Theorem 4.6.6, the problem (4.54) along with (4.55) can be written in the form (4.82) by letting

$$F_{\mathrm{MABV}}(x, \nabla u(x), \nabla^2 u(x)) := \max\{F_{\mathrm{MA}}(u(x)), F_{\mathrm{BV}}(\nabla u(x))\}. \tag{4.83}$$

For the PDE in the form (4.82), we introduce a type of weak solutions.

Definition 4.8.4. A function $u : \overline{K} \to \mathbb{R}$ is a viscosity subsolution to (4.82) if

1. u is upper semicontinuous.

2. For any $\phi \in C^2(\overline{K})$, if x is a local maximum of $u - \phi$ in $\overline{K}$, then

$$\liminf F(x, \nabla\phi(x), \nabla^2\phi(x)) \leq 0.$$

The function u is a viscosity supersolution if

1. u is lower semicontinuous.

2. For any $\phi \in C^2(\overline{K})$, if x is a local minimum of $u - \phi$ in $\overline{K}$, then

$$\limsup F(x, \nabla\phi(x), \nabla^2\phi(x)) \geq 0.$$

Finally, u is a viscosity solution if it is both a viscosity subsolution and supersolution.

Now, we relate a numerical scheme to a certain PDE as in (4.82) by the following definition.

Definition 4.8.5. A numerical scheme $S^h : \mathbb{R}^{\mathcal{G}_h} \to \mathbb{R}^{\mathcal{G}_h}$ is consistent with respect to a PDE that has the form (4.82) if for any $\phi \in C^\infty(\overline{K})$ and $x \in \overline{K}$,

$$\limsup_{\substack{x' \in \mathcal{G}_h, x' \to x \\ h \to 0^+}} S^h\phi[x'] \leq \limsup F(x, \nabla\phi(x), \nabla^2\phi(x)),$$

$$\liminf_{\substack{x' \in \mathcal{G}_h, x' \to x \\ h \to 0^+}} S^h\phi[x'] \geq \liminf F(x, \nabla\phi(x), \nabla^2\phi(x)).$$

Note that our numerical scheme (4.79) has a parameter α. Thus, to further discuss consistency between numerical schemes and PDEs in our specific setting, we generalize the form for PDEs as in (4.82) to one that also has a parameter α. Specifically, we add a parameter $\alpha \in \mathbb{R}$ to modify the formulation (4.83), i.e., define

$$F^{\alpha}_{\text{MA}}(u(x)) :=$$
$$\alpha + \max_{M \in \mathcal{P}, \operatorname{Tr} M = 1} \left[n \cdot (B(x, \nabla u(x)) \cdot \det M)^{1/n} - \operatorname{Tr}(M \cdot (\nabla^2 u(x) - A(x, \nabla u(x)))) \right].$$

Next, consider

$$F^{\alpha}_{\text{MABV}}(x, \nabla u(x), \nabla^2 u(x)) := \begin{cases} \max\{F^{\alpha}_{\text{MA}}(u(x)), F_{\text{BV}}(\nabla u(x))\}, & \text{if } x \in K, \\ -\infty, & \text{if } x \in \overline{K} \setminus K. \end{cases} \tag{4.84}$$

Then, when $\alpha = 0$ the formulation (4.84) coincides with (4.83) assuming that K is an open set.

We are ready to show the consistence between the numerical scheme (4.79) and the PDE (4.84).

Proposition 4.8.6. *For any sequence of $(\alpha_h)_{h>0}$ such that $\lim_{h\to 0^+} \alpha_h = \alpha$ for some α, the scheme S^{h,α_h}_{MABV} is consistent with respect to the corresponding $F^{\alpha_h}_{\text{MABV}}$ in terms of Definition 4.8.5.*

Proof. First, we prove the proposition assuming the following: let $\phi \in C^\infty(\overline{K})$ and $(\alpha_h)_{h>0}$ be a sequence such that $\lim_{h\to 0^+} \alpha_h = \alpha \in \mathbb{R}$. Then assume for any compact subset $\tilde{K}$ of K, there hold

$$\begin{aligned} S^{h,\alpha_h}_{\text{MABV}}\phi[x] &\le F^{\alpha}_{\text{MABV}}(x, \nabla\phi(x), \nabla^2\phi(x)) + o_{h\to 0^+}(1), \quad \text{uniformly for } x \in \mathcal{G}_h, \\ S^{h,\alpha_h}_{\text{MABV}}\phi[x] &\ge F^{\alpha}_{\text{MABV}}(x, \nabla\phi(x), \nabla^2\phi(x)) + o_{h\to 0^+}(1), \quad \text{uniformly for } x \in \tilde{K} \cap \mathcal{G}_h. \end{aligned} \tag{4.85}$$

Assuming (4.85), then to prove the proposition, it suffices to prove

$$\begin{aligned} \limsup_{h\to 0^+, x'\in\mathcal{G}_h, x'\to x} S^{h,\alpha_h}_{\text{MABV}}\phi[x'] &\le \limsup F^{\alpha}_{\text{MABV}}(x, \nabla\phi(x), \nabla^2\phi(x)), \\ \liminf_{h\to 0^+, x'\in\mathcal{G}_h, x'\to x} S^{h,\alpha_h}_{\text{MABV}}\phi[x'] &\ge \liminf F^{\alpha}_{\text{MABV}}(x, \nabla\phi(x), \nabla^2\phi(x)). \end{aligned} \tag{4.86}$$

If x in (4.86) belongs to some compact subset $\tilde{K}$ of K, then (4.86) follows from (4.85). If not, then (4.86) still holds as in this case

$$\liminf F^{\alpha}_{\mathrm{MABV}}(x, \nabla\phi(x), \nabla^2\phi(x)) = -\infty.$$

Now, let us prove (4.85). Denote by $\tilde{K}$ an arbitrary compact subset of K. It suffices to show that for any $h > 0$ and $x \in \mathcal{G}_h \cap \tilde{K}$, there hold

$$\begin{aligned} S^h_{\mathrm{MA}}\phi[x] &= F^0_{\mathrm{MA}}(x, \nabla\phi(x), \nabla^2\phi(x)) + o(1), \\ S^h_{\mathrm{BV}}\phi[x] &= F_{\mathrm{BV}}(\nabla\phi(x)) + o(1), \end{aligned} \tag{4.87}$$

uniformly with respect to x, if $x \in \tilde{K}$, and

$$\begin{aligned} S^h_{\mathrm{MA}}\phi[x] &\le F^0_{\mathrm{MA}}(x, \nabla\phi(x), \nabla^2\phi(x)) + o(1), \\ S^h_{\mathrm{BV}}\phi[x] &\le F_{\mathrm{BV}}(\nabla\phi(x)) + o(1), \end{aligned} \tag{4.88}$$

uniformly if $x \in \mathcal{G}_h$ but not necessarily belong to $\tilde{K}$.

We first deal with the F_{BV} operator in (4.87) and (4.88). Note that by Definition 4.7.2, there always holds $\delta^{e_i}_h u[x] \ge u[x + he_i] - u[x]$. Thus, we choose h small enough so that for any x in the compact subset $\tilde{K}$, there holds $\delta^{e_i}_h u[x] = u[x + he_i] - u[x]$. And then the two equations that involve F_{BV} hold by Definition 4.7.10.

Now, we consider the F^0_{MA} operator in (4.87) and (4.88). We first treat the $B(\cdot, \cdot)$ function. If there holds $\Delta_h\phi[x] < +\infty$. Then this enforces that

$$x \pm he_i \in \mathcal{G}_h,$$

for each e_i. Hence, it follows from Definition 4.7.4 and Definition 4.7.5 that

$$\nabla_h \phi[x] = \nabla \phi(x) + O(h^2),$$

$$\Delta_h \phi[x] = \Delta \phi(x) + O(h^2).$$

Then by the Lipschitz continuity of $B(\cdot, \cdot)$, we have:

$$B(x, \nabla_h \phi[x])^{1/n} - \frac{h}{2} b_1 \Delta_h \phi[x] = B(x, \nabla \phi(x))^{1/n} + O(h).$$

Then it follows from Definition 4.7.6 that

$$B_h \phi[x]^{1/n} = B(x, \nabla \phi(x))^{1/n} + O(h). \tag{4.89}$$

On the other hand, if $\Delta_h \phi[x] = +\infty$, then we must have $x \notin \tilde{K}$. By Definition 4.7.6, this forces $B_h \phi[x] = 0$, which in particular means $B_h \phi[x] \leq B(x, \nabla \phi(x))$. Then we also have

$$-\infty = B_h \phi[x]^{1/n} \leq B(x, \nabla \phi(x))^{1/n} + O(h) \tag{4.90}$$

for $x \in K \setminus \tilde{K}$.

Next, we treat the $A(\cdot, \cdot)$ function. More precisely, we consider $A_h^e \phi[x]$ and $\Delta_h^e \phi[x]$ for an arbitrary superbase $\mathbf{v} \in V_h$ and $e \in \mathbf{v}$. As before, assume we choose h small enough so that $x + he \in \mathcal{G}_h$ if $x \in \tilde{K}$.

Then by the Lipschitz continuity of $A(x, \nabla \phi(x), \nabla^2 \phi(x))$, there holds

$$A_h^e \phi[x] \leq \langle e, A(x, \nabla \phi(x)) e \rangle + O(h|e|^2)$$

for any x, and the equality holds when $x \in \tilde{K}$.

By Definition 4.7.5, we also have

$$-\Delta_h^e \phi[x] \leq -\langle -e, \nabla^2 \phi(x) e \rangle + O(h^2 |e|^4)$$

for any x, and the equality holds when $x \in \tilde{K}$.

Now, consider any superbase $\mathbf{v} \in V_h$ and $\gamma \in \mathbb{R}_+^3$ such that

$$\operatorname{Tr}(P(\mathbf{v}, \gamma)) = 1, \tag{4.91}$$

then (4.91) requires

$$\sum_{i=1}^{3} \gamma_i |v_i|^2 = 1.$$

For the term we care in (4.77), there then holds

$$\begin{aligned}
-\langle \gamma, \Delta_h^{\mathbf{v}} \phi[x] - A_h^{\mathbf{v}} \phi[x] \rangle &= -\sum_{i=1}^{3} \gamma_i (\Delta_h^{v_i} \phi[x] - A_h^{v_i} \phi[x]) \rangle \\
&\leq -\sum_{i=1}^{3} \gamma_i \langle v_i, (\nabla^2 \phi(x) - A(x, \nabla \phi(x)) v_i \rangle + \sum_{i=1}^{3} \gamma_i O(h |v_i|^2) \\
&= -\langle P(\mathbf{v}, \gamma), \nabla^2 \phi(x) - A(x, \nabla \phi(x)) \rangle + O(h) \\
&= -\langle P(\mathbf{v}, \gamma), \nabla^2 \phi[x] - A(x, \nabla \phi(x)) \rangle + o(1)
\end{aligned} \tag{4.92}$$

for any x, and the equality holds when $x \in \tilde{K}$.

Then by definition in (4.62), and (4.89), (4.90) and (4.92), we proved that

$$S_{\mathrm{MA}}^h \phi[x] \leq \max_{\mathbf{v} \in V_h} \max_{\gamma \in \mathbb{R}_+^3, \operatorname{Tr} P(\mathbf{v}, \gamma) = 1} L_{\mathbf{v}, \gamma}(B(x, \nabla \phi(x)), \nabla^2 \phi(x) - A(x, \nabla \phi(x))) + o(1).$$

for any x, and the equality holds when $x \in \tilde{K}$. Then by (4.57), we have shown the inequality (4.87) for S^h_{MA} and F^0_{MA}. This finishes the proof. $\square$

The final property of our numerical scheme is as follows: roughly speaking, we will show that the numerical scheme admits subsolutions. This fact will play a crucial role when we proceed to construct a solution to the numerical scheme, following a modification of Perron's argument, see Theorem 4.8.10.

Definition 4.8.7. A numerical scheme S^α_h with parameter $\alpha \in \mathbb{R}$ is said to be stable if

- For any small $h > 0$, there exists a subsolution (α, u) to the scheme, i.e.,

$$S^\alpha_h u[x] \leq 0, \quad \forall x \in \mathcal{G}_h.$$

- There exists a function $\omega : \mathbb{R} \times \mathbb{R}_+ \to \mathbb{R}_+$ that is non-increasing w.r.t. its first variable and satisfies $\lim_{t \to 0} \omega(\alpha, t) = 0$ for any $\alpha \in \mathbb{R}$, such that for any small $h > 0$, and any subsolution (α, u) and any $x_1, x_2 \in \mathcal{G}_h$ there holds

$$|u[x_1] - u[x_2]| \leq \omega(\alpha, |x_1 - x_2|).$$

- There exists $\overline{\alpha}$ such that for any small $h > 0$ and any subsolution (α, u) there holds $\alpha \leq \overline{\alpha}$.

- There exists $\underline{\alpha}$ such that for any small $h > 0$ and any solution (α, u), there holds $\underline{\alpha} \leq \alpha$.

Proposition 4.8.8. *Assume there exists a function $\phi \in C^\infty(\overline{K})$ such that $\nabla\phi(x) \in P$ for all $x \in \overline{K}$. Assume there exists a positive constant $C_{\mathcal{G}}$ such that for any small $h > 0$ and any* *function* $u : \mathcal{G}_h \to \mathbb{R}$,

$$\max_{x_1 \neq x_2 \in \mathcal{G}_h} \frac{|u[x_1] - u[x_2]|}{|x_1 - x_2|} \leq C_{\mathcal{G}} \max_{x_1, x_2 \in \mathcal{G}_h, |x_1 - x_2| = h} \frac{|u(x_1) - u(x_2)|}{h}. \tag{4.93}$$

Then the numerical scheme $S^{h,\alpha}_{MABV}$ is stable in terms of Definition 4.8.7.

Remark 4.8.9. The existence of such ϕ in Proposition 4.8.8 is indeed satisfied in our applications; the potential function u itself, defined as in Theorem 4.2.11 fulfills this requirement.

Proof of the Proposition. First, let us establish the existence of subsolutions. By the assumption that $\phi(x)$ satisfies

$$F_{\mathrm{BV}}(\nabla\phi(x)) < 0, \quad \text{for } x \in \overline{K}.$$

Additionally, recalling that $A(x, \nabla\phi(x))$ and $B(x, \nabla\phi(x))$ are bounded, we can choose $\alpha \leq 0$ negative enough so that

$$F^0_{\mathrm{MA}}(x, \nabla\phi(x), \nabla^2\phi(x)) < -\alpha, \quad \text{for } x \in \overline{K}.$$

By combining these two inequalities, we obtain

$$\limsup F^{\alpha}_{\mathrm{MABV}}(x, \nabla\phi(x), \nabla^2\phi(x)) < 0.$$

Then, using (4.85) from the proof of Proposition 4.8.6, for any small $h > 0$ and $x \in \mathcal{G}_h$, we have

$$S^{h,\alpha}_{\mathrm{MABV}}\phi[x] < 0. \tag{4.94}$$

Thus, for any small $h > 0$, (α, ϕ) is a subsolution.

Next, let us construct the function $\omega(\alpha, t)$. Let $h > 0$ be small enough, and then let (α, u) be a subsolution, as previously demonstrated. In particular, we have

$$S^h_{\mathrm{BV}} u[x] \leq 0, \quad \text{for } x \in \mathcal{G}_h.$$

By the construction in (4.78), this inequality implies

$$-\delta_h^{\pm e_i} \leq h_P(\mp e_i) \tag{4.95}$$

for all e_i. As the closure of P is compact, there exists a constant $C_P \geq 0$ such that

$$h_P(\mp e_i) \leq C_P.$$

Consequently:

$$-\delta_h^{\pm e_i} u[x] \leq C_P.$$

Replacing the right hand side in assumption (4.93) with $\delta_h^{\pm e_i}$, we obtain

$$\max_{x_1 \neq x_2, x_1, x_2 \in \mathcal{G}_h} \frac{|u[x_1] - u[x_2]|}{|x_1 - x_2|} \leq C_P \cdot C_{\mathcal{G}}.$$

Therefore, we just need to define $\omega(\alpha, t) := C_P C_{\mathcal{G}} t$, which is independent of α.

Finally, let us address the existence of aforementioned $\overline{\alpha}$ and $\underline{\alpha}$. Still, let $h > 0$ be small and let (α, u) be a subsolution. In particular,

$$S^h_{\text{MA}} u[x] \leq -\alpha, \quad \text{for } x \in \mathcal{G}_h.$$

By (4.53) from the Proposition 4.5.16, we consider the superbase $\mathbf{v} \in V_h$ and $\gamma \in \mathbb{R}^3_+$ such that

$$P(\mathbf{v}, \gamma) = e_1 e_1^T.$$

Choosing this pair of $\mathbf{v} = (e_1, v_2, v_3)$ and $\gamma = (1, \gamma_2, \gamma_3)$ in S^h_{MA} yields

$$S^h_{\text{MA}} u[x] \leq -\alpha \Longrightarrow A^{e_1}_h u[x] - \Delta^{e_1}_h u[x] \leq -\alpha.$$

Combining this inequality with the assumption that $A^{e_1}_h u[x] \geq a_2$, we have

$$\Delta^{e_1}_h u[x] \geq a_2 + \alpha.$$

Now let $\ell > 0$ be small enough that the segment $[0, \ell e_1]$ belongs to K. Note that such ℓ is independent of h. Let $n_h := \lceil \ell / h \rceil$. We choose h small enough such that $ihe_1 \in K$ for $i \in \{0, \ldots, n_h + 1\}$. Then for any such i,

$$\begin{aligned} h\Delta^{e_1}_h u[ihe_1] &= \delta^{e_1}_h u[ihe_1] + \delta^{-e_1}_h u[ihe_1] \\ &= \delta^{e_1}_h u[ihe_1] - \delta^{e_1}_h u[(i-1)he_1]. \end{aligned}$$

Hence, there hold

$$\delta^{e_1}_h u[ihe_1] = \delta^{e_1}_h u[(i-1)he_1] + h\Delta^{e_1}_h u[ihe_1],$$

and in particular

$$\delta_h^{e_1} u[n_h h e_1] = \delta_h^{e_1} u[0] + h \sum_{i=1}^{n_h} \Delta_h^{e_1} u[ihe_1]$$

$$\geq \delta_h^{e_1} u[0] + n_h h(\alpha + a_2).$$

Since $n_h h \geq \ell$, if $\alpha \geq -a_2$, then

$$\delta_h^{e_1} u[n_h h e_1] \geq \delta_h^{e_1} u[0] + \ell(a_2 + \alpha)$$

$$= -\delta_h^{-e_1} u[he_1] + \ell(\alpha + a_2).$$

Finally, since

$$\delta_h^{e_1} u[n_h h e_1] \leq C_P$$

$$\delta_h^{-e_1} u[he_1] \leq C_P,$$

we obtain

$$\overline{\alpha} \leq \frac{2C_P}{\ell} - a_2.$$

To address the existence of $\underline{\alpha}$, let us assume in this part that (α, u) is a solution. Let $\alpha_1 \geq 0$ be the α we have in (4.94). Up to a constant, we have for u there exists $x \in \mathcal{G}_h$ such that

$$u[x] = \phi[x], \quad u \geq \phi, \quad \text{in } \mathcal{G}_h.$$

By the Proposition 4.8.2,

$$S_{\text{MABV}}^{h,\alpha_1} u[x] \leq S_{\text{MABV}}^{h,\alpha_1} \phi[x].$$

We have shown that $S^{h,\alpha_1}_{\text{MABV}}\phi[x] < 0$. Thus $S^{h,\alpha_1}_{\text{MABV}}u[x] < 0$ and in particular

$$S^h_{\text{MA}}u[x] < -\alpha_1,$$

$$S^h_{\text{BV}}u[x] < 0.$$

On the other hand, the equality $S^{h,\alpha}_{\text{MABV}}u[x] = 0$ yields

$$\max\{S^h_{\text{BV}}u[x], S^h_{\text{MA}}u[x] + \alpha\} = 0.$$

Since $S^h_{\text{BV}}u[x] < 0$, we deduce that $\alpha = -S^h_{\text{MA}}u[x] > \alpha_1$. I.e., we just choose $\underline{\alpha} = \alpha_1$.

□

4.8.2 Existence of solutions to the numerical scheme

Thanks to these properties enjoyed by $S^{h,\alpha}_{\text{MABV}}$, especially the stability of the scheme which guarantees the existence of subsolutions, cf. Proposition 4.8.8, the idea of the Perron's method can be applied to show the existence of solution to this scheme.

Theorem 4.8.10. [5, Theorem 2.15] *For small $h > 0$ there exists a solution to* (4.80).

Remark 4.8.11. The Perron's method, formally speaking, aims to construct a solution $u_{\text{sol}} \in \mathbb{R}^{\mathcal{G}_h}$ to a numerical scheme S^h by considering

$$u_{\text{sol}}[x] := \sup\{\tilde{u}[x] : \forall y \in \mathcal{G}_h, S^h\tilde{u}[y] \leq 0\}.$$

In other words, a solution is constructed by taking supremum over all the subsolutions. However, in our case the numerical scheme $S^{h,0}_{\text{MABV}}$ has a property that if $\tilde{u}$ is a subsolution then $\tilde{u} + c$ is also a subsolution for any constant c. Hence, a supremum over all the subsolutions will lead to $+\infty$. To overcome this, an extra real number α is introduced in (4.79).

Proof. For ease of notations, we use $S^{h,\alpha}$ as a shorthand for $S^{h,\alpha}_{\mathrm{MABV}}$.

Define the set of subsolutions to the numerical scheme to be the following:

$$U := \{(\alpha, u) \in \mathbb{R} \times \mathbb{R}^{\mathcal{G}_h} : S^{h,\alpha}u[x] \leq 0\}$$

Then since $S^{h,\alpha}$ is stable, it always admits subsolutions and U is not empty. We define

$$\overline{\alpha} := \sup_{(\alpha,u)\in U} \alpha.$$

The first step is to show that there exists $\overline{u}$ defined on grid points such that $(\overline{\alpha}, \overline{u})$ is a subsolution. To achieve so, let $\{(\alpha_k, u_k)\}_{k\in\mathbb{N}}$ be an increasing sequence in α_k that gives the supremum in the definition of $\overline{\alpha}$. Set $\alpha_{\min} := \min_{k\in\mathbb{N}} \alpha_k$. Assume further that up to a constant $u_k[0] = 0$ for all k. Then by the stability in Definition 4.8.7, there holds

$$|u_k[x] - 0| \leq \omega(\alpha_k) \leq \omega(\alpha_{\min}).$$

In particular, this shows that $\{u_k\}_{k\in\mathbb{N}}$ is bounded in $\mathbb{R}^{\mathcal{G}_h}$, and up to a subsequence we proved that $\{u_k\}_{k\in\mathbb{N}}$ converges to some $\overline{u} \in \mathbb{R}^{\mathcal{G}_h}$. Now, by the continuity of the scheme, there holds

$$S^{h,\overline{\alpha}}\overline{u}[x] \leq 0, \quad \forall x \in \mathcal{G}_h$$

as desired. We have found that $(\overline{\alpha}, \overline{u})$ is a subsolution.

We have shown that the set

$$\tilde{U} := \{u : \mathcal{G}_h \to \mathbb{R} | (\overline{\alpha}, u) \text{ is a subsolution}\}$$

is not empty. Next, for any $u \in \tilde{U}$, consider the set

$$\mathcal{G}_u := \{x \in \mathcal{G}_h : S^{h,\overline{\alpha}}_{\text{MABV}} u[x] < 0\}.$$

and denote by $\mathcal{G}_*$ the set among all $\mathcal{G}_u$ that has a max cardinality. Denote by $\tilde{u}$ the subsolution corresponding to $\mathcal{G}_*$.

The first observation is that $\mathcal{G}_* \neq \mathcal{G}_h$. Otherwise, there would exist $\tilde{\alpha} > \overline{\alpha}$ such that $(\tilde{\alpha}, \tilde{u})$ is also a subsolution, and this violates the definition of $\overline{\alpha}$.

Thus, inspired by Perron's method, we can consider a family of functions

$$u_\epsilon(x) := \sup\{u(x) : (\overline{\alpha}, u) \in U, u = \tilde{u} \text{ in } \mathcal{G}_h \setminus \mathcal{G}_*, S^{h,\overline{\alpha}}_{\text{MABV}} u[x] \leq -\epsilon \text{ in } \mathcal{G}_*\}, \tag{4.96}$$

and note that we only consider $\epsilon > 0$ that is small enough so that the set in (4.96), which is

$$\{u(x) : (\overline{\alpha}, u) \in U, u = \tilde{u} \text{ in } \mathcal{G}_h \setminus \mathcal{G}_*, S^{h,\overline{\alpha}}_{\text{MABV}} u[x] \leq \epsilon \text{ in } \mathcal{G}_*\}$$

contains $\tilde{u}$ and hence is not empty.

Finally, the idea is to apply a type of Perron's method argument to the family of functions $\{u_\epsilon\}$, and show the limit $\lim_{\epsilon\to 0} u_\epsilon$ is a solution to the scheme.

For a fixed $\epsilon > 0$ that is small enough, for any $x \in \mathcal{G}_h$, there exists u such that $(\overline{\alpha}, u) \in U$,

$S^{h,\overline{\alpha}}_{\text{MABV}} u[x] \leq -\epsilon$ in $\mathcal{G}_*$, $u_\epsilon \geq u$ in $\mathcal{G}_h$ and $u_\epsilon[x] = u[x]$. Then by the monotonicity,

$$S^{h,\overline{\alpha}}_{\text{MABV}} u_\epsilon[x] \leq S^{h,\overline{\alpha}}_{\text{MABV}} u[x],$$

and thus $(\overline{\alpha}, u_\epsilon)$ is a subsolution and satisfies that

$$S^{h,\overline{\alpha}}_{\text{MABV}} u_\epsilon[x] \leq -\epsilon, \quad \forall x \in \mathcal{G}_*.$$

Furthermore, there indeed holds $S^{h,\overline{\alpha}}_{\text{MABV}} u_\epsilon[x] = -\epsilon$, by the definition (4.96).

We define $u_{\text{can}}[x] := \lim_{\epsilon \to 0^+} u_\epsilon[x]$. Then by the continuity, for any $x \in \mathcal{G}_*$, there already holds

$$S^{h,\overline{\alpha}}_{\text{MABV}} u_{\text{can}}[x] = 0,$$

and $(\overline{\alpha}, u_{\text{can}})$ is a subsolution.

Then assume, for sake of contradiction, that u_{can} is not a solution. Then there must exist $x \in \mathcal{G}_h \setminus \mathcal{G}_*$ such that

$$S^{h,\overline{\alpha}}_{\text{MABV}} u_{\text{can}}[x] < 0.$$

Then there also exists small enough ϵ such that

$$S^{h,\overline{\alpha}}_{\text{MABV}} u_{\epsilon,\text{can}}[x] < 0 \tag{4.97}$$

as well. But note that such $(\overline{\alpha}, u_\epsilon)$ belongs to $\tilde{U}$, and (4.97) indicates that $\mathcal{G}_*$ which is associated with $\tilde{u}$ does not have the maximum cardinality. A contradiction arises. We have finished the proof.

$\square$

4.8.3 Convergence results: relating numerical scheme's solution to original equations.

In the previous section, we established the existence of solutions to (4.80). In this section, we aim to show that such solutions do converge to the original Monge–Ampère equation, which is (4.54) combined with (4.55), as $h \to 0^+$. However, this convergence result requires to assume that in (4.54), the functions $A(x, \nabla u(x))$ and $B(x, \nabla u(x))$ have the following form:

$$\begin{aligned} A(x,p) &= 0, \\ B(x,p) &= \frac{f(x)}{g(p)}, \end{aligned} \tag{4.98}$$

where $f, g : \mathbb{R}^n \to \mathbb{R}$ are bounded.

In our application, the Ricci iteration, as presented in (4.17) and (4.18), does have the same form as in Definition 4.6.1, with the feature that the functions A and B satisfy that $A \equiv 0$ and $B(x, \nabla u(x)) = f(x)$ in (4.54). Thus, our $A(\cdot,\cdot)$ and $B(\cdot,\cdot)$ functions do take the desired form, making the convergence results readily applicable.

There are three equations under consideration. The first one is the original problem we defined in (4.54) and (4.55). The second one is the equation $F^{\alpha}_{\mathrm{MABV}}(x, \nabla u(x), \nabla^2 u(x)) = 0$, where $F^{\alpha}_{\mathrm{MABV}}$ is defined in (4.84). The third one is the numerical scheme (4.80). In this section we aim to show, roughly speaking, the solutions to (4.80) converge to a type of weak solutions to (4.84), and such weak solutions to (4.84) are also weak solutions to (4.54) and (4.55).

Theorem 4.8.10 guarantees us the existence of solutions to the numerical scheme (4.80).

The following result then builds a connection between solutions to the scheme and the viscosity solutions to the corresponding continuous problem (4.84).

Let $\{h_n\}_{n\in\mathbb{N}}$ be a sequence of positive numbers such that $\lim_{n\to\infty} h_n = 0$. Let $\{\alpha_n\}_{n\in\mathbb{N}}$ be a sequence of real numbers such that $\lim_{n\to\infty} \alpha_n = \alpha \in \mathbb{R}$. Assume $\{u_n\}$ is a sequence of functions $u_n : \mathcal{G}_{h_n} \to \mathbb{R}$ such that (α_n, u_n) is a solution to (4.80). Define for $x \in K$,

$$\overline{u}(x) := \limsup_{\substack{x'\in\mathcal{G}_{h_n}, x'\to x\\ n\to\infty}} u_n[x'],$$

$$\underline{u}(x) := \liminf_{\substack{x'\in\mathcal{G}_{h_n}, x'\to x\\ n\to\infty}} u_n[x'].$$

Theorem 4.8.12. *The functions $\overline{u}$ and $\underline{u}$ above are respectively a viscosity subsolution and viscosity supsolution to* (4.84).

Remark 4.8.13. In [4, Theorem 2.1], the authors proved that the limit inferior and limit superior of a solution u_h to a monotone, stable and consistent numerical scheme S^h, in terms of Definitions 4.8.1, 4.8.5 and 4.8.7, are respectively viscosity sub- and supersolutions of the original equation. This result can be directly applied to prove Theorem 4.8.12.

The next result links viscosity solutions to (4.84) with weak solutions to the corresponding problem defined in Definition 4.6.1. We first give the definition of such weak solutions. Assuming that $u : K \to \mathbb{R}$ is a convex function, we will denote by

$$\partial u(x) := \{y \in \mathbb{R}^n : u(x') \geq u(x) + \langle y, x' - x\rangle, \forall x' \in K\}$$

its subgradient.

Definition 4.8.14. A function $u : K \to \mathbb{R}$ is an Aleksandrov solution to (4.54) and (4.55) if it is convex and for any Borel subset $E \subset K$,

$$\int_E B(x)dx = \text{Volume}(P \cap \partial u(E)).$$

An Aleksandrov solution is minimal if $\partial u(K) \in P$.

Remark 4.8.15. Such Aleksandrov solution can be seen as a weak solution by considering the integral $\int_E 1dy$. Then we can calculate the integral using a change of variable $y = \nabla u(x)$ and (4.54).

Theorem 4.8.16. *If $u : K \to \mathbb{R}$ is a viscosity solution to* (4.84) *for some $\alpha \in \mathbb{R}$, then $\alpha = 0$ and u is a minimal Aleksandrov solution to* (4.54) *and* (4.55).

Remark 4.8.17. A detailed proof of this result can be found in [5, Section 5].

We conclude this section by the following convergence result. It shows that the solutions to the numerical scheme converge to a weak solution to the original second boundary value problem.

Theorem 4.8.18. [5, Theorem 5.25] *Assume that K is strongly convex and* (4.98) *is satisfied in* (4.54)*. Then there exists a sequence of solutions (α_h, u_h) to* (4.80) *such that $u_h[0] = 0$ for small $h > 0$. Furthermore, as $h \to 0^+$, it follows that $\alpha_h \to 0$, and u_h converges to a minimal Aleksandrov solution u to* (4.54) *and* (4.55) *satisfying that $u(0) = 0$.*

Proof. The existence of sequence (α_h, u_h) follows from Theorem 4.8.10. Given the stability of the scheme by Proposition 4.8.8, the sequence $\{\alpha_h\}$ is bounded, and $\{u_h\}$ is uniformly bounded and equicontinuous. It follows from the sequential compactness of $\mathbb{R}$ and Arzelà–Ascoli theorem that, up to a subsequence, $\{\alpha_h\}$ converges to some $\alpha \in \mathbb{R}$ and $\{u_h\}$ converges to a continuous function $u : K \to \mathbb{R}$. By Theorem 4.8.12, u is both a viscosity sub- and supsolution, hence a viscosity solution to (4.84). By Theorem 4.8.16, there also hold $\alpha = 0$ and u is a minimal Aleksandrov solution to (4.54) and (4.55). $\square$

4.9 Numerical implementation of the Ricci iteration

We are ready to implement the Ricci iterations. The equations under consideration, namely (4.17), (4.18) and (4.20), have the same form as (4.54) and (4.55). Hence, the numerical Ricci iteration can be done by solving an associated numerical scheme (4.80) for a sequence of functions.

The equation (4.17) will be solved for P_1, P_2 and P_3. The equations (4.18) and (4.20) are solved for P_4 and P_5.

4.9.1 (Non)existence of exact solutions to the Ricci iteration

When $P = P_1$ (respectively, P_2), the solutions to the Ricci iteration (4.17) correspond to potential functions of the Kähler–Einstein metrics on the surface $\mathbb{P}^2$ (respectively, $\mathbb{P}^1 \times \mathbb{P}^1$). These metrics are the Fubini–Study metrics, cf. Example 1.1.3. The explicit forms of the metrics, equivalently, of the solutions to (4.17) when $P = P_1, P_2$ are as follows:

$$\begin{aligned} \psi_1^{\mathrm{sol}}(x) &:= -2\log 3 - x_1 - x_2 + 3\log(1 + e^{x_1} + e^{x_2}), \\ \psi_2^{\mathrm{sol}}(x) &:= -2\log 2 - x_1 - x_2 + 2\log(1 + e^{x_1}) + 2\log(1 + e^{x_2}). \end{aligned} \tag{4.99}$$

When $P = P_3$, the exact solution to (4.17) is the potential function of the Kähler–Einstein metric on $\mathbb{P}^2\#3\overline{\mathbb{P}^2}$. There is no explicit form available for this metric (Indeed, finding its closed-form is still an open problem [2, p. 12]). We implement the Ricci iteration in this case and obtain a numerical approximation to the metric.

When $P = P_4$, the equation 4.17 is not solvable as $\mathbb{P}^2\#2\overline{\mathbb{P}^2}$ does not admit any Kähler–Einstein metric. Instead, we solve (4.18). Its solution corresponds to the Kähler-Ricci soliton on $\mathbb{P}^2\#2\overline{\mathbb{P}^2}$. The explicit form of this metric is not available. We also solve (4.20) to approximate the soliton. When $P = P_5$, due to the same reason we also consider (4.18) and (4.20). The Kähler-Ricci soliton on $\mathbb{P}^2\#\overline{\mathbb{P}^2}$ is known to satisfy certain ODE and that was discovered independently by Koiso [41] and Cao [13].

4.9.2 Approximation of $\mathbb{R}^2$ using bounded domains, Guillemin potentials and mass balance condition

It is worth noting that in equations (4.17), (4.18), the functions ψ_{i+1} and ψ_i are defined on $\mathbb{R}^2$, and the equation should ideally be solved over the entire $\mathbb{R}^2$. However, in practical implementations, it is necessary to confine the solution to a bounded domain. Thus, we constrain ourselves to solving equations within a finite domain represented by a box,

$$[-b, b]^2, \quad 0 < b < +\infty, \tag{4.100}$$

and discretize this domain by dividing each axis into n equal parts. We refer to the lattice generated by this approach as $\mathcal{G}_n$, and we conduct the Ricci iterations for a total of I times.

Remark 4.9.1. To choose an appropriate value for b in (4.100), we consider the Guillemin potentials on these toric del Pezzo surfaces [28]. Recall from Theorem 4.2.8 that each toric del Pezzo surface is associated with a Delzant polytope, P, with the formula (4.10). To simplify notation, we define

$$\ell_\alpha(y) := \langle n_\alpha, y\rangle + 1, \quad y \in P,\ n_\alpha \in \mathbb{R}^2,$$

where n_α, y are specified in (4.10). Then on such toric del Pezzo surface S associated with the Delzant polytope P, for any $y \in \operatorname{int} P$, there holds $\ell_\alpha(y) > 0$, and the following Guillemin potential is well defined in the symplectic coordinates, cf. (4.8),

$$G(y) := \frac{1}{2}\sum_\alpha \ell_\alpha(y)\log \ell_\alpha(y), \quad y \in \operatorname{int} P.$$

The Guillemin potential is convex and its Legendre transform is a function defined in the complex coordinates, cf. (4.4),

$$\psi_G(x) := \log\left(\sum_\gamma e^{\langle x, z_\gamma\rangle}\right), \quad \text{where } z_\gamma \text{ is lattice point in } P,\ x \in \mathbb{R}^2. \tag{4.101}$$

For example, when $S = \mathbb{P}^2$, the polytope P is the triangle in Figure 4.1. Each ℓ_α satisfies

$$\ell_1(y) = y_1 + 1,\ \ell_2(y) = y_2 + 1,\ \ell_3(y) = -y_1 - y_2 + 1,$$

and lattice points in P include

$$(-1,2), (-1,1), (0,1), (-1,0), (0,0), (1,0), (-1,-1), (0,-1), (1,-1), (2,-1).$$

The function $\psi_G(x)$ in this case recovers the Kähler potential of the Fubini–Study metric on $\mathbb{P}^2$.

More generally, for any toric del Pezzo surface S with its Delzant polytope P, its Guillemin potential $\psi_G(x)$ is still a convex function in $\mathbb{R}^2$ whose gradient image is P. We can see $\psi_G(x)$ as a model metric potential for S. Motivated by that, we choose b large enough so that

$$\nabla\psi_G([-b,b]^2) \approx P,$$

i.e., the gradient image is a good approximation to P. In practice, a choice of $b = 7.5$ fulfills this requirement for all surfaces we concern.

Remark 4.9.2. The integral equality in (4.17) or (4.18) is to ensure a specific solution can be chosen at each iteration, as solutions are only unique up to an additive constant. Indeed, taking (4.17) as an example, the requirement

$$\int_{\mathbb{R}^2} e^{-\psi_i(x)}\, dx = |P| \tag{4.102}$$

is essentially the so-called mass balance condition when regarding (4.17) as an optimal transport problem and ensuring the mass given by $e^{-\psi}$ on $\mathbb{R}^2$ and 1 on P being the same.

In practice, we compute this integral over the bounded domain $[-b,b]^2$, as previously discussed.

Chapter 5: Approximating Kähler–Einstein metrics

In this chapter, we present a new method to approximate Kähler–Einstein metrics based on numerical implementation of the Ricci iteration. In Section 5.1, we survey existing works on numerically compute Kähler–Einstein metrics. Analysis on our numerical results are presented in Section 5.2. We show the accuracy results of our method in tables and plots. We also present several visualizations of our solutions. Accuracy results and comparison to other works are summarized in 5.3.

5.1 Related works on numerically approximating Kähler–Einstein metrics

The existence results for Kähler–Einstein metrics on toric manifolds have been reviewed in Section 4.2. These theoretical results are remarkable, yet the majority of them are of a constructive nature. Indeed, there are plenty of canonical metrics known to exist that do not admit an exact formula. Consequently, mathematicians and physicists have been trying to obtain concrete estimations of these geometries through numerical methods.

Headrick and Wiseman pioneered the study on numerically computing Kähler–Einstein metrics in 2005 [33]. Their method essentially simulates the Ricci flow and uses the fact that Kähler–Einstein metrics are limit of the flow. Following the same idea, Doran, Headrick, Herzog, Kantor and Wiseman approximate the Kähler–Einstein metric on $\mathbb{P}^2\#3\overline{\mathbb{P}^2}$ [19]. Essentially, they consider the parabolic equation:

$$\frac{\partial \psi_t}{\partial t} = \log \det \nabla^2 \psi_t + \psi_t + c_t \tag{5.1}$$

where c_t is a constant at given time t and ψ_t is the Kähler potential at t. The evolution of (5.1) is simulated by choosing an initial function $u_t|_{t=0}$ and applying finite difference method. Their simulation was done for up to a grid of 400×400 points. Their approximation to the potential function of the metric is therefore at an array of points.

At around the same time, in 2005, Donaldson proposed a distinct approach to numerically approximate Kähler–Einstein and more broadly, extremal metrics [17]. Given a line bundle $L \to M$ over an n-dimensional compact Kähler manifold M and a large integer $k > 0$, denote by $H^0(L^k)$ the complex vector space of holomorphic sections. Suppose that M can be embedded into the projective space $\mathbb{P}(H^0(L^k)^*)$. For an arbitrary Hermitian matrix $G = (G_{i\bar{j}})$, it gives a metric on $H^0(L^k)$ and there is correspondingly a metric g on L^k satisfying that if (s_i) is any orthonormal basis of $H^0(L^k)$, the function

$$\sum_i |s_i|_G^2$$

is equal to 1 pointwise on M. The curvature of this metric induces a Kähler metric ω_G on M. Let z be coordinates on $\mathbb{P}(H^0(L^k)^*) \supset M$. Define

$$(T(G))_{i\bar{j}} := R \int_M \frac{z_i \bar{z}_j}{\sum_{k,\ell=1} G^{k\bar{\ell}} z_k \bar{z}_\ell} \frac{\omega_G^n}{n!}, \tag{5.2}$$

where $R := \dim H^0(L^k)/\text{volume of } (X, \omega_G^n)$ is a constant. Then T maps G to another Hermitian matrix. Donaldson's algorithm starts with an initial Hermitian metric G_0 on $H^0(L^k)$, which is essentially a Hermitian matrix. Then, for large enough r, the Hermitian metric $T^r(G_0)$ leads to a metric on M that approximates the Kähler–Einstein metric.

Following the same idea, Bunch–Donaldson [6] numerically compute the Kähler–Einstein metric on $\mathbb{P}^2\#3\overline{\mathbb{P}^2}$ and also other extremal metrics on toric surfaces. In this specific setting, they consider Kähler potential $u_{\mathrm{BD}} : \mathbb{R}^2 \to \mathbb{R}$ in the form

$$\psi_{\mathrm{BD}}(x) = \log\left(\sum_{\gamma} a_\gamma e^{\langle x, z_\gamma\rangle}\right) \tag{5.3}$$

where z_γ takes values of lattice points in certain polytope and $a_\gamma \in \mathbb{R}$ serves as parameters that will be tweaked to vary the metric. This metric should be compared to (4.101). This metric relates to the general discussion in [17] as it is the specific form of aforementioned metrics ω_G for certain G. The T-map in (5.2) will be evaluated iterative to update the metric u_{BD} and lead to an approximation to the Kähler–Einstein metric.

In [19], the authors also proposed another numerical method that shares some similarity with Bunch–Donaldson's formulation, other than their simulation approach. They consider a space of polynomials in the symplectic coordinates up to certain order. Their goal is to choose a polynomial from this space that approximates well the smooth part of the Kähler–Einstein potential for $\mathbb{P}^2\#3\overline{\mathbb{P}^2}$. This amounts to finding one polynomial that almost solve the Monge–Ampère equation (4.11) pointwise. To this end, they insert the polynomial into (4.11) and move every term to one side of the equality. Then minimizing a resulting objective function determines the unknown coefficients in the polynomial.

The two methods in [19] give similar results in terms of accuracy [19, p. 359, line 17].

5.2 Analysis on numerical results

In this section we show the numerical results we obtained after computing the Kähler–Einstein metrics on $\mathbb{P}^2$, $\mathbb{P}^1 \times \mathbb{P}^1$ and $\mathbb{P}^2 \# 3\overline{\mathbb{P}^2}$.

5.2.1 Parameters

In implementation of the Ricci iteration, three parameters affect the accuracy: range of the domain in which we solve the equation, denoted by $[-b, b]^2$, number of grid points along each axis, denoted by n, and number of the iterations, denoted by I.

For the three concerned surfaces, we find that the gradient image of corresponding Guillemin potentials on $[-7.5, 7.5]^2$ has already closely approximates the desired polytopes, cf. Remark 4.9.1. Hence, we use $b = 7.5$ for most cases. We also examine the convergence of numerical solutions against different b experimentally in Table 5.3 and Figures 5.4, 5.5 and 5.6.

We obtain more accurate results for a larger n. In our experiments we tried $n = 64, 128, 256, 512$ and 896. Accuracy result for different n is shown in Tables 5.1, 5.2, 5.5 and 5.6.

If not specified, the number of the iterations is taken as $I = 10$, since the Ricci iteration numerically converge at $I = 10$ for all three surfaces, cf. Figures 5.2 and 5.3.

Remark 5.2.1. Other than the three aforementioned parameters, the numerical solver by Bonnet–Mirebeau itself also admits some parameters.

In particular, we experiment with different choices for the parameter `condition number`, whose meaning is explained in Section 4.5.5, which determines the number of superbases included in V_h in Proposition 4.6.2 that are used to discretize the equation (4.54). Different choices $15, 30$ and 60 for `condition number` lead to different numbers of superbases used, which are $6, 10$ and 18. Experiment results for the three cases only have a difference in residuals no more than 1%. Moreover, we observe that in some cases, using more superbases causes even larger residuals, indicating that this parameter cannot be directly adjusted to guarantee improved accuracy.

Due to these findings, in our experiments, we keep using the same setting, where `condition number = 15` for the numerical solver as in their demo on Bonnet's website. [1]

5.2.2 Initial choice

To make a good initial choice $\psi_0(x)$ in (4.17), we recall the solution to (4.17) is expected to be the potential function of Kähler–Einstein metrics. Thus, it is natural to take the Guillemin potential (4.101) for an initial choice as it provides a model metric potential. However, for $\mathbb{P}^2$ and $\mathbb{P}^1 \times \mathbb{P}^1$, the Guillemin potential coincides with the true solution we want to approximate. In these two cases, we simply use the quadratic function $|x|^2 = x_1^2 + x_2^2$ as an initial choice.

For $\mathbb{P}^2 \# 3\overline{\mathbb{P}^2}$, the Guillemin potential no longer represents the Kähler–Einstein metric, so it can serve as an initial choice. In our experiments, we indeed use the numerical solution obtained by Bunch–Donaldson as an initial choice. Their solution has a closed form (5.3) and it has a similar form as the Guillemin potential. We also experiment using the quadratic function as an initial choice. We observe that for grid whose size is no bigger than 512×512, the initial choice does not cause much difference, in terms of both computing time and accuracy. However, to obtain a very high resolution solution, we employ Bunch–Donaldson's solution as an initial choice to save computing time.

[1] https://github.com/gbonnet1/ma-ot-monotone

5.2.3 Residual functions

We always denote by ψ_{num} our numerical solution obtained from the Ricci iteration, and by $\psi_{\text{benchmark}}$ any solution to which we want to compare. We use two types of residual functions to assess the accuracy of our numerical method.

Let $\mathcal{G}_n$ be a set of $n \times n$ grid points, cf. (4.73). First, define

$$\ell_{\text{relative}}(\psi_{\text{num}}) := \frac{1}{|\mathcal{G}_n|} \sum_{x \in \mathcal{G}_n} \left| \frac{\psi_{\text{num}}(x) - \psi_{\text{benchmark}}(x)}{\psi_{\text{benchmark}}(x)} \right|. \tag{5.4}$$

The function ℓ_{relative} will be only used for $\mathbb{P}^2$, $\mathbb{P}^1 \times \mathbb{P}^1$. We use the true solutions in (4.99) as $\psi_{\text{benchmark}}$.

Next, define

$$\ell_{\text{remainder}}(\psi_{\text{num}}) := \frac{1}{|\mathcal{G}_n|} \sum_{x \in \mathcal{G}_n} \left(\det(\nabla^2 \psi_{\text{num}}(x)) - e^{-\psi_{\text{num}}(x)} \right).$$

The function ℓ_{relative} assesses the proximity of our numerical solutions to the true solutions (or any other function chosen as a benchmark). The function $\ell_{\text{remainder}}$ measures the extent to which our numerical solutions satisfy the objective equation (4.17).

5.2.4 Dependence on the parameters

Resolution of the grid

Fix $b = 7.5$ and $I = 10$. For ℓ_{relative}, the result is presented in Table 5.1.

For $\ell_{\text{remainder}}$, the result is presented in Table 5.2.

$b = 7.5, I = 10$	$\mathbb{P}^2$	$\mathbb{P}^1 \times \mathbb{P}^1$
$n = 64$	2.58%	0.115%
$n = 128$	1.16%	0.077%
$n = 256$	2.09%	0.069%
$n = 512$	1.78%	0.064%

Table 5.1: For $\mathbb{P}^2$, our numerical solutions differ from the existing solutions by on average 1.78% when $n = 512$. For $\mathbb{P}^1 \times \mathbb{P}^1$, the approximation is extremely close.

$b = 7.5, I = 10$	$\mathbb{P}^2$	$\mathbb{P}^1 \times \mathbb{P}^1$	$\mathbb{P}^2\#3\overline{\mathbb{P}^2}$
$n = 64$	1.5×10^{-3}	3.2×10^{-5}	3.5×10^{-4}
$n = 128$	8.1×10^{-4}	1.5×10^{-5}	1.9×10^{-4}
$n = 256$	4.2×10^{-4}	7.4×10^{-6}	9.9×10^{-5}
$n = 512$	2.4×10^{-4}	3.5×10^{-6}	5.2×10^{-5}

Table 5.2: For all cases, the residual $\ell_{\text{remainder}}$ decreases as n increases.

Size of the box

To explore dependence of convergence on b, we experiment with $\mathbb{P}^2$, as in this case we have a true solution to assess accuracy of our numerical results.

The number of iteration I is set to be 20 and we pick the smallest residual we reach during the iteration. To maintain a consistent resolution of the grid, we fix the ratio b/n, and more precisely we use a 64×64 grid for $b = 7.5$ and accordingly a 256×256 grid for $b = 30$.

We observe that solutions obtained from a larger box approximate the true solution better. This is illustrated in Table 5.3 and Figure 5.1.

Number of iterations

We experiment with $\mathbb{P}^2$. Fix $b = 7.5$ and $n = 256$. In Table 5.4, we record the evolution of residuals ℓ_{relative} and $\ell_{\text{remainder}}$ against iteration times. More pictures regarding the convergence against iteration times are shown in the next section.

$b/n = 0.117, I \leq 20$	ℓ_{relative} for $\mathbb{P}^2$	$\ell_{\text{remainder}}$ for $\mathbb{P}^2$
$b = 7.5$	0.0187	0.00144
$b = 11.7$	0.0157	0.00061
$b = 15$	0.0149	0.00039
$b = 17.6$	0.0146	0.00029
$b = 23.4$	0.0142	0.00018
$b = 30$	0.0139	0.00011

Table 5.3: The Residual is calculated for $\mathbb{P}^2$ by comparing u_{num} to the true solution.

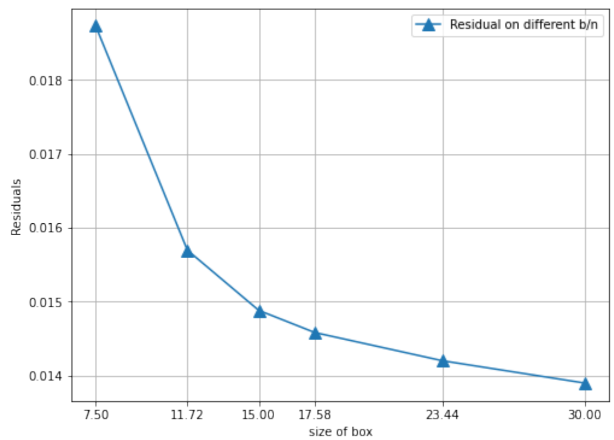

Figure 5.1: For $\mathbb{P}^2$, by keeping b/n constant and iterating less than 20 times to pick a smallest residual among the iterations, the function value of ℓ_{relative} decreases as we enlarge the size of box on which we solve the equation.

5.2.5 Rate of convergence

Fix $b = 7.5$ and $n = 256$. The residual function ℓ_{relative} against iteration times is presented in Figure 5.2. Note that the Ricci iteration is essentially a process to produce a solution that minimizes the $\ell_{\text{remainder}}$ function, not ℓ_{relative}, as the iteration itself discretizes the original equation (4.11) from which we define $\ell_{\text{remainder}}$. This may be related to the fact that ℓ_{relative} not necessarily decreases after more iterations.

The residual function $\ell_{\text{remainder}}$ against iteration times is presented in Figure 5.3. As expected, more iterations lead to smaller residuals in $\ell_{\text{remainder}}$, and a convergence is observed once

$b = 7.5, n = 256$	$I = 5$	$I = 10$	$I = 15$	$I = 20$
ℓ_{relative} for $\mathbb{P}^2$	0.0209	0.0055	0.0219	0.0415
$\ell_{\text{remainder}}$ for $\mathbb{P}^2$	0.00042	0.00045	0.00044	0.00043

Table 5.4: The convergence is relatively fast regarding the iteration times needed.

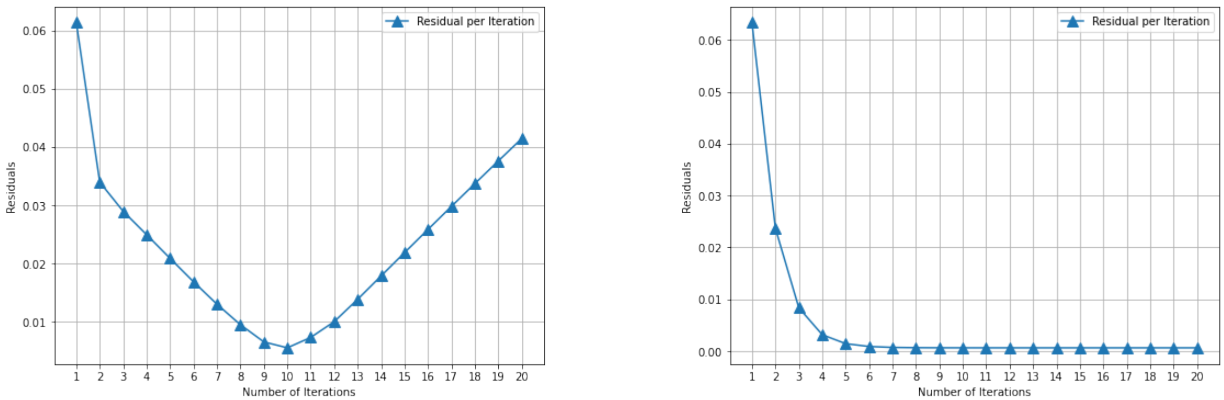

Figure 5.2: Fix $b = 7.5, n = 256$. The left plot is for $\mathbb{P}^2$. It shows that after 10 iterations, our numerical solution reached its best estimate of the true value. Continuing to iterate, the estimation accuracy worsened. The right plot is for $\mathbb{P}^1 \times \mathbb{P}^1$.

$\ell_{\text{remainder}}$ does not change too much any more.

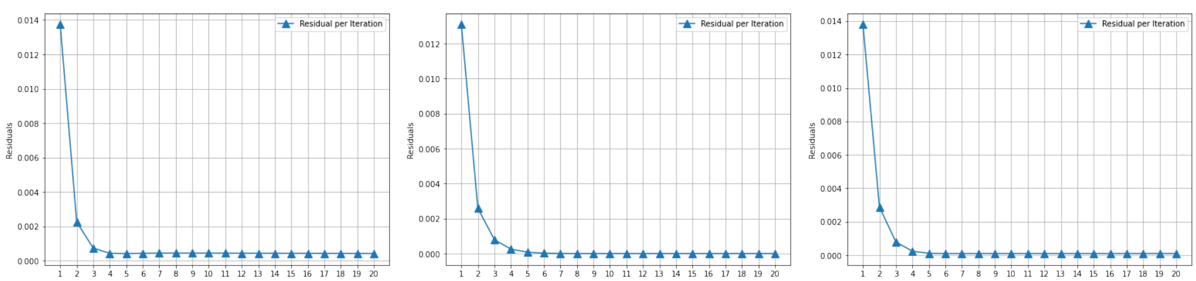

Figure 5.3: Fix $b = 7.5, n = 256$. From left to right, the plots correspond to $\mathbb{P}^2$, $\mathbb{P}^1 \times \mathbb{P}^1$, $\mathbb{P}^2 \# 3\overline{\mathbb{P}^2}$ respectively. The plots themselves represent the relationship between $\ell_{\text{remainder}}$ and iteration times.

We also experiment with different n, while fixing $b = 7.5$ and $I = 10$, to examine corresponding convergence rate. The plots suggest a first order convergence.

For $\mathbb{P}^2$, the log-log plots of ℓ_{relative} (respectively, $\ell_{\text{remainder}}$) against different n are shown in Figures 5.4.

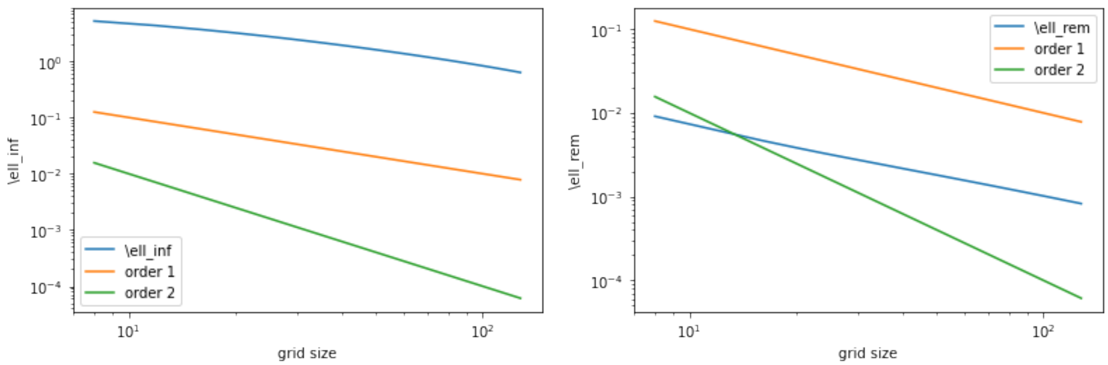

Figure 5.4: Plots are for $\mathbb{P}^2$ with fixed $b = 7.5$ and $I = 10$. The left plot shows ℓ_{relative} against the grid size n. The right plot shows $\ell_{\text{remainder}}$.

For $\mathbb{P}^1 \times \mathbb{P}^1$, the log-log plots of ℓ_{relative} (respectively, $\ell_{\text{remainder}}$) against the grid size are shown in Figure 5.5.

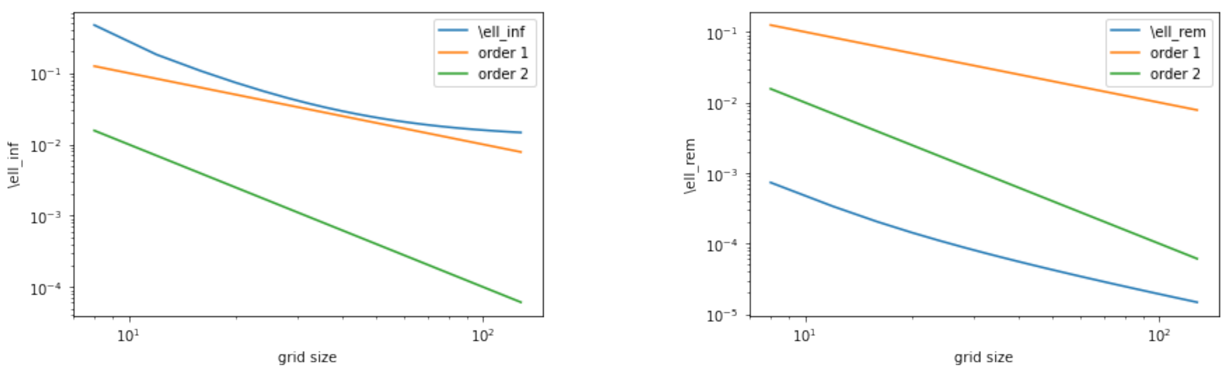

Figure 5.5: Plots are for $\mathbb{P}^1 \times \mathbb{P}^1$ with fixed $b = 7.5$ and $I = 10$. The left plot shows ℓ_{relative} against the grid size n. The right plot shows $\ell_{\text{remainder}}$.

For $\mathbb{P}^2 \# 3\overline{\mathbb{P}^2}$, the log-log plot of $\ell_{\text{remainder}}$ against the grid size is in Figure 5.6.

5.2.6 Visualization

The triangle

We plot color maps on $[-7.5, 7.5]^2$ for both the numerical solution and the exact solution in Figure 5.7. From the figure, we find that the numerical solution closely approximates the exact solution.

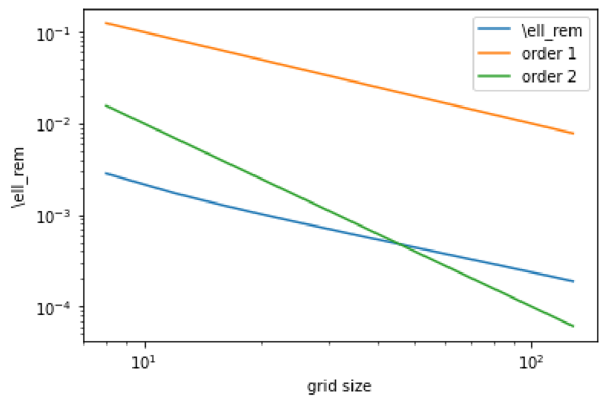

Figure 5.6: The plot is for $\mathbb{P}^2\#3\overline{\mathbb{P}^2}$ with fixed $b = 7.5$ and $I = 10$. It shows behavior of the residual function $\ell_{\mathrm{remainder}}$ against the grid size.

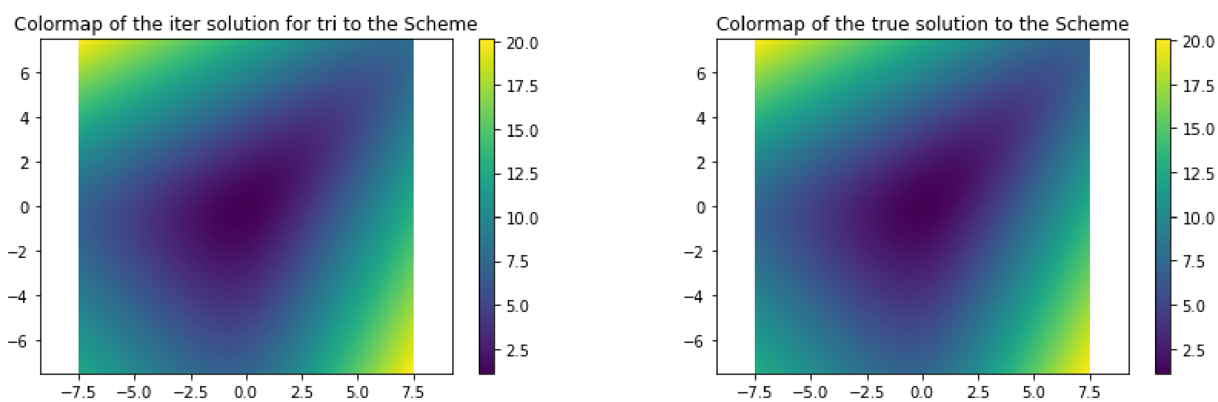

Figure 5.7: Take $b = 7.5, n = 256$ and $I = 10$. The left plot shows the colormap of the numerical solution to the Kähler–Einstein equation on $\mathbb{P}^2$. This numerical solution serves as an approximation to the Kähler–Einstein potential function. The right plot shows the colormap of the a priori known Kähler–Einstein potential function on $\mathbb{P}^2$.

The colormap of the difference from the numerical solution to the exact solution is shown in Figure 5.8.

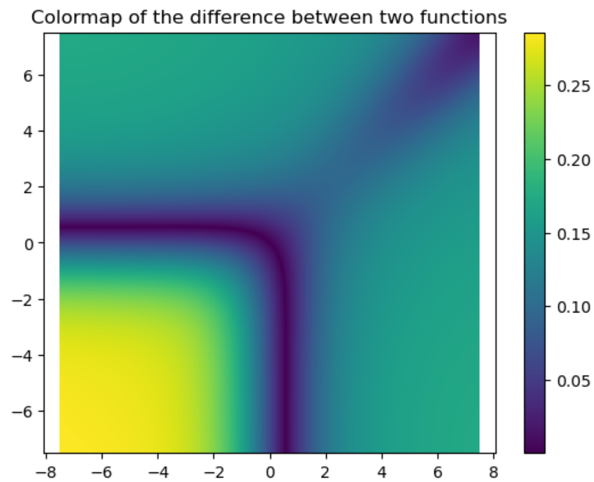

Figure 5.8: Take $b = 7.5, n = 256$ and $I = 10$. For $\mathbb{P}^2$, the difference between the exact and numerical solutions are shown in the figure.

We plot the colormaps of the Legendre transform of both solutions in Figure 5.9. We find that their Legendre transforms have very similar colormaps.

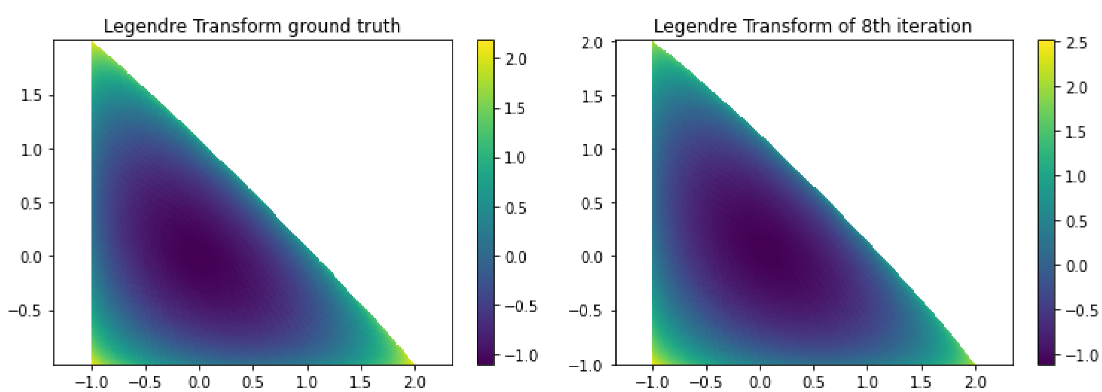

Figure 5.9: Take $b = 7.5, n = 256$ and $I = 8$. For $\mathbb{P}^2$, the left plot shows the colormap of the Legendre transform of the exact solution. The right plot shows that of the numerical solution.

The square

We plot the color maps of both the numerical solution and the exact solution in Figure 5.11. We find from the figure that the numerical solution approximates well the true solution.

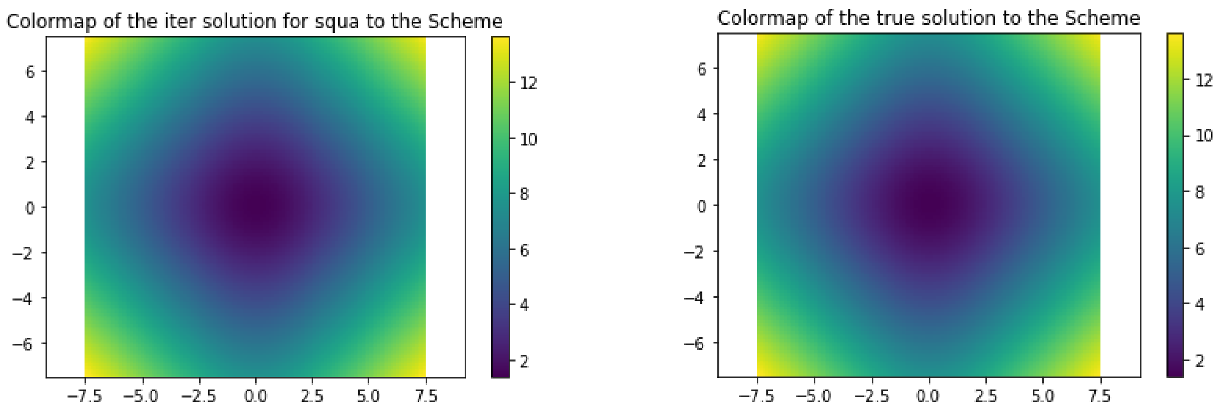

Figure 5.10

Figure 5.11: Take $b = 7.5, n = 256$ and $I = 10$. The left plot shows the colormap of the numerical solution to the Kähler–Einstein equation on $\mathbb{P}^1 \times \mathbb{P}^1$. The numerical solution aims to approximate the Kähler–Einstein potential function. The right plot shows the colormap of the exact solution.

The difference between the exact solution and the numerical solution is plotted in Figure 5.12.

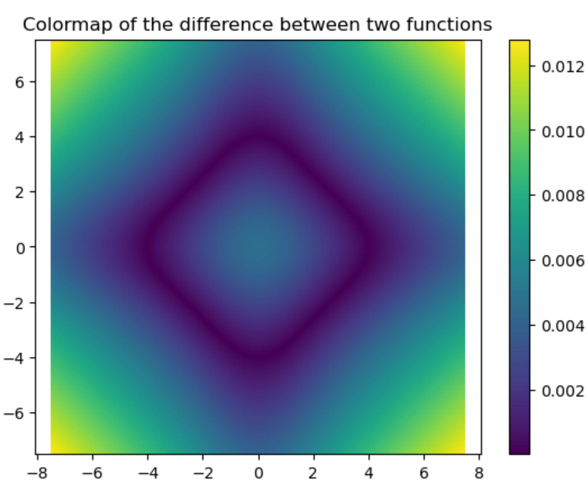

Figure 5.12: Take $b = 7.5, n = 256$ and $I = 10$. Plot is the difference between the exact solution and the numerical solution for $\mathbb{P}^1 \times \mathbb{P}^1$.

The colormap of the Legendre transform of the numerical solution on the square is Figure 5.13.

The value of ℓ_{rem} is plotted in Figure 5.14. We found from the figure that the numerical

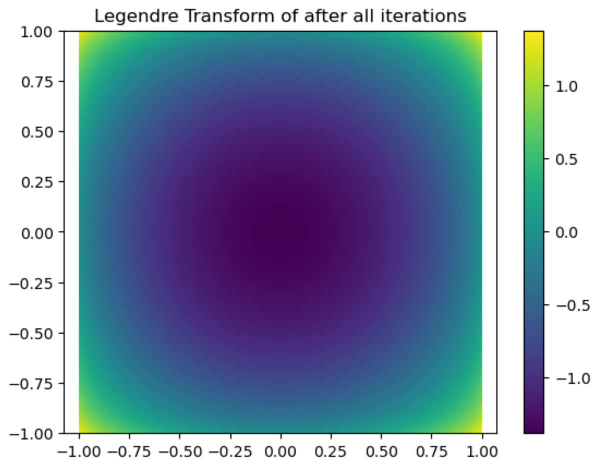

Figure 5.13: Take $b = 7.5, n = 256$ and $I = 10$. The colormap of the Legendre transform of the numerical solution is plotted on the Delzant polytope, which is a square, for $\mathbb{P}^1 \times \mathbb{P}^1$.

solution act as a good approximation of the Einstein metric.

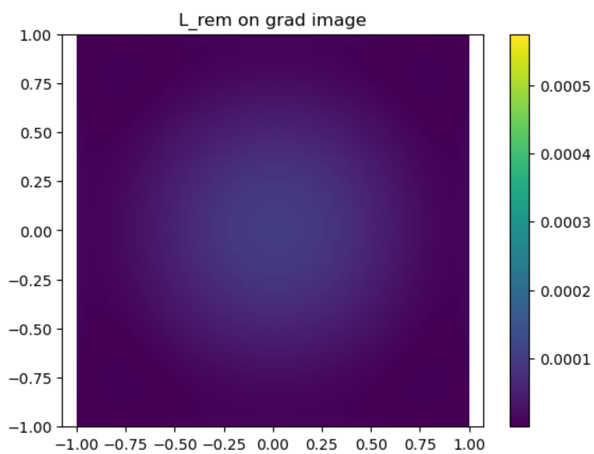

Figure 5.14: Take $b = 7.5, n = 256$ and $I = 10$. The loss function ℓ_{rem} is plotted for $\mathbb{P}^1 \times \mathbb{P}^1$ on its Delzant polytope.

The hexagon

The colormap of the Legendre transform of the numerical solution is plotted on the hexagon in Figure 5.15. From the figure, we roughly see the symmetry of this function governed by a dihedral group of order 12.

The value of the loss function ℓ_{rem} is plotted on Figure 5.16, and we see from the figure that

Figure 5.15: Take $b = 7.5, n = 256$ and $I = 10$. The numerical solution to the Kähler–Einstein equation on $\mathbb{P}^2\#3\overline{\mathbb{P}^2}$ has a symmetry under a dihedral group of order 12.

the numerical solution approximates well the Einstein metric.

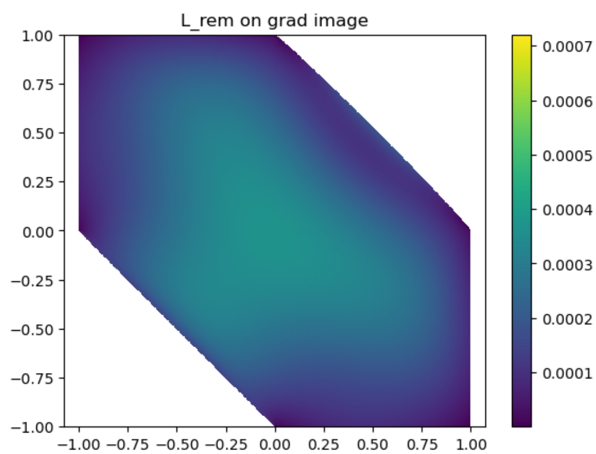

Figure 5.16: Take $b = 7.5, n = 256$ and $I = 10$. The colormap of the loss function ℓ_{rem} is plotted for $\mathbb{P}^2\#3\overline{\mathbb{P}^2}$ on its Delzant polytope, which is the hexagon.

5.3 Accuracy results and comparison to other works

5.3.1 An overview

The simulation procedure in [19, 34] is claimed to be slow, which may take many hours on a 400×400 grid [19, p. 389, line -14]. As the number of integral grid points grows larger, the method in [6] also becomes slow [6, p. 12, line -11]. On the other hand, the optimization approaches in [19] do not admit a convergence guarantee.

Our method seems to be more efficient and can be run on a personal computer for a gird of 256×256 within 12 minutes and a 512×512 grid within 1 hour and 10 minutes.

5.3.2 The triangle

The highest resolution result we obtained for $\mathbb{P}^2$, correspondingly $P = P_1$ in (4.17), is under the setting $n = 512, b = 7.5, I = 10$. Residuals of this solution have been shown in Table 5.1 and Table 5.2.

5.3.3 The square

The highest resolution result we obtained for $\mathbb{P}^1 \times \mathbb{P}^1$, correspondingly $P = P_2$ in (4.17), is under the setting $n = 512, b = 7.5, I = 10$. Residuals of this solution have been shown in Table 5.1 and Table 5.2.

5.3.4 The hexagon

Due to lack of an existing explicit solution, for our numerical solution on $\mathbb{P}^2 \# 3\overline{\mathbb{P}^2}$, we compare it to the numerical solution presented in [6], denoted by ψ_{BDResult}. We do so in two ways. First, taking ψ_{BDResult} as a benchmark solution $\psi_{\text{benchmark}}$ in (5.4), we compute ℓ_{relative} accordingly in Table 5.5:

Second, we compute $\ell_{\text{remainder}}$ for both ψ_{num} and ψ_{BD} in Table 5.6. The result shows that our solution serves better as an approximation to the solution to equation (4.17). However, it is

	compare ψ_{num} to ψ_{BDResult}
$n = 64$	5.82%
$n = 128$	3.48%
$n = 256$	2.21%
$n = 512$	1.64%
$n = 896$	1.22%

Table 5.5: When $n = 896$, the two solutions differ by on average 1.22%.

noted on [6, p. 14] that better solutions are obtained although not presented in the text.

	ψ_{num}	ψ_{BDResult}
$n = 64$	3.5×10^{-4}	5.749×10^{-3}
$n = 128$	1.9×10^{-4}	5.661×10^{-3}
$n = 256$	9.9×10^{-5}	5.618×10^{-3}
$n = 512$	5.2×10^{-5}	5.597×10^{-3}
$n = 896$	2.9×10^{-5}	5.588×10^{-3}

Table 5.6

A high resolution solution

Using Bunch–Donaldson's approximation as an initial choice, we implement the Ricci iteration on a relatively high resolution of 896×896 lattice. The $\ell_{\text{remainder}}$ residual of this solution is 2.9×10^{-5}. The ℓ_{relative} residual of this solution w.r.t. u_{BD} is 1.22%. We regard this solution as the most accurate result we achieved. We expect it to be of practical use for certain cases.

Visualization

We now present some pictures showing similarity between our numerical solution and that of [6, 19].

Recall our numerical solution takes values on $[-7.5, 7.5]^2 \subset \mathbb{R}^2$. The corresponding numerical solution in [6] take values on the whole $\mathbb{R}^2$, while in [19] it takes values on the subset $\{(x_1, x_2) \in \mathbb{R}^2 : x_1 \geq 2x_2, 2x_1 \geq x_2\}$. Therefore, when we plot the results of ours and [6] we consider grid points within $[-7.5, 7.5]^2$. For our result and that of [19], we only use grid points within $[0, 1] \times [-1, 0]$.

The colormaps of our result and that in [6] are shown in Figure 5.17. The colormaps of our result and that in [19] are shown in Figure 5.18.

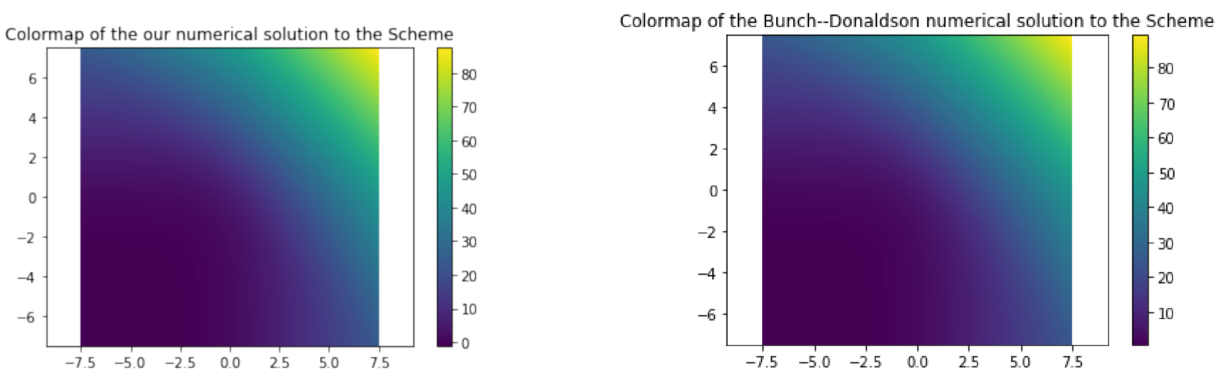

Figure 5.17: Take $b = 7.5, n = 256$ and $I = 10$. The left plot shows our numerical solution for the potential function of the Kähler–Einstein metric on $\mathbb{P}^2 \# 3\overline{\mathbb{P}^2}$. The right plot shows the numerical solution obtained by Bunch–Donaldson.

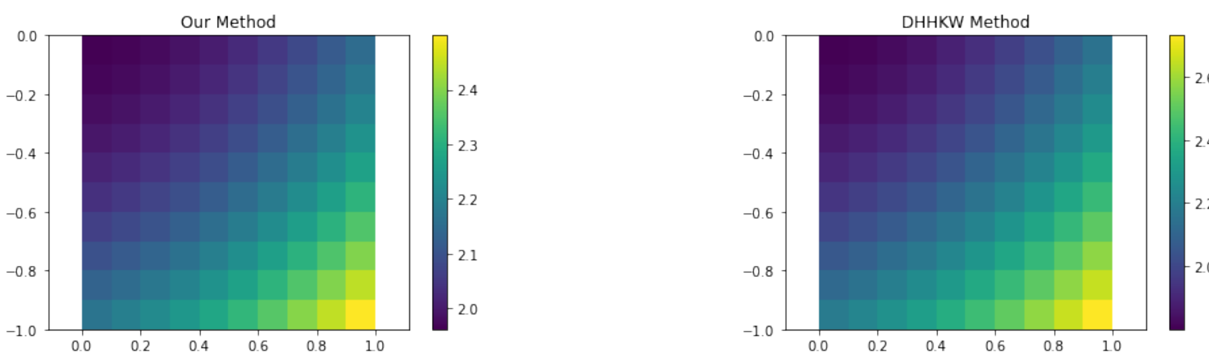

Figure 5.18: The left plot shows our numerical solution for the potential function of the Kähler–Einstein metric on $\mathbb{P}^2 \# 3\overline{\mathbb{P}^2}$. The right plot shows the numerical solution obtained by DHHKW. Note that the solutions are plotted on $[0, 1] \times [-1, 0] \subset \mathbb{R}^2$, which is a piece of common area where both methods provide a numerical solution. Our numerical solution is calculated by taking $b = 7.5, n = 160$ and $I = 10$.

Chapter 6: Approximating Ricci solitons

In Section 6.1, we summarized previous works that numerically compute Kähler Ricci solitons on $\mathbb{P}^2\#\overline{\mathbb{P}^2}$ and $\mathbb{P}^2\#2\overline{\mathbb{P}^2}$. Analysis on our numerical results are presented in Section 6.2. The accuracy results and comparison to related works is presented in Section 6.3. In Section 6.4, we use the numerical results to explore a geometric property of the Kähler–Ricci solitons on $\mathbb{P}^2\#\overline{\mathbb{P}^2}$ and $\mathbb{P}^2\#2\overline{\mathbb{P}^2}$: the scalar curvature. This shows the potential of applying our method to study geometric structure of these manifolds from a numerical perspective.

6.1 Related works on numerically approximating Ricci solitons

Headrick and Wisemen [34] applied the method developed in aforementioned works [19, 33] to simulate the Ricci flow on $\mathbb{P}^2\#2\overline{\mathbb{P}^2}$. Numerical Kähler–Ricci soliton then arises as the convergence point of the simulation.

Hall and Murphy [30] treated both $\mathbb{P}^2\#\overline{\mathbb{P}^2}$ and $\mathbb{P}^2\#2\overline{\mathbb{P}^2}$ using a way that is similar to the second method proposed in [19]. They solve certain optimization problems in a space of polynomials to search for Kähler–Ricci soliton metrics in that form. The objective function of the optimization is directly derived from the Kähler–Ricci soliton equation.

6.2 Analysis on numerical results

6.2.1 Parameters, initial choice and residual functions

We implement the Ricci iteration for solitons using two formulations. We solve both (4.18) and (4.20).

It is the same three parameters in Section 5.2.1 that will affect the experimental results in the soliton case. If not specified, the settings of these parameters are $b = 7.5, I = 10$ and n takes values from 64 to 512.

Note that when we solve (4.20), we will start from the box $[-7.5, 7.5]^2$. However, after every iteration, the box will be translated by c. We continue the next iteration in the translated box. Hence, each solution u_i will take values on a grid $\mathcal{G}_i$ that discretizes a different B_i, and we always assume the boundary condition $\nabla\psi_i(B_i) = \operatorname{int} P$.

We experiment with both the Guillemin potential and the quadratic function as an initial choice, and the results does not vary much. The results presented are obtained using the quadratic function as an initial choice.

The only residual function that we will use is as follows:

$$\ell_{\text{remainder}}(\psi_{\text{num}}) := \frac{1}{|\mathcal{G}_n|}\sum_{x\in\mathcal{G}_n}\left(\det(\nabla^2\psi_{\text{num}}(x)) - e^{-\psi_{\text{num}}(x)-\theta(x)}\right),$$

where

$$\theta(x) = -0.434748\frac{\partial\psi_{\text{num}}}{\partial x_1}(x) - 0.434748\frac{\partial\psi_{\text{num}}}{\partial x_2}(x)$$

for $\mathbb{P}^2 \# 2\overline{\mathbb{P}^2}$ and

$$\theta(x) = 0.52762 \frac{\partial \psi_{\text{num}}}{\partial x_1}(x) + 0.52762 \frac{\partial \psi_{\text{num}}}{\partial x_2}(x),$$

for $\mathbb{P}^2 \# \overline{\mathbb{P}^2}$. The constant numbers in θ are determined by Propositions 4.2.14 and 4.2.15.

The function $\ell_{\text{remainder}}$ measures the extent to which our numerical solutions satisfy the objective equation (4.18).

6.2.2 Dependence on grid size

We fix $b = 7.5$ and $I = 10$. For $\ell_{\text{remainder}}$, the residual against different n is presented in Table 6.1.

$b = 7.5, I = 10$	$\mathbb{P}^2 \# \overline{\mathbb{P}^2}$ w/ translation	$\mathbb{P}^2 \# 2\overline{\mathbb{P}^2}$ w/ translation	$\mathbb{P}^2 \# \overline{\mathbb{P}^2}$	$\mathbb{P}^2 \# 2\overline{\mathbb{P}^2}$
$n = 64$	2.5×10^{-3}	6.0×10^{-4}	1.3×10^{-3}	2.7×10^{-4}
$n = 128$	1.6×10^{-3}	5.2×10^{-4}	9.3×10^{-3}	4×10^{-4}
$n = 256$	1.2×10^{-3}	5.9×10^{-4}	8.7×10^{-3}	6×10^{-4}
$n = 512$	9.9×10^{-4}	6.5×10^{-4}	1.9×10^{-3}	5.9×10^{-4}

Table 6.1: Fix $b = 7.5, I = 10$. For $\mathbb{P}^2 \# 2\overline{\mathbb{P}^2}$, we found the residual may increase as we enlarge n. This may be caused by the definition of $\ell_{\text{remainder}}$, in which we a priori need the solution to be accurate to guarantee the residual function itself to be a good measure.

6.2.3 Rate of convergence

The residual function $\ell_{\text{remainder}}$ against iteration times is presented in Figure 6.1.

6.2.4 Visualization

The pentagon

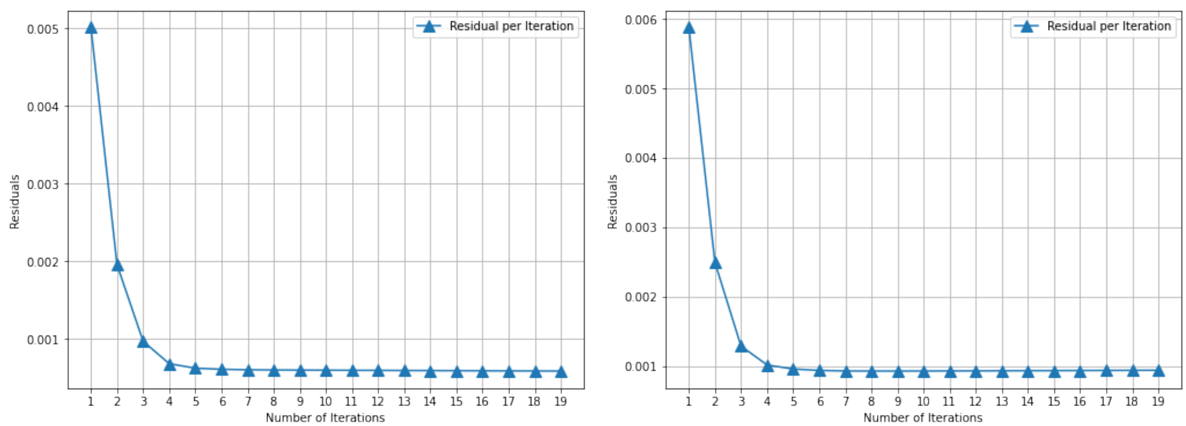

Figure 6.1: Fix $b = 7.5$ and $n = 256$. From left to right, the plots correspond to $\mathbb{P}^2\#2\overline{\mathbb{P}^2}$ and $\mathbb{P}^2\#\overline{\mathbb{P}^2}$. The plots themselves represent the relationship between $\ell_{\text{remainder}}$ and iteration times. The result shown here comes from the Ricci iteration without translation of variables.

We compare our numerical solution on the pentagon to the solution obtained by Headrick–Wiseman [34] and Hall–Murphy [30]. As the two previous works have similar numerical solutions [30, p. 629, line -3], we only compare ours to [30]. The colormaps of each numerical solution are shown in Figures 6.2.

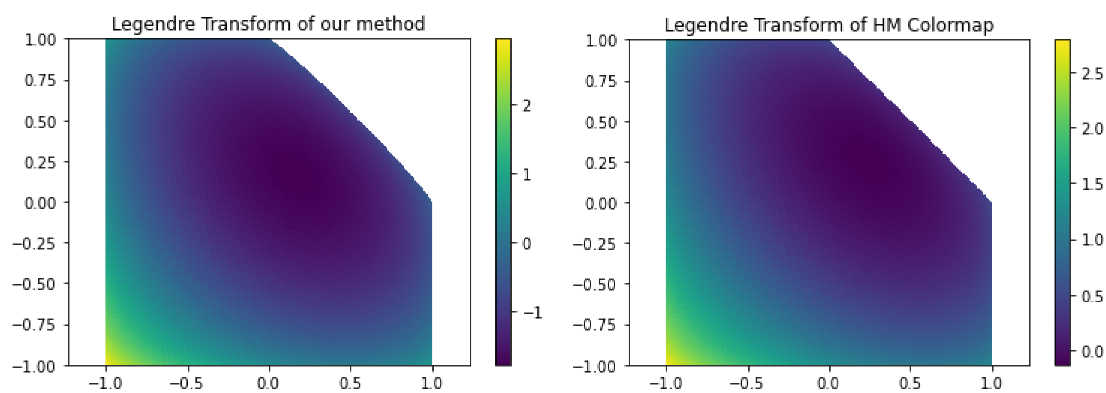

Figure 6.2: We take $b = 7.5, n = 256$ and $I = 10$. The left plot shows the colormap of our numerical solution for the potential function of the Kähler–Ricci soliton on $\mathbb{P}^2\#2\overline{\mathbb{P}^2}$, plotted on the pentagon. The right plot shows that of Hall–Murphy.

The trapezoid

We compare our numerical solution on the trapezoid to the solution obtained by Hall–Murphy [30]. The colormaps of each numerical solution are shown in Figure 6.3.

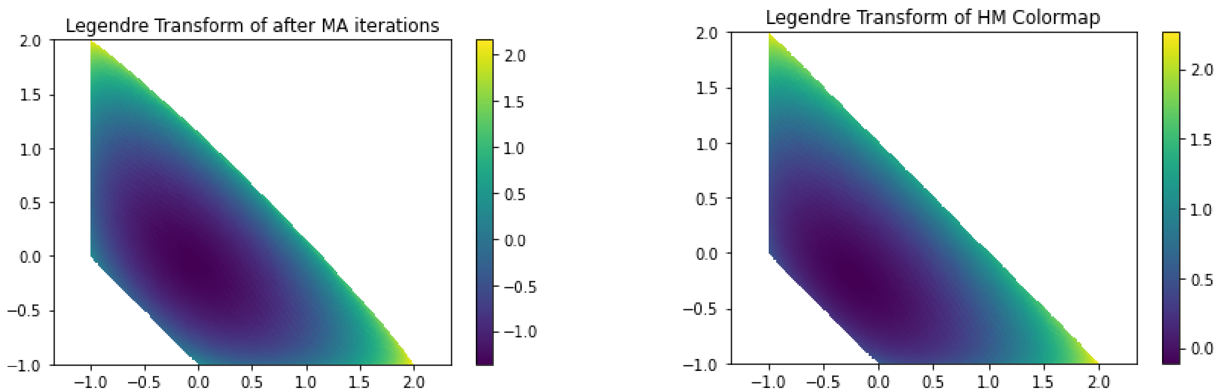

Figure 6.3: We take $b = 7.5, n = 256$ and $I = 10$. The left plot shows the colormap of our numerical solution for the potential function of the Kähler–Ricci soliton on $\mathbb{P}^2\#\overline{\mathbb{P}^2}$, plotted on the trapezoid. The right shows that of Hall–Murphy.

6.3 Accuracy results and comparison to other works

The highest resolution result we obtained is on a grid of 512×512. The accuracy of these results is shown in Table 6.1.

Comparison in picture between our results and previous works have been presented in Figures 6.2 and 6.3.

6.4 Numerical scalar curvature of Kähler–Ricci solitons

Focusing on the first and the second del Pezzo $\mathbb{P}^2\#\overline{\mathbb{P}^2}$ and $\mathbb{P}^2\#2\overline{\mathbb{P}^2}$, We aim to exploit our numerical solutions for Ricci solitons to study *scalar curvature* of the metrics.

Let (M, ω) be an n-dimensional Kähler manifold. Assume in local coordinates the metric satisfies $\omega = \sqrt{-1}\sum_{i,j}^n g_{i\bar{j}} dz^i \wedge d\bar{z}^j$ and $\mathrm{Ric}\,\omega = \sqrt{-1}\sum_{i,j}^n R_{i\bar{j}} dz^i \wedge d\bar{z}^j$.

Definition 6.4.1. The scalar curvature of (M, ω) is defined by

$$S := \sum_{i,j}^{n} g^{i\bar{j}} R_{i\bar{j}}, \tag{6.1}$$

where $\{g^{i\bar{j}}\}$ is the inverse matrix of $\{g_{i\bar{j}}\}$.

6.4.1 Numerical results on scalar curvature of Kähler–Einstein potentials

By Definition 6.4.1, any Kähler–Einstein metric has constant scalar curvature, as in that case there holds $R_{i\bar{j}} = \mu g_{i\bar{j}}$ for some $\mu \in \mathbb{R}$, and it follows $S = \mu n$. We calculate numerically the scalar curvature of the Kähler–Einstein metrics we solved for $\mathbb{P}^2$, $\mathbb{P}^1 \times \mathbb{P}^1$ and $\mathbb{P}^2\#3\overline{\mathbb{P}^2}$, and the following colormaps indicate constant functions (whose values are approximately 2 at all grid points):

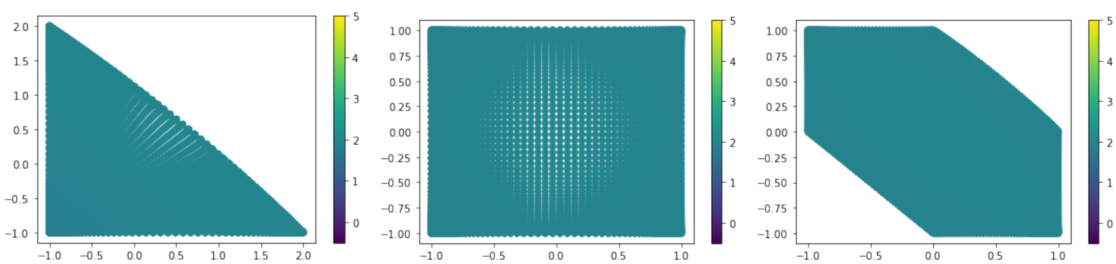

Figure 6.4: Scalar Curvatures of KE metrics on $\mathbb{P}^2$ (left), on $\mathbb{P}^1 \times \mathbb{P}^1$ (middle), and on $\mathbb{P}^2\#3\overline{\mathbb{P}^2}$ (right). We take $b = 7.5, n = 256$ and $I = 10$.

The plot of scalar curvature on $\mathbb{P}^1 \times \mathbb{P}^1$ against iterations is shown in the Figure 6.5.

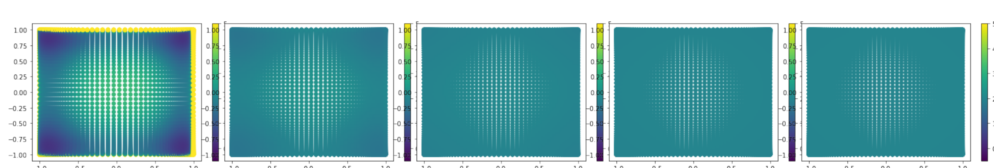

Figure 6.5: Fix $b = 7.5, n = 256$. From iteration 2 to 6. The scalar curvature converges to the constant 2 as the iterations progress; it changes dramatically from iteration 2 to 3.

6.4.2 Numerical results on scalar curvature of Ricci solitons

Kähler–Ricci solitons may have non-constant scalar curvature. By definitions (6.1) and (1.11), the scalar curvature of an n-dimensional Kähler–Ricci soliton (M, ω) with soliton potential θ is given by

$$
\begin{aligned}
S &= \sum_{i,j} g^{i\bar{j}} R_{i\bar{j}} \\
&= \sum_{i,j} g^{i\bar{j}} \left(g_{i\bar{j}} + \frac{\partial^2 \theta}{\partial z^i \partial \bar{z}^j} \right) \\
&= n + \sum_{i,j} g^{i\bar{j}} \frac{\partial^2 \theta}{\partial z^i \partial \bar{z}^j}.
\end{aligned}
\tag{6.2}
$$

We are interested when M is either $\mathbb{P}^2 \# \overline{\mathbb{P}^2}$ or $\mathbb{P}^2 \# 2\overline{\mathbb{P}^2}$, and ω is its unique Ricci soliton metric. In those cases, we numerically solved the Ricci iteration (4.18) and let us denote by ψ_{i+1} and ψ_i in that equation respectively the $(i+1)$th and ith Kähler potential functions we obtained. Denote by ω_{i+1} and ω_i respectively the corresponding Kähler metrics. In local complex coordinates, cf. (4.4), assume $\omega_{i+1} = \sqrt{-1}(g_{i+1})_{k\bar{\ell}} dz^k \wedge d\bar{z}^\ell$ and $\omega_i = \sqrt{-1}(g_i)_{k\bar{\ell}} dz^k \wedge d\bar{z}^\ell$. Then there hold

$$
\operatorname{Ric} \omega_{i+1} = \omega_i + \sqrt{-1}\partial\bar{\partial}\theta_i,
$$

and recalling that u_{i+1} and u_i is written in $(x_1, x_2) \in \mathbb{R}^2$, which is the real part of the complex coordinates,

$$
\begin{aligned}
(g_{i+1})_{k\bar{\ell}} = \frac{\partial^2 \psi_{i+1}}{\partial x_k \partial x_\ell}&, \; (g_i)_{k\bar{\ell}} = \frac{\partial^2 \psi_i}{\partial x_k \partial x_\ell}, \\
\theta_i(x) &= c \left(\frac{\partial \theta_i}{\partial x_1}(x) + \frac{\partial \theta_i}{\partial x_2}(x) \right), \\
\frac{\partial}{\partial z_k} \frac{\partial \theta_i}{\partial \bar{z}_\ell} &= \frac{\partial}{\partial x_k} \frac{\partial \theta_i}{\partial x_\ell},
\end{aligned}
$$

where $c = 0.52762$ for $\mathbb{P}^2 \# \overline{\mathbb{P}^2}$ and $c = -0.434748$ for $\mathbb{P}^2 \# 2\overline{\mathbb{P}^2}$. Hence, the scalar curvature S_{i+1}

of the metric ω_{i+1} can be calculated numerically in the same spirit of (6.2):

$$S_{i+1} = \sum_{k,\ell}^{2} g_{i+1}^{k\bar{\ell}} \left((g_i)_{k\bar{\ell}} + \frac{\partial^2 \theta_i}{\partial x_k \partial x_\ell} \right).$$

The colormaps of the scalar curvatures of u_i, for $i = 5$, against the gradient image of u_i (which is the Delzant polytope) is plotted in Figure 6.6.

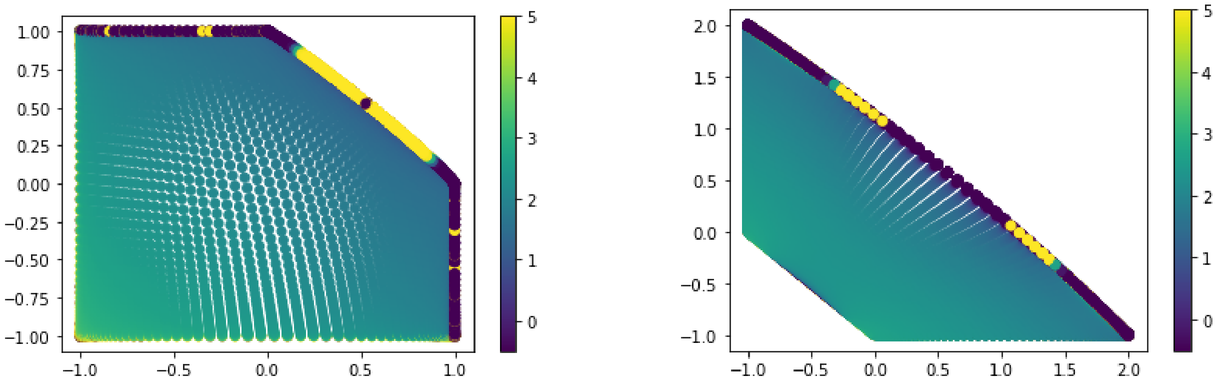

Figure 6.6: The left shows the scalar curvature as a function plotted on pentagon, which is the Delzant polytope of the second del Pezzo, for the numerical Kähler–Ricci soliton. The function values range roughly from 1 to 3. The right shows that on trapezoid, which is the Delzant polytope of the first del Pezzo The function values range roughly from 1 to 5. We take $b = 7.5, n = 256$ and $I = 10$.

Appendix A: Code

A.1 Overview of the code

Our implementation is in Python. The libraries we use in our code include the following:

```
from agd                    import Domain
import agd.LinearParallel as lp
import matplotlib.pyplot  as plt
import numpy              as np
import ma
```

The full name of the agd library is Adaptive Grid Discretizations using Lattice Basis Reduction. It will be used to discretize PDEs on cartesian grids and implement finite difference method. The ma library is developed by Bonnet and Mirebeau [5] and provides a numerical solver for the second boundary value problem for Monge–Ampère equations.

The numerical solver we will call has the following general form:

```
u = ma.NewtonRootBV2(u, x, domain, A_func, B_func, u0, F_func, stencil)
```

Each variable has the following meanings: u is the array of function values at all grid points, x is the array of grid points, domain serves as a helper to take finite difference, A_func and B_func respectively correspond to the A and B function in (4.54), u0 is the value of u at the origin, `F_func` corresponds to F_{BV} in Definition 4.6.4, and `stencil` determines the number of superbases in V_h in (4.56), which is used to discretize the equation (4.54), cf. Proposition 4.6.2.

We will use the numerical solver in five different cases, corresponding to the five toric del Pezzo surfaces. We need to specify all those inputs for the solver.

In the next section, we will explain in detail our implementation using our code, including the main function's definition, how to specify the `A_func`, `B_func` and `F_func`, normalize the solution obtained from the iteration, how the plots are generated and how to implement the Ricci iteration coupled with translation in each step.

A.2 Explanation of some code

A.2.1 Main function

Our main function is as follows:

```
def ric_iter(poly: str, grid_size: int, grid_scale: float, iter_num: int):
```

We have five options for `poly`, corresponding to the five toric del Pezzo surfaces. The parameters have such correspondence: `grid_size` is n, `grid_scale` is b and `iter_num` is I, cf. Section 5.2.1.

A.2.2 `A_func`

In our case, `A_func` in the code is as follows:

```
def A_func(x: np.ndarray, r: np.ndarray, p: np.ndarray) -> np.ndarray:
    return np.zeros((2, 2) + x.shape[1:])
```

It reflects the fact that A in (4.54) is zero in our case, cf. (4.17) and (4.18).

A.2.3 B_func

B_func has different forms in the Kähler–Einstein case and soliton case, cf. (4.17) and (4.18). Our code is as follows:

```
global cur_u
cur_u = np.copy(u)

global cur_dx
tmp_dx = bc.DiffUpwind(u, [1, 0])
cur_dx = np.copy(tmp_dx)

global cur_dy
tmp_dy = bc.DiffUpwind(u, [0, 1])
cur_dy = np.copy(tmp_dy)

def B_func(x: np.ndarray, r: np.ndarray, p: np.ndarray) -> np.ndarray:
    # cur_u refers to u_i, and will be updated in each iteration
    return np.exp(-1. * cur_u)

def pen_B_func(x: np.ndarray, r: np.ndarray, p: np.ndarray) -> np.ndarray:
    # cur_u refers to u_i, and will be updated in each iteration
    return np.exp(-1. * cur_u - 0.434748 * cur_dx - 0.434748 * cur_dy)
```

```python
def trap_B_func(x: np.ndarray, r: np.ndarray, p: np.ndarray) -> np.ndarray:
    # cur_u refers to u_i, and will be updated in each iteration
    return np.exp(-1. * cur_u +  0.52762 * cur_dx +  0.52762 * cur_dy)
```

Global variables `cur_u`, `cur_dx` and `cur_dy` respectively correspond to the array of function values of

$$\psi_i, \quad \frac{\partial \psi_i}{\partial x_1}, \quad \frac{\partial \psi_i}{\partial x_2}$$

in (4.17) and (4.18). They are updated after each iteration. The numerical derivative is taken using `bc.DiffUpwind`, which is the finite difference helper in `agd`.

In the Kähler–Einstein case, the right hand side in (4.17) reads

$$e^{-\psi_i(x)}$$

and in the code we use `B_func` for it. In the soliton case, the right hand side of (4.18) reads

$$e^{-\psi_i(x)-\theta_i(x)}$$

and in the code we use respectively `pen_B_func` and `trap_B_func` for $\mathbb{P}^2\#2\overline{\mathbb{P}^2}$ and $\mathbb{P}^2\#\overline{\mathbb{P}^2}$.

A.2.4 `F_func`

We define different `F_func` for different polytopes. In this section, we take `squa_F_func`, which is the `F_func` for the square to illustrate its definition.

```python
def squa_F_func(x, r, p0, p1):
    tmp = np.maximum(-p0[0]-1, -p0[1]-1)
    tmp = np.maximum(tmp, -p1[0]-1)
    return 20 * np.maximum(tmp, -p1[1]-1)
```

The square has four facets. And the square is defined to be the intersection:

$$\{y_1 - 1 \leq 0\} \cap \{-y_1 - 1 \leq 0\} \cap \{y_2 - 1 \leq 0\} \cap \{-y_2 - 1 \leq 0\}$$

Equivalently, a single inequality that defines it is

$$\max\{y_1 - 1, -y_1 - 1, y_2 - 1, y_2 - 1\} \leq 0.$$

Now, to define `squa_F_func`, we first have that the input `p0` and `p1` have the following meanings: `p0[0]` is y_1, `p0[1]` is y_2, `p1[0]` is $-y_1$ and `p1[1]` is $-y_2$.

To define `squa_F_func`, we translate from the polytope's definition to

$$\begin{aligned} y_1 - 1 &\text{ becomes } -p1[0] - 1, \\ -y_1 - 1 &\text{ becomes } -p0[0] - 1, \\ y_2 - 1 &\text{ becomes } -p1[1] - 1, \\ -y_2 - 1 &\text{ becomes } -p0[1] - 1. \end{aligned}$$

And the `squa_F_func` returns maximum of these four terms.

In other cases, we also write the polytope as an intersection of inequalities $n_1 y_1 + n_2 y_2 + c \leq$

0. Then we recast this inequality by replacing y_1, y_2 using `p0` and `p1`. For example, if $n_1 > 0$, then $n_1 y_1$ becomes $-n_1$ `p1[0]`; if $n_1 < 0$, then $n_1 y_1$ becomes n_1 `p0[0]`.

A.2.5 Normalization of the solution

Recall (4.102), we normalize the solution $\psi_i(x)$ obtained by requiring the integral of $e^{-\psi_i}$ over $\mathbb{R}^2$ to be equal to the area of the polytope. Using $\mathbb{P}^1 \times \mathbb{P}^1$ as an example, the code for normalization is as follows:

```
if poly == 'squa':
    area = 4
for i in range(iter_num):
    if poly == 'squa':
        u = ma.NewtonRootBV2(u,x,domain,A_func,B_func,u0,squa_F_func,stencil)
        c = -1 * np.log(area / (4*d_l**2/n**2*np.sum(np.exp(-1*u))))
        u += c
```

The integral is numerically computed by taking a sum of the value $e^{-\psi_i}$ at all points and then multiplying it by the area of the small square produced by the discretization.

A.2.6 Plot functions

The gradient image is numerically computed as follows:

```
def grad_img(u_d: np.ndarray) -> None:
    '''
    plot gradient image given u_d, the function values on the grid
    '''
```

```
    grad = bc.DiffUpwind(u_d, [[1, 0], [0, 1]])
    grad_x, grad_y = grad[0].flatten(), grad[1].flatten()
    plt.scatter(grad_x, grad_y)
```

Given any array representing function values at a grid of points, we calculate for each point its corresponding gradient value. However, the calculation is done for numpy array and thus efficient.

The Legendre transform is calculated using:

```
def legendre_transform(x_grid, u, title: str, poly: str):
    # plot Legendre transform of a function u(x) on its gradient image

    u_x0 = bc.DiffUpwind(u, [1, 0])
    u_x1 = bc.DiffUpwind(u, [0, 1])
    y = np.stack([u_x0, u_x1])

    new_y0, new_y1 = y[0][:-1, :-1], y[1][:-1, :-1]
    new_x0, new_x1 = x_grid[0][:-1, :-1], x_grid[1][:-1, :-1]
    u = u[:-1, :-1]

    x_grid = np.stack([new_x0, new_x1])
    y = np.stack([new_y0, new_y1])

    u_l = x_grid[0] * y[0] + x_grid[1] * y[1] - u

    y_0, y_1 = y[0].flatten(), y[1].flatten()
    plt.scatter(y_0, y_1)
```

```
    plt.title('Gradient Image {}'.format(title))
    plt.show()


    im = plt.pcolormesh(*y, u_l, shading='nearest')
    plt.colorbar(im)
    plt.axis('equal')
    plt.title('Legendre Transform of {}'.format(title))
    plt.show()
    return u_l
```

Given an array of function values u and a grid x_grid, we find at each point its gradient, and then calculate u_l, the numerical Legendre transform using the formula of Legendre transform, as shown in the line starting with u_l in the code block.

Colormaps are generated using the following code:

```
def colormaps(u_1, u_2, x_grid, name1, name2):
    plt.title("Colormap of {}".format(name1))
    im = plt.pcolormesh(*x_grid, np.where(bc.interior, u_1, np.nan))
    plt.colorbar(im)
    plt.axis("equal")
    plt.show()


    plt.title("Colormap of {}".format(name2))
    im = plt.pcolormesh(*x_grid, np.where(bc.interior, u_2, np.nan))
    plt.colorbar(im)
    plt.axis("equal")
    plt.show()
```

A.2.7 The Ricci iteration coupled with translation

The implementation of (4.20) for $\mathbb{P}^2\#\overline{\mathbb{P}^2}$ and $\mathbb{P}^2\#2\overline{\mathbb{P}^2}$ is as follows:

```python
def manual_version(poly: str,grid_size: int,grid_scale: float,iter_num: int):
    stencil = ma.StencilForConditioning(15)
    n = grid_size
    d_l = grid_scale
    b_l = d_l * 2

    x = np.stack(
        np.meshgrid(
            np.linspace(-d_l, d_l, n + 1),
            np.linspace(-d_l, d_l, n + 1),
            indexing="ij",
        )
    )

    domain = Domain.Box(sides=((-b_l, b_l), (-b_l, b_l)))
    global bc
    bc = Domain.Dirichlet(domain, np.inf, x)

    u = lp.dot_VV(x, x) # Initial value of the solution = |x|^2
    u0 = 0

    global cur_u
    cur_u = np.copy(u)
```

```
    if poly == 'trap':

        area = 4.

    if poly == 'pen':

        area = 3.5


    for i in range(iter_num):

        if poly == 'pen':

            u = ma.NewtonRootBV2(u,x,domain,A_func,B_func, u0,pen_F_func,stencil)

        elif poly == 'trap':

            u = ma.NewtonRootBV2(u,x,domain,A_func,B_func,u0,trap_F_func,stencil)


        c = -1 * np.log(int_const / (4*d_l**2/n**2*np.sum(np.exp(-1*u))))

        u += c


        if poly == 'pen':

            x -= 0.434748

            bc = Domain.Dirichlet(domain, np.inf, x)

        else:

            x += 0.527620

            bc = Domain.Dirichlet(domain, np.inf, x)


        cur_u = np.copy(u)
```

When we initialize the `domain`, we make it twice as large as the box where we start solving (4.20). We use a global variable `bc` to keep track of the translated grids. After each iteration, `x`, which represents the grid, gets translated accordingly. This has the same effect as defining a new function $\psi(x + a)$ for an existing $\psi(x)$ and a vector a.

Bibliography

[1] M. Abreu. Kähler metrics on toric orbifolds. *J. Differential Geom.*, 58(1):151–187, 2001.

[2] M. Abreu. Kähler geometry of toric manifolds in symplectic coordinates. In *Symplectic and contact topology: interactions and perspectives (Toronto, ON/Montreal, QC, 2001)*, volume 35 of *Fields Inst. Commun.*, pages 1–24. Amer. Math. Soc., Providence, RI, 2003.

[3] M. Atiyah and C. Lebrun. Curvature, cones and characteristic numbers. *Math. Proc. Cambridge Philos. Soc.*, 155(1):13–37, 2013.

[4] G. Barles and P. E. Souganidis. Convergence of approximation schemes for fully nonlinear second order equations. *Asymptotic Anal.*, 4(3):271–283, 1991.

[5] G. Bonnet and J.-M. Mirebeau. Monotone discretization of the Monge-Ampère equation of optimal transport. *ESAIM Math. Model. Numer. Anal.*, 56(3):815–865, 2022.

[6] R. S. Bunch and S. K. Donaldson. Numerical approximations to extremal metrics on toric surfaces. In *Handbook of geometric analysis. No. 1*, volume 7 of *Adv. Lect. Math. (ALM)*, pages 1–28. Int. Press, Somerville, MA, 2008.

[7] D. Burago, Y. Burago, and S. Ivanov. *A course in metric geometry*, volume 33 of *Graduate Studies in Mathematics*. American Mathematical Society, Providence, RI, 2001.

[8] E. Calabi. Métriques kählériennes et fibrés holomorphes. *Ann. Sci. École Norm. Sup. (4)*, 12(2):269–294, 1979.

[9] E. Calabi. Extremal Kähler metrics. In *Seminar on Differential Geometry*, volume 102 of *Ann. of Math. Stud.*, pages 259–290. Princeton Univ. Press, Princeton, N.J., 1982.

[10] F. Campana, H. Guenancia, and M. Păun. Metrics with cone singularities along normal crossing divisors and holomorphic tensor fields. *Ann. Sci. Éc. Norm. Supér. (4)*, 46(6):879–916, 2013.

[11] P. Candelas, G. T. Horowitz, A. Strominger, and E. Witten. Vacuum configurations for superstrings. *Nuclear Phys. B*, 258(1):46–74, 1985.

[12] A. Cannas da Silva. *Lectures on symplectic geometry*, volume 1764 of *Lecture Notes in Mathematics*. Springer-Verlag, Berlin, 2001.

[13] H.-D. Cao. Existence of gradient Kähler-Ricci solitons. In *Elliptic and parabolic methods in geometry (Minneapolis, MN, 1994)*, pages 1–16. A K Peters, Wellesley, MA, 1996.

[14] I. A. Cheltsov and Y. A. Rubinstein. Asymptotically log Fano varieties. *Adv. Math.*, 285:1241–1300, 2015.

[15] T. Darvas and Y. A. Rubinstein. Convergence of the Kähler-Ricci iteration. *Anal. PDE*, 12(3):721–735, 2019.

[16] S. K. Donaldson. Kähler geometry on toric manifolds, and some other manifolds with large symmetry. In *Handbook of geometric analysis. No. 1*, volume 7 of *Adv. Lect. Math. (ALM)*, pages 29–75. Int. Press, Somerville, MA, 2008.

[17] S. K. Donaldson. Some numerical results in complex differential geometry. *Pure Appl. Math. Q.*, 5(2):571–618, 2009.

[18] S. K. Donaldson. Kähler metrics with cone singularities along a divisor. In *Essays in mathematics and its applications*, pages 49–79. Springer, Heidelberg, 2012.

[19] C. Doran, M. Headrick, C. P. Herzog, J. Kantor, and T. Wiseman. Numerical Kähler-Einstein metric on the third del Pezzo. *Comm. Math. Phys.*, 282(2):357–393, 2008.

[20] M. R. Douglas, R. L. Karp, S. Lukic, and R. Reinbacher. Numerical Calabi-Yau metrics. *J. Math. Phys.*, 49(3):032302, 19, 2008.

[21] T. Eguchi and A. J. Hanson. Self-dual solutions to Euclidean gravity. *Ann. Physics*, 120(1):82–106, 1979.

[22] B. Gaveau. Méthodes de contrôle optimal en analyse complexe. I. Résolution d'équations de Monge Ampère. *J. Functional Analysis*, 25(4):391–411, 1977.

[23] D. Gilbarg and N. S. Trudinger. *Elliptic partial differential equations of second order*, volume 224 of *Grundlehren der Mathematischen Wissenschaften [Fundamental Principles of Mathematical Sciences]*. Springer-Verlag, Berlin, second edition, 1983.

[24] M. B. Green, J. H. Schwarz, and E. Witten. *Superstring theory. Vol. 2. Loop amplitudes, anomalies and phenomenology*. Cambridge University Press, Cambridge, anniversary edition, 2012.

[25] H. Guenancia. Kähler-Einstein metrics with mixed Poincaré and cone singularities along a normal crossing divisor. *Ann. Inst. Fourier (Grenoble)*, 64(3):1291–1330, 2014.

[26] H. Guenancia. Kähler-Einstein metrics: from cones to cusps. *J. Reine Angew. Math.*, 759:1–27, 2020.

[27] H. Guenancia and M. Păun. Conic singularities metrics with prescribed Ricci curvature: general cone angles along normal crossing divisors. *J. Differential Geom.*, 103(1):15–57, 2016.

[28] V. Guillemin. Kaehler structures on toric varieties. *J. Differential Geom.*, 40(2):285–309, 1994.

[29] S. J. Hall. Computing Perelman's ν-functional. *Differential Geom. Appl.*, 29(3):426–432, 2011.

[30] S. J. Hall and T. Murphy. Approximating Ricci solitons and quasi-Einstein metrics on toric surfaces. *New York J. Math.*, 22:615–635, 2016.

[31] R. S. Hamilton. Three-manifolds with positive Ricci curvature. *J. Differential Geometry*, 17(2):255–306, 1982.

[32] G. H. Hardy, J. E. Littlewood, and G. Pólya. *Inequalities*. Cambridge, at the University Press,, 1952. 2d ed.

[33] M. Headrick and T. Wiseman. Numerical Ricci-flat metrics on $K3$. *Classical Quantum Gravity*, 22(23):4931–4960, 2005.

[34] M. Headrick and T. Wiseman. Numerical Kähler-Ricci soliton on the second del Pezzo. *arXiv preprint arXiv: 0706.2329*, 2007.

[35] F. Hirzebruch. Über eine Klasse von einfachzusammenhängenden komplexen Mannigfaltigkeiten. *Math. Ann.*, 124:77–86, 1951.

[36] R. Hunter. *Monge-Ampère Iteration*. ProQuest LLC, Ann Arbor, MI, 2017. Thesis (Ph.D.)–University of Maryland, College Park.

[37] R. Hunter. Monge-Ampère iteration. *Selecta Math. (N.S.)*, 25(5):Paper No. 73, 70, 2019.

[38] T. Jeffres, R. Mazzeo, and Y. A. Rubinstein. Kähler-Einstein metrics with edge singularities. *Ann. of Math. (2)*, 183(1):95–176, 2016.

[39] C. Jin and Y. A. Rubinstein. Tian's stabilization problem for toric fanos. *arXiv preprint arXiv:2403.17262*, 2024.

[40] R. Kobayashi. Kähler-Einstein metric on an open algebraic manifold. *Osaka J. Math.*, 21(2):399–418, 1984.

[41] N. Koiso. On rotationally symmetric Hamilton's equation for Kähler-Einstein metrics. In *Recent topics in differential and analytic geometry*, volume 18-I of *Adv. Stud. Pure Math.*, pages 327–337. Academic Press, Boston, MA, 1990.

[42] R. K. Lazarsfeld. *Positivity in Algebraic Geometry I: Classical setting: Line bundles and Linear Series*, volume 48. Springer, 2017.

[43] M. Lindsey and Y. A. Rubinstein. Optimal transport via a Monge-Ampère optimization problem. *SIAM J. Math. Anal.*, 49(4):3073–3124, 2017.

[44] R. Mazzeo and Y. A. Rubinstein. The Ricci continuity method for the complex Monge-Ampère equation, with applications to Kähler-Einstein edge metrics. *C. R. Math. Acad. Sci. Paris*, 350(13-14):693–697, 2012.

[45] Y. A. Rubinstein. The Ricci iteration and its applications. *C. R. Math. Acad. Sci. Paris*, 345(8):445–448, 2007.

[46] Y. A. Rubinstein. *Geometric quantization and dynamical constructions on the space of Kahler metrics*. ProQuest LLC, Ann Arbor, MI, 2008. Thesis (Ph.D.)–Massachusetts Institute of Technology.

[47] Y. A. Rubinstein. Some discretizations of geometric evolution equations and the Ricci iteration on the space of Kähler metrics. *Adv. Math.*, 218(5):1526–1565, 2008.

[48] Y. A. Rubinstein. Smooth and singular Kähler-Einstein metrics. In *Geometric and spectral analysis*, volume 630 of *Contemp. Math.*, pages 45–138. Amer. Math. Soc., Providence, RI, 2014.

[49] Y. A. Rubinstein and K. Zhang. Small angle limits of Hamilton's footballs. *Bull. Lond. Math. Soc.*, 52(1):189–199, 2020.

[50] Y. A. Rubinstein and K. Zhang. Angle deformation of Kähler-Einstein edge metrics on Hirzebruch surfaces. *Pure Appl. Math. Q.*, 18, special issue in honor of Bernard Shiffman(1):343–366, 2022.

[51] E. Selling. Uber die binären und ternären quadratischen Formen. *J. Reine Angew. Math.*, 77:143–229, 1874.

[52] G. Székelyhidi. *An Introduction to Extremal Kähler Metrics*, volume 152. American Mathematical Soc., 2014.

[53] G. Tian. On Calabi's conjecture for complex surfaces with positive first Chern class. *Invent. Math.*, 101(1):101–172, 1990.

[54] G. Tian. Kähler-Einstein metrics on algebraic manifolds. In *Transcendental methods in algebraic geometry (Cetraro, 1994)*, volume 1646 of *Lecture Notes in Math.*, pages 143–185. Springer, Berlin, 1996.

[55] G. Tian and S.-T. Yau. Existence of Kähler-Einstein metrics on complete Kähler manifolds and their applications to algebraic geometry. In *Mathematical aspects of string theory (San Diego, Calif., 1986)*, volume 1 of *Adv. Ser. Math. Phys.*, pages 574–628. World Sci. Publishing, Singapore, 1987.

[56] X.-J. Wang and X. Zhu. Kähler-Ricci solitons on toric manifolds with positive first Chern class. *Adv. Math.*, 188(1):87–103, 2004.